

Copyright is owned by the Author of the thesis. Permission is given for a copy to be downloaded by an individual for the purpose of research and private study only. The thesis may not be reproduced elsewhere without the permission of the Author.

MATHEMATICAL MODELLING FOR DESIGN OF HORTICULTURAL PACKAGING

A thesis presented in partial fulfilment of the requirements for the degree
of Doctor of Philosophy in Food Engineering at Massey University.

David James Tanner
B.Hort. (Tech.) (Hons)

1998



'The roots of education are bitter, but the fruit is sweet'
- Aristotle

ABSTRACT.

A simulation system for design and optimisation of horticultural packaging systems was developed. This computer-based system is applicable to a range of horticultural products and package designs and predicts product cooling rate, product weight loss, local in-package relative humidity, and package material moisture properties.

A zone definition methodology was developed which related geometric characteristics of a wide range of packaging systems to specific model input data. The methodology also allowed the important intra- and inter-zonal heat and mass transfer pathways to be delineated and characterised. The model component hierarchy treated the fluid, packaging and product as equally important. This decision, differing from some previous models, was instrumental in achieving both greater flexibility and improved alignment between the modelled system and reality.

The dynamic simulation system was developed, with two model components. The pre-cooling (heat transfer) model within the 'Packaging Simulation for Design' software included ten major convective or conductive heat transfer pathways between air, packaging and product. Whilst these were the most significant modes of heat transfer envisaged, not all are necessarily significant for any particular package design. The dynamic bulk storage (mass transfer) model, also within the 'Packaging Simulation for Design' software, included six major mass transfer pathways associated with: packaging material moisture uptake, water vapour transport across packaging and ventilation boundaries, and product mass transfer.

In addition, a quasi-steady-state simulation system 'Weight Loss Simulator' was developed. The associated software incorporates a database of packaging configurations, and product specific data. The user inputs only a sub-set of the data needed by the dynamic model.

With the exception of in-package fluid velocity, most data needed for using the models could be adequately estimated using previously available methods. An experimental technique was developed for characterisation of airflow distribution within horticultural product packages. This technique used CO₂ as a tracer gas, measuring

arrival times at different locations following injection of CO₂ into the air stream entering the package. Several package designs for apples were characterised and in-pack air velocities estimated.

The heat transfer model was successfully applied to a range of both small and large packaging units (from single cardboard packs to apple pallets and bins). Both time-temperature data collected as part of this research and data from three external sources were predicted as well as could be expected, taking into account model input data uncertainties.

The dynamic and quasi-steady-state mass transfer models were tested for apple and tomato packaging systems (including both commercially used and prototype configurations). Where good quality input data were available, both models accurately predicted the mass loss from product/package systems.

Overall, the generalised simulation systems developed in this research were shown to be of sufficient accuracy for confidence to be placed in their application to design, optimisation and comparison of packaging system performance across a range of typical horticultural food cooling and storage operations. Nevertheless, areas for possible improvement are identified. The models may be applicable beyond horticultural commodities, but require testing for other products to substantiate this.

ACKNOWLEDGEMENTS

To the supervision team, without whom I could not have completed this project:

- Professor Andrew Cleland, Professor of Food Engineering and Academic Director (Technology and Engineering), Massey University (Chief Supervisor). Thank you greatly for your inspiring wisdom, professional attitude and confidence throughout this enjoyable programme.
- Mr Tom Robertson, Senior Lecturer in Packaging Technology (Institute of Technology and Engineering), Massey University. Thank you for the introduction into the packaging research industry, suggestions and advice.
- Dr Linus Umetz Opara, Lecturer in Postharvest Engineering (Institute of Technology and Engineering), Massey University. Thank you for your helpful guidance, advice and professional attitude, which assisted greatly in completion of this project.

Thank you all for your patience and professionalism in what was a cross-departmental, cross-faculty and cross-institute journey – a true learning experience for us all.

I would also like to thank the following people for their technical, administrative and logistical support:

- ENZAFRUIT New Zealand (International). Thank you to this progressive horticultural export company for providing project funding, enabling this programme to be completed successfully with real commercial benefit. The wider horticultural, and scientific, communities need more leaders such as you to help create a technological resource for New Zealand industry.
- The Frank Sydenham Memorial Trust. Thank you for investing in what I believe to be a worthwhile project, benefiting the wider horticultural industries of New Zealand.
- Byron McKillop, Garry Radford, Mark Dorsey, Sue Nicholson, John Alger, Don McLean and Bruce Collins from the greater Technology community and Centre for Postharvest and Refrigeration Research, Massey University. Thank you for assistance and guidance in making and/or maintaining experimental equipment.

Your combined knowledge and expertise make you all an invaluable resource for postgraduate and academic researchers. Keep up the great work.

- Dr Doug King, Research Manager, ENZAFRUIT New Zealand (International), Hastings. Thank you for providing information from the ‘coal-face’ and offering quality guidance. I look forward to further interaction in the future.

And finally, I would like to thank the following people for their support, encouragement and understanding, without which this project would have been a long and lonely road:

- My wife Kim, without whom all this would not be worthwhile, and probably would not have been possible. Your understanding throughout this personal journey is a very special quality. Thank you for your patience.
- My family, particularly my parents, Brian and Judy, for their continued support (not always just emotional). Hope it is worth the wait.
- To the fellow postgraduate students and more recently staff I have had the pleasure of interacting, conversing and playing tennis with – Thanks for the memories and best of luck to you all in your endeavours.

TABLE OF CONTENTS

Abstract	<i>i</i>
Acknowledgements	<i>iii</i>
Table of Contents	<i>v</i>
List of Figures	<i>xi</i>
List of Tables	<i>xix</i>
 <i>Chapter 1:</i>	
Introduction	1.1
 <i>Chapter 2:</i>	
Mathematical Modelling of Horticultural Packaging -	
A Literature Review	2.1
2.1 Introduction	2.1
2.2 Principles of Mathematical Modelling	2.1
2.2.1 Formulation	2.2
2.2.2 Complexity	2.2
2.2.2.1 Time Discretisation	2.3
2.2.2.1 Space Discretisation	2.3
2.3 Modelling of Horticultural Product Behaviour in the Cool Chain	2.4
2.3.1 Product Heat Transfer	2.5
2.3.1.1 Analytical Models	2.6
2.3.1.2 Approximate Analytical Models	2.8
2.3.1.3 Empirical Models	2.8
2.3.1.4 Numerical Models	2.11
2.3.2 Product Respiration	2.13
2.3.3 Product Mass Transfer	2.15
2.3.3.1 Evaporation Models	2.15
2.3.3.2 Models for Product Mass Transfer including Evaporation	2.16
2.4 Modelling of Airspace within Horticultural Packages	2.17
2.4.1 Modelling of Airflow Pathways	2.17
2.4.1.1 Zoned Models	2.18
2.4.1.2 Fully Distributed (or Fluid Dynamics) Models	2.19
2.4.1.3 Airflow Visualisation	2.21
2.4.2 Modelling Airspace Relative Humidity	2.22
2.5 Modelling of Horticultural Packaging Materials	2.23
2.5.1 Packaging Material Thermal Capacity	2.23
2.5.2 Moisture Accumulation in Packaging Materials	2.24
2.5.3 Moisture Transport through Packaging Materials	2.25
2.5.4 Moisture Transport through Packaging Ventilation	2.26
2.6 Model Validation	2.27
2.7 Literature Summary	2.28

Chapter 3:

Research Objectives	3.1
3.1 Introduction	3.1
3.2 Objectives	3.1
3.3 Customisation to the needs of the Project Sponsor	3.3

Chapter 4:

Simulation Model Development Strategy	4.1
4.1 Introduction	4.1
4.2 Physical Models of Packaging Systems	4.1
4.3 Sub-model Hierarchy	4.9
4.4 General Modelling Philosophy	4.10
4.4.1 Zone Definition	4.10
4.4.2 Zone Fluid	4.12
4.4.3 Packaging Materials	4.12
4.4.4 Product	4.13
4.5 Concluding Remarks	4.13

Chapter 5:

Formulation and Implementation of Simulation Models	5.1
5.1 Formulation of the Pre-cooling Model	5.1
5.1.1 Heat Transfer Pathways	5.1
5.1.2 Mathematical Formulation of Heat Transfer Equations	5.4
5.1.2.1 Formulation of the ODE for Zone Product Temperature	5.4
5.1.2.2 Formulation of the ODE for Zone Fluid Temperature	5.7
5.1.2.3 Determination of Actual Heat Transfer Coefficients	5.10
5.1.2.4 Determination of 'Effective' Heat Transfer Coefficients ..	5.15
5.1.2.5 Determination of Velocity Data	5.17
5.1.2.6 Determination of Thermo-physical Properties	5.17
5.1.2.7 Determination of Area Values	5.17
5.1.2.8 Respiration Correlation	5.18
5.2 Formulation of the Bulk Storage Model	5.18
5.2.1 Mass Transfer Pathways	5.18
5.2.2 Mathematical Formulation of Mass Transfer Equations	5.20
5.2.2.1 Determination of Mass Transfer Coefficients	5.23
5.2.2.2 Determination of Velocity Data	5.25
5.2.2.3 Determination of Area Values	5.26
5.2.2.4 Determination of Moisture Properties of Fluid and Product	5.26
5.2.2.5 Determination of Moisture Properties of Packaging Materials	5.26
5.2.2.6 Respiratory Mass Loss	5.29
5.3 Formulation of the Database-linked Steady-state Model	5.29
5.3.1 Mass Transfer Pathways	5.30
5.3.2 Mathematical Formulation of Mass Transfer Equations	5.31
5.3.2.1 Process A (Packaging Material Moisture Uptake)	5.31
5.3.2.2 Process B (Steady-state Mass Loss)	5.32
5.3.2.3 Determination of Mass Transfer Coefficients	5.34

5.3.2.4	Determination of Velocity Data	5.35
5.3.2.5	Determination of Area Values	5.35
5.3.2.6	Determination of Moisture Properties of Fluid and Product	5.35
5.3.2.7	Respiratory Mass Loss	5.35
5.3.3	Complete Steady-state Model	5.35
5.4	Model Implementation	5.36
5.4.1	Solution Method	5.36
5.4.2	Computer Implementation	5.36
5.4.2.1	Dynamic ‘Packaging Simulation for Design’	5.36
5.4.2.2	Steady-state ‘Weight Loss Simulator’	5.40
5.5	Concluding Remarks	5.42

Chapter 6:

	Determination of Velocity Profiles for Horticultural Packages	6.1
6.1	Introduction	6.1
6.2	Development of a Flow Characterisation and Visualisation Technique	6.1
6.2.1	Development of the CO ₂ Trace Pulsing Technique	6.2
6.2.2	Calculation of Flow-Relativity Coefficients	6.3
6.2.2.1	Complete Velocity Profiles (with no cross mixing)	6.6
6.2.2.2	Complete Velocity Profiles (with cross mixing)	6.10
6.2.2.3	Measurement of Fluid-Fluid Boundary Areas for 2D Velocity Profiles	6.11
6.3	Experimental Work Undertaken on Apple Packaging	6.12
6.3.1	Pre-1996 ‘Standard’ Apple Packaging	6.14
6.3.2	1996 ‘Zeus’ Apple Packaging	6.20
6.3.3	A Pallet Layer of 1997 ‘Zeus’ Apple Packages	6.23
6.4	Other Packaging Configurations	6.28
6.4.1	Wooden Bin filled with Pears.....	6.28
6.4.2	Packed Bed of Apples	6.28
6.4.3	Further Apple Packaging Configurations assessed for Mass Transfer	6.29
6.4.4	Tomato Packages	6.29
6.5	Concluding Remarks	6.29

Chapter 7:

	Heat Transfer (Pre-Cooling) Model Testing	7.1
7.1	Introduction	7.1
7.2	Analytical and Numerical Integrity Testing	7.1
7.3	Experimental Data Collection and Testing	7.2
7.3.1	Data collected and presented by Amos (1995)	7.2
7.3.2	Data collected and presented by Falconer (1995a)	7.14
7.3.3	Packed Bed Experiment	7.20
7.3.4	Data collected by staff at UC-Davis (1996)	7.24
7.4	Discussion of Model Performance	7.29
7.5	Recommendations for Future Work.....	7.30

Chapter 8:

Mass Transfer (Bulk Storage) Model Testing	8.1
8.1 Introduction	8.1
8.2 Experimental Data Collection	8.1
8.2.1 Previous Data Collected for Apple Package Configurations	8.1
8.2.2 Mass Loss Data Collection	8.4
8.2.2.1 Experimental Methodologies	8.5
8.2.2.2 Results and Other Observations	8.10
8.2.2.2 Summary of Experimental Observations and Discussion ..	8.15
8.3 Model Testing - Apple Packaging Systems	8.16
8.3.1 Mass Loss from Palletised, Unmodified, 1997 ‘Zeus’ Apple Packages	8.16
8.3.2 Mass Loss from Palletised, Cling-wrapped, 1997 ‘Zeus’ Apple Packages	8.22
8.3.3 Mass Loss from Palletised, Non-ventilated, 1997 ‘Zeus’ Apple Packages	8.23
8.3.4 Mass Loss from Palletised, Polylined, 1997 ‘Zeus’ Apple Packages	8.24
8.3.5 Mass Loss from Palletised Vented Polylined, 1997 ‘Zeus’ Apple Packages	8.26
8.3.6 Mass Loss from Different Configurations of the 1997 Apple ‘Retail Display Tray’	8.26
8.4 Prediction of Tomato Packaging Systems	8.27
8.4.1 Mass Loss from a 10kg Cardboard Tomato Package	8.27
8.4.2 Mass Loss from a 15kg Plastic Tomato Package	8.29
8.5 Sensitivity Analysis	8.31
8.5.1 Sensitivity to Variation in Product Mass Transfer Coefficient, $K_{f,pr}=K_{skin}$	8.31
8.5.2 Sensitivity to Variation in Product Respiration Rate	8.33
8.5.3 Effect of Poor Knowledge of Fruit Temperature - Package Air Temperature Difference.....	8.34
8.5.4 Sensitivity to Variation in Product Water Activity	8.35
8.5.5 Sensitivity to Variation in Effective Packaging Material Mass Transfer Coefficient, $K_{eff,pk}$	8.36
8.5.6 Sensitivity to Variation in External Fluid Relative Humidity	8.37
8.5.7 Effect of Variation in the In-package Air – Coolstore Air Temperature Difference	8.38
8.5.8 Sensitivity to Variation in the Lower Limit for Packaging Thickness, x_{pk}	8.39
8.6 Discussion of Model Performance	8.41
8.7 Recommendations for Future Work	8.42

<i>Chapter 9:</i>	
Conclusions	9.1
 <i>Chapter 10:</i>	
References	10.1
 <i>Appendix 1:</i>	
Table of Nomenclature	A1.1
 <i>Appendix 2:</i>	
Determination of Model Input Data	A2.1
A2.1 Introduction	A2.1
A2.2 Thermo-physical Properties	A2.1
A2.2.1 Thermal Conductivity	A2.1
A2.2.1.1 Prediction Methods for Thermal Conductivity	A2.1
A2.2.1.2 Experimental Values of Thermal Conductivity	A2.3
A2.2.1.3 Data Used	A2.3
A2.2.2 Specific Heat Capacity	A2.5
A2.2.2.1 Prediction Methods for Specific Heat Capacity	A2.5
A2.2.2.2 Experimental Values of Specific Heat Capacity	A2.6
A2.2.2.3 Data Used	A2.6
A2.2.3 Density	A2.8
A2.2.3.1 Prediction Methods for Density	A2.8
A2.2.3.2 Experimental Values of Density	A2.9
A2.2.3.3 Data Used	A2.10
A2.2.4 Fluid Kinematic Viscosity	A2.10
A2.2.5 Product Surface Area	A2.11
A2.2.5.1 Data Used	A2.12
A2.2.6 Energy Release by Product Respiration	A2.12
A2.2.6.1 Prediction of Respiration Phenomena	A2.12
A2.2.6.2 Cultivar-specific Respiration Data	A2.14
A2.2.6.3 Measured Data.....	A2.15
A2.2.6.4 Data Used	A2.15
A2.3 Hydro-physical Properties of Products	A2.16
A2.3.1 Product Water Activity	A2.16
A2.3.1.1 Theoretical Determination of Product Water Activity	A2.16
A2.3.1.2 Experimental Determination of Product Water Activity	A2.16
A2.3.1.3 Data Used	A2.17
A2.3.2 Effective Diffusivity of Water Vapour in Air.....	A2.17
A2.3.3 Mass Transfer Coefficient Correlations.....	A2.18
A2.3.3.1 Skin to Fluid	A2.18
A2.3.3.2 Experimental Determination of Skin Mass Transfer Coefficients	A2.18
A2.3.3.3 Data Used	A2.20
A2.3.4 'Effective' Mass Transfer Coefficients for Packaging Materials	A2.20

A2.3.4.1	Measurement of ‘Effective’ Mass Transfer Coefficients for Packaging Materials	A2.21
A2.3.5	Mass Transfer Coefficients for Fluid - Packaging Material Contact.....	A2.23
A2.3.6	Guggenheim-Anderson-De Boor (G.A.B) Moisture Isotherm Coefficients.....	A2.23
A2.4	Concluding Remarks	A2.24

Appendix 3:

	Practical Guide to ‘Packaging Simulation for Design’	A3.1
A3.1	Computer Requirements.....	A3.1
A3.2	Installation	A3.1
A3.3	Running the Software	A3.1
A3.3.1	Pre-cooling Simulation Model	A3.2
A3.3.2	Bulk Storage Simulation Model	A3.5
A3.4	Creating Heat and Mass Transfer Datafiles	A3.8
A3.5	Using Other Components of the Simulation Software	A3.10
A3.6	Future Modifications of Software	A3.10
A3.7	Files Included for Software Operation	A3.11

Appendix 4:

	Practical Guide to ‘Weight Loss Simulator’	A4.1
A4.1	Computer Requirements.....	A4.1
A4.2	Installation	A4.1
A4.3	Running the Software	A4.1
A4.4	Editing the Product, Package and Packaging Materials Databases.....	A4.6
A4.5	Current Package and Product Inclusions in the Weight Loss Simulator.	A4.10
A4.6	Future Modifications of Software	A4.11
A4.7	Files Included for Software Operation	A4.11

LIST OF FIGURES

Chapter 1:

- 1.1 Example plots of product temperature and product mass in both pre-cooling (a) and bulk static storage (b) of apples1.3
- 1.2 Example plots of packaging material moisture content and in-package relative humidity in both pre-cooling (a) and bulk static storage (b) of apples.....1.3
- 1.3 Example plots of package O₂ and CO₂ concentration in both pre-cooling (a) and bulk static storage (b) of modified atmosphere packed apples.....1.3

Chapter 2:

- 2.1 Effect of model complexity on accuracy and implementation cost (After Cleland and Cleland, 1989a).2.2
- 2.2 Log-transformed temperature-time profile for a single stage chilling process (modified from Cleland and Davey, 1995).2.8

Chapter 3:

- 3.1 Proposed technology transfer process for model application in the design of horticultural packaging systems3.3

Chapter 4:

- 4.1 Physical model of the system described in Example 14.2
- 4.2 Conceptualisation of the main pathways existing for heat and mass transfer in Example 1 (a corrugated apple package).4.3
- 4.3 Physical model of the system described in Example 2 (after Merts, 1996).4.4
- 4.4 Conceptualisation of the main pathways existing for heat and mass transfer in Example 2 (an apple carton with the product enclosed in a polyliner).4.5
- 4.5 Physical model of the trays in the system described in Example 3.4.5
- 4.6 Conceptualisation of the main pathways existing for heat and mass transfer in a pallet.4.6
- 4.7 Physical model of the systems described in Examples 4 and 5.4.7
- 4.8 Conceptualisation of the main pathways existing for heat and mass transfer in a bulk storage unit.....4.8
- 4.9 Conceptualisation of the main pathways existing for mass transfer in a bulk storage container placed in static storage, where heat transfer has reached steady state.4.9
- 4.10 Sub-model interaction within a zone in the proposed modelling system.4.10
- 4.11 Examples of the zone and zone boundary numbering and coding utilised in the modelling system.4.11

Chapter 5:

5.1	Major heat transfer pathways for product and fluid in a modelling zone (shaded region).....	5.2
5.2	Product interactions with components in adjacent zones across the zone boundary	5.4
5.3	Zone fluid interactions with components across adjacent boundaries.....	5.8
5.4	Major mass transfer pathways for product, packaging materials and fluid in an example-modelling zone (shaded region).	5.19
5.5	Zone fluid interactions with components across adjacent boundaries.....	5.20
5.6	Moisture sorption isotherm model predictions for “outer” corrugated apple packaging (at 1°C and 40°C) undergoing both sorption (in which the material is taken from dry conditions to a higher humidity) and desorption (from saturated conditions to a lower humidity). After Eagleton and Marcondes (1994).	5.29
5.7	Indicative plot of modelling results for the dynamic and the steady-state simulation models.	5.30
5.8	Water mass interactions modelled as instantaneous processes in the steady-state simulation model	5.31
5.9	Water mass interactions modelled in the steady-state simulation model.....	5.33
5.10	Structure of the dynamic simulation system and the individual component linkages.....	5.37
5.11	Structure of the steady-state simulator and the individual component linkages.....	5.42

Chapter 6:

6.1	CO ₂ Tracer Pulsing System set-up.....	6.3
6.2	Typical concentration versus time curves, which are used to determine flow profiles for different packaging systems.....	6.3
6.3	Methodology used in development of single plane (<i>y</i> direction) velocity relativity curves for positions in a horticultural package.....	6.5
6.4	Velocity relativity data and visualisation curves for planes down the height (or <i>y</i> direction) at three positions across the width (<i>x</i> direction) in an apple package, at different inlet air temperatures.....	6.7
6.5	Velocity relativity data and visualisation curves for planes down the height (or <i>y</i> direction) at three positions across the width (<i>x</i> direction) in an apple package, at different inlet air velocities.	6.8
6.6	Allowable pathways of fluid flow as a result of assuming that flow in the dominant flow direction does not undergo cross-mixing.....	6.10
6.7	Illustration of pathways of fluid flow exhibiting cross-mixing between zones in the counter-current flow directions.....	6.11
6.8	Concept utilised for measurement of actual fluid-fluid boundary areas (the shaded region indicates $A_{i,jff}$ for an individual position).	6.11
6.9	Plan view of two possible ‘Friday’ tray orientations in complete package configurations (NB these are for the top layer of the package).	6.12

6.10	Velocity relativity data and visualisation curves for planes down the height (or y direction) at three positions across the width (x direction) in an apple package, with different ‘Friday’ tray orientations.	6.13
6.11	The “Standard” apple packaging used in the determination of velocity relativity coefficients.	6.14
6.12	Velocity relativity data and visualisation curve for positions across the width (or x direction) in a 5-layer ‘Standard’ apple package.	6.15
6.13	Velocity relativity data and visualisation curve for positions down the height (or y direction) in a 5-layer ‘Standard’ apple package.	6.15
6.14	Velocity relativity data and visualisation curve for positions across the width (or x direction) in a 6-layer ‘Standard’ apple package.	6.16
6.15	Velocity relativity data and visualisation curve for positions down the height (or y direction) in a 6-layer ‘Standard’ apple package.	6.16
6.16	Velocity relativity data and visualisation curves for planes down the height (or y direction) at three positions across the width (x direction) in a 5-layer ‘Standard’ apple package.	6.18
6.17	Velocity relativity data and visualisation curves for planes down the height (or y direction) at three positions across the width (x direction) in a 6-layer ‘Standard’ apple package.	6.19
6.18	The “Zeus” apple packaging used in the determination of velocity relativity coefficients.	6.20
6.19	Velocity relativity data and visualisation curve for positions across the width (or x direction) in a 4-layer ‘Zeus’ apple package.	6.21
6.20	Velocity relativity data and visualisation curve for positions down the height (or y direction) in a 4-layer ‘Zeus’ apple package.	6.21
6.21	Velocity relativity data and visualisation curve for positions down the length (or z direction) of a 4-layer ‘Zeus’ apple package.	6.22
6.22	Velocity relativity data and visualisation curve for positions down the height (or y direction) in a 4-layer ‘Zeus’ apple package.	6.22
6.23	Velocity relativity data and visualisation curves for planes down the height (or y direction) at three positions across the width (x direction) in a 4-layer ‘Zeus’ apple package.	6.24
6.24	Velocity relativity data and visualisation curves for planes down the height (or y direction) at three positions down the length (z direction) of a 4-layer ‘Zeus’ apple package.	6.25
6.25	The pallet layer configuration of “Zeus” apple packaging used in the determination of velocity relativity coefficients (left - top view, right (top and bottom) - the two possible package orientations).	6.26
6.26	Numbering system and flow directions used in CO ₂ tracer studies for the ‘Zeus’ apple pallet layer. The zone coordinates in the x , y and z directions are also illustrated.	6.26
6.27	Example flow patterns for both directions across a pallet layer of “Zeus” apple packages.	6.27

Chapter 7:

7.1	Configuration used in the model datafiles constructed for comparison of Amos (1995) data.....	7.3
7.2	Predicted and measured air temperatures vs time for the centre of layer 3 of a 'standard' apple package undergoing 'conduction-only' cooling – Experimental data from Amos (1995).....	7.3
7.3	Predicted and measured fruit temperature vs time for the centre of layer 3 in a 'standard' apple package undergoing 'conduction-only' cooling – Experimental data from Amos (1995).....	7.5
7.4	Predicted and measured product temperature vs time for the centre fruit in layer 4 in a 'standard' apple package undergoing 'suppressed' heat transfer – Experimental data from Amos (1995).....	7.6
7.5	Predicted and measured product temperatures vs time for positions in 2 layers of a 'standard' apple package undergoing forced draft cooling – Experimental data from Amos (1995).....	7.7
7.6	Air temperatures for two positions in a 'conduction-only' apple package for 3 levels of inter-zone natural convection.....	7.8
7.7	Product temperatures for two positions in a 'conduction-only' apple package layer for 3 levels of inter-zone natural convection.....	7.9
7.8	Air temperatures for two positions in a force-draft cooled apple package for 3 levels of inter-zone natural convection.....	7.9
7.9	Product temperatures for two positions in a force-draft cooled apple package for 3 levels of inter-zone natural convection.....	7.10
7.10	Product temperatures vs time for simulations both including and excluding packaging thermal capacity in a 'conduction-only' apple package.....	7.10
7.11	Product temperatures vs time for simulations both including and excluding packaging thermal capacity in a forced-draft cooled apple package.....	7.11
7.12	Assessment of sensitivity of predictions to the uncertainty in the inlet air velocity (for the apple forced-draft cooling scenario, 1.4 m.s^{-1}) using two positions in a force-draft cooled apple package.	7.12
7.13	Assessment of the importance of inclusion of respiratory heat generation to prediction of product temperatures for two positions in a forced-draft cooling scenario (for apples, the respiratory coefficients for inclusion in the model of Gaffney <i>et al.</i> (1985b) are $a= 4.59 \times 10^{-6}$ and $b= 2.66$).....	7.13
7.14	Assessment of the importance of inclusion of respiratory heat generation to prediction of product temperatures for two positions in a 'conduction-only' cooling scenario (for apples, the respiratory coefficients for inclusion in the model of Gaffney <i>et al.</i> (1985b) are $a= 4.59 \times 10^{-6}$ and $b= 2.66$).....	7.13
7.15	Configuration used in the model datafiles constructed for comparison of Falconer (1995a) data for the single Z-Pack.....	7.14
7.16	Predicted and measured fruit temperatures vs time located at the centre of layers 1 - 4 for the 1996 'Zeus' apple package – Experimental data from Falconer (1995a).	7.16

7.17	Pallet Layer configuration of the 1996 Zeus Apple Packaging - Modified from Falconer (1995a).	7.17
7.18	Predicted and measured fruit temperatures vs time for 'Zeus' apple packages in a pallet layer configuration (Cartons 1, and 2 - as shown in Figure 7.17) – Experimental data from Falconer (1995a).	7.18
7.19	Predicted and measured fruit temperatures vs time for 'Zeus' apple packages in a pallet layer configuration (Cartons 4 and 6 - as shown in Figure 7.17) – Experimental data from Falconer (1995a).	7.19
7.20	Predicted and measured air outlet temperature vs time for 'Zeus' apple packages in a pallet layer configuration - Modified from Falconer (1995a).	7.20
7.21	Predicted and measured product and air temperature vs time at the centre position of a packed bed container of apples – undergoing forced-air cooling.	7.21
7.22	Predicted and measured fruit temperature vs time for the centre position of the packed bed container of apples – undergoing hydro-cooling.	7.23
7.23	Predicted and measured fruit temperatures vs time for three positions in a bin of pears using airflow of $0.313\text{m}^3\cdot\text{s}^{-1}$	7.25
7.24	Positions where measurements were taken within the pear bin by UC – Davis Research Staff, and simulation positions in a 27-zone pear bin model datafile.	7.25
7.25	Assessment of sensitivity to variation in of product specific heat capacity (simulated value for pears: $3750\text{J}\cdot\text{kg}^{-1}\cdot\text{K}^{-1}$) of $\pm 10\%$. The position used is the middle (centre) zone of the 27-zone pear bin.....	7.26
7.26	Assessment of sensitivity to variation in product thermal conductivity (simulated value for pears: $0.51\text{W}\cdot\text{m}^{-1}\cdot\text{K}^{-1}$) of $\pm 10\%$	7.27
7.27	Assessment of sensitivity to variation in fluid specific heat capacity (simulated value for air: $1005\text{J}\cdot\text{kg}^{-1}\cdot\text{K}^{-1}$) of $\pm 10\%$	7.28
7.28	Assessment of sensitivity to variation in fluid density (simulated value for air: $1.28\text{kg}\cdot\text{m}^{-3}$) of $\pm 10\%$	7.28

Chapter 8:

8.1	Royal Gala weekly fruit weights during 13 weeks coolstorage (After Frampton and Ahlborn, 1994).	8.3
8.2	Outline of the construction of the ventilation holes in the prototype ENZA vented polyliner.	8.6
8.3	Measured mass changes in (a) a single apple fruit, (b) a layer of fruit within a package and (c) a complete apple package, after removal from coolstorage conditions to laboratory-controlled ambient conditions (23°C and $65\% \text{RH}$) for mass loss measurements.....	8.8
8.4	The two package configurations used to assess tomato fruit mass loss (left - 10kg corrugated cardboard carton used for local market packaging; right - 15kg plastic cube crate used to reduce water vapour transport pathways).....	8.9
8.5	Mass loss vs time from three Hawke's Bay Z-Pack configurations during storage (with 95% confidence interval bars).	8.11

8.6	Plot of tomato package mass vs time in the mass loss trial.....	8.14
8.7	Plot of tomato package mass vs time in mass loss trial.....	8.14
8.8	The positioning of an ‘average’ palletised Z-Pack.....	8.16
8.9	Predicted and measured fruit mass loss vs time for a single palletised apple Z-Pack in commercial storage. This configuration was modelled as a single zone, using both the dynamic, and steady state, simulation systems.	8.18
8.10	Predicted relative humidity and packaging material moisture uptake vs time for an ‘average’ palletised apple Z-Pack in commercial storage, modelled as a single zone, using the dynamic simulation system, ‘PackSim’.....	8.19
8.11	Differences in partial pressure driving force as simulated by the dynamic simulation system, ‘PackSim’ (solid lines) and the steady-state ‘Weight Loss Simulator’ (dashed lines).	8.20
8.12	Predicted and measured fruit mass loss vs time for individual layers of an ‘average’ palletised apple Z-Pack in commercial storage, modelled as 4 zones, using the dynamic simulation system.....	8.21
8.13	Predicted and measured fruit mass loss vs time for an ‘average’ palletised apple Z-Pack, wrapped in cling-film, in commercial storage. This package was modelled as a single zone, using both the dynamic, and steady state, simulation systems.....	8.23
8.14	Predicted and measured fruit mass loss vs time for an ‘average’ palletised apple Z-Pack, with no ventilation, in commercial storage. This configuration was modelled as a single zone, using both the dynamic, and steady state, simulation systems.....	8.24
8.15	Predicted and measured fruit mass loss vs time for an ‘average’ palletised apple Z-Pack, with a polyliner, in commercial storage. This configuration was modelled as a single zone, using both the dynamic, and steady state, simulation systems.....	8.26
8.16	Predicted and measured fruit mass loss vs time for a 10kg corrugated paperboard tomato package in controlled laboratory storage. This configuration was modelled as a single zone, using both the dynamic, and steady state, simulation systems.....	8.29
8.17	Predicted and measured fruit mass loss vs time for a 15kg plastic tomato package in controlled laboratory storage. This configuration was modelled as a single zone, using both the dynamic, and steady state, simulation systems.	8.31
8.18	Assessment of sensitivity of predictions to variation/inaccuracy in the product mass transfer coefficient (control for apples was $3.51 \times 10^{-10} \text{ kg.s}^{-1}.\text{m}^{-2}.\text{Pa}^{-1}$). The dashed lines are the relative humidity predictions whilst the solid lines predict mass loss.....	8.33
8.19	Assessment of the effect of variation in the product respiration rate on total mass loss and relative humidity prediction (control for apples: $2.53 \times 10^{-11} \text{ kgmol.kg}^{-1}.\text{s}^{-1}$). The dashed lines are the relative humidity predictions whilst the solid lines predict mass loss.	8.34

8.20	Assessment of sensitivity of predictions to variation/inaccuracy in the product-package air temperature difference (control for apples: +0.05°C). The dashed lines are the relative humidity predictions whilst the solid lines predict mass loss.	8.35
8.21	Assessment of sensitivity of predictions to variation in the product water activity (control for apples, 0.995). The dashed lines are the relative humidity predictions whilst the solid lines predict mass loss.	8.36
8.22	Assessment of sensitivity to variation in the effective packaging material mass transfer coefficient on predictions of product mass loss and packaging internal air relative humidity (control for corrugated material, $2.95 \times 10^{-9} \text{ kg.s}^{-1}.\text{m}^{-2}.\text{Pa}^{-1}$). The dashed lines are the relative humidity predictions whilst the solid lines predict mass loss.	8.37
8.23	Assessment of sensitivity of variation in the external relative humidity on prediction of product mass loss and packaging internal air relative humidity (control for this configuration was 89%). The dashed lines are the relative humidity predictions whilst the solid lines predict mass loss.....	8.38
8.24	Assessment of sensitivity to variation in the package - coolstore air temperature difference (control for this configuration was a 0°C temperature difference). The dashed lines are the relative humidity predictions whilst the solid lines predict mass loss.	8.39
8.25	Assessment of sensitivity to variation in the packaging thickness lower limit on predictions of product mass loss and relative humidity (control for this configuration was a 1mm lower limit). The dashed lines are the relative humidity predictions whilst the solid lines predict mass loss.	8.40

Appendix 2:

A2.1	Graph showing the two portions of the water vapour transport into and through packaging materials.	A2.22
-------------	---	-------

Appendix 3:

A3.1	The initial ‘splash’ screen for the ‘Packaging Simulation for Design’ software.	A3.2
A3.2	The main screen for the ‘Packaging Simulation for Design’ software - where the decision, on which simulation model to activate, is required.	A3.3
A3.3	The first implementation screen for the Pre-cooling Simulation of the ‘Packaging Simulation for Design’ software.....	A3.3
A3.4	The simulation duration and output frequency screen for the Pre-cooling Simulation of the ‘Packaging Simulation for Design’ software.	A3.4
A3.5	The dialog box requiring input of the results file for the Pre-cooling Simulation. Multiple results files will be required for modelling scenarios of greater than 125 zones.....	A3.4
A3.6	The main simulation screen which remains active throughout the duration of the Pre-cooling Simulation.	A3.5
A3.7	A summary of a 3 zone results file as produced by the ‘Packaging Simulation for Design’ software.....	A3.6

A3.8	The main simulation screen which remains active throughout the duration of the Bulk Storage Simulation.	A3.7
A3.9	A summary of the results file as produced by the 'Bulk Storage Simulation' component of the 'Packaging Simulation for Design' software.....	A3.7
A3.10	The setup conditions required for generation of a datafile template, used to generate a heat transfer or mass transfer datafile.....	A3.8
A3.11	The main screen in the datafile generator worksheet which is used to develop a pre-cooling simulation datafile for inclusion in the 'Packaging Simulation for Design' software.	A3.9
A3.12	An example of a portion of the input datafile as produced by the datafile generator worksheet.....	A3.9
A3.13	The data input screen for the Convection Factor calculator.....	A3.10
A3.14	The output screen for the Convection Factor calculator.....	A3.10

Appendix 4:

A4.1	The initial 'splash' screen for the 'Weight Loss Simulator' software.....	A4.2
A4.2	The main screen for the 'Weight Loss Simulator' software - where the simulation model is activated using the Run Simulation Speed Button.	A4.2
A4.3	The first dialogue screen for implementation of product data for the 'Weight Loss Simulator' software.	A4.3
A4.4	The second dialogue screen for implementation of storage data for the 'Weight Loss Simulator' software.	A4.4
A4.5	The third dialogue screen for implementation of packaging system data for the 'Weight Loss Simulator' software.	A4.4
A4.6	The packaging materials dialogue box. The data this dialogue contains is shown only for information, and cannot be edited at this time.....	A4.5
A4.7	The status of the screen during simulation by the 'Weight Loss Simulator' software.	A4.5
A4.8	The summary of results as produced upon completion by the Simulation software.....	A4.6
A4.9	A summary of the results file as produced by the Simulation software. This can be readily imported into a spread-sheeting package for data analysis.....	A4.7
A4.10	The product database editor, which allows input of specialised data regarding products in package configurations.	A4.8
A4.11	The package configuration database editor, which allows input of data for packaging configurations and constructions.....	A4.9
A4.12	The packaging materials database editor, which allows input of data for packaging materials.	A4.9

LIST OF TABLES

Chapter 2:

- 2.1 Summary of some empirical models of heat transfer based on semi-logarithmic temperature reduction with time, outlining some strengths and weaknesses.....2.9
- 2.2 Some researchers who have reported experimental measurements of fresh produce cooling rates.....2.10
- 2.3 Summary of some numerically based models for heat transfer of fruits and vegetables.2.11
- 2.4 Respiratory coefficients for Eqn. (2.14) for a range of horticultural products (calculated from Hardenburg *et al.*, 1986)2.14

Chapter 5:

- 5.1 A comparison of actual and effective heat transfer coefficients for a range of typical Bi conditions (**NB** $k_{pr} = 0.5 \text{ W.m}^{-2}\text{K}^{-1}$ and $R = 0.025\text{m}$).....5.17
- 5.2 Specific data required by the datafile generator to create the 'PackSim' input datafile for both the pre-cooling simulation model and the bulk-storage simulation model.5.38
- 5.3 Specific data required for 'PackSim', created in an input datafile for both the pre-cooling simulation model and the bulk-storage simulation model by the datafile generator.5.39
- 5.4 Information delivered in the 'PackSim' results file for both the pre-cooling simulation model and the bulk-storage simulation model.5.40
- 5.5 Specific data requiring for the 'Weight Loss Simulator'5.41
- 5.6 Information delivered in the 'Weight Loss Simulator' results file.5.41

Chapter 6:

- 6.1 Two-dimensional velocity relativity coefficients, as calculated from the VRC 's presented, for the 4-layer apple package.6.9
- 6.2 Two-dimensional velocity relativity profile for the pre-1996 'Standard' apple package packed with 5 layers of fruit.....6.17
- 6.3 Two-dimensional velocity relativity profile for the pre-1996 'Standard' apple package packed with 6 layers of fruit.....6.17
- 6.4 Two-dimensional velocity relativity profile for the 'Zeus' apple package (flow in the z direction).....6.23
- 6.5 Two-dimensional velocity relativity profile for the 'Zeus' apple package (flow in the x direction).6.23
- 6.6 Two-dimensional velocity relativity profile for a pallet layer of 'Zeus' apple packages (flow in Direction A). Note that each package's velocity profile is independent of others in the pallet configuration.....6.27

6.7	Two-dimensional velocity relativity profile for a pallet layer of 'Zeus' apple packages (flow in Direction B). Note that each package's velocity profile is independent of others in the pallet configuration.	6.27
6.8	Assumed two-dimensional velocity relativity profile for a wooden bin filled with pears.....	6.28
6.9	Assumed two-dimensional velocity relativity profile for a packed bed of apples.	6.29

Chapter 7:

7.1	Major data used for construction of a 150 zone, pre-cooling simulation model datafile for 'conduction-only' cooling of a 'standard' apple package.....	7.4
7.2	Amended data (to those of Table 7.1) for development of a 150-zone, pre-cooling simulation model datafile for a 'suppressed' heat transfer 'standard' apple package.....	7.5
7.3	Amended data (to those of Table 7.1) for development of a 150-zone, pre-cooling simulation model datafile for an unmodified 'standard' apple package.....	7.6
7.4	Major data used for construction of a 100 zone, pre-cooling simulation model datafile for forced-draft cooling of an unmodified apple Z-Pack.....	7.15
7.5	Amended major data (to those of Table 7.4) for development of a 144-zone, pre-cooling simulation model datafile for a pallet layer of apple Z-Packs.....	7.17
7.6	Major data used for construction of a 45 zone, simulation model datafile for forced-draft cooling of a packed bed.....	7.22
7.7	Amended major data (to those of Table 7.6) for development of a 45-zone, pre-cooling simulation model datafile for a hydro-cooled packed bed of apples.	7.23
7.8	Major data used for construction of a 27 zone, pre-cooling simulation model datafile for forced-draft cooling of a bin of pears.	7.24

Chapter 8:

8.1	Assessment of mass loss as a result of storage regime and variety for the 1986 apple season - After Bartholomew (1990).	8.2
8.2	Assessment of mass loss as a result of polyliner use for 'Braeburn' apples in the 1985 season - After Bartholomew (1990).	8.2
8.3	Mass changes in a carton of Royal Gala apples after 13 weeks coolstorage (g) - After Frampton and Ahlborn (1994).	8.3
8.4	Package configurations and their modifications tested in the mass loss trial.	8.5
8.5	Fruit mass loss results from all package configurations measured after \approx 4, 8 and 12 weeks (mean \pm 95% confidence limits, assuming replicates are normally distributed).	8.10

8.6	Mean temperature and in-package relative humidity conditions (in comparison with mean coolstore conditions of 90% RH and 0.1°C). The contribution of carbon loss to mass loss is also presented.....	8.12
8.7	Mean moisture content of packaging materials at the conclusion of the mass loss trial.....	8.13
8.8	Major data used for development of a single zone, bulk-storage simulation model datafile for an 'average' palletised Z-Pack.	8.17
8.9	Amended data (to those of Table 8.8) for development of a 4-zone, bulk-storage simulation model datafile for an 'average' palletised Z-Pack.....	8.21
8.10	Amended data (to those of Table 8.8) for development of a single zone, bulk-storage simulation model datafile for an 'average' palletised cling-wrapped Z-Pack.....	8.22
8.11	Amended data (to those of Table 8.8) for development of a single zone, bulk-storage simulation model datafile for an 'average' palletised Z-Pack, with no ventilation.	8.23
8.12	Major data used for development of a single zone, bulk-storage simulation model datafile for an 'average' palletised Z-Pack, with a polyliner.	8.25
8.13	Model predictions of fruit mass loss and relative humidity for four Retail Display Tray packaging configurations after 12 weeks in commercial storage.	8.27
8.14	Major data used for development of a single zone, bulk-storage simulation model datafile for a corrugated paperboard tomato pack.....	8.28
8.15	Major data used for development of a single zone, bulk-storage simulation model datafile for a plastic tomato pack.	8.30
8.16	Major data used for development of a single zone, bulk-storage simulation model datafile as a control for sensitivity analysis.....	8.32

Appendix 2:

A2.1	Experimental values of thermal conductivity for a range of horticultural and packaging products.....	A2.4
A2.2	Values for thermal conductivity of air and water (After McCabe <i>et al.</i> , 1993).....	A2.4
A2.3	Values for specific heat capacity of packaging materials.	A2.6
A2.4	Experimentally determined values for horticultural product composition and measured or calculated specific heat capacity.	A2.7
A2.5	Literature presented values for specific heat capacity of air and water.....	A2.8
A2.6	Experimental values of density for a range of horticultural and packaging products.	A2.9
A2.7	Values of density of air and water.	A2.10
A2.8	Parameter values for linear regression models relating product mass to product surface area (Chau <i>et al.</i> , 1987).....	A2.11
A2.9	Parameter values for non-linear regression models relating apple surface area to fruit mass and fruit volume for four apple cultivars and the combined dataset (Clayton <i>et al.</i> , 1995).....	A2.12

A2.10	Respiratory coefficients for Eqn. (A2.20) for a range of horticultural products, based on data presented by Hardenburg <i>et al.</i> (1986).	A2.14
A2.11	Parameter values for non-linear regression models relating apple cultivar respiration rate to temperature (Dadzie, 1992).	A2.15
A2.12	Respiration rates for a range of horticultural products (After Hardenburg <i>et al.</i> , 1986).	A2.15
A2.13	Commodity surface water activities (Chau <i>et al.</i> , 1988).	A2.17
A2.14	Values of effective diffusivity of water vapour in air.	A2.18
A2.15	Commodity skin mass transfer coefficients (Chau <i>et al.</i> , 1987; Gan and Woods, 1989; and Becker <i>et al.</i> , 1994).	A2.19
A2.16	Apple variety mass transfer coefficients (Maguire <i>et al.</i> , 1996).	A2.19
A2.17	Effective' mass transfer coefficients for packaging materials, including percentage of rate relative to rate through a still air gap of the same thickness (at 0°C).	A2.22
A2.18	GAB moisture-sorption isotherm model equation coefficients for paper-based packaging materials used in construction of transport packaging for apples (After Eagleton and Marcondes, 1994).	A2.24

Appendix 3:

A3.1	Table of files included in Appendix 5	A3.11
-------------	---	-------

Appendix 4:

A4.1	A list of products and packaging materials included in the Beta Version of the 'Weight Loss Simulator'	A4.10
A4.2	A list of packages included in the Beta Version of the 'Weight Loss Simulator'	A4.11
A4.3	Table of files included in Appendix 5	A4.12

CHAPTER 1

INTRODUCTION

The New Zealand horticultural industry was worth \$1.56 billion in export earnings in 1995/96, of which 63.4% was fresh fruit and 10.7% was fresh vegetable exports (Mirams, 1996). Of these products, apples (52.1%) and kiwifruit (41.1%) made up the majority of the fresh fruit turnover, whilst onions (38.9%) and squash (33.0%) topped the fresh vegetables export earnings.

An important factor in the export of fresh horticultural items is the maintenance of product quality. After harvesting, fresh produce is generally graded for quality, packaged, palletised and stored in a cooling environment. The major purpose of this cooling is to slow the metabolic activity of the commodity's tissue, such as respiration rate, to decrease the rate of degradation and extend the product's shelf life.

By packaging the produce, a number of benefits can be gained such as; reductions in mass loss (also influenced by the relative humidity control in the coolstore), protection from handling damage, and greater inventory control as a result of larger unitisation for transport. However, reduction in product cooling rate can occur due to the lowering of cooling medium flow through the package. This delays the lowering of the rate of respiration, which can reduce the product storage life. A further disadvantage can be a localised and detrimental increase in undesirable volatile concentrations, (e.g. ethylene, carbon dioxide) and a deleterious reduction in oxygen level.

The packaging component can be up to 10% of the weight of palletised apples destined for export markets. It cost the apple industry (and ENZAFRUIT New Zealand International in particular) approximately \$75 million in 1997 (King, pers. comm.). This is the third largest postharvest cost to this industry behind shipping and coolstorage.

Both the pipfruit industry and the kiwifruit industry presently use a small number of relatively standard packs. However, future trends will include the need to:

- minimise packaging (e.g. to meet European packaging legislation, reduce transportation costs),
- protect fruit better (e.g. reduce bruising),
- maintain the best possible local environment (better control relative humidity, temperature, gas composition) and,
- accommodate market-led customisation of packs for particular consumer groups.

Thus package design will increase in importance, and it is vital that the market needs are reconciled with sound engineering practice to maintain product quality, and achieve cost-effective storage and handling systems. When a new package design is proposed, the implications for the whole fruit handling chain should be easily predictable (Figures 1.1 - 1.3), rather than requiring a costly experimental re-development of, for example, fruit cooling and handling systems.

The development and application of predictive models in horticultural refrigeration has increased markedly in the past decade. By applying appropriate mathematical tools to the packaging design process, quantitative prediction of important variables can be made. This will allow designs to be screened prior to any prototype testing, reducing the need to perform experimentation and “trial and error” testing which is both time consuming and can be expensive.

The aim of this research was to develop a computer-based mathematical simulation model applicable to a range of horticultural product and package designs that will predict product cooling rate, product mass loss, local pack relative humidity, and package material moisture properties. This prediction system should be useful for a variety of post-harvest produce management organisations as well as packaging supply companies.

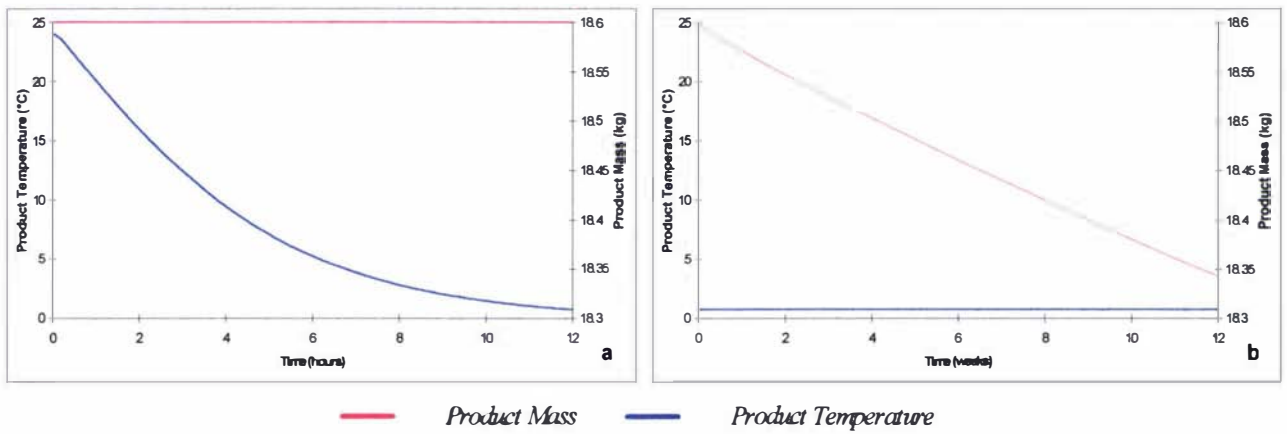


Figure 1.1. Example plots of product temperature and product mass in (a) pre-cooling and (b) bulk static storage of apples.

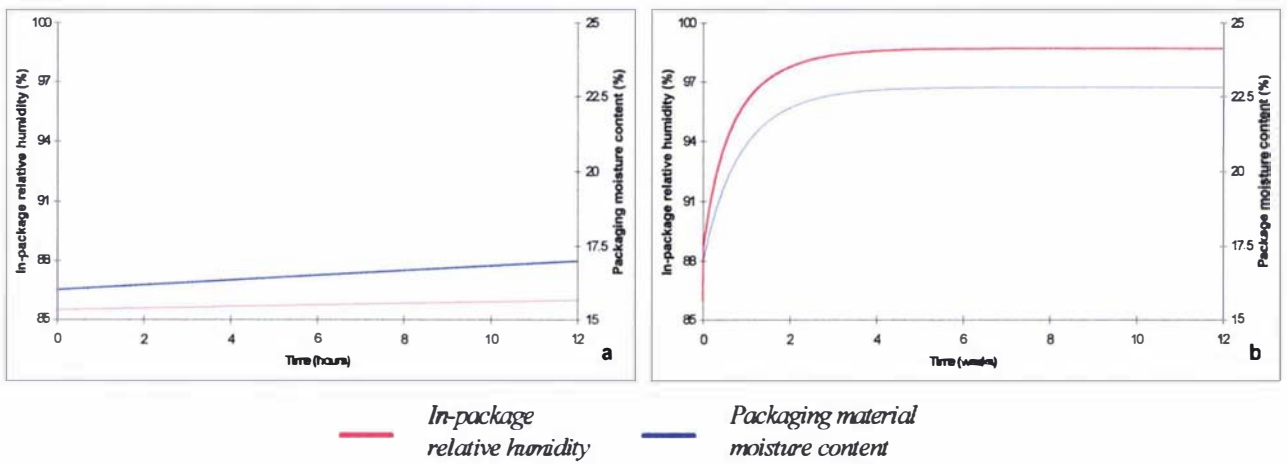


Figure 1.2. Example plots of packaging material moisture content and in-package relative humidity in (a) pre-cooling and (b) bulk static storage of apples.

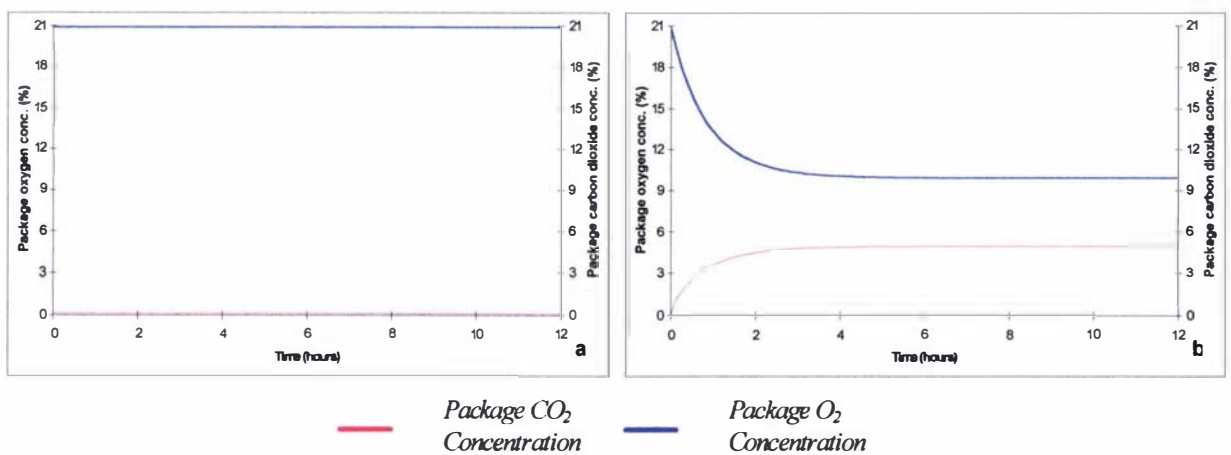


Figure 1.3. Example plots of in-package O₂ and CO₂ concentration in (a) pre-cooling and (b) bulk static storage of modified atmosphere packed apples.

CHAPTER 2

LITERATURE REVIEW

2.1. INTRODUCTION

This literature review encompasses topics of importance to the research undertaken in this study. Section 2.2 covers general principles of mathematical modelling and reviews modelling approaches taken by previous researchers. Section 2.3 introduces modelling concepts related to heat and mass transfer within horticultural produce. Section 2.4 covers modelling of airspace within the horticultural packaging system, whilst Section 2.5 covers modelling of the packaging materials. The final section covers methods of model validation, both graphical and statistical, that have been used by previous researchers.

2.2. PRINCIPLES OF MATHEMATICAL MODELLING

A mathematical model is a model created using mathematical concepts such as functions and equations (Edwards and Hamson, 1989). Such a model is used to provide a solution to a mathematical problem, which is then translated into a useful solution to a ‘real world’ problem.

The use of mathematical models and computer simulation as aids in designing and describing systems has rapidly increased in refrigeration research. Researchers have explored the interactions between the physical refrigeration system and various products using both simple and complex models. The approach taken when formulating a mathematical model is generally dependant on the problem being considered. The level of model complexity must be balanced with the time and cost required to ensure that an adequately accurate yet ‘appropriate’ model results (Figure 2.1).

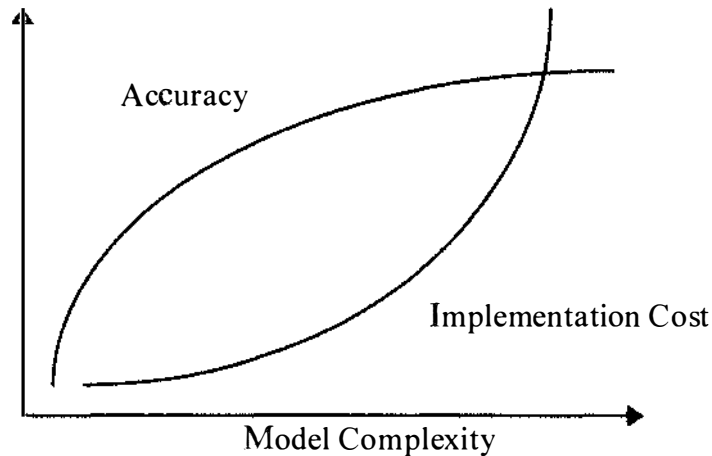


Figure 2.1. Effect of model complexity on accuracy and implementation cost (After Cleland and Cleland, 1989a).

2.2.1. Formulation

The development of mathematical models can be based upon an empirical (black box) approach or a mechanistic (white box) approach. Empirical models involve the development of equations for the system output variables based only on the input conditions and without reference to the internal operations of the system (Cleland, 1990). This reduces their flexibility, as changes in the internal mechanisms often mean complete reworking of the model. Mechanistic models are based on fundamental laws and scientific principles that describe the internal workings of the system (Touber, 1984). Therefore one model can predict the output of the system for a range of situations by alteration of the inputs and the internal parameters. In practice there is a continuous spectrum of modelling approaches between mechanistic and empirical. The main advantage of mechanistic models over empirical models is that they can be used to predict a wider range of systems or used beyond the limits of testing with greater confidence.

2.2.2. Complexity

The accuracy of a mathematical model and its outputs depends on both the validity of the assumptions made and the quality of the knowledge of system data (Cleland, 1983). Any model of a refrigerated airspace must take account of the major sources of variation in a realistic manner if accurate prediction of product conditions is to be

achieved (Amos *et al.* 1993a). However, a model that incorporates all known physical effects might be prohibitively complicated, or the measurements required too expensive to gather (Cleland, 1990). Therefore, a highly detailed model may not be as appropriate as a simple model. Incorporating only the most important effects, may provide a sufficiently accurate description of the application under consideration, provided the important effects can be accurately elucidated using engineering judgement or other means.

2.2.2.1. *Time Discretisation*

Both mechanistic and empirical models can be developed by using either of two methods for describing time variability.

i). Step-wise steady-state modelling.

Steady-state models give an instantaneous output in response to input variables. These have been widely used for modelling refrigerated facilities due to their low level of complexity. They generally require little computational time and only a small amount of data (Pham *et al.*, 1993). These models can only predict time trends by using a time averaging or step-wise procedure (typically hourly or 24 hourly) that neglects thermal storage (Cleland, 1990). They are not expected to be accurate unless all the important system transients are very rapid. Steady-state models can be applied to systems with short transient phases as a strategy to simplify an unsteady-state model. Generally only algebraic equations are required.

ii). Unsteady-state or dynamic modelling.

Unsteady-state or dynamic simulation allows the behaviour of a system to be continuously predicted under time-variable conditions. Unsteady-state models are more computationally and data-intensive, but are more accurate for time variable systems with significant thermal capacity (Cleland, 1990; Amos, 1995). They require differential equations.

2.2.2.2. *Space Discretisation*

There are a number of approaches available for modelling positional variability of conditions, whether the time-variability of the system is steady state or unsteady-state. These include single-zoned, multi-zoned and fully distributed or fluid dynamic modelling approaches (Wang and Toubert, 1990). These are discussed below in the

context of air in a room, but the same principles apply to a region of space occupied by other materials, whether fluid or solid.

i). Single-Zoned Models.

These assume that the defined airspace can be modelled as a single, perfectly mixed, zone. One ordinary differential equation (ODE) is used for air temperature (or energy content with temperature estimated algebraically) and one for humidity. Models such as these assume that any interaction with components within the zone affects the entire zone equally. Single-zoned models do not allow variability within the airspace to be modelled (Amos, 1995).

ii). Multi-Zoned Models.

These models split the region up into a series of zones, which are then individually treated as perfectly mixed. Air transfer between zones will occur. This transfer was modelled as both plug-flow down a well-defined airflow path from air outlet to intake and via a less direct, user defined path by Amos *et al.* (1993b). Multi-zoned models may also include air interchange or cross mixing between zones to represent the real mixing effects in the room (Amos, 1995).

iii). Fully Distributed (or Fluid Dynamic) Models.

The space region is discretised using a complete finite difference, control volume or finite element grid. Fundamental partial differential equations (PDE's) describing momentum, heat and mass transfer are solved within the region by numerical means. This methodology requires few assumptions regarding fluid cross-mixing as the extent of this is calculated by solving the appropriate fundamentally derived equation. The use of this type of modelling methodology has increased markedly in recent years, mainly due to the enhancement of computational speed and capacity, and the availability of software codes (Wang, 1991).

2.3. MODELLING OF HORTICULTURAL PRODUCT BEHAVIOUR IN THE COOL CHAIN

Modelling the heat and mass transfer to and within an entire horticultural package requires understanding of the interactions between heat and mass transfer processes within the commodity and between the commodity and its surrounding medium.

2.3.1. Product Heat Transfer

Product heat transfer models must describe two types of situations. Firstly, there are situations where warm product, either packaged or unpackaged, is at temperatures significantly greater than the cooling environment and is actively cooled. Secondly, once the product is very close to storage temperature there are still important, but often slower, processes occurring such as respiration, evaporative cooling and/or fluctuations in cooling medium (Gaffney *et al.*, 1985b). Published models of these situations differ substantially.

In the first situation, where heat transfer is encouraged, there is generally a significant temperature gradient between the product surface and its centre. This is a common circumstance with horticultural commodities where the surface heat transfer coefficient (h) is often numerically much larger than the thermal conductivity (k). The rate of the change in internal temperature of a solid body can be described by Fourier's Law:

$$\rho c \frac{\partial \theta}{\partial t} = \frac{\partial}{\partial x} \left(k \frac{\partial \theta}{\partial x} \right) + \frac{\partial}{\partial y} \left(k \frac{\partial \theta}{\partial y} \right) + \frac{\partial}{\partial z} \left(k \frac{\partial \theta}{\partial z} \right) \quad (2.1)$$

If the thermal properties of the product can be assumed to be constant with respect to both temperature and time, this simplifies to:

$$\frac{\partial \theta}{\partial t} = \frac{k}{\rho c} \left(\frac{\partial^2 \theta}{\partial x^2} + \frac{\partial^2 \theta}{\partial y^2} + \frac{\partial^2 \theta}{\partial z^2} \right) = \alpha \left(\frac{\partial^2 \theta}{\partial x^2} + \frac{\partial^2 \theta}{\partial y^2} + \frac{\partial^2 \theta}{\partial z^2} \right) \quad (2.2)$$

where c	=	specific heat capacity of the solid ($\text{J.kg}^{-1} \text{K}^{-1}$)
ρ	=	density of the solid (kg.m^{-3})
θ	=	temperature of the solid (K or $^{\circ}\text{C}$)
t	=	time (s)
k	=	thermal conductivity of the solid ($\text{W.m}^{-1} \text{K}^{-1}$)
x, y, z	=	space position within the solid (m)
α	=	thermal diffusivity of the solid ($\text{m}^2.\text{s}^{-1}$)

In the second type of situation the resistance to heat transfer between the cooling medium and the surface is usually higher in comparison with the internal resistance to conduction. Under these conditions of slow cooling, Newton's law of cooling (third kind of boundary condition) may adequately describe the rate of cooling:

$$c \rho V \frac{\partial \theta}{\partial t} = h_c A (\theta_f - \theta) \quad (2.3)$$

where V	=	volume of the solid (m^3)
θ_f	=	fluid temperature (K or $^{\circ}\text{C}$)
h_c	=	surface convective heat transfer coefficient ($\text{W}\cdot\text{m}^{-2}\text{K}^{-1}$)
A	=	surface area of the solid (m^2)

Eqn. (2.3) implicitly models a convection boundary condition.

Gaffney *et al.* (1985b), Cleland (1990), Amos (1995), and Chuntranuluck (1995) have presented comprehensive reviews of models of both types for product heat transfer including those models for both single product items and interacting multiple items either packaged and/or in bulk stacked configurations. These models utilise a variety of solution methods, such as analytical, approximate analytical, empirical and numerical.

2.3.1.1. Analytical Models

Analytical or exact solutions that apply for the cooling of horticultural produce have been derived for one-dimensional heat flow in regularly shaped objects (e.g. sphere, infinite cylinder or infinite slab) subject to the following conditions (Carslaw and Jaeger, 1959):

- i). The object is homogeneous;
- ii). The initial temperature of the object is uniform;
- iii). The surrounding temperature is constant with time;
- iv). There is no temperature- or time-variable internal heat generation;
- v). There is no mass transfer (evaporation) at the surface;
- vi). The object's thermal properties are constant with time and temperature.

With appropriate boundary and initial conditions, analytical methods can be used to solve Eqn. (2.1) for single product items. For the third kind of boundary condition, which examines convective heat transfer at the surface, and with no internal heat generation the following analytical solution to Eqn. (2.2) for a sphere can be derived, provided neither h nor θ_f changes with time (Newman, 1936; Carslaw and Jaeger, 1959; Smith *et al.* 1967):

$$Y_r \equiv \frac{\theta_r - \theta_f}{\theta_{in} - \theta_f} = \sum_{m=1}^{\infty} j_m(r) e^{-(\beta_m^2) \frac{\alpha t}{R^2}} \quad (2.4)$$

$$Y_{av} \equiv \frac{\theta_{av} - \theta_f}{\theta_{in} - \theta_f} = \sum_{m=1}^{\infty} j_m(av) e^{-(\beta_m^2) \frac{\alpha t}{R^2}} \quad (2.5)$$

where the values of β are found by solving:

$$Bi = 1 - \beta_m \cot(\beta_m) \quad (2.6)$$

and the values of j_m are given by:

$$j_m(r) = \frac{2BiR}{r} \frac{(\beta_m^2 + (Bi - 1)^2)}{\beta_m^2(\beta_m^2 + (Bi - 1)Bi)} \sin(\beta_m) \sin(\beta_m \frac{r}{R}) \quad (2.7)$$

$$j_m(av) = \frac{6Bi^2}{\beta_m^2(\beta_m^2 + (Bi - 1)Bi)} \quad (2.8)$$

where Y_r	=	dimensionless temperature ratio as a function of time and position within the solid.
Y_{av}	=	dimensionless temperature ratio as a function of time for the mass average position within the solid.
θ_f	=	fluid temperature (K or °C)
θ_{in}	=	initial product temperature (K or °C)
θ_{av}	=	mass average product temperature (K or °C)
θ_r	=	temperature at position r in the solid (K or °C).
$j_m(r)$	=	function of β_m , geometry and position.
$j_m(av)$	=	function of β_m , and geometry.
Bi	=	Biot number, $h_c R / k$.
β_m	=	m^{th} root of the transcendental equation for, in this case, the sphere (Eqn. 2.6).
R	=	characteristic dimension of the solid (m).
r	=	space position within solid relative to the centre position (m).

Similar solutions exist for the infinite slab, infinite cylinder, infinite rectangular rod, finite cylinder, and brick and for some situations where there is a constant rate of internal heat generation (Carslaw and Jaeger, 1959). There are also analytical solutions for some situations in which cooling medium temperature (θ_f), or surface heat transfer coefficient (h_c), changes with time in a predetermined manner. For example, by use of Duhamel's Theorem, the effect of a step change in θ_f or h_c can be predicted (Cleland and Davey, 1995; Tanner *et al.*, 1995).

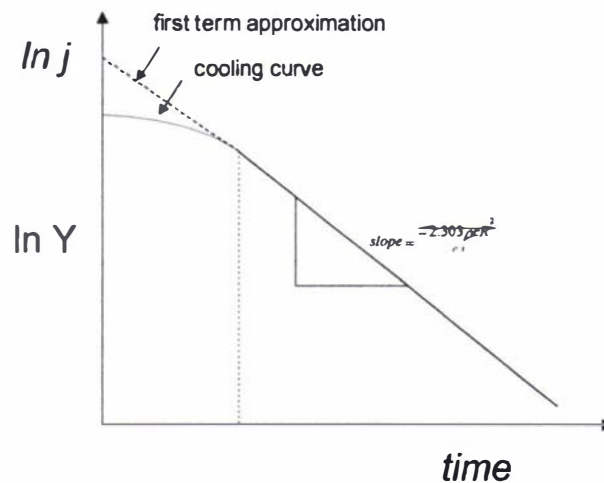
2.3.1.2. Approximate Analytical Models

Where one or more of the conditions assumed in derivation of the exact analytical solution are not met, then approximate analytical solutions may be used. These solutions involve assumptions to simplify the differential equations so that they can then be solved. An example is the work of Goodman (1958; 1961; 1964) who assumed polynomial temperature profiles in the solid to simplify the analytical solution to Eqn. (2.2).

2.3.1.3. Empirical Models

Analytical and approximate analytical solutions are of limited value when the assumptions made during their derivation are not satisfied by the products under investigation e.g. irregular product shape, heat transfer mechanisms other than conduction and convection. As a result, researchers have resorted to the use of empirical prediction methods.

Conductive cooling curves for most horticultural commodities follow a similar trend to the analytical solutions (Figure 2.2). After an initial “lag” period, the temperature of the product decreases at an exponential rate, often referred to as the “constant half-life” period (Cleland, 1990).



where	j	=	intercept coefficient.
	Y	=	fractional unaccomplished temperature change for a process with constant cooling medium temperature.
	f	=	slope index (time for 90% reduction in Y ; s) = $2.303t_{1/2}$.
	$t_{1/2}$	=	half-cooling time (s).

Figure 2.2. Log-transformed temperature-time profile for a single stage chilling process (modified from Cleland and Davey, 1995).

For simple shapes (e.g. sphere), this period corresponds to only one term in the analytical series solution being significant. This period can be identified as the straight-line portion on the semi-log plot of fractional unaccomplished temperature change (Y) versus time, of which the slope is inversely proportional to the half-cooling time. Many empirical methods assume this semi-log behaviour, and thus mimic the analytical solutions (Table 2.1). However, where experimental data were used to curve-fit the formula, the prediction method is probably system specific, and therefore the empirical formulae suggested may be inaccurate beyond the situation from which the data were collected. Table 2.2 lists researchers who have measured fruit and vegetable cooling rates that have been, or might be, processed to develop an empirical method.

Table 2.1.
Summary of empirical models of heat transfer based on
semi-logarithmic temperature reduction with time.

Author(s)	Characteristics
Pflug and Blaisdell (1963)	Presented 1st term approximation to heat transfer in an infinite slab.
Smith <i>et al.</i> (1967)	Defined a generalised shape factor, G , as a ratio of semi-log plots at Bi_{∞} for a real shape and a sphere of the same dimensions
Kopelman and Pflug (1968)	Presented 1st term approximations to heat transfer in an infinite slab, infinite cylinder and sphere.
Clary <i>et al.</i> (1971)	Developed charts using the method of Smith <i>et al.</i> (1967).
Fikiin and Fikiina (1971)	Curve-fitted analytical solutions to develop a relationship between Bi , Fo , and Y during the chilling of different shapes.
Fikiin (1983)	Performed 256 tests of the above relationship and found accuracy was within $\pm 9\%$.
Cleland and Earle (1982)	Developed a generalised shape factor, E , for a range of shapes.
Wade (1984)	Used an empirical technique to predict the cooling rate of complex shapes by treating individual fruit pieces as spheres and pallets as infinite slabs.
Chuntranuluck <i>et al.</i> (1989)	Developed methods for predicting thermal centre and mass average temperatures using E , which would apply to all shapes.
Lin <i>et al.</i> (1993)	Extended work of Chuntranuluck <i>et al.</i> (1989) and presented and tested equations for a range of shapes, including irregular shapes.
Yilmaz. (1995)	Presented equations for centre, surface and mean temperatures during heating and cooling of a range of shapes.

Table 2.2

Researchers who have reported experimental measurements of fresh produce cooling rates.

Author(s)	Characteristics
Hall (1962)	Determined cooling rates of cartonised apples and pears in different pallet stacking configurations.
Parsons <i>et al.</i> (1972)	Determined cooling rates of pears and plums in different carton stacking configurations on a pallet.
Haas <i>et al.</i> (1976)	Determined cooling rates of oranges packed in cartons with variable vent areas.
Haas and Felsenstein (1985)	Determined cooling rates of avocados packed in cartons with different vent area, with different approach air velocities and carton stack heights.
Arifin and Chau (1988)	Determined cooling rates of strawberries packed in cartons with different vent designs, and with different approach air velocities.
ASHRAE (1990)	Published hydro-cooling rates for a range of products.
McDonald (1990)	Determined forced-air and bulk storage cooling rates of apples and pears in a range of packaging and stacking configurations.
Watkins (1990)	Determined forced-air cooling rates for a wide range of produce.
Dincer <i>et al.</i> (1992)	Determined hydro-cooling rates and empirical parameters for packaged apricots, plums and peaches.
McDonald <i>et al.</i> (1993)	Determined forced-air cooling rates of kiwifruit in different coolstorage facilities.
Frampton and Ahlborn (1994)	Determined cooling rates of packaged apples during both forced-air and bulk storage cooling.
Amos (1995)	Determined cooling rates of apples in one package type, but with varied boundary conditions.
Dincer (1995)	Determined forced-air precooling rates of individual grapes.
Falconer and Billing (1995), Falconer (1995a,b)	Determined cooling rates of apples and pears in a range of ventilated and non-ventilated packages.
Frampton (1995; 1996)	Determined rates of cooling of both apples and pears in a range of packaging configurations.
Thompson <i>et al.</i> (1996)	Determined cooling rates, and subsequent moisture loss, of carrots and waxed oranges during forced draft cooling.
Faubion and Kader (1997)	Assessed the influence of wrapping of pears on the cooling rate of this palletised produce.
Hellickson and Baskins (1997)	Determined the effect of tight-stacking of bins on temperature reduction in pear fruit

2.3.1.4. Numerical Models

Numerical methods such as finite element analysis (FE) and finite difference (FD) are often used for solving heat conduction problems where the conditions required for analytical solutions cannot be met. Finite differences are most applicable to situations where simple, regular shapes are used and are more difficult to implement for irregular shapes. In such cases, finite element schemes are more efficient at dealing with arbitrary product shape (Cleland, 1990).

In addition to these methods, Ordinary Differential Equation (ODE) - based modelling approaches have been utilised by some researchers for finite volume or zoned modelling. Such approaches assume that the zones are homogeneous and solve an ODE for each important variable within the zone boundaries (e.g. temperature and moisture content in air or product). Table 2.3 summarises applications of such approaches.

Table 2.3.
Summary of numerically based models for heat transfer of fruits and vegetables (key overleaf).

Author(s)	Type	Product (shape)	Characteristics ¹	Experimentally Validated
Baird and Gaffney (1976)	FD	Orange (sphere)	Only considered internal conduction and convective surface heat transfer from the product.	Yes
Hayakawa (1978)	FD	N/A	Included respiratory heat generation and evaporative cooling in model.	No
Hayakawa and Succar (1982)	FE	Tomato, Potato (sphere)	Included respiratory heat generation and evaporative cooling in model.	Yes
Holdredge and Wyse (1982)	FD	Sugarbeet (?)	Included respiratory heat generation and evaporative cooling in model.	Yes
Ansari <i>et al.</i> (1984)	FD	Apple, Potato (sphere)	Included evaporative cooling in model.	Yes
Chau <i>et al.</i> (1984)	FD	Orange (sphere)	Included respiratory heat, evaporative cooling and product surface radiation in model.	No

Table 2.3 cont.
Summary of numerically based models for heat transfer of fruits and vegetables.

Author(s)	Type	Product (shape)	Characteristics ¹	Experimentally Validated
Jiang <i>et al.</i> (1987)	FE	Broccoli (?)	Assumed that moisture transfer from the stalk was zero.	Yes
Romero and Chau (1987)	FD	Orange (sphere)	Included respiratory heat generation and product mass transfer in model.	Yes
Haghighi and Segerlind, (1988)	FE	Soybean (?)	Included evaporative cooling in model.	Yes
Patel and Sastry, (1988)	FE	Tomato, Mushroom (?)	Included respiratory heat and product surface radiation in model.	Yes
Bazan <i>et al.</i> (1989)	FD	Tomato (sphere)	Included respiratory heat generation in model.	Yes
Gan and Woods (1989)	FD	Swede (sphere)	Included respiratory heat generation and product mass transfer in model.	No
Chau and Gaffney (1990)	FD	Tomato (sphere)	Included respiratory heat, evaporative cooling and product surface radiation in model.	Yes
Pan and Bhowmik, (1991)	FE	Tomato (?)	Only considered internal conduction in the product.	Yes
Mackinnon and Balinski (1992)	FD	Lettuce (?)	Included respiratory heat generation and evaporative cooling in model.	Yes
Lovatt <i>et al.</i> (1993a,b)	ODE	General	A generalised approach which can include extra heat transfer terms as they are required	Yes
Becker <i>et al.</i> (1994)	FD	General (sphere)	Another generalised approach which includes respiratory heat generation	Yes
Camponone <i>et al.</i> (1995)	FD	Apple (sphere)	Included respiratory heat and product evaporation.	Yes

where ¹ = In addition to internal conduction and convective product surface heat transfer.

FD = Finite difference scheme.

FE = Finite element method.

ODE = ODE - based method.

(?) = Product shape not reported or irregular.

2.3.2. Product Respiration

Respiration is the chemical process by which fresh horticultural products convert sugars and O_2 into CO_2 , water and energy. This process is comprised of a series of 50 or more component reactions but is often expressed as a summary equation for the common respiration of glucose (Salisbury and Ross, 1992):



Most of the released energy is eventually converted into heat (approximately 2870 $\text{kJ}\cdot\text{mol}^{-1}$ of glucose). The rate of internal heat generation during the chilling process is generally low in comparison with the rate of heat removal during the cooling of horticultural produce. Hood (1964) showed that the heat due to respiration of a cucumber raised the centre temperature of the commodity by only 0.006°C after 30 minutes of cooling. Gaffney *et al.* (1985b) stated that there are only a few situations during industrial cooling, such as conduction-only cooling, where respiratory heat may slow the chilling process significantly. However, if the product is to be chilled very slowly or to a final temperature close to that of the cooling medium, the heat of respiration becomes important (Cleland, 1990), and therefore must be considered.

Respiration of most horticultural commodities is dependant upon temperature and so is most easily modelled using numerical methods, such as finite difference or finite elements (Cleland, 1990). Empirical equations for respiration as a function of temperature have been developed for a range of fresh horticultural products by Hayakawa and Succar (1982), Gaffney *et al.* (1985b), Wang (1991) and Dadzie (1992). Analytical solutions to the heat transfer problem only exist if the rate of respiration is constant or a simple function of temperature (Carslaw and Jaeger, 1959).

The empirical equation used by Gaffney *et al.* (1985b) is widely used to calculate the heat of respiration as a function of product temperature (Eqn. 2.10). This has a correlation coefficient of greater than 0.99 for the temperature range of $0 - 27^\circ\text{C}$.

$$q = a[\theta_{pr} + 17.8]^b \quad (2.10)$$

where q = heat generation rate ($\text{W}\cdot\text{kg}^{-1}$).
 θ_{pr} = product temperature ($^\circ\text{C}$).
 a, b = product specific constants.

Gaffney *et al.* (1985b) obtained, by regression of data from USDA Handbook 66 (latest edition edited by Hardenburg *et al.* 1986), the following constants for use in Eqn. 2.10.

$$\begin{array}{llll} \text{Apples:} & a = 4.59 \times 10^{-6} & \text{and} & b = 2.66 \\ \text{Peaches:} & a = 1.37 \times 10^{-7} & \text{and} & b = 3.88 \end{array}$$

Becker and Fricke (1996) presented a relationship for calculation of respiratory heat generation. This equation (Eqn. 2.11) requires that the respiration rate be known for the commodity, and is temperature specific. The basis of this relationship is that in the respiratory chemical reaction, for every 1 milligram of carbon dioxide produced, 10.7 joules of heat are generated (Hardenburg *et al.*, 1986).

$$q = \frac{10.7m_{CO_2}}{3600} \quad (2.11)$$

where m_{CO_2} = carbon dioxide production per unit mass of product ($\text{mg.kg}^{-1}.\text{hr}^{-1}$).

Becker and Fricke (1996) used a correlation equivalent to Eqn (2.10), for which the coefficients were fitted to data given by Hardenburg *et al.* (1986), which related a commodity's carbon dioxide production rate to its temperature:

$$m_{CO_2} = o \left(\frac{9}{5} \theta_{pr} + 32 \right)^p \quad (2.12)$$

where o, p = respiratory coefficients (as presented in Table 2.4).
 θ_{pr} = product temperature ($^{\circ}\text{C}$).

Table 2.4
Respiratory coefficients for Eqn. (2.14) for a range of horticultural products (calculated from Hardenburg *et al.*, 1986).

Product	Coefficients	
	o	p
Apple	2.34×10^{-3}	2.25
Apricot	2.69×10^{-4}	3.09
Avocado	2.01×10^{-7}	5.17
Orange	3.27×10^{-5}	3.23
Peach	1.36×10^{-5}	3.65
Pear	3.16×10^{-5}	3.42

Lee *et al.* (1991) proposed a respiration model, based on enzyme kinetics, for predicting respiration rates of fresh produce as a function of O₂ and CO₂ concentration. In this model, the dependence of respiration on O₂ was assumed to follow the Michaelis-Menten relationship:

$$rr_{pr} = \frac{V_m [O_2]}{K_m + [O_2]} \quad (2.13)$$

and the effect of CO₂ on respiration was assumed to follow an uncompetitive inhibition model:

$$rr_{pr} = \frac{V_m [O_2]}{K_m + (1 + [CO_2] / K_i) [O_2]} \quad (2.14)$$

where rr = respiration rate of product (kgmol.kg⁻¹.s⁻¹).
 V_m = maximum respiration rate (kgmol.kg⁻¹.s⁻¹).
 K_m = Michaelis-Menten constant (% O₂).
 K_i = inhibition constant (% CO₂).
 $[O_2]$ = oxygen concentration (%).
 $[CO_2]$ = carbon dioxide concentration (%).

Model predictions were assessed against published data for a variety of commodities and experimentally collected data for cut broccoli and were judged to agree well.

2.3.3. Product Mass Transfer

Weight loss in horticultural products is a combination of carbon loss due to CO₂ evolution in the respiration process and product moisture loss. The carbon loss is generally an insignificant component of total product weight loss, except when moisture loss rates are low (Gaffney *et al.*, 1985b). Moisture loss from a fruit or vegetable is driven by the gradient in partial pressure of water vapour between the boundary layer over the product surface and its immediate environment. Whilst the product surface boundary layer is sometimes assumed to be saturated ($a_w = 1.0$), the partial pressure at the evaporating surface is not equal to the vapour pressure at the product surface temperature if there are dissolved substances present as these lower the water activity at the evaporating surface (Sastry *et al.* 1978).

2.3.3.1. Evaporation Models

The basic form of the evaporation model is:

$$m = K \cdot A (p_s - p_a) \quad (2.15)$$

where:

$$p_s = a_w p_{sat, surf} \quad (2.16)$$

$$p_a = H_R \cdot p_{sat, amb} \quad (2.17)$$

where m = evaporation rate at product surface ($\text{kg}\cdot\text{s}^{-1}$).
 p_s = partial pressure of water vapour in boundary layer at product surface (Pa).
 p_a = partial pressure of water vapour in ambient air (Pa).
 K = mass transfer coefficient ($\text{kg}\cdot\text{s}^{-1}\cdot\text{m}^{-2}\cdot\text{Pa}^{-1}$).
 A = product area (m^2).
 a_w = water activity at the product surface.
 $p_{sat, surf}$ = saturated vapour pressure of water vapour at product surface temperature (Pa).
 H_R = relative humidity (fraction).
 $p_{sat, amb}$ = saturated vapour pressure of water vapour at ambient air temperature (Pa).

Fockens and Meffert (1972) presented a formulation for the evaporation rate at the product surface. This model defined the water activity immediately below the skin rather than at the product surface and then treated the skin as a mass transfer resistance. This allowed the authors to model variable skin permeability:

$$\frac{1}{K_t} = \frac{1}{K_f} + \frac{1}{K_{skin}} \quad (2.18)$$

where K_t = mass transfer coefficient ($\text{kg}\cdot\text{m}^{-2}\cdot\text{s}^{-1}\cdot\text{Pa}^{-1}$).
 K_f = fluid film mass transfer coefficient ($\text{kg}\cdot\text{m}^{-2}\cdot\text{s}^{-1}\cdot\text{Pa}^{-1}$).
 K_{skin} = skin mass transfer coefficient ($\text{kg}\cdot\text{m}^{-2}\cdot\text{s}^{-1}\cdot\text{Pa}^{-1}$).

2.3.3.2. Models for Product Mass Transfer including Evaporation

Sastry and Buffington (1982; 1983) developed a mathematical model for predicting the steady-state evaporation rate of stored horticultural commodities of approximately spherical shape. Heat transfer was assumed to occur only in a radial direction and arose from effects related to the latent heat of vapourisation of water and respiratory heat generation. An expression was derived for the surface temperature of the product using an energy balance for one-dimensional airflow through a tubular reactor. This model predicted evaporation rates in close agreement with experimentally collected data for tomatoes.

Gaffney *et al.* (1985b) considered the influence of carbon loss as part of the total weight loss; the effects of air film resistance on the overall mass transfer coefficient; respiratory heat generation, evaporative cooling, convective and radiative heat flow effects on the evaporating surface temperature; and, the influence of dissolved substances on the lowering of water activity. Using a finite difference model developed by Chau *et al.* (1984), testing was conducted against experimental data for apples, peaches and brussel sprouts as these commodities represented products with low, medium and high susceptibility to weight loss. Model predictions agreed well with experimental weight loss data.

Van Beek (1985) outlined a method for calculating the level of protection that packaging provides against moisture loss of commodities (Eqn. 2.19). A protection factor of 1 indicates that the packaging does not influence moisture loss.

$$P_f = \frac{w_{unpkd}}{w_{pkd}} \quad (2.19)$$

where P_f = protection factor (dimensionless).
 w_{unpkd} = moisture loss rate of the unpacked product ($\text{kg}\cdot\text{s}^{-1}$).
 w_{pkd} = moisture loss rate of the packed product ($\text{kg}\cdot\text{s}^{-1}$).

Romero and Chau (1987) presented a finite difference model, which simulated evaporation from fruits and vegetables in bulk storage. This model accounted for respiratory heat generation and evaporative cooling. This model was validated using oranges packaged in a wooden box and stored at 7.5 - 8.5°C and 85% R.H.

Chau *et al.* (1988) presented a steady state, mathematical model for describing the moisture loss of fruits and vegetables with shapes of spheres, cylinders and slabs. This model considered the internal heat of respiration, the convective and radiative heat transfer at the surface, surface cooling due to evaporation, and the effects of reduced water activity. Validation against experimental data was not presented.

2.4. MODELLING OF AIRSPACE WITHIN HORTICULTURAL PACKAGES

2.4.1. Modelling Airflow Pathways

Modelling of the interaction between fruits and vegetables and the air in a refrigerated airspace can be approached in two ways:

2.4.1.1. Zoned Models.

As stated earlier, modelling of the air within a space, be it a package or a coolstore, using a single zoned approach assumes that the air is perfectly mixed. For this zone, temperature (or energy content with temperature derived algebraically) and humidity are calculated using an ordinary differential equation (ODE) (Amos, 1995).

Multi-zoned models split the airspace into a series of zones that are commonly linked either in a plug-flow orientation or with a defined airflow pathway (Amos, 1995). This approach also assumes that the zones are perfectly mixed.

i) Plug-flow Zoned Models

Becker *et al.* (1994) utilised a model assuming plug flow between zones in a porous medium to estimate the latent and sensible heat loads and moisture loss in bulk storage of fruits and vegetables. The model was tested against experimental data, obtained from literature, for a range of fruits and vegetables. The results showed good agreement between the experimental data and the numerical results.

Marchant *et al.* (1994) derived a model of heat and mass transfer in a bed of potatoes. The airflow model was developed to fit published empirical data, based on the observed behaviour of air in storage rooms, especially the results of Wang and Touber (1988). The airflow was treated as a one-dimensional plug-flow system between zones. The authors considered that the model gave good agreement with experimental data collected from 3 locations in a potato store.

ii) Zoned Models with Cross-mixing between Zones

Marshall and James (1975) modelled a quick freezing plant for vegetables by treating the air space as eight perfectly mixed zones, with an ordinary differential equation (ODE) representing the energy content of air in each zone. The extent of cross-mixing was measured. This model was system-specific with predictions fitting experimental data well.

Amos (1995) developed two multi-zoned models of refrigerated airspaces. Firstly, an apple carton-cooling model was developed to predict apple temperature and weight loss with position and time within the carton. This model required the user to define the airflow pathway as input data. Cross-mixing was estimated using empirical relationships presented by Holman (1990). The second, a multi-zoned heat and mass transfer model, was developed for predicting conditions in large horticultural

coolstores. This model took into account heat and water vapour transfer pathways, which interacted with the zone air, and the operational characteristics of the system. These zones were also linked by a user defined airflow path, based on knowledge of the airflow characteristics of the coolstore. Cross-mixing was again estimated using an empirical relationship based on measured data for an industrial coolstore. This model was experimentally validated in a large commercial apple coolstorage facility in New Zealand with model predictions reported to have satisfactory agreement with measured data taking into account data uncertainties.

2.4.1.2. Fully Distributed (or Fluid Dynamics) Models

The physical behaviour of any fluid is governed by three fundamental principles: Conservation of mass, conservation of energy and conservation of momentum. These fundamental principles can be expressed in terms of governing partial differential equations (PDE's). Computational fluid dynamics (CFD) is the science of determining a numerical solution to the governing equations of fluid flow for a system with both time and space discretisation and subject to appropriate boundary conditions. This mathematical tool was primarily developed for use in the nuclear, aerospace, automobile and defence industries (Gigiel *et al.*, 1994) but can now be applied to almost any process utilising the flow of fluids.

Such models predict airflow based on the Reynolds time-averaging Navier-Stokes equations for momentum conservation, in which the concepts of a turbulent viscosity and turbulent diffusivity are employed to give turbulent stress and fluxes (Wang and Janssens, 1994). These models can be solved using a complete finite difference, control volume or finite element discretisation of the equations in the airspace.

Chan and Scott (1988) extensively reviewed mathematical models for predicting air movement in rooms. Many of these utilised computational fluid dynamics. Fletcher (1991) reviewed computational techniques.

Van der Ree *et al.* (1974) developed a finite element computer program for predicting the transient behaviour of air in a refrigerated container. Heat transmission was considered to be non-steady-state and spatially distributed. The airflow model assumed flow was exclusively in one direction, and that the spaces between boxes were of the same width. Water vapour transport was neglected. Predictions indicated that the rate of air circulation and the product-stacking pattern significantly affected the temperature distribution, although no testing of this model against experimental findings was reported.

Nielson *et al.* (1978) calculated values of the velocity characteristics of a room with high and low level slot arrangements. The two-dimensional TEACH computer code, developed by Patankar and Spalding (1972), was used to estimate velocity values which were compared to measurements obtained using Laser-doppler anemometry in a model room. These researchers concluded that it was possible to represent the velocity characteristics of a ventilated room using the two-dimensional calculation procedure.

Gosman *et al.* (1980) used a three-dimensional version of the TEACH fluid dynamics code to calculate the isothermal flow field in a rectangular enclosure having with a single square inlet. Calculated values were reported to be in good agreement with experimental measurements.

Wang and Toubert (1988) developed three models of refrigeration rooms. The first predicted the mass flow of air within the room using the Navier-Stokes equation in isolation from the heat and mass transfer models. This method assumed that the airflow pattern was not time-variable due to domination by forced convection, and thus free convection could be neglected. The second stage (Wang and Toubert, 1987) assumed the flow distribution from the first stage was fixed and then predicted energy and mass flows within a room and compared these to measured temperatures. The third model used a resistance network analogy to simplify the Navier-Stokes equation, effectively replacing the first model. The models were used to model temperature and humidity distribution within a room. Model predictions were found to agree well with measured data for a small coolstore loaded with 24 wooden boxes containing electrical heating mats.

Van Gerwen and Van Oort (1989, 1990), Van Gerwen *et al.* (1991), Wang and Toubert (1990) and Wang (1991) all used computational fluid dynamics models in which the momentum equation was decoupled from the heat and mass transport equations. This enabled air velocity patterns to be predicted, which were then assumed to be unaffected by changing heat transfer conditions. Temperature and humidity patterns within the rooms were then predicted using the air velocities calculated in the first stage as input data. Laboratory-scale experiments were conducted by Wang and Toubert (1990) to validate their model, with good agreement between measured and predicted data being reported, although the computational time for predictions of airflow patterns was approximately 100 hours on a SUN workstation (Series 3/60). Further computational time was required for prediction of temperature and humidity fields.

Talbot *et al.* (1990) used a finite element solution to determine 3-D pressure and velocity distributions of airflow through an orange carton using porous media flow analysis. The predicted airflow was then incorporated into an existing heat transfer model to provide a predicted temperature response. These calculations were compared with data from 12 tests of oranges packed in an experimental carton. The porous media flow analysis was found to provide adequate information if variable porosity within the carton was considered.

Wang and Janssens (1994) described a two-stage mathematical simulation model for the thermodynamic behaviour of a pre-cooling process for cut flowers. Firstly, using the computational fluid dynamics package *PHOENICS*[®], airflow was modelled by treating the region as flow through a homogeneous porous medium. The flow was assumed to be turbulent and governed by the rate of turbulent kinetic energy dissipation (k - ϵ) model. This model was based on the Reynolds time-averaged Navier-Stokes equations. The resulting velocity field was then used as an input to solve the heat and mass equations for the product and cooling medium. Validation of this model against experimental data collected for roses showed good agreement with model predictions.

Baleo *et al.* (1995) also used the k - ϵ model and the Reynolds time-averaged Navier-Stokes equations to predict a flow pattern for air in a refrigerated display case. These researchers used the CFD package *FLUENT*[®], which utilises a finite volume method and the *SIMPLE* algorithm developed by Patankar (1980), to solve the equations. The predictions were compared to anemometry measurements taken from a display cabinet. Differences in results were reported to be due to k - ϵ model overestimation of air entrainment at the edge of the air delivery jet, which lead to overestimation of the velocity magnitude.

2.4.1.3. Airflow Visualisation

Airflow patterns in a confined space can be examined in a number of ways: visualisation of flow using smoke (Mueller, 1983; Amos *et al.*, 1993b); scale modelling (Lovatt *et al.*, 1993c); or laser anemometry (Baleo *et al.*, 1995).

Mueller (1983) described the use of smoke to visualise airflow patterns. The word ‘smoke’ is used in a very broad sense in flow visualisation and includes a variety of smoke-like materials such as vapours, fumes and mists. The smoke must be generated in a safe manner and possess the necessary light-scattering qualities so that it can be

photographed. The particles must be small enough so that they follow the flow pattern being studied and be large enough to scatter a sufficient amount of light. Mueller (1983) also introduced the use of less popular agents for airflow visualisation, such as helium bubbles.

Amos *et al.* (1993b) carried out a smoke test in a large horticultural coolstore to ascertain airflow patterns. The test was carried out in a closed store with the fans operating on low speed, with smoke being released from a number of positions, and showed significant cross-mixing between three major airflow pathways.

Lovatt *et al.* (1993c) used a scale model approach, using water as the flow medium, to emulate airflows in beef chillers. The model was designed to achieve fluid dynamic similarity with the full-scale system. This required the Reynolds numbers (Re) in both the model and full-scale regimes to be similar. The principal flow patterns of interest to the authors were two-dimensional, so a slice across a chiller was used in the model. Characterisation of forced-convection flow patterns was carried out using small hydrogen bubbles created by electrolysis.

Baleo *et al.* (1995) visualised the trajectories of injected particles in a refrigerated display case air curtain using a 5W LASER plane lighting system. Flow velocity profile measurements were also made using hot wire anemometry. These measurements along with the visual pattern, were used to validate the flow pattern predicted by *FLUENT*[®], a computational fluid dynamics code. The simulation gave good predictions of the air jet flow patterns.

2.4.2. Modelling of Airspace Relative Humidity

Humidity affects many aspects of postharvest horticulture including product moisture loss, growth of microorganisms, texture, colour and palatability of fruits and vegetables (Gaffney, 1978). Humidity also affects factors not directly related to the products themselves, such as condensation of moisture on, and adsorption into, packaging, which can affect package strength and downgrade the package appearance (Marcondes, 1992b; 1996).

Airspace relative humidity is usually calculated from temperature and water concentration (mass) using psychrometric relationships. These relationships are developed from a set of basic equations that include Dalton's law of partial pressures and the perfect gas law. Empirical formulae have been developed from

experimentation (Wexler and Greenspan, 1971; Wilhelm, 1976; ASHRAE, 1993) to approximate the fundamental equations.

Cleland *et al.* (1982) and Cleland (1983) used a single zoned modelling approach for applications in the meat industry with ODEs for temperature and water mass. A weakness of the water mass model was that it allowed relative humidity to exceed 100%. Lovatt (1992) used a similar model, but assumed condensation to occur if humidity exceeded saturation.

Amos (1995) modelled water concentration directly for horticultural packaging systems. As the configurations studied were largely ventilated and water vapour transport across packaging materials occurred readily, inclusion of a model for condensation was not considered necessary.

2.5. MODELLING OF HORTICULTURAL PACKAGING MATERIALS

2.5.1. Packaging Material Thermal Capacity

In some models it has been assumed that packaging materials have negligible thermal capacity, i.e. that the heat extracted due to temperature change in the packaging is negligible compared to that extracted from the product (Cleland, 1990). It is then assumed that the prime action of the packaging is to decrease the surface heat transfer coefficient between product and air by adding thermal resistance. An effective heat transfer coefficient might then be used to take into account the effect of packaging on heat transfer.

When calculating the cooling load for packaging materials in a model for power consumption and weight loss in a cold store, Pala and Devres (1988) assumed that the packaging cooled to room temperature within a day. Devres and Bishop (1992) used an updated version of the same model and compared model predictions with experimentally collected data.

Adre and Hellickson (1989) modelled transient refrigeration load throughout a storage season in apple and pear coolstores. Fruit were stored in wooden bins and the heat load due to the bin material was calculated.

Jamieson *et al.* (1993) modelled cartons of cheese packaged in pallet loads during cooling in coolstores. The pallet boundary was assumed to be the outermost cheese

surface and the packaging outside this surface affected only the heat transfer coefficient. All packaging, air voids and cheese inside the boundary were assumed to affect only the mean product/package thermal properties. A series model (Miles *et al.*, 1983) was used to estimate effective thermal conductivity, whilst the effective heat transfer coefficient was based on the combined effect of convection from the packaging surface to air, radiation from this surface to surrounding objects (acting in parallel) and conduction through packaging layers and trapped air. Model predictions agreed satisfactorily with measured data.

2.5.2. Moisture Accumulation in Packaging Materials

Packaging can readily adsorb or desorb moisture when introduced into a storage environment, depending on the initial moisture content of the packaging material and the relative humidity of the storage atmosphere. Storage atmospheres for horticultural products are generally maintained at high relative humidity to decrease product weight loss. However, by introducing paper-based packaging materials to an environment with high relative humidity, strength properties will be reduced due to moisture uptake (Wink, 1961; Marcondes, 1992a,b; Amos *et al.*, 1993c). Fundamental studies and modelling of the accumulation of moisture in packaging materials have been undertaken by a number of researchers.

Wink (1961) and Liebenspacher and Weisser (1989) presented models for determining moisture contents of paper-based packaging materials in response to air relative humidity. The later measured the spin-spin relaxation time with pulsed nuclear magnetic resonance (NMR) spectroscopy to determine the mobility of water molecules in packaging materials. By freezing the paper samples and interpreting their NMR-signal decay, it was found that most of the moisture absorbed by packaging exists in a mobile state.

Marcondes (1992a) studied the effects of moisture content in corrugated fibreboard on its shock absorbing properties. The relative humidity of the air was found to have a significant effect on the shock absorbing properties of corrugated fibreboard. The author noted that the common conception that high relative humidity gives poor carton performance only applies to compression strength, as cushioning properties are enhanced at high relative humidities.

Eagleton and Marcondes (1994) applied two common moisture-sorption isotherm models for food materials to fibreboard packaging for transport of apples. The

Guggenheim-Anderson-de Boer (GAB) model was compared with the Brunauer-Emmett-Teller (BET) isotherm model. In the range of temperatures (1 - 40°C) and humidities (43 - 96%) studied, the GAB model was found to fit experimental data adequately.

Amos (1995) stated that un-waxed cardboard packaging continuously absorbs or desorbs water to reach an equilibrium moisture content (ψ_e), depending only on the surrounding air relative humidity (R.H.). The ψ_e was determined using the GAB moisture isotherm model (Eqn. 2.22). When modelling the water uptake process, this researcher assumed a first order model. Thus:

$$emc = \frac{H_R}{\chi_1(H_R)^2 + \chi_2 H_R + \chi_3} \quad (2.22)$$

$$\frac{dmc}{dt} = k_{mc}(emc - mc) \quad (2.23)$$

where emc = equilibrium moisture content ($\text{kg}_{\text{H}_2\text{O}} \cdot \text{kg}^{-1}$).
 mc = moisture content ($\text{kg}_{\text{H}_2\text{O}} \cdot \text{kg}^{-1}$).
 H_R = relative humidity (fraction).
 χ_1, χ_2, χ_3 = G.A.B. coefficients for the packaging material.
 k_{mc} = rate constant for water adsorption or desorption (s^{-1}).

Amos (1995) also assumed the rate constants for adsorption and desorption to be the same and that emc did not change over small temperature ranges. The author also ignored any retardation or lag effect on emc , and added the associated latent heat of evaporation/condensation into the energy balance equation for the packaging.

Foss *et al.* (1997) studied the dynamics of moisture accumulation in paper, as well as the diffusional paths and location of the sorbed moisture. These authors proposed that the transient adsorption / desorption of moisture by a paper sheet occurs by a different process and at a significantly slower rate than the steady-state diffusion (or transport) through the sheet.

2.5.3. Moisture Transport through Packaging Materials

In addition to the accumulation of moisture by packaging materials, moisture transport across a packaging material boundary bordered by different relative humidity states is another important moisture transport pathway. The resistance of water vapour

movement is largely a function of the porosity of the material, as the transport is commonly believed to occur in the pore-space of the material.

Contreras-Medellin (1980) studied the effect of both relative humidity and temperature on the permeance of ten food-packaging films. No clear-cut relationship was shown between permeance, relative humidity and temperature. It was shown however, that the Arrhenius relationship explained the temperature dependence of permeance at each relative humidity. Labuza (1982) stated that temperature and relative humidity on either side of a film can have a significant effect on permeability due to water dissolving in the film, which can plastize it, cause it to swell, and influence the temperature at which the polymer changes from an amorphous to a crystalline state.

Samaniego-Esquerria and Robertson (1991) developed a mathematical model describing water vapour permeance of laminates or films as a function of external relative humidity and temperature. The relationship between water vapour permeability and temperature followed the Arrhenius model for the three films (Low Density Polyethylene (LDPE), Polyethylene terephthalate (PET) and a laminate of both films) tested.

Nilsson *et al.* (1993) studied the diffusion of water vapour through both pulp and paper experimentally. Data presented indicated that the effective diffusivity of a solid paper product was correlated to its density (the data did not include corrugated cardboard samples). Nilsson *et al.* (1993) also showed that the effective diffusivity was relatively constant over the relative humidity range examined (10 - 60%).

In the work of Foss *et al.* (1997), the movement of water vapour through paper sheets was characterised to be of the order of $10^{-6} \text{ m}^2 \cdot \text{s}^{-1}$ whilst diffusivity of water through the fibre wall was of the order of $10^{-12} \text{ m}^2 \cdot \text{s}^{-1}$.

2.5.4. Moisture Transport through Packaging Ventilation

Renault *et al.* (1994a) described the transport of gases (including water vapour) through micro-perforations using the Stephan-Maxwell laws. These laws assume that gas transport is due simultaneously to diffusion and convection. In this work, the boundaries of each micro-perforation were assumed to be defined by the inside and outside boundaries of the film, leading to neglect of the resistance to diffusion of gases in the surrounding gas volume. Renault *et al.* (1994b) noted that this assumption led to overestimation of gas transport rates measured experimentally.

Merts (1996) considered the diffusion of gases through perforations in MAP packaging configurations. This author assumed that the gas immediately outside the perforation was uniform and perfectly mixed. An empirical factor was included in the model to correct for the absence of boundary layer effects in the model.

2.6. MODEL VALIDATION

Visual inspection of graphical data has been applied widely. For example, Marshall and James (1975) used graphical comparisons of predicted and measured data to verify their model of refrigeration system behaviour. These comparisons showed that the model did not accurately predict the product freezing process, but the heat load was accurate enough for the purpose of investigating capacity control.

Cleland *et al.* (1982) described validation of a mathematical model for a refrigerated fishing vessel. In this case, graphical shapes and trends from predicted and actual data were compared to assess the level of agreement. Cleland (1985) also used graphical comparison to deduce the level of agreement between predicted and experimentally collected data in a New Zealand meat processing plant, which had a total refrigeration capacity of 2.5 MW. Predicted air temperatures followed the same trends as measured data with differences being attributed more to uncertainties in the data than to deficiencies in the formulation of the mathematical model.

Use of statistical measures of model accuracy is relatively uncommon in the validation of mathematical models. Wells (1992) developed and tested mathematical models of a greenhouse environment and growth of a cucumber crop in that environment. This researcher used graphical trends as well as calculations of daily root mean square (RMS) error, daily mean error (ME) and daily coefficient of correlation to assess the accuracy of predicted air temperature conditions against measured conditions.

Clayton (1995) developed a mathematical model of temperature and weight loss from onion bulbs in a transport container. This researcher presented graphical comparisons of predicted and measured data, as well as calculations of % ME, % RMS error and *r* statistic.

2.7. CONCLUDING REMARKS

This chapter has outlined the ‘state of the art’ pertaining to mathematical modelling of heat and mass transfer in horticultural packaging systems. The following chapter summarises the collective concepts drawn from currently published literature and sets the objectives of the research programme.

CHAPTER 3

RESEARCH OBJECTIVES

3.1. INTRODUCTION

The goal of this research project was to develop a computer-based dynamic simulation modelling system for predicting cooling rates during pre-cooling and mass loss during long-term storage for a range of packaged horticultural products and packaging configurations. This system was intended to improve the design of horticultural packaging systems. In order to achieve this, as well as advance intellectual understanding, aggregation of mathematical model descriptions for individual components of horticultural packaging systems were required.

A number of models of individual products, without incorporation of the packaging system as a limiting element, already existed. Airflow characterisation had generally been modelled by previous researchers in one of two ways. Firstly, there were models using either a user defined airflow pathway or an assumed plug-flow orientation. Such pathways were generally defined using experimental data and thus the models tended to be system specific. Secondly, the flow pattern could be characterised using computational fluid dynamics packages. These packages require large amounts of input data for prediction of accurate flow patterns, and high levels of computational power for rapid calculations. Mathematical descriptors of packaging materials also existed, but required incorporation into an overall description of the greater physical system to accurately predict all the system components interactions.

3.2. OBJECTIVES

Taking into account the overall goal and the 'state of the art' revealed by the literature review, the objectives of this work were to:

- (1) Develop a simple, generalised and flexible mathematical modelling framework for implementation in both pre-cooling and bulk storage processes.
- (2) Assess the shortcomings of existing heat transfer models and, if necessary, refine and generalise these models so that accurate predictions can be made for a range of packaging systems.
- (3) Assess the shortcomings of existing mass transfer models for water vapour movement and, if necessary, refine and generalise these models so that accurate predictions can be made for a range of packaging systems.
- (4) Assess the shortcomings of existing airflow representation methodologies and, if necessary, implement more accurate or user-friendlier methods for characterisation of packaging geometries.
- (5) Assess the quality of previously collected data and, if necessary, measure important parameters (during both pre-cooling and bulk storage) within horticultural packages with different designs and constructions to provide high quality data for model testing.
- (6) Implement these models into a prototype, generalised computer simulation system that will predict the dynamic and/or steady state behaviour of pre-cooling and mass loss in storage given a small number of user-defined initial conditions.
- (7) Test the overall modelling system using examples of existing and possible new package designs.

In the longer term and with further refinement, the proposed modelling system will enable a wide variety of proposed package designs to be quickly and simply assessed for their impact on both fruit quality and the logistics of fruit cooling and storage systems. This approach will speed up the package development cycle significantly.

The concepts underpinning a suitable computer software package, incorporating both the heat and mass transfer processes (pre-cooling and bulk storage respectively) are illustrated in Figure 3.1. This block diagram illustrates how the results of each stage in the research were integrated to meet the technology transfer needs of the project sponsor.

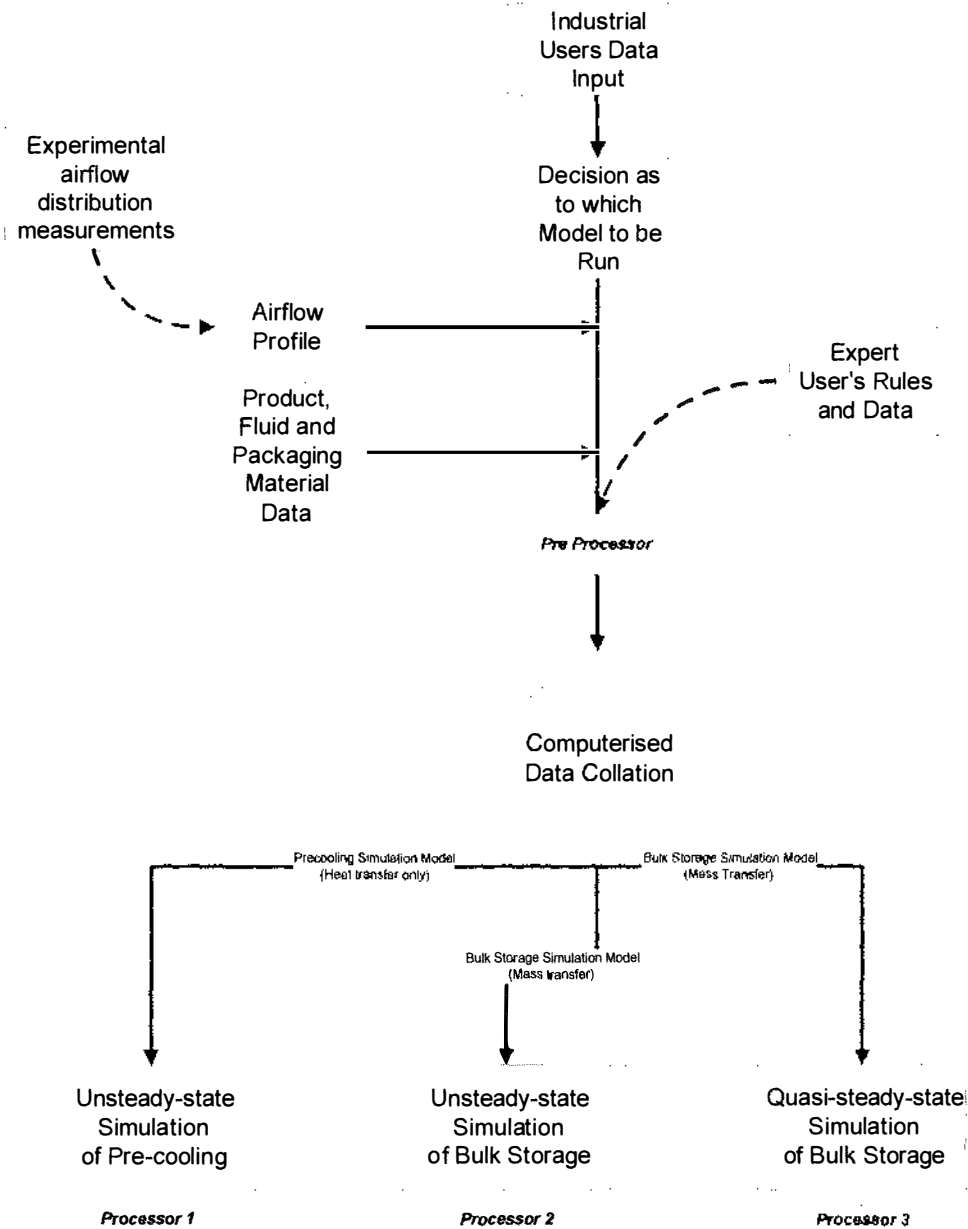


Figure 3.1. Proposed technology transfer process for model application in the design of horticultural packaging systems.

3.3. CUSTOMISATION TO THE NEEDS OF THE PROJECT SPONSOR

A goal for the project sponsor was to develop prototype simulation software for use by industrial practitioners. It was envisaged that this software would require only those product, fluid, package and packaging material property data that are likely to be available to industry representatives. The required simplicity was achieved by development of a quasi-steady-state model in addition to an unsteady-state model. The latter was more flexible as a research tool, and better suited for developing fundamental understanding of rate controlling processes.

CHAPTER 4

SIMULATION MODEL DEVELOPMENT STRATEGY

4.1. INTRODUCTION

This chapter describes the development of the overall strategy of the modelling system, which make up both the pre-cooling (heat transfer), the steady-state bulk-storage (mass transfer) and the dynamic bulk-storage (mass transfer) simulation models. It describes the basis of the generalised modelling methodology used to construct simulation models for prediction of product cooling rates and product mass loss, and states major simplifying assumptions.

The purpose of the pre-cooling simulation model is to predict product and fluid temperatures with respect to both position within the entity such as a carton or bin and time. The bulk storage models will predict product mass loss with respect to time in storage and, in the case of the unsteady-state model, position within an entity. To serve as generalised models, all must have the capability to adjust to changes in packaging configuration, fluid properties and flow directions, initial conditions, and stacking arrangements.

4.2. PHYSICAL MODELS OF PACKAGING SYSTEMS

An entire physical model can be visualised as an 'entity' of which the outer boundary separates the entity from some exterior conditions, e.g. this may be an outer packaging wall. The entity can be subdivided by the use of interleaving packaging and is cooled by the flow of a cooling medium. The entity may also contain heat and water sources, which may or may not be items of product such as fruit.

When transforming the physical models into a mathematical model system, the first decision is to define the model boundary, and the second is to define the sub-zoning

within. These decisions need to be taken with an abstract rather than specific view of each system so that the model retains generality. A number of examples of systems encompassed by this model are illustrated here. These examples represent some of the packaging systems currently used, or in development, in the major horticultural industries of New Zealand. The basic structure of a suitable generalised model must be able to accommodate these and any other reasonable configurations without any change to the model (although data must change to define specific systems).

Example 1 – A corrugated cardboard apple carton (Figure 4.1)

The total system is an individual corrugated cardboard carton of apples. The apples are packed onto moulded pulp interleaving packaging called ‘Friday’ trays with four or five layers of ‘Friday’ trays in each carton. These fruit are initially at about 25°C and are placed in a forced draft air pre-cooling system with air at 0°C flowing onto the front face of the tray, typically at 1.5 m.s⁻¹.



Figure 4.1. Physical model of the system described in Example 1.

For this example, a number of heat and mass transfer pathways exist as shown in Fig. 4.2. These include;

- a) Energy and mass flow due to flow of cooling medium through the package.
- b) Heat conduction within product (apple).
- c) Heat convection from the product to the cooling medium (air).
- d) Evaporation of water vapour from the product to the cooling medium.
- e) Radiation from the product to other surfaces.
- f) Heat conduction between the product and layer packaging (‘Friday’ tray).

- g) Water vapour transport between the product and layer packaging ('Friday' tray).
- h) Water vapour transport through packaging materials by diffusion, capillary action or both.
- i) Heat conduction within packaging materials.
- j) Heat convection between the cooling medium and packaging materials.
- k) Absorption or desorption of water vapour by the packaging materials.

To enable an accurate description of the total system to be developed, sub-zoning is required. In this example, a logical zoning in the x (vertical) dimension is the division between layers. In the y (length) dimension, the subdivision could be each item of product along the length and in the z (width) direction, the rows in the interleaving packaging might make a logical division. A major task is then to define the conditions at each sub-zone boundary.

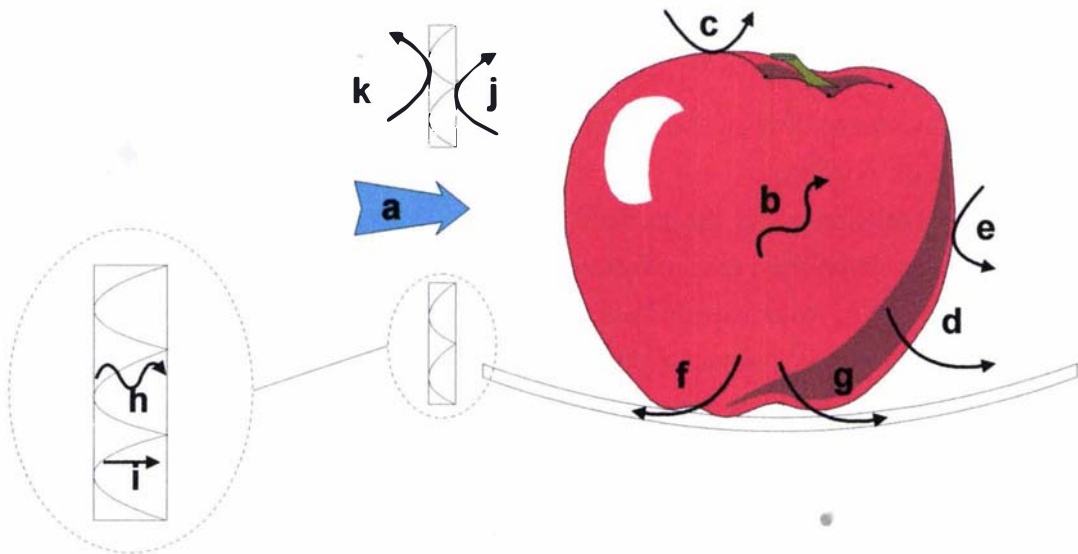


Figure 4.2. Conceptualisation of the main pathways existing for heat and mass transfer in Example 1 (a corrugated apple package).

Example 2 – A corrugated cardboard apple carton, with a polyethylene liner (Figure 4.3)

The total system is also an individual corrugated cardboard carton of apples, but the fruit within the carton are fully enclosed in a 45 μm low-density polyethylene film liner (polyliner) which prevents the flow of the cooling medium through the product. The apples are packed in 4 or 5 layers, which are subdivided by moulded pulp interleaving packaging. The apples are initially at about 25°C and are placed in a forced draft air pre-cooling system with air at about 0°C flowing onto the front face of the carton, typically at 1.5 $\text{m}\cdot\text{s}^{-1}$.

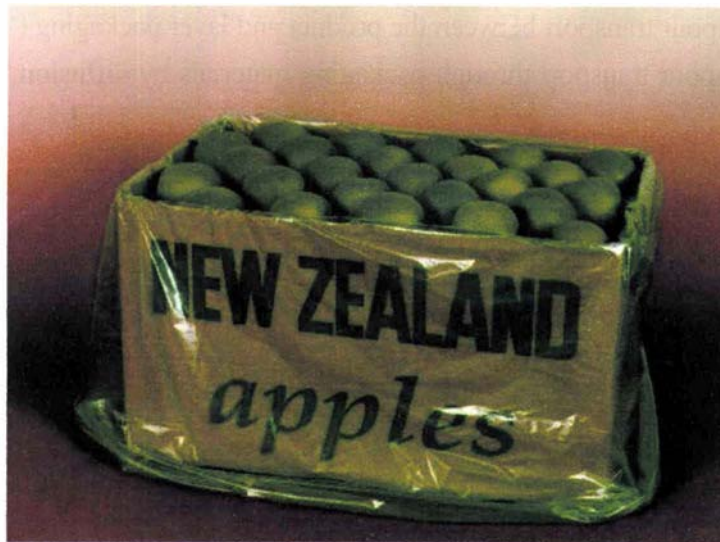


Figure 4.3. Physical model of the system described in Example 2 (after Merts, 1996).

For this example, a number of heat and mass transfer pathways may exist as shown in Fig. 4.4. These include;

- a) Heat and mass flow of the external-cooling medium through the package, but outside the polyliner.
- b) Heat conduction within the product (apple).
- c) Heat convection from the product to the cooling medium (air).
- d) Evaporation of water vapour from the product to the cooling medium.
- e) Radiation from the product to other surfaces.
- f) Heat conduction between the product and layer packaging ('Friday' tray).
- g) Water vapour transport between the product and layer packaging ('Friday' tray).
- h) Water vapour transport through packaging materials by diffusion, capillary action or both.
- i) Heat conduction within packaging materials.
- j) Heat convection between the cooling medium and packaging materials.
- k) Absorption or desorption of water vapour by the packaging materials.
- l) Heat conduction between the product and the polyliner.
- m) Convection between the internal cooling medium and the polyliner.
- n) Convection between the external cooling medium and the polyliner.

Several approaches could be made to sub-zoning of the system. The first approach involves subdivision as implemented in Example 1. An alternative approach is to treat the entire sub-system within the polyliner as one zone. The sub-system outside the polyliner but within the carton subdivided could then be subdivided into more than one zone.

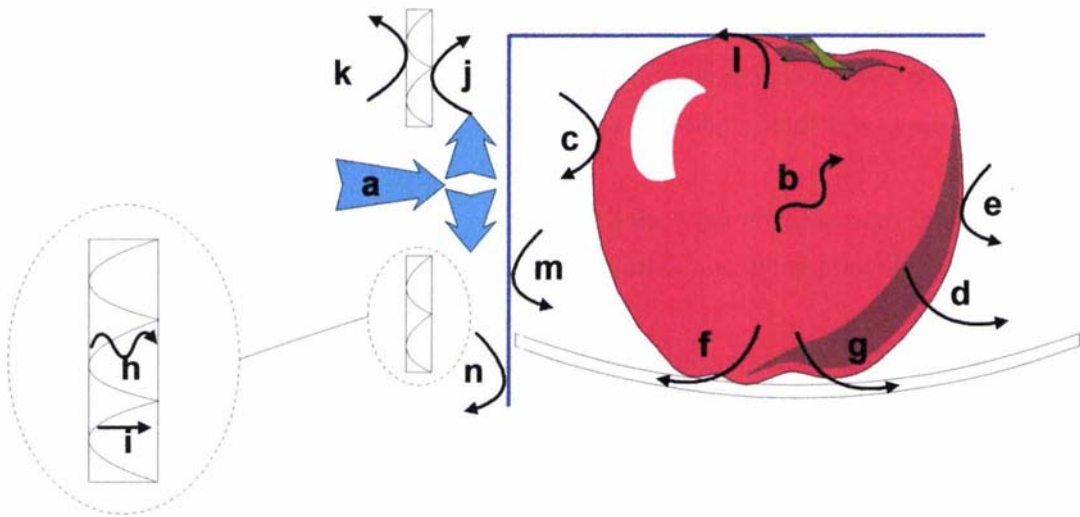


Figure 4.4. Conceptualisation of the main pathways existing for heat and mass transfer in Example 2 (an apple carton with the product enclosed in a polyliner).

Example 3 – A corrugated cardboard apple tray (Figure 4.5)

The total system is a pallet of apple retail display trays (RDT's). These two layer corrugated cardboard trays are stacked 13 layers high with 5 trays per pallet layer. The ventilation slots in the trays align with others in the same layer only. The pallet is stacked two high in a coolstore with the air at 2°C and velocity onto one face of the pallet typically at $0.25 \text{ m}\cdot\text{s}^{-1}$.



Figure 4.5. Physical model of the trays in the system described in Example 3.

For this example, a number of heat and mass transfer pathways exist between and within the cartons. These include:

- All those that occur in Example 1 and (as Figure 4.6 shows),
 - l) Mass flow and thus embodied energy flow in the cooling medium between the trays.
 - m) Heat and mass transfer between the trays.
 - n) Heat conduction between the trays on the bottom layer and the wooden pallet.

The sub-zoning of this example might be tray-based. In the x dimension, each of the 13 pallet layers would be an appropriate sub-division, while individual trays within layers in the y and z dimensions would be logical. Differences in conditions between different positions in a tray may then be difficult to model. A more complex zoning configuration could include within tray variability (as in examples 1 and 2) as well as between tray variability.

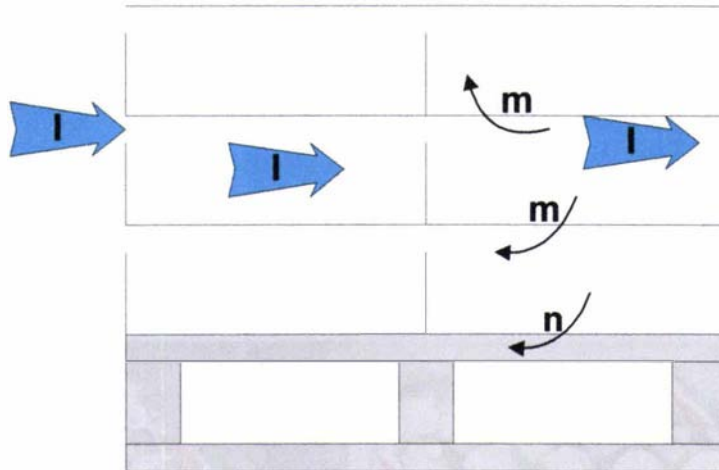


Figure 4.6. Conceptualisation of the main pathways existing for heat and mass transfer in a pallet.

Example 4 – A wooden or plastic bin (Figure 4.7)

In this case, the total system is a wooden or plastic bin, containing 500kg of produce at 25°C. The fruit are bulk-packed in this container and submerged in 5°C water flowing at 1 m.s⁻¹ through the bin sides.

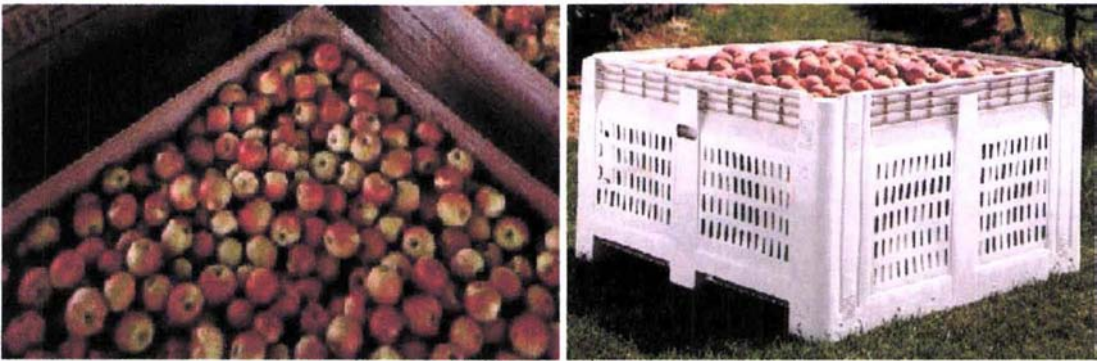


Figure 4.7. Physical model of the systems described in Examples 4 and 5.

For this example, a number of heat and mass transfer pathways may exist (Figure 4.8). These include:

- a) Energy and mass flow due to flow of the cooling medium through the container.
- b) Heat conduction within items of product.
- c) Heat conduction between items of product.
- d) Convection from the product to the cooling medium (water).
- e) Heat conduction between the product and the container (wooden bin).
- f) Heat conduction within the container material.
- g) Convection between cooling medium and the container material.

The subdivision of the total system in this example might best be accomplished by arbitrarily dividing the total length of each of the x, y, and z dimensions equally into a grid of, for example, $5 \times 5 \times 5$.

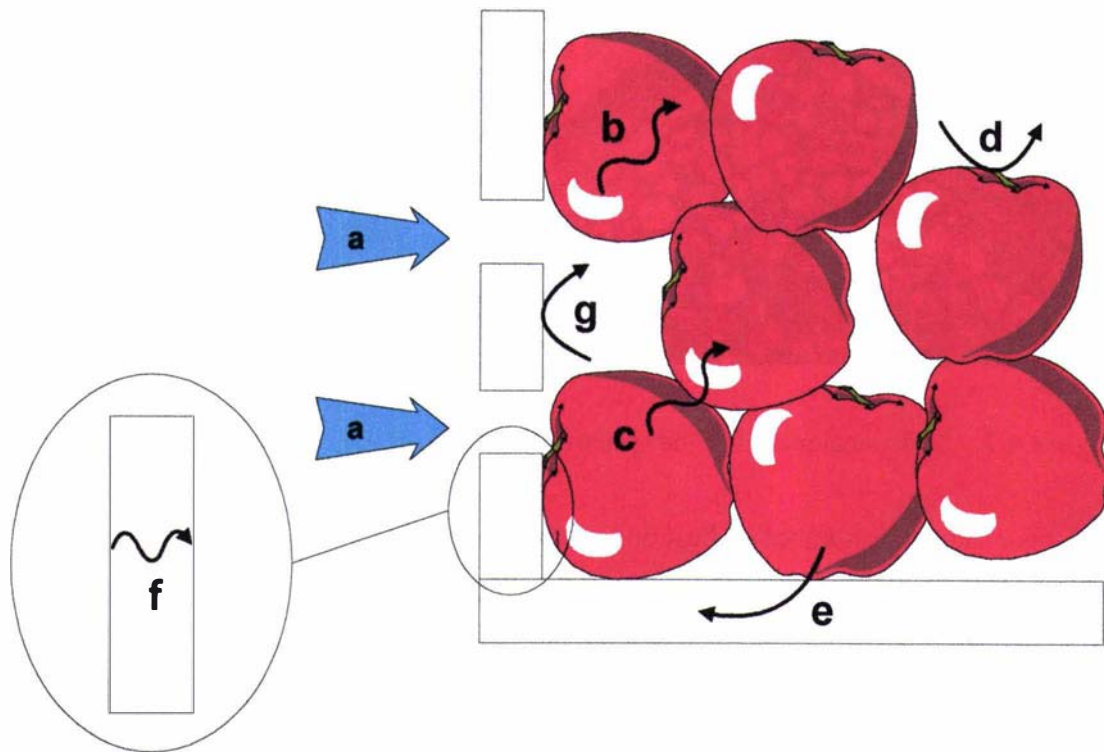


Figure 4.8. Conceptualisation of the main pathways existing for heat and mass transfer in a bulk storage unit.

Example 5 – A wooden or plastic bin (also Figure 4.7).

In this case, the total system is again a 500kg capacity bin, constructed of either plastic or wood, with produce at 0.5°C in a bulk-storage facility. The fruit have been bulk-packed in this container and pre-cooled prior to storage, such that the heat transfer process is nominally steady state. The process examined in this scenario is therefore mass transfer-based.

For this example, a number of mass transfer pathways may exist (Figure 4.9). These include:

- a) Mass flow due to flow of the cooling medium through the container.
- b) Water movement within items of product.
- c) Evaporation of water vapour from the product to the fluid medium.
- d) Water vapour movement from the product to the container.
- e) Water vapour transport through the container material.
- f) Adsorption or desorption from the container material to the fluid medium.

Again, as in Example 4, the subdivision of the total system might best be accomplished with a grid of, for example, 5×5×5.

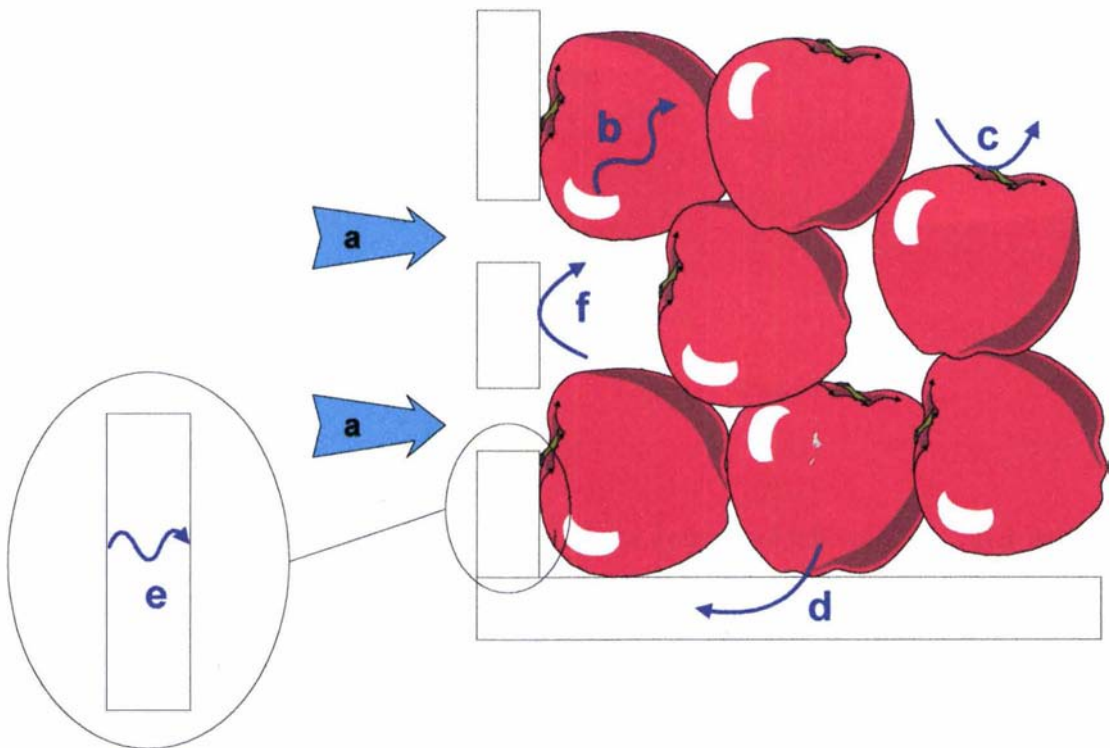


Figure 4.9. Conceptualisation of the main pathways existing for mass transfer in a bulk storage container placed in static storage, where heat transfer has reached steady state.

4.3. SUB-MODEL HIERARCHY

The subdivision of any total system model into sub-models allows simplification of the problem into manageable components but requires the development of appropriate interface models between components. Previous researchers have incorporated a sub-model hierarchy during model development, which regarded the flow medium (usually air) as most dominant in the system (Cleland *et al.*, 1982; Cleland, 1985). This required all processes to interface with the flow medium within a modelling zone, and neglected possible interactions between model components within the zone other than through the air. Inter-zone interactions were generally solely via the flow medium. Amos (1995), however, included the convection from apples to air and conduction from apples to 'Friday' trays. This allowed some components to interact as they would in a physical system and not through the air.

The approach taken in the present work reduced the flow medium to a level of equal importance, where all components can interact freely with each other given an appropriate interface model (Figure 4.10).

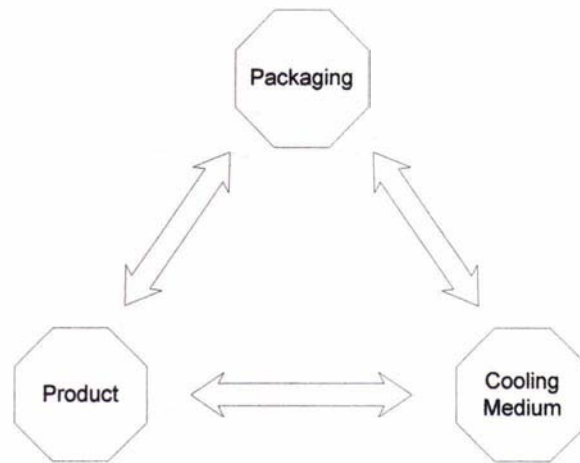


Figure 4.10. Sub-model interaction within a zone in the proposed modelling system.

4.4. GENERAL MODELLING PHILOSOPHY

In developing a modelling methodology to facilitate construction of simple, yet flexible models, a multi-zoned or control volume modelling approach was selected. Each of the ‘zones’ contained appropriate sub-models depending on the composition of the system to be modelled. These sub-models include the cooling fluid, product items, packaging and/or other heat sources or sinks. For all selected cases, the relationships between the sub-models were characterised using general modelling rules.

4.4.1. Zone Definition

The definition of a modelling zone is:

A physical space within a packaging geometry which may or may not contain product, cooling fluid, packaging materials or other sources of heat and/or mass. A single or greater number of zones may be used to represent the physical system in a modelling scenario.

The rules regarding zone size and positioning were defined as follows:

- All zones are essentially rectangular (although the sides may not be truly flat) and thus must have six interfaces to other zones. Unless constrained by ‘natural’ boundaries (eg. carton walls) they should also have dimension ratios of less than 2:1 (must be approximately cuboidal). This latter requirement eliminates any difficulties that might arise by modelling “stretched” regions with too few zones.
- External boundaries of the system would normally be physical (e.g. bin walls, packaging); there may or may not be fluid medium flow through holes in the boundary. This allows delineation of the interaction with the external conditions.

- The environment external to the outer boundary wall can consist of either a fluid medium or, a perfect insulating material through which no heat or water vapour flows, or a combination of both. This allows the model to simulate systems only partially exposed to an external fluid medium. Fluid flow across a boundary, e.g. via ventilation holes, will usually dominate the net energy or water vapour transfer involved (except in circumstances where fluid flow over the boundary is very low). In such circumstances, other energy or water vapour transfer processes over the boundary need not be as precisely modelled.

Zone and zone boundary numbering within a packaging configuration required development of general rules. These were defined as follows:

- The front face is defined as the face through which the largest incoming airflow occurs. Direction x is horizontal to this face, y is vertical, and z is perpendicular to this face.
- Zones are numbered starting at the front left, top corner and proceed across each plane from left to right, then down each plane (top to bottom). This is repeated for each plane in the z – direction.
- For each zone, the zone boundaries are both numbered and coded. For the vertical direction they are numbered top to bottom (for a single zone model, V_1 and V_2); boundaries for the horizontal direction are numbered left to right (for a single zone model, H_1 and H_2); and boundaries for the perpendicular direction are numbered front to back (for a single zone model, P_1 and P_2). Figure 4.11 illustrates the numbering and coding used for zones and zone boundaries.

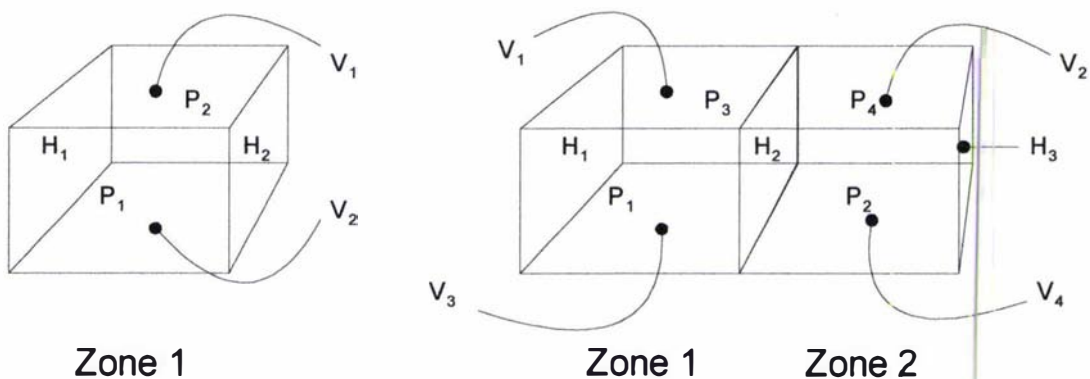


Figure 4.11. Examples of the zone and zone boundary numbering and coding utilised in the modelling system.

4.4.2. Zone Fluid

- The zone fluid within a zone is considered perfectly mixed.
- Inter-zonal interactions across zone boundaries to the zone fluid in the next zone can occur (e.g. cross-mixing by dispersion or eddy currents, pressure difference induced flows).
- The density of the zone fluid is considered constant, therefore treating mass accumulation within the zone fluid as negligible.
- It is not necessary to assume that the flows across boundaries or the external environmental conditions are independent of time, as these are input variables.

A generalised energy balance around the zone fluid is then:

$$\begin{aligned} \text{Rate of accumulation} \\ \text{of energy in zone fluid} \\ \text{within a zone} \end{aligned} = \sum \begin{aligned} \text{Energy flow into the} \\ \text{zone fluid from across} \\ \text{the zone boundaries} \end{aligned} + \sum \begin{aligned} \text{Energy flow into the} \\ \text{zone fluid from heat} \\ \text{generators within the zone} \end{aligned} \quad (4.1)$$

A generalised mass balance around the zone fluid is then:

$$\begin{aligned} \text{Rate of accumulation of} \\ \text{water vapour in zone} \\ \text{fluid within a zone} \end{aligned} = \sum \begin{aligned} \text{Water vapour flows into the} \\ \text{zone fluid from across the} \\ \text{zone boundaries} \end{aligned} + \sum \begin{aligned} \text{Water vapour flows into the} \\ \text{zone fluid from components} \\ \text{within the zone} \end{aligned} \quad (4.2)$$

4.4.3. Packaging Materials

- In heat transfer terms, zone boundary packaging is assumed to have only thermal resistance at that position. The packaging thermal capacity is distributed evenly to within the zones either side of the boundary and lumped with the zone fluid thermal capacity of each zone. This reduced packaging model complexity as well as reducing the simulation time. By treating the boundary packaging layer as having resistance only, the mathematical model for its behaviour is an algebraic equation. (Calculations for typical package configurations showed that the thermal capacity of the packaging is generally less than 5% of the thermal capacity of the product in bulk horticultural packages).
- In heat transfer terms, packaging internal to a zone is assumed to have no thermal resistance, whilst its thermal capacity is lumped with that of the fluid medium or product in the zone.
- In mass transfer terms, the packaging material was assumed to adsorb/desorb water vapour from the fluid and product with which it is in contact, seeking to reach its equilibrium moisture holding capacity at the local air and/or product conditions.

- In assessing mass transfer dynamics, where a packaging material lies on a boundary between two zones, 50% of the material was assumed to be seeking equilibrium with the zone components in each zone. In steady-state mass transfer, 50% of the boundary packaging material was assumed to be in equilibrium with the internal zone fluid water partial pressure and 50% with the external environment's fluid water partial pressure.

In the unsteady-state mass transfer case, a generalised mass balance around the packaging material in a zone is therefore:

$$\begin{aligned} \text{Rate of accumulation of} \\ \text{water vapour in packaging} \\ \text{material(s) within a zone} \end{aligned} = \sum \begin{aligned} \text{Water vapour flows into the} \\ \text{packaging material(s) from} \\ \text{zone fluid within the zone} \end{aligned} + \sum \begin{aligned} \text{Water vapour flows into the} \\ \text{packaging material(s) from} \\ \text{components within the zone} \end{aligned} \quad (4.3)$$

4.4.4. Product

- Product within a zone was assumed to be 'perfectly mixed' in terms of temperature (heat transfer modelling) and water status (mass transfer modelling).
- Product to product contact within a zone was assumed to create no net energy or water vapour flow.
- It was not necessary to assume a uniform initial product temperature as this is an input variable.
- Inter-zonal product contact across zone boundaries can occur,

The generalised energy balance is:

$$\begin{aligned} \text{Rate of accumulation} \\ \text{of energy in product} \\ \text{within a zone} \end{aligned} = \begin{aligned} \text{Energy flow into the} \\ \text{product from zone} \\ \text{fluid within the zone} \end{aligned} + \sum \begin{aligned} \text{Energy flows into the} \\ \text{product from across the} \\ \text{zone boundaries} \end{aligned} + \begin{aligned} \text{Energy generation} \\ \text{in product due} \\ \text{to respiration} \end{aligned} \quad (4.4)$$

A generalised water mass balance can also be developed for the product:

$$\begin{aligned} \text{Rate of accumulation} \\ \text{of water in product} \\ \text{within a zone} \end{aligned} = \sum \begin{aligned} \text{Water (vapour) flows into} \\ \text{the product from zone} \\ \text{fluid within the zone} \end{aligned} + \sum \begin{aligned} \text{Water (vapour) flows into the} \\ \text{product from packaging} \\ \text{materials within the zone} \end{aligned} \quad (4.5)$$

4.5. CONCLUDING REMARKS

This chapter has outlined the heuristics underpinning the mathematical modelling methodology. These heuristics allow the overall physical model to be conceptualised prior to development of specific sub-models. In the following chapter (Chapter 5), the mathematical equations for the various sub-models used in prediction of both heat transfer (pre-cooling model) and mass transfer (bulk storage model) are presented.

CHAPTER 5

FORMULATION AND IMPLEMENTATION OF SIMULATION MODELS

5.1. FORMULATION OF THE PRE-COOLING MODEL

This unsteady-state model considers pre-cooling of packaged products; predicting product temperature variations as a function of cooling medium flow pattern, vent position and packaging configuration.

5.1.1. Heat Transfer Pathways

The heat transfer pathways occurring across each zone boundary to the product or cooling medium within the zone are dependent on the formation and structure of the zone boundaries which were established via heuristics in Chapter 4. The resultant zone component interactions and their heat transfer pathways are illustrated in Figure 5.1. Where internal packaging exists (such as ‘Friday’ trays), zone boundaries also usually exist.

External energy flows to the fluid in the zone include:

- a) That arising from cooling fluid flow between adjacent zones.
- b) Convective and conductive (through packaging) heat flow from the cooling fluid in an adjacent zone, or from the external environment.

The ‘heat generators’ within a zone, such as product, interact with other components within the zone and components immediately across zone boundaries, giving a number of additional heat transfer pathways:

- c) Convective and conductive heat flow from heat generators in an adjacent zone, through packaging to the cooling fluid.

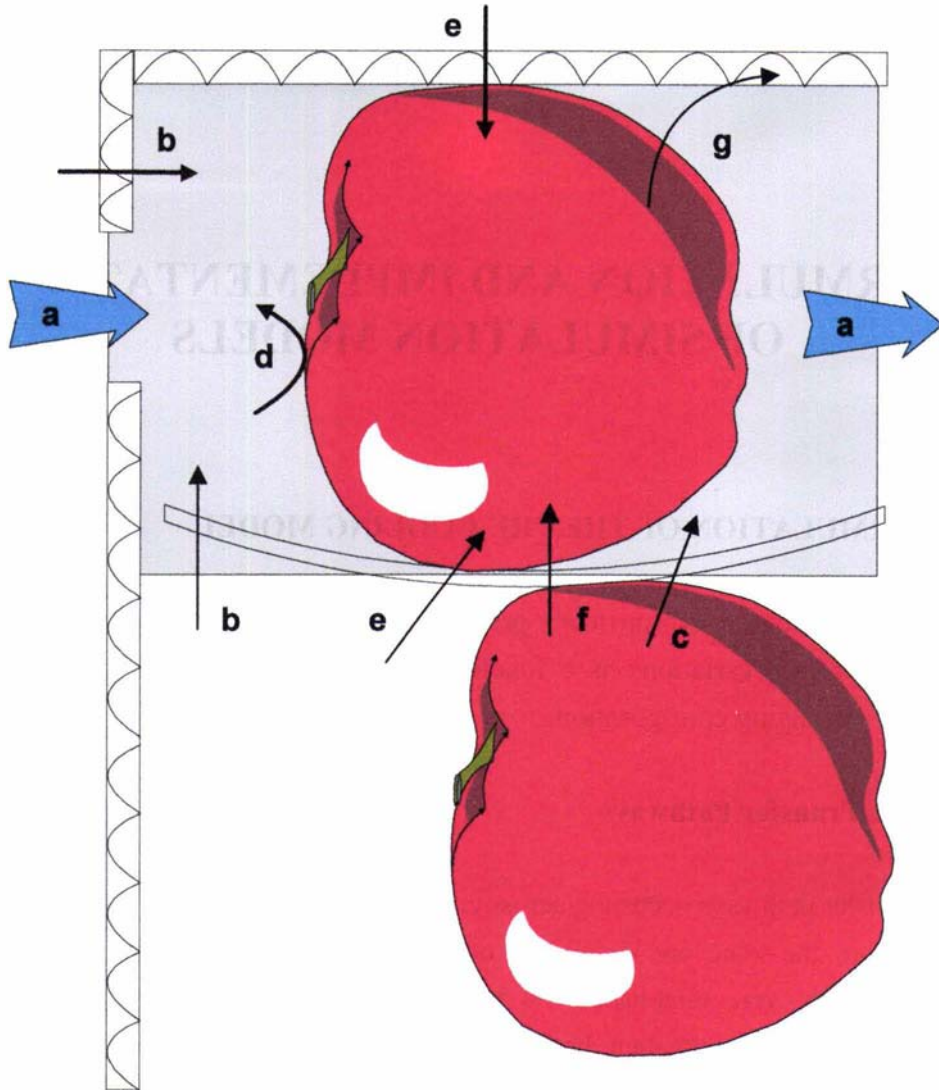


Figure 5.1. Major heat transfer pathways for product and fluid in a modelling zone (shaded region). Pathways are described in Section 5.1.1.

- d) Convective heat flow from the product in the zone to the zone fluid.
- e) Convective and conductive heat flow from fluid in an adjacent zone, through packaging to the product.
- f) Conductive heat flow from product in an adjacent zone, through packaging to the product.
- g) Radiative heat flow from product to surfaces within the zone.

As a result of application of the heuristics in Chapter 4, all zones contain one ordinary differential equation (ODE) for product temperature and one ODE for flow medium temperature (and could contain an ODE for humidity should this be modelled at a later time). To minimise model complexity, engineering judgment was applied to develop

simplifying assumptions, which reduced the number of pathways to be modelled. The following assumptions were adopted:

- Moisture movement from the product, and its contribution to energy flow, was ignored (Over the relatively short pre-cooling period, generally <24hours, the total change in mass of horticultural products such as apples and pears, due to mass loss, is less than 0.1% and the temperature change over 4 - 12 hours is 15 - 25°C. The contribution of evaporation during pre-cooling to the total energy loss of fruit is typically 0 - 5%, a negligible amount).
- Product respiration was likely to contribute negligibly to the total heat load (In a typical pre-cooling process, the rate of heat generation by respiration is often very low, $\approx 0.5\%$ of the total heat load, and in comparison with the total heat load for these conditions, respiration contributes negligibly. Awberry (1927) calculated the excess temperature at the centre of an apple, caused by its heat of respiration, to be 0.023°C after two hours. Camponone *et al.* (1995) also verified that respiratory heat has no practical influence on the pre-cooling time). However, to account, in the longer term, for situations where forced fluid flow is negligible, heat generation by respiration was included so that the modeller could 'turn it on' if required. The numerical value was generally set to 0 in the present work.
- The influence of radiative heat transfer was considered sufficiently small to be ignored. (Gaffney *et al.* (1985a) stated that if a product was packaged in a bin or box, it was likely that the individual product item would receive minimal nett radiative heat transfer from adjacent product items).
- A linear relationship between air temperature, and each of air internal energy and enthalpy was assumed, thus ignoring water vapour contributions. Although not physically correct, the error was considered to be sufficiently small over the limited temperature and humidity ranges likely to be modelled.

The boundary-related modes of heat transfer positively included in this model are those considered necessary to retain reasonable generality and are illustrated in Figure 5.2. They are:

1. Heat transfer from adjacent zone fluid to zone product touching the zone boundary (modelled as forced and/or natural convection).
2. Heat transfer from adjacent zone product to zone product touching the zone boundary (modelled as contact heat transfer).
3. Heat transfer from adjacent zone product through packaging to zone product (modelled as contact and packaging heat transfer).

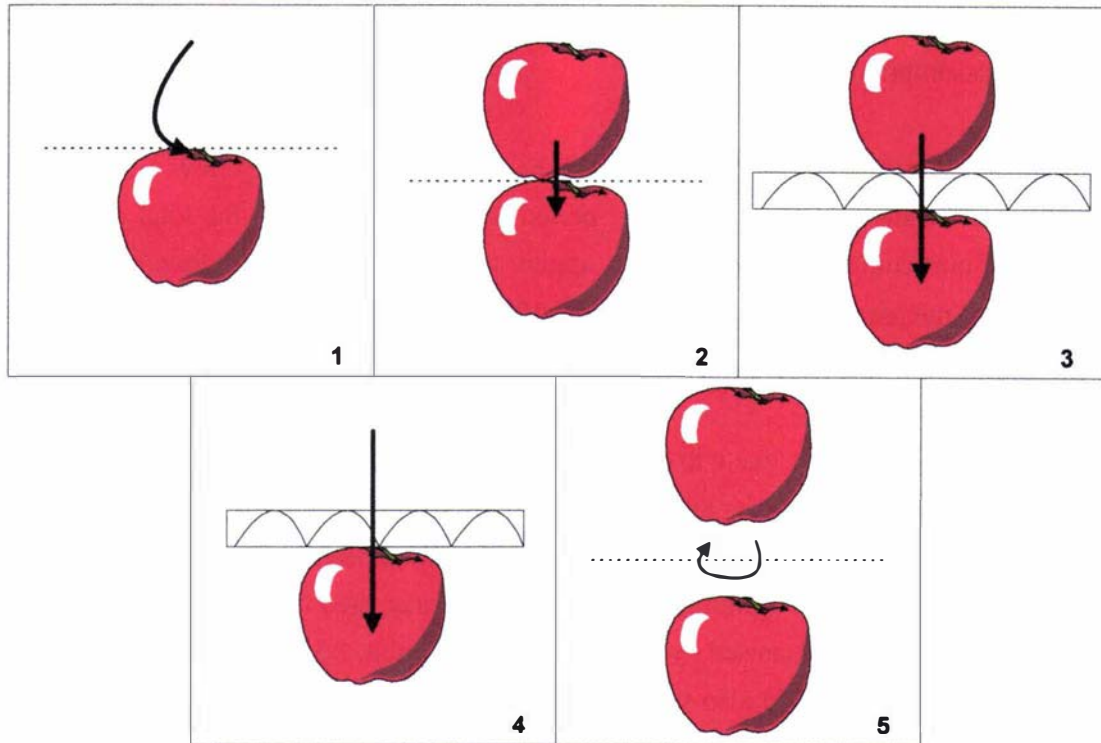


Figure 5.2. Product interactions with components in adjacent zones across the zone boundary (numbers correspond to the modes of heat transfer explained in Section 5.1.1).

4. Heat transfer from adjacent zone fluid through packaging to zone product (modelled as forced and/or natural convection, packaging and contact heat transfer).
5. Heat transfer from adjacent zone product through air to zone product (modelled as natural convection).

5.1.2. Mathematical Formulation of Heat Transfer Equations

5.1.2.1. Formulation of the ODE for Zone Product Temperature

The energy balance for product in a generalised zone is:

$$\begin{array}{l}
 \text{Rate of accumulation} \\
 \text{of energy in product} \\
 \text{within a zone}
 \end{array}
 =
 \begin{array}{l}
 \text{Energy flow into the} \\
 \text{product from flow} \\
 \text{medium within the zone}
 \end{array}
 +
 \sum
 \begin{array}{l}
 \text{Energy flows into the} \\
 \text{product from across the} \\
 \text{zone boundaries}
 \end{array}
 +
 \begin{array}{l}
 \text{Energy generation} \\
 \text{in product due} \\
 \text{to respiration}
 \end{array}
 \quad (5.1)$$

The mathematical representation of Eqn. (5.1) is:

$$(M_{pr}c_{pr})\frac{d\theta_{pr}}{dt} = \phi_{flpr} + \sum_{i=1}^6 \sum_{j=1}^5 \phi_{i,j} + Q_{resp} \quad (5.2)$$

where	M_{pr}	=	mass of the product (kg).
	c_{pr}	=	(constant) specific heat capacity of the product ($J.kg^{-1}.K^{-1}$).
	θ_{pr}	=	temperature of the product ($^{\circ}C$).
	t	=	time (s).
	ϕ_{flpr}	=	convective heat transfer from fluid to product within the zone (W).
	i	=	boundary number (maximum of six).
	j	=	heat transfer mode (as indicated by Figure 5.2 - maximum of five).
	$\phi_{i,j}$	=	heat flow via j^{th} mode of heat transfer across i^{th} boundary (W).
	Q_{resp}	=	respiratory heat generation within product (W).

Within any zone, Figure 4.11 defined the six surfaces as $H1, H2, V1, V2, P1$ and $P2$. The value of i for a single zone is defined in sequence ie. $i = 1$ ($H1$), $i = 2$ ($H2$), $i = 3$ ($V1$), $i = 4$ ($V2$), $i = 5$ ($P1$) and $i = 6$ ($P2$).

The individual heat transfer terms in Eqn. (5.2) were modelled using:

$$\phi_{flpr} = h_{eff,flpr} A_{flpr} (\theta_{fl} - \theta_{pr}) \quad (5.3)$$

and, for $j = 1 - 5$:

$$\phi_{i,j} = h_{eff,i,j} A_{i,j} (\Delta\theta_{i,j}) \quad (5.4)$$

where	$h_{eff,flpr}$	=	'effective' surface heat transfer coefficient from fluid to product in the zone by convection ($W.m^{-2}.K^{-1}$).
	A_{flpr}	=	surface area of the product in contact with zone fluid (m^2).
	θ_{fl}	=	temperature of the fluid in the zone ($^{\circ}C$).
	$h_{eff,i,j}$	=	'effective' surface heat transfer coefficient between objects at the i^{th} boundary for the j^{th} mode of heat transfer ($W.m^{-2}.K^{-1}$).
	$A_{i,j}$	=	surface area for the j^{th} mode of heat transfer at the i^{th} boundary (m^2). (NB: $\sum A_{i,j}$ = total boundary area).
	$\Delta\theta_{i,j}$	=	temperature difference expressed on an inwards directional basis between components at the i^{th} boundary for the j^{th} mode of heat transfer (K).

For calculation of $h_{i,j}$, sums of resistances were used (see p. 5.7 for nomenclature):

For $j = 1$:

$$\frac{1}{h_{eff,i,1}} = \frac{1}{h_{adj,flpr}} + R_{pr} \quad (\text{convection}) \quad (5.5)$$

where:

$$R_{pr} = \frac{1}{h_{eff,pr}} - \frac{1}{h_{act,pr}} \quad (5.6)$$

The value of $h_{act,pr}$ is defined as the reciprocal of the heat transfer resistance between the product surface and the adjacent material, whose temperature is used to define $\Delta\theta_{ij}$. This may be adjacent fluid or product. Thus:

$$h_{act,pr} = h_{adj,flpr} \quad (5.7)$$

(h_{act} and h_{eff} values are inter-related in Section 5.1.2.4 and h_{act} values are defined in Section 5.1.2.3)

For $j = 2$:

$$\frac{1}{h_{eff,i,2}} = R_c + 2R_{pr} \quad (\text{contact only}) \quad (5.8)$$

R_{pr} is calculated using Eqn. (5.6) with $h_{act,pr}$ for $j = 2$ defined by:

$$\frac{1}{h_{act,pr}} = R_c \quad (5.9)$$

For $j = 3$:

$$\frac{1}{h_{eff,i,3}} = \frac{x_{pk}}{k_{pk}} + 2R_c + 2R_{pr} \quad (\text{contact + packaging}) \quad (5.10)$$

R_{pr} is calculated using Eqn. (5.6) with $h_{act,pr}$ for $j = 3$ defined by:

$$\frac{1}{h_{act,pr}} = \frac{x_{pk}}{k_{pk}} + 2R_c \quad (5.11)$$

For $j = 4$:

$$\frac{1}{h_{eff,i,4}} = \frac{1}{h_{adj,flpk}} + \frac{x_{pk}}{k_{pk}} + R_c + R_{pr} \quad (\text{convection + packaging + contact}) \quad (5.12)$$

R_{pr} is calculated using Eqn. (5.6) with $h_{act,pr}$ for $j = 4$ defined by:

$$\frac{1}{h_{act,pr}} = \frac{1}{h_{adj,flpk}} + \frac{x_{pk}}{k_{pk}} + R_c \quad (5.13)$$

The fifth heat transfer term ($j = 5$) was incorporated into the modelling methodology to represent the natural convection present between product items close to but not contacting zone boundaries and where such product items were at different temperatures. This fifth mode of heat transfer is only significant if the extent of forced convection is low.

For $j = 5$:

$$\frac{1}{h_{eff,i,5}} = \frac{x_i}{k_{fl}CF} + 2R_{pr} \quad (\text{natural convection}) \quad (5.14)$$

R_{pr} is calculated using Eqn. (5.6) with $h_{act,pr}$ for $j = 5$ defined by:

$$h_{act,pr} = \frac{k_{fl}CF}{x_i} \quad (5.15)$$

where $h_{adj,flpr}$	=	actual convection heat transfer coefficient from fluid in an adjacent zone to product at the zone boundary ($\text{W.m}^{-2}.\text{K}^{-1}$).
R_{pr}	=	resistance associated with heat transfer between the product surface and the product mass average position ($\text{m}^2.\text{K}^{-1}.\text{W}^{-1}$).
$h_{eff,pr}$	=	'effective' heat transfer coefficient between the fluid / adjacent body and the product mass average position ($\text{W.m}^{-2}.\text{K}^{-1}$).
$h_{act,pr}$	=	actual heat transfer coefficient between the fluid / adjacent body and the product surface ($\text{W.m}^{-2}.\text{K}^{-1}$).
R_c	=	actual contact resistance between two objects (can be product-product or product-packaging) ($\text{m}^2.\text{K}^{-1}.\text{W}^{-1}$).
x_{pk}	=	thickness of the boundary packaging material (m).
k_{pk}	=	thermal conductivity of boundary packaging material ($\text{W.m}^{-1}.\text{K}^{-1}$).
$h_{adj,flpk}$	=	convection heat transfer coefficient from fluid in an adjacent zone to the boundary packaging material ($\text{W.m}^{-2}.\text{K}^{-1}$).
k_{fl}	=	thermal conductivity of the fluid ($\text{W.m}^{-1}.\text{K}^{-1}$).
CF	=	correction factor for modelling natural convection as conduction.
x_i	=	distance, taken across and through the i^{th} zone boundary, between adjacent zone product and product in zone (m).

5.1.2.2. Formulation of the ODE for Zone Fluid Temperature

The interactions between the zone fluid and components of adjacent zones to be modelled are shown in Figure 5.3.

The modes of heat transfer included in the model are:

6. Energy flow by direct fluid movement from an adjacent zone to the zone (energy flow associated with forced air movement).
7. Heat transfer from adjacent zone fluid through packaging to zone fluid (modelled as forced convection and packaging heat transfer).

8. Heat transfer from adjacent zone product through packaging to zone fluid (modelled as contact, packaging heat transfer and forced convection).
9. Heat transfer from adjacent zone product directly to zone fluid (modelled as forced convection).

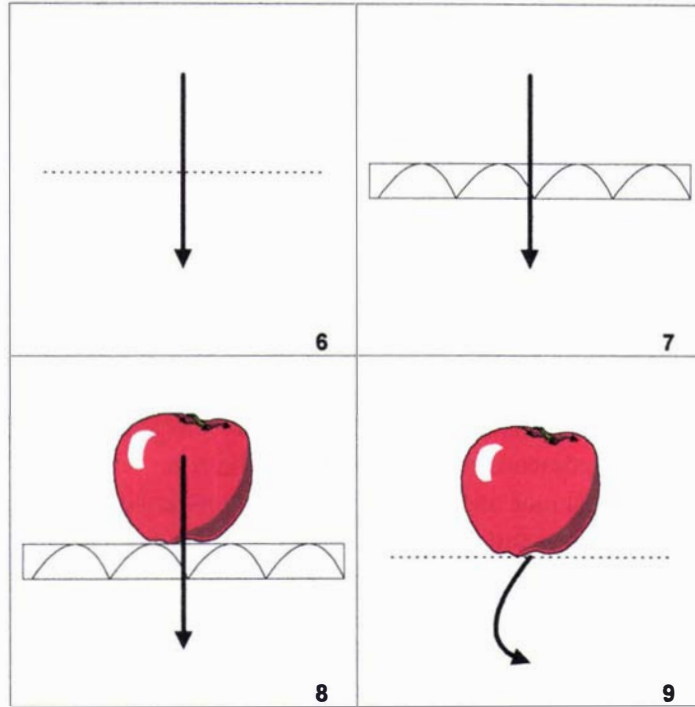


Figure 5.3. Zone fluid interactions with components across adjacent boundaries (numbers, which continue from Figure 5.2, correspond to the modes of heat transfer explained above).

The energy balance for the fluid in a generalised zone is:

$$\begin{array}{l}
 \text{Rate of accumulation} \\
 \text{of energy in zone fluid} \\
 \text{within a zone}
 \end{array}
 =
 \begin{array}{l}
 \text{Energy flow into the} \\
 \text{zone fluid from across} \\
 \text{the zone boundaries}
 \end{array}
 -
 \begin{array}{l}
 \text{Energy flow into the} \\
 \text{product from fluid within} \\
 \text{the zone}
 \end{array}
 \quad (5.16)$$

Taking into account the various pathways considered and earlier assumptions, especially that relating to packaging thermal mass placement, the energy balance can be expressed as:

$$(M_{pk} c_{pk} + M_{fl} c_{eff}) \frac{d\theta_{fl}}{dt} = \sum_{i=1}^6 \sum_{j=6}^9 \phi_{i,j} - \phi_{flpr} \quad (5.17)$$

where M_{pk} = mass of packaging material associated with the zone (kg).
 c_{pk} = specific heat capacity of the packaging materials ($\text{J.kg}^{-1}.\text{K}^{-1}$).
 M_{fl} = (constant) mass of fluid in the zone (kg).

$$\begin{aligned} c_{eff} &= \text{(constant) 'effective' specific heat capacity of the fluid (J.kg}^{-1}.\text{K}^{-1}\text{)}. \\ \phi_{i,j} &= \text{energy flow via } j^{\text{th}} \text{ mode of heat transfer across } i^{\text{th}} \text{ boundary (W)}. \end{aligned}$$

The 'effective' fluid specific heat capacity was calculated as a combination of the specific heat capacities of the fluid and the water vapour in the fluid:

$$c_{eff} \approx c_{fl} + H_{fl}c_{wv} \quad (5.18)$$

where

$$\begin{aligned} c_{fl} &= \text{actual specific heat capacity of the fluid (J.kg}^{-1}.\text{K}^{-1}\text{)}. \\ H_{fl} &= \text{absolute humidity of the fluid (if air) (kg}_{\text{water}}.\text{kg}_{\text{dry air}}^{-1}\text{)}. \\ c_{wv} &= \text{(constant) specific heat capacity of water vapour (J.kg}^{-1}.\text{K}^{-1}\text{)}. \end{aligned}$$

The second term in Eqn. (5.18) is relatively small so an H_{fl} value, corresponding to 90% RH @ 0°C, (typical operating conditions) was used rather than re-evaluating this parameter for each simulation. The individual energy transfer modes in Eqn. (5.17) were modelled using:

For $j = 6$ and if v_i is positive (incoming):

$$\phi_{i,6} = v_i A_{i,6} \rho_{fl} (c_{eff} \theta_{fl,adj}) \quad (5.19)$$

For $j = 6$ and if v_i is negative (outgoing):

$$\phi_{i,6} = v_i A_{i,6} \rho_{fl} (c_{eff} \theta_{fl}) \quad (5.20)$$

For $j = 7 - 9$:

$$\phi_{i,j} = h_{eff,i,j} A_{i,j} (\Delta\theta_{i,j}) \quad (5.21)$$

where

$$\begin{aligned} v_i &= \text{mean incoming fluid velocity across the } i^{\text{th}} \text{ zone boundary} \\ &\quad \text{expressed on inwards directional basis (m.s}^{-1}\text{)}. \\ A_{i,6} &= \text{area of } i^{\text{th}} \text{ boundary undergoing the } 6^{\text{th}} \text{ mode of heat transfer (m}^2\text{)}. \\ \rho_{fl} &= \text{(constant) density of the fluid (kg.m}^{-3}\text{)}. \\ \theta_{fl,adj} &= \text{temperature of fluid in zone from which flow across the boundary} \\ &\quad \text{is incoming (}^\circ\text{C)}. \end{aligned}$$

For calculation of the individual heat transfer coefficients, $h_{i,j}$, for $j = 7 - 9$, sums of resistances were used.

For $j = 7$:

$$\frac{1}{h_{eff,i,7}} = \frac{1}{h_{adj,flpk}} + \frac{x_{pk}}{k_{pk}} + \frac{1}{h_{int,flpk}} \quad \text{(convection + packaging)} \quad (5.22)$$

For $j = 8$:

$$\frac{1}{h_{eff,i,8}} = R_{pr} + R_c + \frac{x_{pk}}{k_{pk}} + \frac{1}{h_{int,flpk}} \quad (\text{contact + packaging + convection}) \quad (5.23)$$

R_{pr} is calculated using Eqn. (5.6) where $h_{act,pr}$ is defined by:

$$\frac{1}{h_{act,pr}} = R_c + \frac{x_{pk}}{k_{pk}} + \frac{1}{h_{int,flpk}} \quad (5.24)$$

For $j = 9$:

$$\frac{1}{h_{eff,i,9}} = \frac{1}{h_{int,flpr}} + R_{pr} \quad (\text{convection}) \quad (5.25)$$

R_{pr} is calculated using Eqn. (5.6) where $h_{act,pr}$ is defined by:

$$h_{act,pr} = h_{int,flpr} \quad (5.26)$$

where $h_{int,flpk} =$ convection heat transfer coefficient from packaging material to the fluid in the zone ($\text{W.m}^{-2}.\text{K}^{-1}$).

$h_{int,flpr} =$ actual convection heat transfer coefficient from product in an adjacent zone to fluid at the zone boundary ($\text{W.m}^{-2}.\text{K}^{-1}$).

5.1.2.3. Determination of Actual Heat Transfer Coefficients

As has been illustrated, overall heat transfer coefficients were determined by summing the appropriate convection, packaging and contact resistances. Heat transfer literature lists a large number of correlations developed for estimating convective heat transfer coefficients between shapes, surfaces and a fluid. The task here was to select those most appropriate to the package geometry and fluid flow conditions.

i) Forced Convection: Product-Fluid (Modes 1, 9, intra-zone product-fluid)

It was judged that the most appropriate, yet simple physical model for flow of a cooling medium through a horticultural package filled with product was a packed bed. The term packed bed refers to a condition for which the position of the particles is fixed (Incropera and DeWitt, 1981). A forced convection correlation presented by Geankoplis (1993) for gas flow in a bed of spheres (Reynolds number range of 10 - 10,000) was selected for calculation of the heat transfer coefficient between products and fluid:

$$\varepsilon \frac{Nu}{Re Pr} Pr^{0.66} = \frac{2.876}{Re} + \frac{0.3023}{Re^{0.35}} \quad (5.27)$$

where:

$$Nu = \frac{h_{act,flpr} d}{k_{fl}} \quad (5.28)$$

where Nu = Nusselt number (dimensionless).
 Re = Reynolds number (dimensionless) = $\rho_{fl} v_s d / \mu_{fl}$.
 Pr = Prandlt number (dimensionless) = $c_{fl} \mu_{fl} / k_{fl}$.
 ε = the mean void fraction or porosity ($m^3 \cdot m^{-3}$).
 $h_{act,flpr}$ = actual surface heat transfer coefficient from fluid to product in the zone by forced convection ($W \cdot m^{-2} \cdot K^{-1}$).
 d = characteristic dimension of the geometry (in this case, the product diameter) (m).
 ρ_{fl} = fluid density ($kg \cdot m^{-3}$).
 v_s = superficial fluid velocity ($m \cdot s^{-1}$).
 μ_{fl} = dynamic viscosity of fluid evaluated at the bulk temperature ($kg \cdot m^{-1} \cdot s^{-1}$).
 c_{fl} = specific heat capacity of fluid ($J \cdot kg^{-1} \cdot K^{-1}$).

Incropera and DeWitt (1981) stated that the correlation presented in Eqn. (5.27) might also be applied to packing materials other than spheres by multiplying the right-hand side by an appropriate correction factor. For a bed of uniformly sized cylinders, with length-to-diameter ratio of 1, the factor is 0.79; for a bed of cubes it is 0.71. For the purpose of finding $h_{act,flpr}$ in the present work, it was assumed that all product items were of equal size and spherical, and that porosity was constant throughout the package.

The correlation presented in Eqn. (5.27) uses the local superficial velocity for calculation of the Reynolds number (the superficial velocity is the velocity that would result if air volumetric flow rate through a zone was maintained but the product volume shrunk to zero). For determination of heat transfer coefficients within a zone, the highest value of v_i across any of the boundaries of the zone was used to represent the dominant velocity that product within the zone was exposed to. The superficial velocity was thus:

$$v_s = v_{i,max} \frac{A_{i,6}}{A_{i,tot}} \quad (5.29)$$

where $v_{i,max}$ = (maximum) velocity across the i^{th} boundary ($m \cdot s^{-1}$).
 $A_{i,6}$ = area of the i^{th} boundary undergoing the 6^{th} mode of heat transfer (m^2).
 $A_{i,tot}$ = total area of the i^{th} boundary (m^2).

It was recognised that the area ratio, $A_{i,6} / A_{i,tot}$, could have any value between 0 and 1,

but good design would have the value approaching unity in a direction in which increased airflow was desired. For all packages examined in this work, the area of the i^{th} boundary with the highest v_i undergoing the δ^{th} mode of heat transfer was physically equal to the total area of the i^{th} boundary, but the model was formulated more generally.

In calculating the forced convection heat transfer coefficients at zone boundaries for fluid - product, $h_{adj,\beta pr}$, (in heat transfer mode $j = 1$), Eqns. (5.27) and (5.29) were applied but the relevant $v_{i,max}$ was taken to be the highest value of v_i in the adjacent zone and the area ratio was set to unity for simplicity.

ii) Forced Convection: Packaging-Fluid (Modes 4, 7, 8)

In addition to the packed bed correlation, used for calculating the heat transfer coefficients for product - fluid interaction, correlations were required for calculating heat transfer coefficients between packaging and fluid. It was decided that the appropriate correlation would be for more planar shapes (as packaging materials are generally planar). Lin *et al.* (1994) presented a number of velocity-dimension dependent correlations, whilst others (Whitaker, 1972; Holman, 1986; Geankoplis, 1993; Kelly *et al.*, 1995) presented reviews of Nusselt-Reynolds-Prandtl correlations. The correlations for heat transfer between packaging and fluid surfaces selected were those of Geankoplis (1993) for heat transfer with fluid flow parallel to a flat plate.

Turbulent flow:

$$Nu = 0.664Re^{0.5}Pr^{0.33} \quad (\text{for } Re > 300000) \quad (5.30)$$

Laminar flow:

$$Nu = 0.0366Re^{0.8}Pr^{0.33} \quad (\text{for } Re < 300000) \quad (5.31)$$

In these cases, the characteristic dimension, d , used for calculation of the Reynolds number was equal to the length of the surface within the zone (ie. packaging material) parallel to the fluid flow.

In calculating the forced convection heat transfer coefficients at zone boundaries for fluid-packaging, $h_{adj,\beta pk}$, (in heat transfer mode $j = 4$) and for fluid - packaging, $h_{adj,\beta pk}$, (in heat transfer mode $j = 7$), Eqns. (5.29) - (5.31) were applied but the relevant $v_{i,max}$ was taken to be the highest value of v_i in the adjacent zone.

iii) Natural Convection: All instances (Mode 5. At low velocity; modes 1, 4, 7, 8, 9, intra-zone product-fluid)

Heat transfer coefficients encountered in forced convection are typically higher than those encountered in natural convection due to the high fluid velocities associated with forced convection. As a result, natural convection was generally ignored in heat transfer analyses involving forced convection, although it was recognised that natural convection heat transfer was still occurring.

As stated earlier, the fifth heat transfer mode ($j = 5$) was incorporated into the modelling methodology to represent the natural convection present between product items close to but not contacting zone boundaries and where such product items were at different temperatures. The correction factor for modelling natural convection as conduction (CF) was determined using the Grashof - Prandtl empirical relationships presented by Holman (1990).

$$CF = \frac{k_{eff}}{k_{fl}} = 1 \quad (Ra < 2000) \quad (5.32)$$

$$CF = \frac{k_{eff}}{k_{fl}} = 0.197 Ra^{0.25} \left(\frac{x_y}{x_x} \right)^{-0.111} \quad (2000 < Ra < 200000) \quad (5.33)$$

where Ra = Raleigh Number (dimensionless) = $GrPr$.
 Gr = Grashof Number (dimensionless) = $g\beta(\theta_1 - \theta_2)(x_x)^3 / \nu$.
 Pr = Prandtl Number (dimensionless) = $c_{pfl} \mu_{fl} / k_{fl}$.
 x_x = separation distance between items in the x direction (m).
 x_y = separation distance between items in the y direction (m).
 g = gravitational acceleration ($m.s^{-2}$).
 β = coefficient of volume expansion (K^{-1}).
 θ_1 = temperature of surface 1 ($^{\circ}C$).
 θ_2 = temperature of surface 2 ($^{\circ}C$).
 ν = kinematic viscosity of the fluid ($m^2.s^{-1}$).

In evaluating this relationship, typical values of the separation distance between items in the x and y directions are 0.01m and 0.05m respectively (representing the distance between product items and distance between horizontal packaging materials). For typical fruit packages and cooling conditions, the Raleigh number was significantly less than 2000 and therefore the CF value equalled 1. This constant value was used in all mode 5 situations unless otherwise specified.

As fluid velocities drop, natural convection could also become significant for product-fluid and packaging-fluid heat transfer. Detailed calculation of natural convection was not carried out in such cases but rather it was decided to only use a single natural convection heat transfer coefficient for all cases. This was defined by:

$$h_{act, fpr} = h_{i,s} \quad \text{and} \quad h_{act, fpk} = h_{i,s} \quad (5.34)$$

iv) Combined Forced and Natural Convection: All instances (Modes 1, 4, 7, 8, 9, intra-zone product-fluid)

The error involved in ignoring natural convection is negligible at high velocities, but may be significant at low velocities. Therefore, it was desirable to assess the relative magnitude of natural convection in the presence of forced convection.

Cengel (1997) states that for a given fluid, the parameter Gr/Re^2 represents the importance of natural convection relative to forced convection. Incropera and DeWitt (1996) indicate that natural convection is negligible if $Gr/Re^2 \ll 1$ and that forced convection is negligible if $Gr/Re^2 \gg 1$. Hence the region where the combined natural and forced (or mixed) convection regime applies is generally where $Gr/Re^2 \approx 1$. In this work, following the recommendation of Cengel (1997), natural convection was considered negligible if $Gr/Re^2 < 0.1$ and forced convection was considered negligible if $Gr/Re^2 > 10$. If this parameter fell between these bounds, a combined heat transfer coefficient was calculated using the following equation:

$$h_{combined} = (h_{forced}^n + h_{natural}^n)^{1/n} \quad (5.35)$$

where $h_{combined}$	=	combined heat transfer coefficient for forced and natural convection (dimensionless)
h_{forced}	=	heat transfer coefficient determined from correlations for forced convection (dimensionless)
$h_{natural}$	=	heat transfer coefficient determined from correlations for natural convection (dimensionless)
n	=	parameter for Eqn. (5.35).

The value of the exponent n varies between 3 and 4, depending on the geometry involved (Cengel, 1997). Incropera and DeWitt (1996) indicate that the best correlation of data is often obtained for $n = 3$ although a value of 4 may be better suited for transverse flows involving cylinders or spheres. In this work, $n = 4$ was utilised.

v) Packaging Resistance (Modes 3, 4, 7, 8)

Packaging material properties such as thermal conductivity and thickness were measured or calculated using equations presented in Appendix 2.

vi) Contact Resistances (Modes 2, 3, 4, 8)

The contact resistance for product – product and product – packaging contact can be characterised in terms of the quality of the contact. Cleland and Valentas (1997) state that in plate freezing applications with poor contact, the contact resistance may be as high as $0.01 - 0.02 \text{ m}^2 \cdot \text{K}^{-1} \cdot \text{W}^{-1}$, and a thin layer of air may also be present (Cowell and Namor, 1974). For good contact, the resistance is typically in the range $0.002 - 0.005 \text{ m}^2 \cdot \text{K}^{-1} \cdot \text{W}^{-1}$. In this case, Creed and James (1985) state that there should not be an air layer trapped between surfaces. In the present work, a mid-range ‘poor contact’ between product and packaging of $0.015 \text{ m}^2 \cdot \text{K}^{-1} \cdot \text{W}^{-1}$ was assumed, as the only ‘contact-improving’ force was that due to bulk unitisation (eg. accumulation of individual cartons in a stacked pallet).

vii) Overall Heat Transfer Coefficients

Using the appropriate combinations of the above methods, actual heat transfer coefficients, $h_{l,j}$, for $j = 1$ to 9 and h_{fpr} were determined.

**5.1.2.4. Determination of ‘Effective’ Heat Transfer Coefficients
(Modes 1, 2, 3, 4, 5, 8, 9, intra-zone product-fluid)**

After the application of Section 5.1.2.3, the surface heat transfer coefficients obtained were those appropriate for using surface and not mass-average temperatures. However, in Eqn. (5.3), it was assumed that Newton’s law of cooling could represent the heat flow between the product as a whole, and the air. As the product mass-average temperature is different from the surface temperature, and the mass-average temperature is used in Eqn. (5.3), an ‘effective’ heat transfer coefficient, h_{eff} , rather than the actual value, h_{act} , must be applied. To derive an expression for h_{eff} , an analogy to a sphere undergoing cooling in a constant temperature environment was used. Under constant environmental conditions, the steady-state solution to Newton’s law of cooling for a sphere, assuming no temperature variation within the sphere, has the form:

$$\frac{\theta_{pr} - \theta_{fl}}{\theta_m - \theta_{fl}} = e^{-\frac{3h_{act}t}{\rho_{pr}c_{pr}R}} \quad (5.36)$$

where the first term approximation to the analytical solution taking into account temperature variation in the sphere is:

$$\frac{\theta_{pr} - \theta_{fl}}{\theta_{in} - \theta_{fl}} = Z e^{-\beta^2 \frac{k_{pr} t}{\rho_{pr} c_{pr} R^2}} \quad (5.37)$$

and:

$$Z = \frac{6Bi^2}{\beta_1^2 (\beta_1^2 + Bi(Bi - 1))} \quad (5.38)$$

For Eqn. (5.36) to give the same predictions as Eqn. (5.37) then it must be assumed that the maximum time (when the 2nd and subsequent terms in the full analytical solution from which Eqn. (5.37) is derived are significant) is short, that:

$$Z = 1 \quad (5.39)$$

and

$$h_{eff} = \frac{\beta_1^2 k_{pr}}{3R} \quad (5.40)$$

where β_1 is the first root of:

$$\beta \cot \beta + Bi - 1 = 0 \quad (5.41)$$

and

$$Bi = \frac{h_{act} R}{k_{pr}} \quad (5.42)$$

where	θ_{in}	=	initial product temperature (°C).
	h_{act}	=	actual surface heat transfer coefficient between product and external medium (W.m ⁻² .K ⁻¹).
	t	=	time (s).
	ρ_{pr}	=	density of product (kg.m ⁻³).
	R	=	radius (or shortest dimension) of product (m).
	k_{pr}	=	thermal conductivity of product (W.m ⁻¹ .K ⁻¹).
	Z	=	dimensionless parameter (Eqn. 5.37 - 5.39).
	Bi	=	Biot number.
	β	=	Root of the transcendental equation (Eqn. 5.41).

In practice, for the sphere, the error in assuming $Z = 1$ is less than 6.5% for $Bi < 2.5$, and as fluid flow rates in a pre-cooler are low, Bi will generally be low (often < 1). Table 5.1 gives an example of the difference between h_{eff} and h_{act} and also shows that Z is close to

unity. As $Bi \rightarrow 0$, the time for which there is significant error in truncating Eqn. (5.37) is also small.

Table 5.1.

A comparison of actual and effective heat transfer coefficients for a range of typical Bi conditions (NB $k_{pr} = 0.5 \text{ W.m}^{-2}\text{K}^{-1}$ and $R = 0.025\text{m}$).

Bi (sphere)	h_{act}	h_{eff}	% Difference	Z
0.05	1	0.99	0.99	0.999
0.25	5	4.76	4.86	0.999
0.5	10	9.06	9.43	0.996
1.25	25	19.62	21.52	0.979
2.5	50	31.53	36.95	0.935
25	500	60.66	87.87	0.677

For non-spherical produce, cooling rates are different to those for a sphere. Hence, the methodology of Lin *et al.* (1996a,b) was applied by scaling $h_{eff,flpr}$ (determined via Eqn. 5.40 to 5.42) by the shape factor E (equivalent heat transfer dimensionality) divided by 3 ($E = 3$ for a sphere and has lower values for other shapes). This approach is broadly similar to that used successfully by Lovatt *et al.* (1993a) and Amos (1995).

Using the h_{act} values, Eqns. (5.40) – (5.42) were used to determine h_{eff} . The results were then applied in Eqn (5.6) to determine the required heat transfer coefficients.

5.1.2.5. Determination of Velocity Data

Velocity data across zone boundaries for packaging configurations were determined using techniques discussed in Chapter 6.

5.1.2.6. Determination of Thermo-physical Properties

Values for thermo-physical properties of the fluid, product and packaging materials, such as thermal conductivity, density, viscosity and specific heat capacity were data inputs to the model. These values, or equations for their calculation, are presented in Appendix 2.

5.1.2.7. Determination of Area Values

Values for area properties of the product were data inputs to the model. These values, or equations for their calculation, are presented in Appendix 2. The methodology for

determining the area of zone boundaries is discussed in Chapter 6 (as this was also required for calculation of velocity data for each package configuration).

5.1.2.8. Respiration Correlation

It has been noted already that respiratory heat generation was not expected to be significant and was normally set to 0. However, Appendix 2 describes how these data can be determined, if required.

5.2. FORMULATION OF THE BULK STORAGE MODEL

This second model considers the dynamic long-term storage scenario, where differences between the product and cooling medium temperatures are small. In this model, relative humidity positional variations and product mass losses are predicted by use of a multi-zone approach.

5.2.1. Mass Transfer Pathways

Water vapour transport pathways occurring across each zone boundary to the cooling medium, product and packaging materials within the zone are dependent on the formation and structure of the zone boundaries (as discussed in Chapter 4). The zone component's interactions and their resulting mass transfer pathways are shown in Figure 5.4. These pathways are:

- a) Water transport in the fluid flow (generally air, and not a liquid for mass loss to be important) between adjacent zones.
- b) Water movement from product to the fluid medium within the zone.
- c) Water movement from the fluid medium in an adjacent zone, through packaging to product.
- d) Water movement from product in an adjacent zone, through packaging to product.
- e) Water movement from fluid in an adjacent zone, through packaging to fluid medium within the zone.
- f) Water movement from product in an adjacent zone, through packaging to fluid medium within the zone.
- g) Water movement through packaging materials by diffusion, capillary action or both.

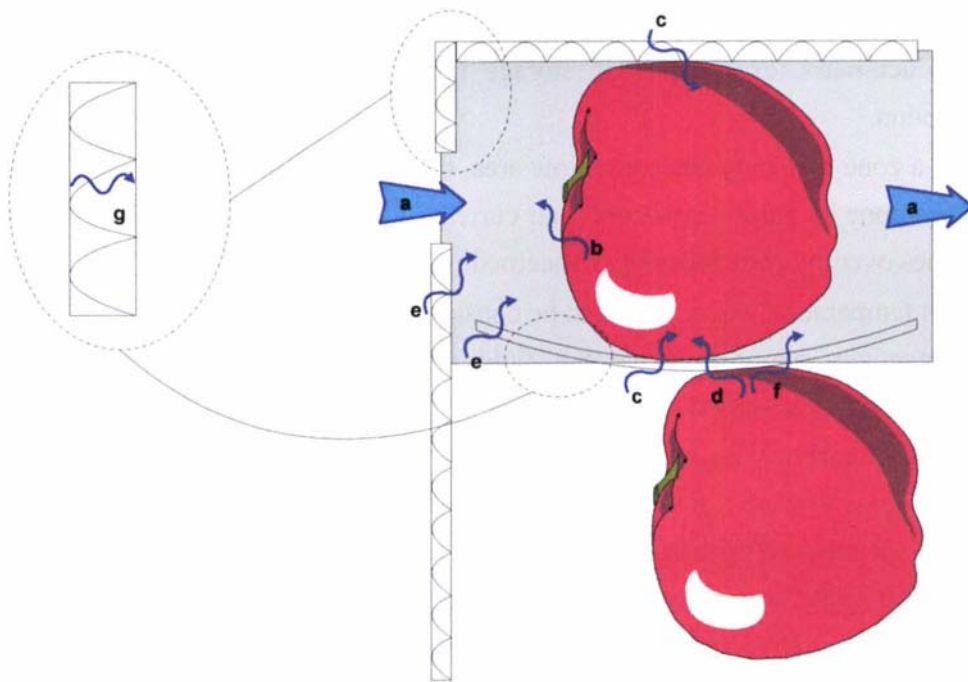


Figure 5.4. Major mass transfer pathways for product, packaging materials and fluid in an example-modelling zone (shaded region). Pathways [a) - g)] are described in Section 5.2.1.

In seeking to develop a bulk storage model, it was recognised that total water loss is low compared to total water present. Thus, provided the environmental conditions remain constant, the process of weight loss by mass transfer between horticultural products and their surrounding environments was expected to be a quasi-steady-state process after an initial establishment period. The necessary equations to define a multi-zoned, steady state model were expected to be non-linear and would have required iterative solution. It was thus only a little more expensive to use an unsteady-state model, which was solved, to steady state. This approach was adopted.

Because the dynamic predictions were only a by-product of the solution method, some of the processes that were more influential on the unsteady-state than the steady-state were modelled simply to reduce model complexity and computation cost. This means that a low level of accuracy in the dynamic response was accepted. Key assumptions and simplifications were:

- All zones contain at least three ordinary differential equations (ODEs). These are; one each for gaseous water mass and product mass, and one for water mass for each type of packaging material present in each zone.
- The product was assumed to have a constant water activity and skin resistance to mass transfer (the latter sometimes described in the literature by a transpiration coefficient).

Given that total mass loss in horticultural produce is generally only a small percentage of product mass, except at long storage times, this was considered a reasonable assumption.

- Where a zone boundary has some flow area, the air in the zone interacts with air in an adjacent zone by natural convection air currents if there is no forced air flow between the zones over the zone boundary concerned.
- Product temperature was assumed to be constant (usually equal to the fluid temperature but potentially elevated above the fluid temperature to allow the influence of respiratory heat generation to be modelled).
- Respiratory carbon loss was included in the modelling methodology as a constant rate transport process between product and the fluid in the zone. This weight loss mechanism may be significant during bulk storage (for some products) where the relative humidity is high and product temperature tends to or is close to that of the fluid medium. At constant storage temperature, it is effectively constant unless changes are made to the product's localised atmosphere composition (eg. it can be reduced by a reduction in available O_2 and increase in CO_2 concentration).
- Zone boundary-located packaging material mass was equally distributed to the zones on either side of the boundary. The packaging mass in a zone was then assumed to solely respond to the moisture content of the fluid within the zone within which it resides.

5.2.2. Mathematical Formulation of Mass Transfer Equations

After application of the simplifying assumptions, the important interactions between zone components and components in adjacent zones included in the modelling methodology are shown in Figure 5.5:

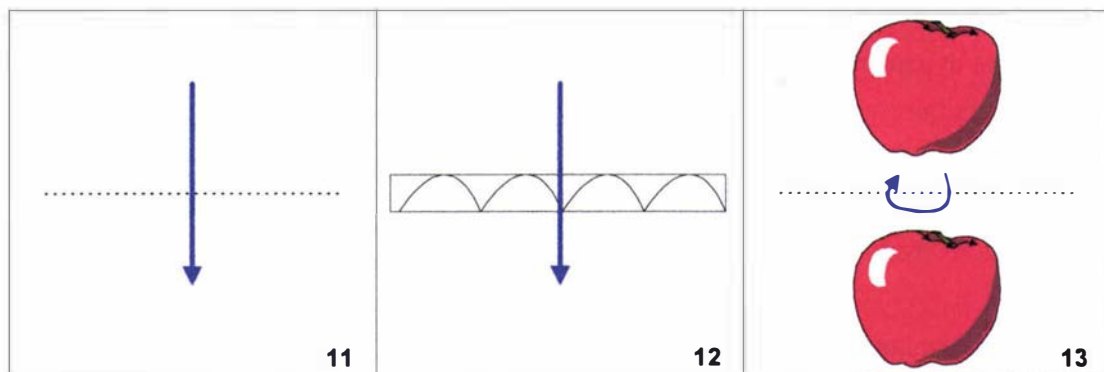


Figure 5.5. Zone fluid interactions with components across adjacent boundaries (numbers correspond to the modes of mass transfer explained below).

11. Water vapour transport from adjacent zone fluid to zone fluid (mass flow associated with forced air movement).
12. Water vapour transport from adjacent zone fluid through the packaging materials to the zone fluid (modelled as ‘effective’ mass transfer).
13. Water vapour transport from adjacent zone air to zone air (modelled as natural convection).

Taking into account the various assumptions and pathways considered, the mass balance for fluid in a generalised zone was stated as:

$$\begin{aligned} \text{Rate of accumulation} \\ \text{of water mass in the} \\ \text{fluid within a zone} \end{aligned} = \sum \begin{aligned} \text{Water mass flows into} \\ \text{the fluid from across} \\ \text{the zone boundary} \end{aligned} - \sum \begin{aligned} \text{Water mass flows to} \\ \text{packaging materials} \\ \text{within the zone} \end{aligned} - \begin{aligned} \text{Water mass flow} \\ \text{from the fluid to} \\ \text{product in the zone} \end{aligned} \quad (5.43)$$

and a mass balance for packaging materials in a generalised zone was stated as:

$$\begin{aligned} \text{Rate of accumulation of} \\ \text{water mass in packaging} \\ \text{materials within a zone} \end{aligned} = \sum \begin{aligned} \text{Water mass flows into} \\ \text{packaging materials from} \\ \text{fluid within the zone} \end{aligned} - \sum \begin{aligned} \text{Water mass flows into} \\ \text{product directly from the} \\ \text{packaging materials in the zone} \end{aligned} \quad (5.44)$$

while a mass balance for product in a generalised zone was stated as:

$$\begin{aligned} \text{Rate of accumulation} \\ \text{of water mass in the} \\ \text{product within a zone} \end{aligned} = \begin{aligned} \text{Water mass flows} \\ \text{into the product from} \\ \text{fluid within the zone} \end{aligned} + \sum \begin{aligned} \text{Water mass flows} \\ \text{into product from packaging} \\ \text{materials within the zone} \end{aligned} \quad (5.45)$$

Mathematical representations are:

$$\frac{dM_{w,fl}}{dt} = \sum_{i=1}^6 m_{i,11} + \sum_{i=1}^6 m_{i,12} + \sum_{i=1}^6 m_{i,13} - \sum_{x=1}^X m_{flpk} - m_{flpr} \quad (5.46)$$

$$\frac{dM_{w,pk}}{dt} = \sum_{x=1}^X m_{flpk} - \sum_{x=1}^X m_{pkpr} \quad (5.47)$$

and

$$\frac{dM_{pr}}{dt} = m_{flpr} + \sum_{x=1}^X m_{pkpr} \quad (5.48)$$

where $M_{w,fl}$ = mass of water in fluid (air) in zone (kg).
 $m_{i,j}$ = water mass flow rate by the j^{th} mode ($j = 11 \dots 13$) across i^{th} boundary where the inwards direction is positive (kg.s^{-1}).

m_{flpk}	=	water mass flow rate from fluid to packaging materials within a zone (kg.s^{-1}).
m_{flpr}	=	water mass flow rate from fluid to product within a zone (kg.s^{-1}).
$M_{w,pk}$	=	mass of water in packaging materials within a zone (kg).
m_{pkpr}	=	water mass flow rate from packaging materials to product within a zone (kg.s^{-1}).
X	=	number of packaging materials within a zone.
M_{pr}	=	mass of product within a zone (kg).

The individual intra-zonal mass flows are;

$$m_{flpr} = K_{flpr} A_{flpr} (p_{fl} - p_{pr}) \quad (5.49)$$

$$m_{flpk} = K_{flpk} A_{flpk} (p_{fl} - p_{pk}) \quad (5.50)$$

$$m_{pkpr} = K_{pkpr} A_{pkpr} (p_{pk} - p_{pr}) \quad (5.51)$$

where	K_{flpr}	=	mass transfer coefficient between fluid and product ($\text{kg.m}^{-2}.\text{s}^{-1}.\text{Pa}^{-1}$).
	p_{fl}	=	partial pressure of water vapour in the fluid (Pa).
	p_{pr}	=	partial pressure of water vapour in the gas voids under the product skin (Pa).
	K_{flpk}	=	mass transfer coefficient between packaging materials and the zone fluid ($\text{kg.m}^{-2}.\text{s}^{-1}.\text{Pa}^{-1}$).
	p_{pk}	=	partial pressure of water vapour in the notional boundary layer over packaging materials (Pa).
	K_{pkpr}	=	mass transfer coefficient between packaging materials and product ($\text{kg.m}^{-2}.\text{s}^{-1}.\text{Pa}^{-1}$).

The individual boundary flow mass transfer components of Eqns. (5.49) – (5.51) are:

For $j = 11$ and if v_i is positive (incoming):

$$m_{i,11} = v_i A_{i,11} \rho_{fl} H_{fl,adj} \quad (\text{transport in forced air mass flow}) \quad (5.52)$$

For $j = 11$ and if v_i is negative (outgoing):

$$m_{i,11} = v_i A_{i,11} \rho_{fl} H_{fl,int} \quad (\text{transport in forced air mass flow}) \quad (5.53)$$

where;

$$H_{fl,z} = \frac{M_{w,fl}}{M_{d,fl}} \quad (5.54)$$

where v_i = inwards fluid velocity across the i^{th} zone boundary (m.s^{-1}).

- $A_{i,11}$ = area of fluid to fluid contact on the i^{th} zone boundary (m^2) – this is equivalent to $A_{i,6}$ and $A_{i,13}$.
 $H_{fl,adj}$ = absolute humidity of fluid in adjacent zone across the i^{th} boundary ($kg_{water} \cdot kg_{dry\ air}^{-1}$).
 $H_{fl,int}$ = absolute humidity of fluid in zone ($kg_{water} \cdot kg_{dry\ air}^{-1}$).
 z = adjacent or internal as appropriate to Eqns. (5.52) and (5.53).
 $M_{d,fl}$ = dry mass of fluid in zone (kg).

For $j = 12$;

$$m_{i,12} = K_{pk,eff} A_{i,12} (p_{fl,adj} - p_{fl,int}) \quad (5.55)$$

For $j = 13$ and if $v_i = 0$, natural convection is assumed to occur and this was modelled as ‘effective’ mass transfer:

$$m_{i,13} = K_{fl,eff} A_{i,13} (p_{fl,adj} - p_{fl,int}) \quad (5.56)$$

- where $K_{pk,eff}$ = ‘effective’ mass transfer coefficient across a packaging material boundary ($kg \cdot m^{-2} \cdot s^{-1} \cdot Pa^{-1}$).
 $A_{i,12}$ = area of i^{th} boundary undergoing the 12^{th} mode of mass transfer (m^2).
 $p_{fl,adj}$ = partial pressure of water vapour of fluid in the adjacent zone across the i^{th} zone boundary (Pa).
 $p_{fl,int}$ = partial pressure of water vapour of fluid in the zone (Pa).
 $K_{fl,eff}$ = ‘effective’ mass transfer coefficient across a fluid-fluid boundary by natural convection ($kg \cdot m^{-2} \cdot s^{-1} \cdot Pa^{-1}$).
 $A_{i,13}$ = area of i^{th} boundary undergoing the 13^{th} mode of mass transfer (m^2).

5.2.2.1. Determination of Mass Transfer Coefficients

For most cases, mass transfer coefficients were calculated using the same correlations presented in Section 5.1.2.1, as mass transfer by convection is analogous to convective heat transfer (Incropera and DeWitt, 1996). The coefficients were calculated by direct conversion of the heat transfer coefficient to a mass transfer coefficient:

$$K_{fl} = \frac{h_{eff}}{k_{fl}} \delta_{fl} \quad (5.57)$$

- where K_{fl} = fluid film mass transfer coefficient ($kg \cdot m^{-2} \cdot s^{-1} \cdot Pa^{-1}$).
 δ_{fl} = diffusivity of water vapour in still air across a fluid-fluid boundary ($kg \cdot m \cdot m^{-2} \cdot s^{-1} \cdot Pa^{-1}$).

However, in some cases, resistance to mass transfer by some components in a system is far greater than the resistance to mass transfer in the boundary layer around such a component and this allowed some simplification by considering only the dominant

resistance. The mass transfer coefficients affected are described below.

i) Mass Transfer Coefficient for Product-Fluid

The mass transfer coefficient for transport between product and fluid is a sum of the resistances of two components: the product skin and the fluid boundary layer (whereas, for heat transfer, skin thermal resistance was negligible):

$$\frac{1}{K_{flpr}} = \frac{1}{K_{fl}} + \frac{1}{K_{skin}} \quad (5.58)$$

where K_{skin} = skin mass transfer coefficient ($\text{kg}\cdot\text{m}^{-2}\cdot\text{s}^{-1}\cdot\text{Pa}^{-1}$).

In line with current practice for products such as apples and pears (Gaffney *et al.* 1985b), it was assumed that the resistance of the product skin was much greater than the resistance of water vapour movement through the boundary layer. Therefore for such products Eqn. (5.58) was simplified to:

$$\frac{1}{K_{flpr}} \approx \frac{1}{K_{skin}} \quad (5.59)$$

Measured values for K_{skin} were utilised in the model and are presented in Appendix 2.

ii) Mass Transfer Coefficient for Fluid-Packaging

Measured values of K_{pkfl} gathered from previous researchers works (Amos, 1995; Merts, 1996) were utilised (Appendix 2).

iii) Mass Transfer Coefficient for Product-Packaging

The resistance of the product skin is much greater than the resistance to water vapour movement into paper-based packaging materials and thus:

$$\frac{1}{K_{pkpr}} \approx \frac{1}{K_{skin}} \quad (5.60)$$

iv) 'Effective' Mass Transfer Coefficient for Fluid-Packaging-Fluid

The 'effective' mass transfer coefficient through a packaging boundary would generally be calculated as a sum of resistances to mass transfer. However, in this work experimental data were collected for mass transfer across layers of the materials and the data analysis method 'lumped' all resistances as one overall effective mass transfer coefficient ($K_{pk,eff}$). The mathematical model used was (Foss, pers. comm.):

$$K_{pk,eff} = R_{pk} \frac{\delta_{fl}}{x_{pk}} \quad (5.61)$$

where R_{pk} = packaging material resistance factor (dimensionless).
 δ_{fl} = diffusivity of water vapour through still air ($\text{kg.m.m}^{-2}.\text{s}^{-1}.\text{Pa}^{-1}$).
 x_{pk} = thickness of packaging material boundary (m).

The conceptual model underpinning Eqn (5.61) is diffusion of water vapour through a still air layer (in the fluted region), which is slowed by the presence of slightly porous paper-based materials. The experimental values of packaging material resistance are presented in Appendix 2, and are < 1.0 .

v) 'Effective' Mass Transfer Coefficient for Fluid-Fluid

It was decided to also apply the model presented in Eqn (5.61) to natural convection mass transfer through fluid-fluid boundaries by treating these boundaries as a “very porous” packaging layer, thus implying that $R_{pk} \rightarrow 1$, and that the still air layer thickness is the packaging thickness. This also implies that the mass transfer resistance is totally within the still air layer. For stiff packaging (eg. paperboard) the material thickness, and thus the still air layer is usually several millimetres thick, but for plastic liners, it can be much less, in which case the assumption that the mass transfer resistance is all in the thin still air layer may not be valid. Rather than attempt to analyse the very complex behaviour known to occur for thin packaging, an empirical decision was made that x_{pk} would never be allowed to be less than 1mm, thus developing a lower bound on the mass transfer coefficient. Numerically, this mass transfer coefficient was physically realistic in comparison to other mass transfer coefficients in the complete system, and was similar to the value used by Merts (1996) for holes in MAP-liners for apple packages. It was accepted that there was little physical justification for the model concept, and that the experimental testing would need to be designed to assess whether this assumption unduly limited the range of applicability of the model.

Equations for calculating the diffusivity of water vapour through still air are presented in Appendix 2. It is noted that natural convection mass transfer across zone boundaries is only significant if the extent of forced convection air movement is low.

5.2.2.2. Determination of Velocity Data

Velocity data were collected using methods described in Chapter 6.

5.2.2.3. Determination of Area Values

Values for area properties were found using the methodology outlined in Section 5.1.2.7 (and are identical to those used in the heat transfer model described in Section 5.1).

5.2.2.4. Determination of Moisture Properties of Fluid and Product

Calculation of the partial pressure conditions for the product surface and the cooling fluid followed standard psychrometric principles:

$$p_{fl} = H_R p_{sat,amb} \quad (5.62)$$

$$p_{pr} = a_w p_{sat,surf} \quad (5.63)$$

and, using an Antoine equation (Cleland and Cleland, 1992) for water;

$$p_{sat,x} = e^{\left[\frac{23.4795 - \frac{3990.56}{\theta_x + 233.833}}{\theta_x + 233.833} \right]} \quad (5.64)$$

- where
- p_{fl} = partial pressure of water vapour in ambient fluid (Pa).
 - H_R = relative humidity (fraction).
 - $p_{sat, amb}$ = (saturation) vapour pressure of water at ambient fluid temperature (Pa).
 - p_{pr} = partial pressure of water vapour in the air voids immediately below the product skin (Pa).
 - a_w = water activity immediately below the product skin (dimensionless).
 - $p_{sat, surf}$ = (saturation) vapour pressure of water at the (constant) product temperature (Pa).
 - x = either *amb* or *surf* depending on the situation being calculated.
 - θ_x = temperature of the component (i.e. product or fluid) ($^{\circ}\text{C}$).

The water activity of the product was assumed to be constant. Experimental values for this parameter are presented in Appendix 2.

5.2.2.5. Determination of Moisture Properties of Packaging Materials

The partial pressure of water vapour in the boundary layer over packaging materials was also determined using standard psychrometric relationships.

$$p_{w,pk} = a_{w,pk} p_{sat,pk} \quad (5.65)$$

where:

$$a_{w, pk} = fn(\text{packaging moisture content}) \quad (5.66)$$

where $a_{w, pk}$ = packaging material water activity.
 $p_{sat, pk}$ = (saturation) vapour pressure of water at the packaging material temperature (Pa).

The determination of $a_{w, pk}$ required several new parameters, such as equilibrium moisture content. The equilibrium moisture content (*emc*) for packaging materials can be determined using the Guggenheim - Anderson - De Boer (G.A.B.) moisture isotherm equation (Bizot, 1983; Eagleton and Marcondes, 1994). The *emc* is largely dependent on the surrounding fluid relative humidity and, where the material is in contact with product, the product's water activity. The appropriate coefficients were fitted from experimental data for each of several packaging materials by Eagleton and Marcondes (1994), and differed slightly for absorption and desorption.

$$emc = \frac{mc_0}{100} \left[\frac{\varphi_1 \gamma_1 RH_{fl}}{(1 - \gamma_1 RH_{fl})(1 - \gamma_1 RH_{fl} + \varphi_1 \gamma_1 RH_{fl})} \right] \quad (5.67)$$

where *emc* = equilibrium packaging material moisture content (dry-weight basis) ($\text{kg}_{\text{water}} \cdot \text{kg}_{\text{dry weight}}^{-1}$).
 RH_{fl} = relative humidity of the fluid.
 mc_0 = moisture content corresponding to saturation of all primary adsorption sites by one water molecule ($\text{g}_{\text{water}} \cdot 100 \text{g}_{\text{dry weight}}^{-1}$).
 φ_1 = Guggenheim constant.
 γ_1 = factor correcting properties of the multi-layer molecules with respect to the bulk liquid.

Eqn. (5.67) was rearranged by Merts (1996) to calculate water activity of the packaging materials as a function of material moisture content.

$$a_{w, pk} = \frac{-(\chi_2 100emc - 1) \pm \sqrt{(\chi_2 100emc - 1)^2 - 4\chi_1 \chi_3 100emc^2}}{2\chi_1 100emc} \quad (5.68)$$

where;

$$\chi_1 = \frac{\gamma_1}{mc_0} \left(\frac{1}{\varphi_1} - 1 \right) \quad (5.69)$$

$$\chi_2 = \frac{1}{mc_0} \left(1 - \frac{2}{\varphi_1} \right) \quad (5.70)$$

$$\chi_3 = \frac{1}{mc_0 \varphi_1 \chi_1} \quad (5.71)$$

and where;

$$emc = \frac{M_{w, pk}}{M_{d, pk}} \quad (5.72)$$

which, when rearranged given the total packaging mass;

$$M_{w, pk} = \frac{M_{tot} emc}{(1 + emc)} \quad (5.73)$$

where χ_1, χ_2, χ_3 = intermediate constants for solution of water activity quadratic.
 $M_{w, pk}$ = mass of water in packaging (kg_{water}).
 $M_{d, pk}$ = mass of dry packaging (kg_{dry weight}).
 M_{tot} = total packaging mass (kg).

Merts (1996) used this approach to model moisture sorption by moulded-pulp ‘Friday’ trays in modified atmosphere apple packaging systems. Assuming that the G.A.B isotherm model was valid for all values of packaging material water activity even though the G.A.B model is only recommended for $a_{w, pk}$ values up to 0.9, and exhibits hysteresis as adsorption and desorption follow dissimilar curves (Figure 5.6). In the present work, the weakness of the model was also tolerated due to an inability to identify a viable alternative model. Further, only the adsorption isotherm was utilised as it was assumed that packaging materials would not be exposed to high relative humidity conditions prior to entry into a bulk-storage facility, and would thus be exposed to adsorption conditions only.

Eqn. (5.64) applies to a fixed temperature. Eagleton and Marcondes (1994) presented packaging material moisture sorption isotherm data for 5 different temperatures between 1°C and 40°C. Their curve-fit coefficients ($mc_0, \varphi_1, \gamma_1$) for the temperature that corresponded most closely to the temperature of the packaging system were used (Appendix 2).

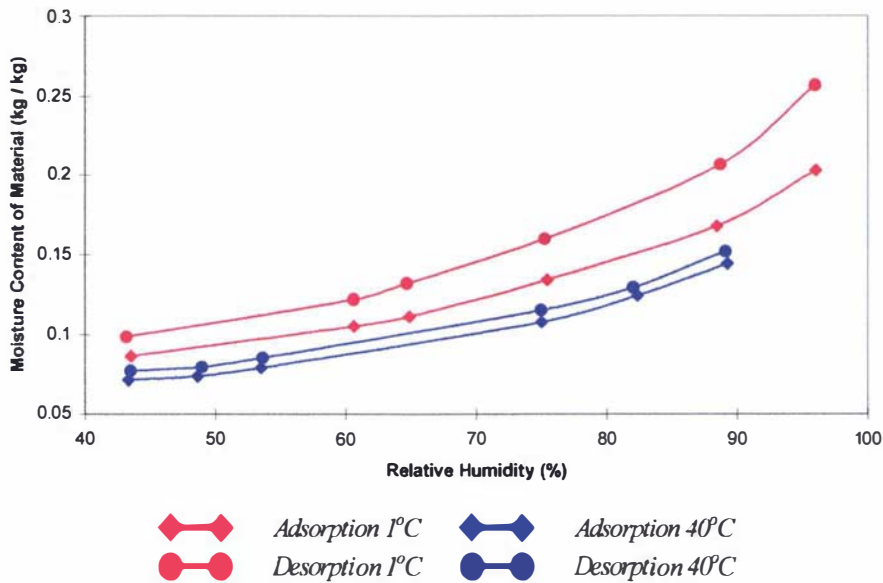


Figure 5.6. Moisture sorption isotherm model predictions for “outer” corrugated apple packaging (at 1°C and 40°C) undergoing both sorption (in which the material is taken from dry conditions to a higher humidity) and desorption (from saturated conditions to a lower humidity). After Eagleton and Marcondes (1994).

5.2.2.6. Respiratory Mass Loss

Respiratory mass loss was included in the model as a constant rate process. This rate was a data input to the model and was measured experimentally, or estimated using product specific equations (as specified in Appendix 2).

5.3. FORMULATION OF THE DATABASE-LINKED STEADY-STATE MODEL

Because the dynamic bulk-storage model involves a complex description of the mass transport pathways within packaging systems, it has substantial data requirements. To meet the needs of the project sponsor, a quasi-steady-state simplified database-linked simulation model with lower data requirements but probably lower accuracy was also developed. Unlike the dynamic mass transfer simulation model described in Section 5.2, the steady-state model did not characterise the rate of uptake of moisture by packaging materials, nor did it consider the position-variable relative humidity of the fluid within the packaging system. The simple model assumed an instantaneous uptake of moisture by packaging materials whereas this process generally takes up to 14 days for packages constructed from paper-based packaging materials (commonly used in the horticultural industry). Figure 5.7 illustrates the different approach of the 2 models for a hypothetical example.

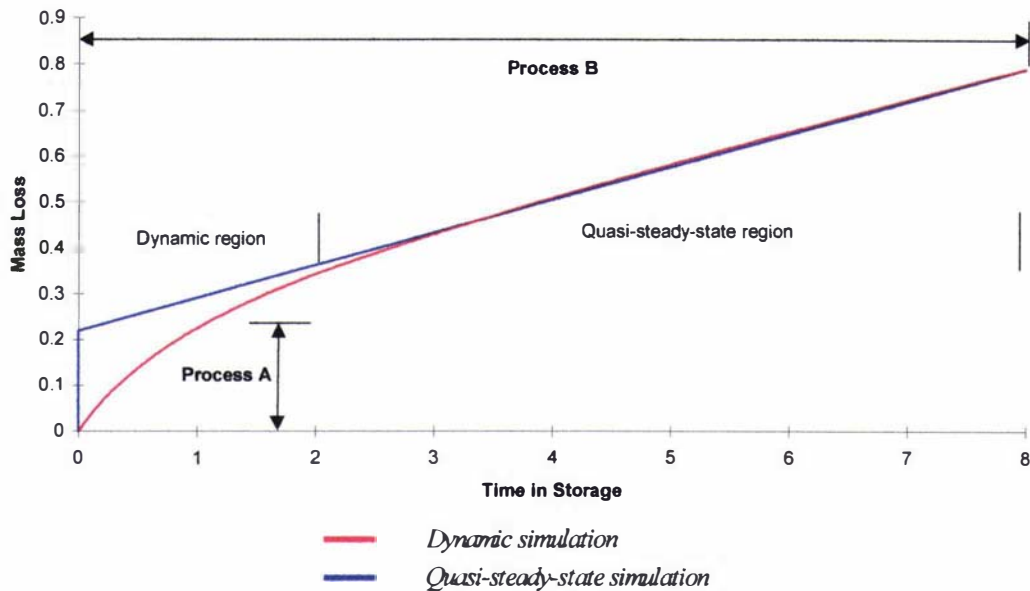


Figure 5.7. Indicative plot of modelling results for the dynamic and the steady-state simulation models. This figure shows the two processes in the quasi-steady-state model (*A* and *B*), explained in Section 5.3.

In Figure 5.7, two processes of the steady-state calculation are shown (*A* and *B*) and are explained below:

- A. This component of the steady-state model incorporates the uptake of moisture by the packaging materials in the horticultural packaging system.
- B. This component is the steady-state mass loss that occurs as a result of characterisation of the steady-state conditions within the packaging system. This is characterised by a rate equation and is the long time solution to the dynamic model.

The greatest error in use of the steady-state simulation model occurs in the representation of the initial packaging material uptake period (termed the Dynamic Region). However, it must be remembered that the dynamic model uses only approximate sub-models during this transient period.

5.3.1. Mass Transfer Pathways

The structure of the simulation model was as simple as possible - only one perfectly mixed zone (generally an entire package) was modelled. Only water vapour transport pathways influencing mass transfer across the package external boundaries were considered. Key assumptions and simplifications were:

- There are no relative humidity gradients with position in the air inside the package - the single zone assumption.
- The product was assumed to have a constant water activity and skin resistance to mass transfer (sometimes specified via a transpiration coefficient).
- Product temperature was assumed to be constant (usually equal to the fluid temperature but potentially elevated above the fluid temperature to allow the influence of respiratory heat generation to be modelled).
- Respiratory carbon loss was included in the modelling methodology as a constant rate transport from the product.

5.3.2. Mathematical Formulation of Mass Transfer Equations

Given that the steady-state simulation of mass transfer in horticultural packages occurs as two distinct processes (termed *A* and *B* in Figure 5.7), formulation of a model requires characterisation of each component individually.

5.3.2.1. Process A (Packaging Material Moisture Uptake)

Process *A* is the adsorption / desorption of water vapour into packaging materials. This process was assessed in two parts (as shown in Figure 5.8):

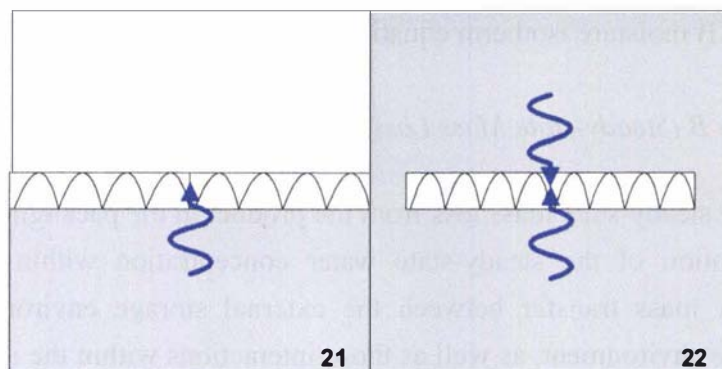


Figure 5.8. Water mass interactions modelled as instantaneous processes in the steady-state simulation model (numbers correspond to the modes of mass transfer explained in Section 5.3.2.5). The shaded region indicates the package configuration boundary.

21. Water vapour adsorption / desorption from the internal package fluid by the boundary packaging materials (in this case, only half the packaging mass is assumed to be in contact with the internal package relative humidity, and half with the external environment relative humidity, so

only the inner half is modelled).

22. Water vapour adsorption / desorption from the internal package fluid by the internal packaging materials.

Total packaging material moisture uptake was calculated using the G.A.B isotherm theory also used in the unsteady-state mass transfer model (explained in Section 5.2.2.5). Then:

$$M_{wv} = M_{d,pk} (mc_{final} - mc_{init}) \quad (5.74)$$

where:

$$M_{d,pk} = M_{d,IP} + 0.5M_{d,BP} \quad (5.75)$$

where M_{wv} = uptake of water vapour by all packaging materials (kg).
 $M_{d,pk}$ = mass of dry packaging (kg_{dry weight}).
 mc_{init} = packaging material moisture content (dry-weight basis) at the initial relative humidity condition (kg_{water}.kg_{dry weight}⁻¹).
 mc_{final} = packaging material moisture content (dry-weight basis) at the steady-state relative humidity condition (kg_{water}.kg_{dry weight}⁻¹).
 $M_{d,IP}$ = total mass of dry internal packaging (kg_{dry weight}).
 $M_{d,BP}$ = total mass of dry boundary packaging (kg_{dry weight}).

Values of mc_{init} and mc_{final} were calculated from the RH at packing time ($RH_{fl,ext}$) and that ultimately developed in the container ($RH_{fl,int}$) respectively, by substitution for RH_{fl} in the G.A.B moisture isotherm equation (Eqn. 5.67).

5.3.2.2. Process B (Steady-state Mass Loss)

Process B is the steady-state mass loss from the product in the packaging system. This requires calculation of the steady-state water concentration within the packaging system. Water mass transfer between the external storage environment, and the internal package environment, as well as those interactions within the internal package environment involving: product, internal packaging materials and the internal airspace, are considered. These are shown in Figure 5.9 and are:

23. Water vapour transport between external environment and internal package environment through ventilation regions (free fluid - fluid boundaries) (modelled as water movement associated with either forced air movement or natural convection).

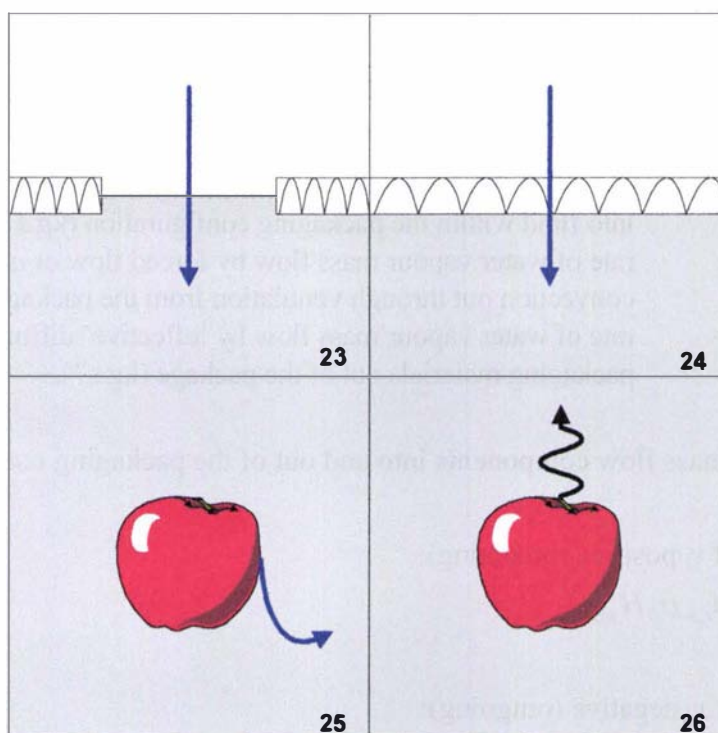


Figure 5.9. Water mass interactions modelled in the steady-state simulation model (numbers correspond to the modes of mass transfer explained in Section 5.3.2). The shaded region indicates the package configuration boundary.

24. Water vapour transport between external environment and internal package environment through boundary packaging materials (modelled as ‘effective’ diffusional mass transfer – and ignoring water storage in the packaging materials).
25. Water vapour transport from product to the fluid medium within the packaging configuration.
26. Respiratory carbon transport from the product to the internal package environment within the packaging configuration.

In order to achieve a convergent solution, and thus define the quasi-steady-state water concentration within the packaging system, the rate of water mass flow into the system must equal the rate of water mass flow out of the system. This rate was estimated by iterative calculation solving the water mass balances for the packaging system:

$$\begin{aligned}
 &\text{Rate of water mass flow by} && \text{Rate of water mass flow} && \text{Rate of water mass flow by mass} \\
 &\text{evaporation from the product} &= & \text{to external environment} &+ & \text{transfer through packaging boundaries} \\
 &\text{to the internal environment} && \text{through ventilation} && \text{to the external environment}
 \end{aligned}
 \tag{5.76}$$

The mathematical representation of Eqn. (5.76) is:

$$m_{flpr} = m_v + m_{flpkfl} \quad (5.77)$$

where m_{flpr} = rate of water vapour mass flow by evaporation from the product into fluid within the packaging configuration (kg.s^{-1}).
 m_v = rate of water vapour mass flow by forced flow or natural convection out through ventilation from the package (kg.s^{-1}).
 m_{flpkfl} = rate of water vapour mass flow by ‘effective’ diffusion through packaging materials out of the package (kg.s^{-1}).

The individual mass flow components into and out of the packaging configuration are:

For $j = 23$ and if v_i positive (incoming):

$$m_v = v_i A_{v,in} \rho_{fl} H_{fl,ext} \quad (5.78)$$

For $j = 23$ and if v_i negative (outgoing):

$$m_v = v_i A_{v,in} \rho_{fl} H_{fl,int} \quad (5.79)$$

For $j = 23$ and if $v_i = 0$, natural convection occurs and was modelled as ‘effective’ mass transfer:

$$m_v = K_{fl,eff} A_{v,all} (P_{fl,int} - P_{fl,ext}) \quad (5.80)$$

For $j = 24$:

$$m_{flpkfl} = K_{pk,eff} A_{pk} (P_{fl,int} - P_{fl,ext}) \quad (5.81)$$

For $j = 25$:

$$m_{flpr} = K_{flpr} A_{flpr} (P_{pr} - P_{fl,int}) \quad (5.82)$$

where $A_{v,in}$ = area of ventilation for flow of fluid into the package (m^2).
 $A_{v,all}$ = area of all ventilation in package configuration (m^2).
 A_{pk} = area of packaging materials exposed to external environment (m^2).

5.3.2.3. Determination of Mass Transfer Coefficients

Mass transfer coefficients were calculated using the same methodology presented in Section 5.2.2.1.

5.3.2.4. Determination of Velocity Data

Velocity data were determined using the methodology presented in Chapter 6.

5.3.2.5. Determination of Area Values

Values for area properties were determined using the methodology presented in Section 5.2.2.3 and Appendix 2.

5.3.2.6. Determination of Moisture Properties of Fluid and Product

Calculation of the partial pressure conditions for the product surface and the cooling fluid used the psychrometric equations outlined in Section 5.2.2.4.

5.3.2.7. Respiratory Mass Loss

Respiratory mass loss was determined using the methodology presented in Appendix 2.

5.3.3. Complete Steady-state Model

The complete model of mass loss in horticultural packaging configurations is a combination of both components outlined in Section 5.3.2. These components were incorporated into a cumulative steady-state balance for the packaging system:

$$\begin{array}{l}
 \text{Cumulative mass loss} \\
 \text{from product within a} \\
 \text{packaging system}
 \end{array}
 =
 \begin{array}{l}
 \text{Water uptake by} \\
 \text{packaging materials} \\
 \text{due to adsorption}
 \end{array}
 +
 \begin{array}{l}
 \text{Cumulative mass loss} \\
 \text{from product by} \\
 \text{evaporation}
 \end{array}
 +
 \begin{array}{l}
 \text{Cumulative mass loss} \\
 \text{from product by} \\
 \text{respiration}
 \end{array}
 \tag{5.83}$$

A mathematical representation of the steady-state mass balance is:

$$WL_{pr} = M_{wv} + m_{fpr}t + m_{resp}t \tag{5.84}$$

where WL_{pr} = cumulative mass loss from product in bulk storage (kg).
 t = time over which mass loss is assessed (s).

Appendix 4 (Practical Guide to the Steady-state Mass Transfer Simulation Model) describes the use of this simple database-linked simulation model.

5.4. MODEL IMPLEMENTATION

The two dynamic mathematical models were developed into computer simulation software entitled ‘Packaging Simulation for Design’ (or PackSim). Both simulation tools were dynamic in nature so required the use of an Ordinary Differential Equation (O.D.E.) solver to calculate the solutions to these simultaneous equations. The following sections will cover the solution method implemented in this software, the software language used and finally the structure that was implemented in the coding.

5.4.1. Solution Method

The Runge-Kutta-Fehlberg method was utilised for solution of the ODEs used in both the dynamic pre-cooling and bulk storage models implemented in the PackSim code. Merts (1996) outlined the benefits of using this ODE integrator.

5.4.2. Computer Implementation

5.4.2.1. *Dynamic ‘Packaging Simulation for Design’*

An internationally recognised standard programming language, C++, was utilised for programming, and in particular, the fifth generation, Rapid Application Development (RAD) software, C++ Builder[®] (Version 1.0, developed by Borland International Inc., Scotts Valley, California). This software has the ability to run on any 32-bit operating system (primarily Windows 95, Microsoft Corporation, Redmond, WA).

This dynamic simulation model incorporated the equations for the pre-cooling model discussed in Section 5.1 and the bulk storage model discussed in Section 5.2. The structure of the code was object-oriented, which is particularly beneficial as it allows the ‘plugging-in’ of component mathematical models, and provides allowance for retrofit of new, improved component models. An outline of the component linkages within the dynamic simulation software is presented in Figure 5.10.

The input datafiles, developed for ‘PackSim’, contain the data required to implement a successful solution of the ODEs. This datafile includes information regarding the product, fluid and packaging materials, a description of the system under investigation and a description of the flows across the external as well as the discretised internal system boundaries.

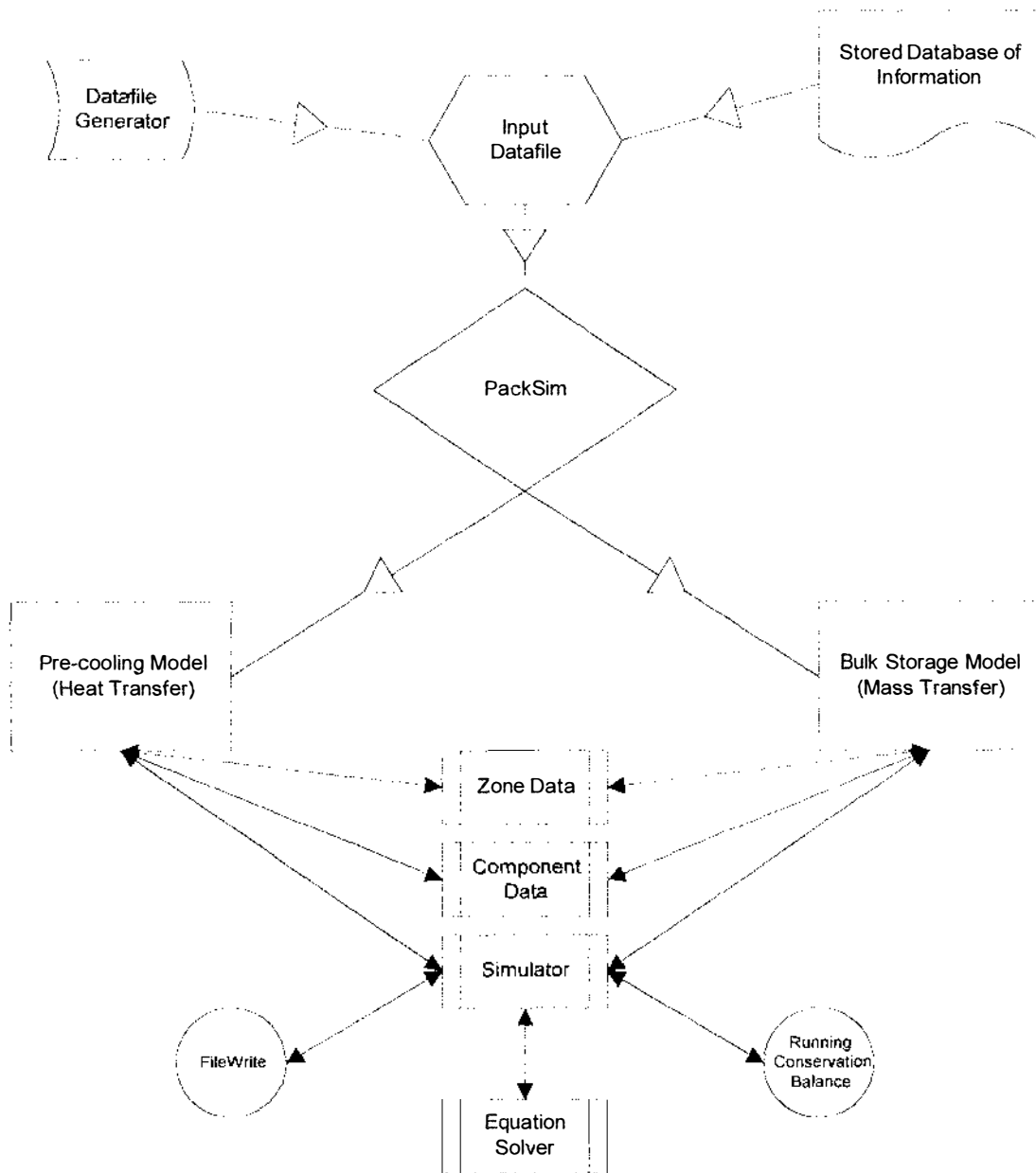


Figure 5.10. Structure of the dynamic simulation system and the individual component linkages.

The datafile generator used for assembly of the data for implementation into the ‘PackSim’ model was developed using Microsoft Excel (Microsoft Corporation, Redmond, WA), a spreadsheet package, which allows rapid, yet efficient calculation of the necessary data. The datafile generator required system specific data for the product, fluid, package and packaging materials for each configuration (the required information varied depending upon which model, pre-cooling or bulk-storage, was being used). These information are summarised in Table 5.2.

Table 5.2.

Specific data required by the datafile generator to create the 'PackSim' input datafile for both the pre-cooling simulation model and the bulk-storage simulation model.

Pre-cooling Simulation Model	Bulk Storage Simulation Model
<i>Package Properties</i>	<i>Package Properties</i>
Dimensions of package	Dimensions of package
Velocity of fluid into, and around package	Velocity of fluid into, and around package
Area of ventilation	Area of ventilation
Flow velocity profile	Flow velocity profile
Number of internal zones in each direction	Number of internal zones in each direction
Number of external zones	Number of external zones
Number of different packaging materials	Number of different packaging materials
<i>Product Properties</i>	<i>Product Properties</i>
Specific heat capacity	Temperature
Thermal conductivity	Water activity
Radius of each item	Mass transfer coefficient
Respiratory coefficients (if required)	Respiration rate
Number of product items	Number of product items
Mass of individual product	Mass of individual product
Volume of individual product	Volume of individual product
Surface area of individual product	Surface area of individual product
<i>Fluid Properties</i>	<i>Fluid Properties</i>
Specific heat capacity	Temperature
Density	Atmospheric pressure
Thermal conductivity	Density
Viscosity	
<i>Packaging Material Properties</i>	<i>Packaging Material Properties</i>
Specific heat capacity	Material adsorption coefficients
Density	Material mass transfer coefficient
Thermal conductivity	Material thickness
Material thickness	
<i>External Zone Properties</i>	<i>External Zone Properties</i>
Initial fluid temperature	Fluid temperature
Final fluid temperature	Fluid relative humidity
<i>Internal Zone Properties</i>	<i>Internal Zone Properties</i>
Initial fluid temperature	Initial fluid relative humidity
Initial product temperature	
<i>For each Zone Boundary:</i>	<i>For each Zone Boundary:</i>
Dimensions of the zone boundary	Dimensions of the zone boundary
Area of boundary occupied by each mode of heat transfer	Area of boundary occupied by each mode of mass transfer

The datafile generator was used to manipulate these input data into a smaller number of specific data, which summarised the physical system for modelling. The resulting data, which are then transferred to the simulation model for implementation, are described in Table 5.3.

Table 5.3.

Specific data created by the datafile generator as an input datafile for both the pre-cooling simulation model and the bulk-storage simulation model.

Pre-cooling Simulation Model	Bulk Storage Simulation Model
<i>Package Properties</i>	<i>Package Properties</i>
Number of internal zones in each direction	Number of internal zones in each direction
Number of external zones	Number of external zones
Number of boundaries in each direction	Number of boundaries in each direction
Number of different packaging materials	Number of different packaging materials
<i>Product Properties</i>	<i>Product Properties</i>
Specific heat capacity	Temperature
Thermal conductivity	Water activity
Radius of each item	Mass transfer coefficient
Respiratory coefficients (if required)	Respiration rate
<i>Fluid Properties</i>	<i>Fluid Properties</i>
Specific heat capacity	Temperature
Density	Atmospheric pressure
Thermal conductivity	Density
<i>Packaging Material Properties</i>	<i>Packaging Material Properties</i>
Specific heat capacity	Material adsorption coefficients
Material thickness	Material mass transfer coefficient
<i>Natural Convection Data</i>	Material thickness
Correction factor	<i>External Zone Properties</i>
Distance between product items	Fluid temperature
<i>External Zone Properties</i>	Initial fluid relative humidity
Initial fluid temperature	Final fluid relative humidity
Final fluid temperature	<i>Internal Zone Properties</i>
<i>Internal Zone Properties</i>	Fluid volume
Initial fluid temperature	Initial fluid relative humidity
Fluid mass in zone	Product mass in zone
Initial product temperature	Product – Fluid KA value
Product mass in zone	Codes for boundaries contacting zone
Product – Fluid UA value.	<i>Packaging Material Data for each Zone</i>
Codes for boundaries contacting zone	Packaging material present (if required)
<i>For Zone Boundaries in each direction:</i>	Packaging material mass
Status of zones on each side of boundary	Mass flow per unit pressure for each mode
Number of such zones	of mass transfer involving packaging
	materials
Packaging material present (if required)	<i>For Zone Boundaries in each direction:</i>
Packaging material mass	Status of zones on each side of boundary
Velocity of fluid across boundary	Number of such zones
UA value across the boundary for	Velocity of fluid across boundary
each mode of heat transfer	KA value across the boundary for each
	mode of mass transfer

The results output from the simulation programme was designed to be brief, yet provide the user with some information as to the accuracy of the modelling solution (the information presented in this results file is described in Table 5.4). A system energy (pre-cooling model) or mass (bulk storage model) balance was completed for each model run and its result presented at the base of the datafile.

Table 5.4.

Information delivered in the ‘PackSim’ results file for both the pre-cooling simulation model and the bulk-storage simulation model.

Pre-cooling Simulation Model	Bulk Storage Simulation Model
Description of packaging system	Description of packaging system
Time of output	Time of output
Fluid temperature for each zone	Relative humidity for each zone
Product temperature for each zone	Product mass for each zone
Successful / Failed solver iterations	Packaging material mass for each zone
Initial and final system energies	Successful / Failed solver iterations
System energy balance	Initial and final system masses
	System mass balance

The guidelines for the successful use of ‘Packaging Simulation for Design’ are included as Appendix 3, whilst the executable code is included as Appendix 5 (on diskette). The author and Massey University hold the full source code.

5.4.2.2. *Steady-state ‘Weight Loss Simulator’*

This simulator incorporated the equations presented for the steady-state bulk storage scenario presented in Section 5.3. In development of this steady-state simulation tool, ease and accuracy of use as well as the ability for use on most computer systems was paramount.

Once again, C++ Builder was utilised for programming. The software was developed so that the user (to reduce the incidence of inaccurate system specification) performed the calculations within the code, with manipulation of a small number of factors. The input data required to implement the simulation model are described in Table 5.5. These data include information regarding the product, fluid and packaging materials, as well as a description of the system under investigation. The results file briefly summarises the results for the packaging system.

Table 5.5.
Specific data required for the ‘Weight Loss Simulator’.

Input data for ‘Weight Loss Simulator’	
<i>Product Properties</i>	<i>Packaging Configuration Properties</i>
Product, type and number	Package dimensions
Mass transfer coefficient	Package porosity factor
Respiration rate	Number of product items in package
Mass of a single product item	Number of boundary packaging materials
Surface area of a single product item	Number of internal packaging materials
Water activity	<i>Packaging Material Properties</i>
<i>Storage Conditions</i>	Total vent area
Fluid type	Total vent area with fluid flow
Atmospheric Pressure	Fluid flow rate
Storage facility temperature	Material mass
Storage facility relative humidity	Material area
In-package fluid temperature	Material thickness
In-package product temperature	Material effective diffusivity
	Material adsorption coefficients

The results output is presented to the user on the screen, but is also stored in a results file (SimResults.txt) in the root directory for the program (the information delivered in this file is described in Table 5.6). This results file is designed to allow easy manipulation of data within a spreadsheet for graphing of results.

Table 5.6.
Information delivered in the ‘Weight Loss Simulator’ results file.

‘Weight Loss Simulator’ Results	
Packaging system description including:	Initial packaging material mass
- product, variety and size	Final packaging material mass
- package construction	Packaging material water vapour uptake
Initial fluid mass	Steady-state internal fluid relative humidity
Final fluid mass	Steady-state rate of product water loss
Fluid water vapour uptake	Steady-state rate of product respiratory loss

The structure of this simulator is shown diagrammatically in Figure 5.11, whilst the essential workings and guidelines for use are presented in Appendix 4. A copy of the executable code for this simulation software is included as Appendix 5 (on diskette).

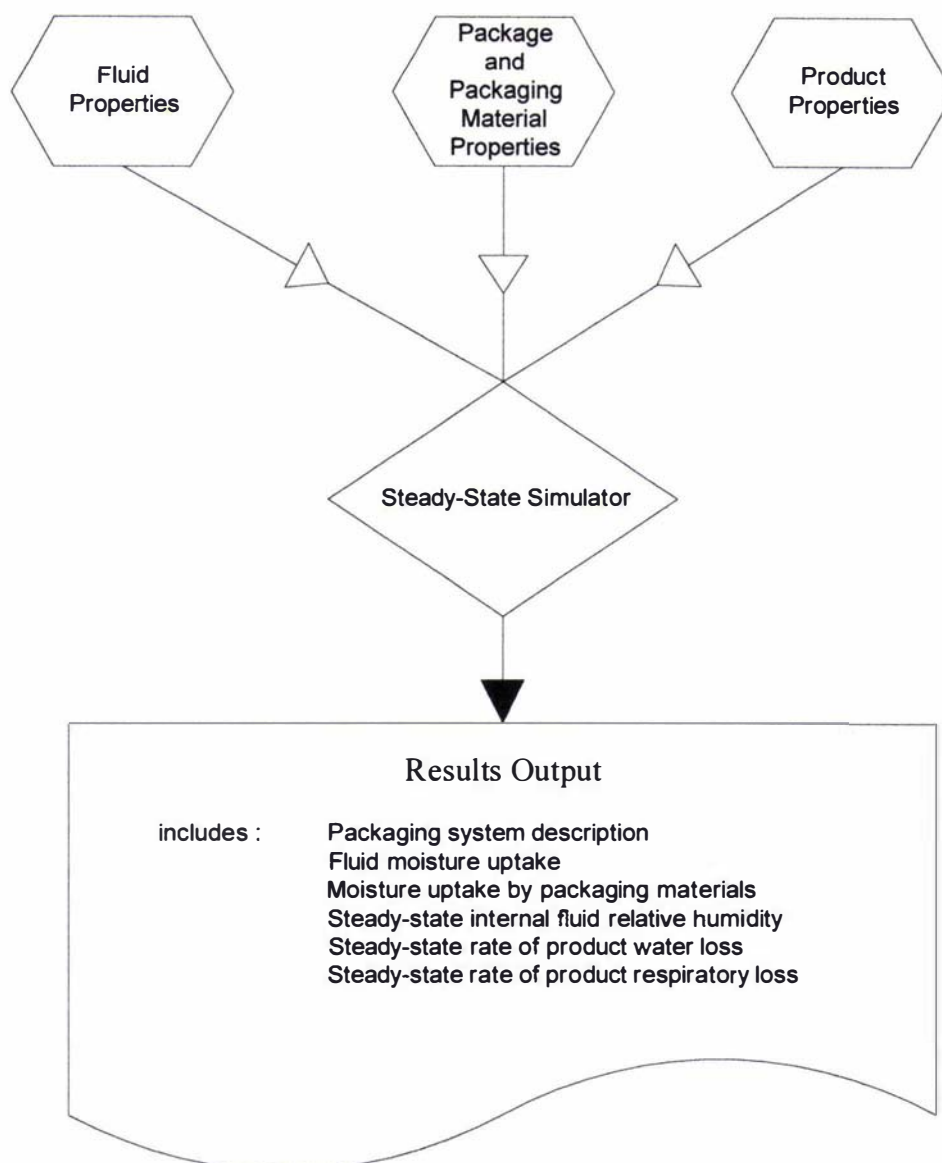


Figure 5.11. Structure of the steady-state simulator and the individual component linkages.

5.5. CONCLUDING REMARKS

This chapter has outlined the generalised mathematical equations used to explain the complex heat and mass transfer relationships within horticultural packaging systems. These generalised equations require system specific data inputs, many of which are covered in Appendix 2.

CHAPTER 6

DETERMINATION OF VELOCITY PROFILES FOR HORTICULTURAL PACKAGES

6.1. INTRODUCTION

This chapter describes the CO₂ trace pulsing technique used to estimate in-package air velocity profiles for different packaging configurations. This profile was used to generate inter-zone velocity data for input to both the pre-cooling and bulk storage simulation models.

6.2. DEVELOPMENT OF A FLOW CHARACTERISATION AND VISUALISATION TECHNIQUE

Published quantitative information about fluid movement through horticultural package configurations is sparse and this limits the ability of all modellers to predict package heat and mass transfer performance. As was outlined in Chapter 1, the data scarcity will represent an increasing problem as market demands lead to more diverse package sizes and shapes. Methods available for estimating in-package velocities include:

1. Use of computational fluid dynamics software (such as *PHOENICS*[®] or *FLOW 3-D*[®]), as discussed in Chapter 2.
2. Use of flow visualisation and scale modelling techniques (Lovatt *et al.*, 1993c).
3. Direct measurement.

For the geometries under consideration, Computational Fluid Dynamics techniques are difficult to use as they require emulation of the complex package geometry with a control volume grid. This is both time consuming and requires significant computational power to provide a solution to the flow pattern. Direct measurement

using velocity measurement devices is difficult in high-density horticultural packages because a relatively bulky instrument is used within the package, thereby changing the package configuration and providing inaccurate data.

Flow visualisation techniques can be classified into a number of groups. These include wall tracing methods (the spreading of a film on the wall of an object to assess surface flow phenomena); tuft methods (tufts are attached to a surface to indicate flow direction); direct injection methods (gas or liquid tracers are injected into the flow stream and their flow paths monitored); electrically controlled tracer methods (these include hydrogen bubble generators and smoke tests) and optical methods (include holograph or shadowgraph methods which indicate density gradients in fluids) (Nakayama, 1993).

In the present research, a direct injection tracer method was developed utilising air as the flow medium and CO₂ as the tracer. CO₂ was utilised as the tracer because instrumentation was available to measure real-time concentration changes in different positions within a package configuration. CO₂ measurement capability is available in the horticultural industry, making the technique inexpensive, thus allowing many horticultural packaging systems to be characterised quickly and easily.

6.2.1. Development of the CO₂ Trace Pulsing Technique

Construction of a system in which a pulse of CO₂ tracer was injected into the inflow stream prior to entry to the full scale model of the package was undertaken (Figure 6.1). A 6.5 mm (4 mm internal dimension, ID) stainless steel hollow pipe or 6.5mm (3.8 mm ID) silicone flexi-pipe (depending on geometry) was connected to a LI - 6262 constant flow gas analyser (LI-COR Inc. Lincoln, Nebraska, USA) so it could be positioned unobtrusively at various places in the package to sample the airflow. In construction of the initial test package, one wall was constructed of Perspex to aid in positioning of the pipe. This Perspex screen also allowed for viewing of smoke patterns (used as a supplementary tool in localised regions of the package to confirm flow directional phenomena).

After injection, the CO₂ concentration at a test location was continuously measured to produce a profile such as that presented in Figure 6.2. The time from insertion of the CO₂ until the time of the CO₂ concentration increase was used to indicate the direct flow stream velocity on the shortest possible flow pathway to the location.

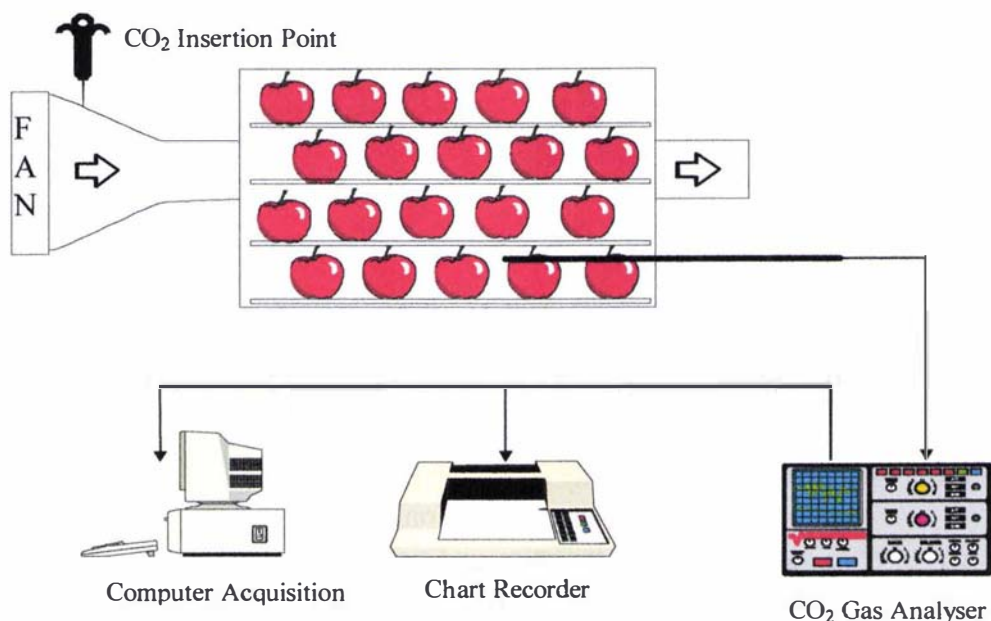


Figure 6.1. CO₂ Tracer Pulsing System set-up.

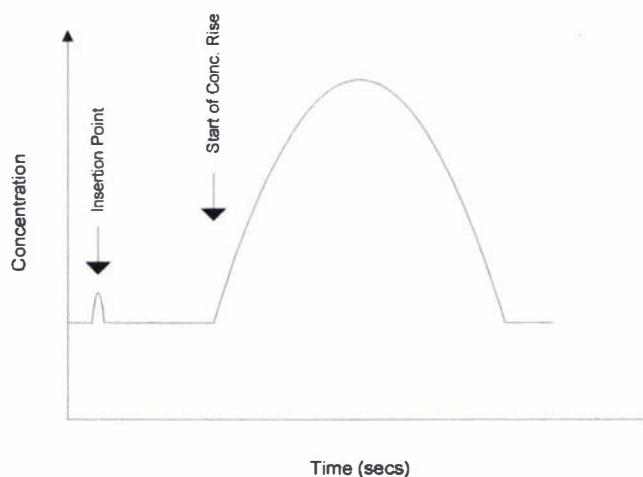


Figure 6.2. Typical concentration versus time curves, which are used to determine flow profiles for different packaging systems.

6.2.2. Calculation of Flow-Relativity Coefficients

Complete characterisation of a package profile would require simultaneous measurement of direct flow stream velocity in all three dimensions (x , y and z directions). This was not possible so each direction was assessed individually. Using data from a number of locations, and measurements for each of the flow path length and the time for first CO₂ arrival, a profile of velocity-relativity coefficients (VRC 's) was generated.

In any plane (vertical or horizontal) perpendicular to the dominant flow direction, one-dimensional velocity relativity coefficients were generated using Eqn. (6.1). These coefficients were taken to indicate the relative proportion of the total flow for each dimension in the packaging system.

$$VRC_i = \frac{\left(\frac{L_i}{\Delta t_i}\right)}{\sum \left(\frac{L_i}{\Delta t_i}\right)} \quad (6.1)$$

where VRC_i = velocity relativity coefficient for position i in one direction in a packaging system (dimensionless).

Δt_i = time between insertion and rise in CO₂ concentration for position i in a packaging system (s).

L_i = length of flow path to measurement position i (m).

Mass (and volumetric at constant density) flow is conserved. In typical horticultural packages, the cross-sectional area down each pathway, L , changes significantly and mean cross-sectional area is not known precisely. Further, there is often only cross-mixing between the more obviously visible flow channels. By using the time for first arrival of CO₂, it was assumed that this CO₂ followed the most direct route, unaffected by cross-mixing effects. Full geometric analysis to remove this assumption would be a very substantial undertaking and was considered beyond the scope of this work. Operating experience suggested that the VRC 's determined by Eqn. (6.1) were broadly representative of the flow distribution, so more sophisticated data analysis was not attempted.

For the types of packaging systems assessed in this research, the observations of smoke transport indicated that flow effects other than in the dominant fluid flow direction were minor and could be neglected. This reduced the complexity in calculation of flow profiles in the packaging system (as only two directions need be analysed for full characterisation), but this simplification may not be appropriate for all packaging systems.

To aid data visualisation 'best fit' profile curves were drawn using a computer graphics software package to interpolate the flow-relativity coefficients. Such curves were constructed for the vertical and horizontal 'planes' in the package (Figure 6.3). For convenience, as the fluid approaches the physical boundaries, the flow was drawn showing reduction to zero at the boundary. Thus, the profile curves are indicative and not a quantitative tool (but they would aid any interpolation process).

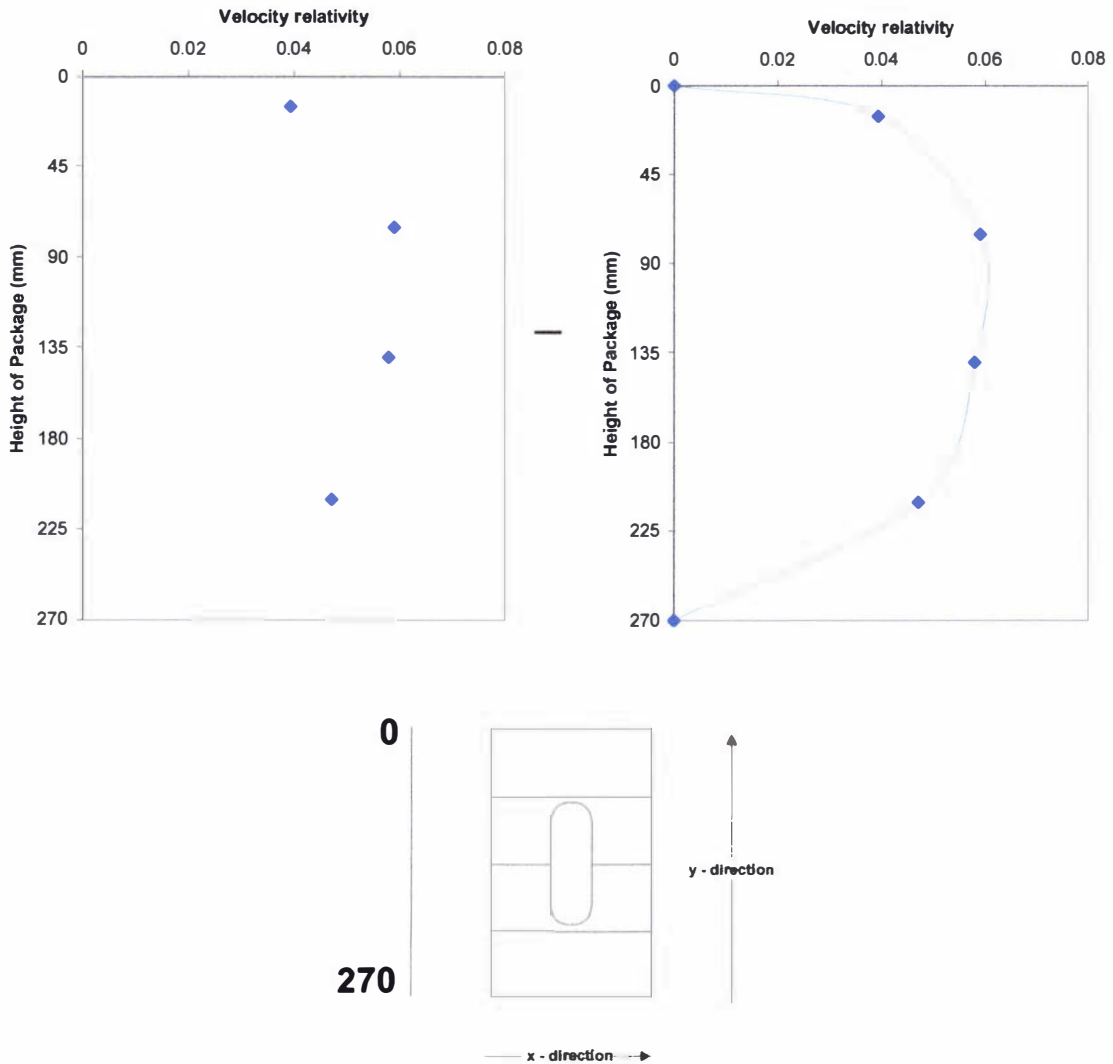


Figure 6.3. Methodology used in development of single plane (y direction) velocity relativity curves for positions in a horticultural package. The flow into the packaging system is in the z direction (into the page).

A number of assumptions were implied by the method of analysis of observed flow profiles for each plane:

- The CO_2 was assumed to be perfectly mixed in the incoming gas flow as it entered the package (this requires turbulent mixing conditions in the inlet port, and sufficient time, and length for mixing). To ensure that CO_2 is well mixed into the air stream as it enters the package requires sufficient length and turbulence in the inlet injection port, downstream of the fan (as shown in Figure 6.1). Direct injection into the fan's turbulent exit stream was used.
- As has been stated, the CO_2 causing the initial concentration increase follows the shortest possible flow path to the measurement point. These path lengths were

measured for each tracer measurement point in a package, using so-called 'streamlines'. The streamlines were the measured lengths between the injection port in the apparatus and the measurement point in the package down the major visually identifiable flow channel.

- The temperature of the cooling medium was assumed to have no effect on the flow profile through the package. Experimentation was conducted to ensure that this assumption was valid. Two air temperatures (22°C and 39°C) were used, whilst product temperatures were maintained close to 8°C. The results (Figure 6.4) showed that fluid temperature had little effect on the flow profile.
- Changing the inlet fluid velocity has little effect on the flow-relativity through the package. Experimental testing was conducted at two air velocities (0.45m.s⁻¹ and 1.5m.s⁻¹), whilst product temperatures were maintained close to 8°C. Results showed that changing inlet air velocity had little effect on flow-relativity curves (Figure 6.5).

In each layer, positioning of the sampling pipe at the central position of any zone within a layer was not physically possible, nor was the central position necessarily representative of the zone as a whole. A pragmatic approach to sample pipe placement was therefore taken with the samples generally offset sideways or upwards from the central location by a constant systematic offset. The actual position is plotted (eg, Figures 6.3 and 6.4) to inform the reader. In analysis, even though the data were not measured from the central position, they were applied for the full zone. The flow visualisation curves are not quantitative and care should be taken in considering them at region edges beyond the last measured data point.

Although the overall technique is not fully based on fundamental principles, it does offer a simple physical system that, with empirical interpretation, provides the necessary information regarding airflow profiles for generating model-input data. Where one-off smoke tests were conducted, the observed visual movement of the smoke, observed through the perspex sidewall, was at a rate consistent with the measured data.

6.2.2.1. Complete Velocity Profiles (with no cross-mixing)

To calculate a complete flow profile (assuming no cross-mixing in the least important dimension) for a packaging system, flow-relativity coefficients for the two directions, other than that of the dominant flow in the system, were combined to give a two-dimensional velocity relativity coefficient (2DVRC).

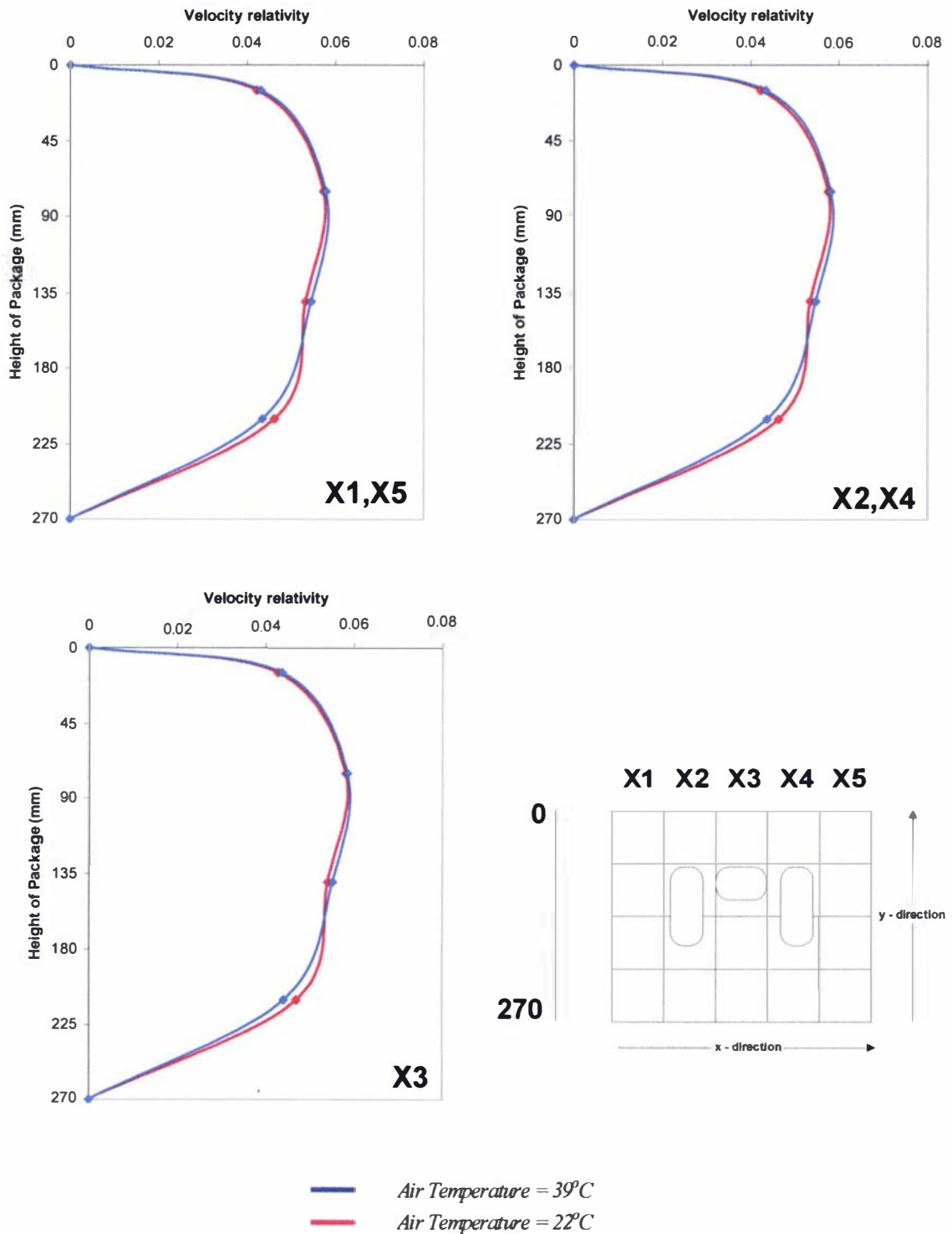


Figure 6.4. Velocity relativity data and visualisation curves for planes down the height (or y direction) at three positions across the width (x direction) in an apple package, at different inlet air temperatures. The data are assumed to be valid for all positions in the direction of the flow into the system, in this case the z direction (into the page).

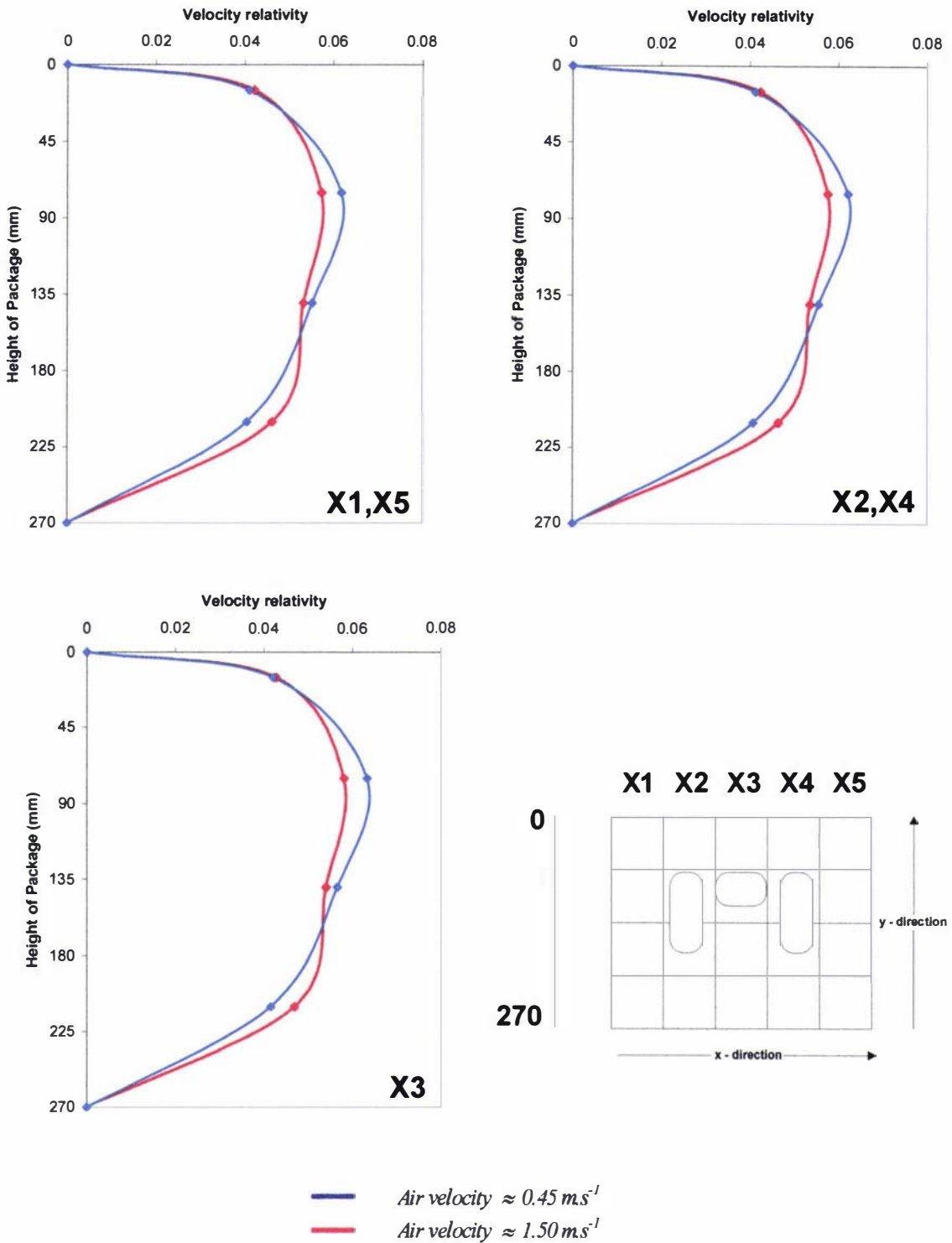


Figure 6.5. Velocity relativeity data and visualisation curves for planes down the height (or y direction) at three positions across the width (x direction) in an apple package, at different inlet air velocities. The data are assumed to be valid for all positions in the direction of the flow into the system, in this case the z direction (into the page).

If the dominant flow is in the x direction (perpendicular to both y and z):

$$2DVRC_i = VRC_{i,y} \times VRC_{i,z} \tag{6.2}$$

If the dominant flow is in the y direction:

$$2DVRC_i = VRC_{i,x} \times VRC_{i,z} \tag{6.3}$$

If the dominant flow is in the z direction:

$$2DVRC_i = VRC_{i,x} \times VRC_{i,y} \tag{6.4}$$

where $2DVRC_i$ = 2 - dimensional velocity relativity coefficient for a zone boundary at position i .

$VRC_{i,x}$ = velocity relativity coefficient for position i in the x direction in a packaging system (dimensionless).

$VRC_{i,y}$ = velocity relativity coefficient for position i in the y direction in a packaging system (dimensionless).

$VRC_{i,z}$ = velocity relativity coefficient for position i in the z direction in a packaging system (dimensionless).

For example, experimental work conducted using the CO₂ tracer system led to the velocity relativity coefficients for a 4-layer apple package, shown in Table 6.1. The coefficients have been determined from experimental data for the x - direction (width) and y - direction (height) in the package (because the dominant flow direction was down the z direction of the package).

Table 6.1.

Two-dimensional velocity relativity coefficients, as calculated from the VRC 's presented in Figure 6.5 for positions X1 – X5, for the 4-layer apple package.

		VRC_x				
		0.3	0.15	0.1	0.15	0.3
VRC_y	0.14	0.042	0.021	0.014	0.021	0.042
	0.41	0.123	0.0615	0.041	0.0615	0.123
	0.36	0.108	0.054	0.036	0.054	0.108
	0.09	0.027	0.0135	0.009	0.0135	0.027

The $2DVRC$ can be used to calculate a two-dimensional velocity profile for the packaging system:

$$v_i = \frac{m_{in}(2DVRC_i)}{\rho_f A_{i,ff}} \quad (6.5)$$

where v_i = fluid velocity across the zone boundary at position i (m.s^{-1}).
 m_{in} = total mass flow rate into package (kg.s^{-1}).
 ρ_f = density of fluid (kg.m^{-3}).
 $A_{i,ff}$ = actual area of fluid-fluid boundary for zone at position i (m^2).

In model application, the data from Table 6.1 were applied for each plane of zones in the dominant flow direction in the packaging system, with no cross-flow between zones to either side, or above or below (ie flow paths are solely parallel, as shown in Figure 6.6). In all cases investigated experimentally, the values of $A_{i,ff}$ were equal.

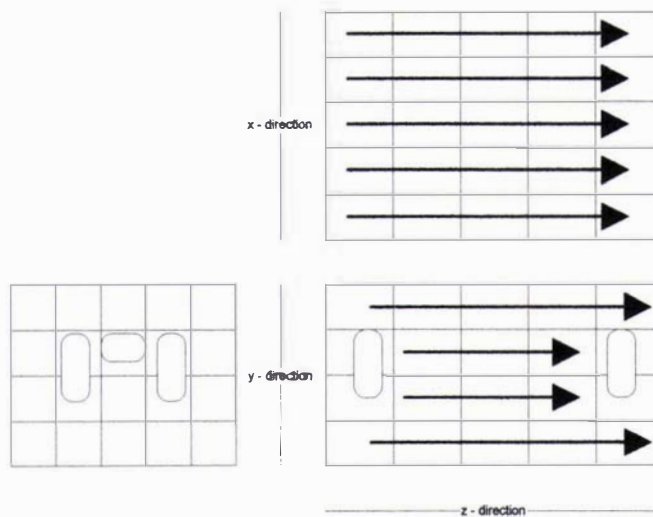


Figure 6.6. Allowable pathways of fluid flow as a result of assuming that flow in the dominant flow direction does not undergo cross-mixing (note that flow in this case is into the end elevation).

6.2.2.2. Complete Velocity Profiles (with cross-mixing)

To calculate a complete velocity profile (including cross-mixing in the third dimension, Figure 6.7) for a packaging system, velocity relativity coefficients for all three directions in the system would be required.

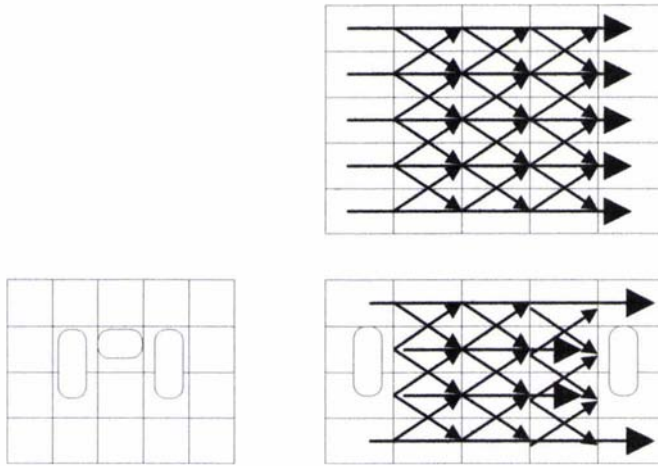


Figure 6.7. Illustration of pathways for fluid flow exhibiting cross-mixing between zones in the counter-current flow directions (note that flow in this case is into the end elevation).

Although the CO₂ tracer technique may be adaptable for this situation, it was not investigated in this research.

6.2.2.3. Measurement of Fluid-Fluid Boundary Areas for 2D Velocity Profiles

The fluid-fluid boundary area utilised in calculation of the two-dimensional velocity profiles may not be the total zone boundary area. In this case, the true area of fluid flow is utilised (as shown in Figure 6.8). This results in Eqn. (6.6).

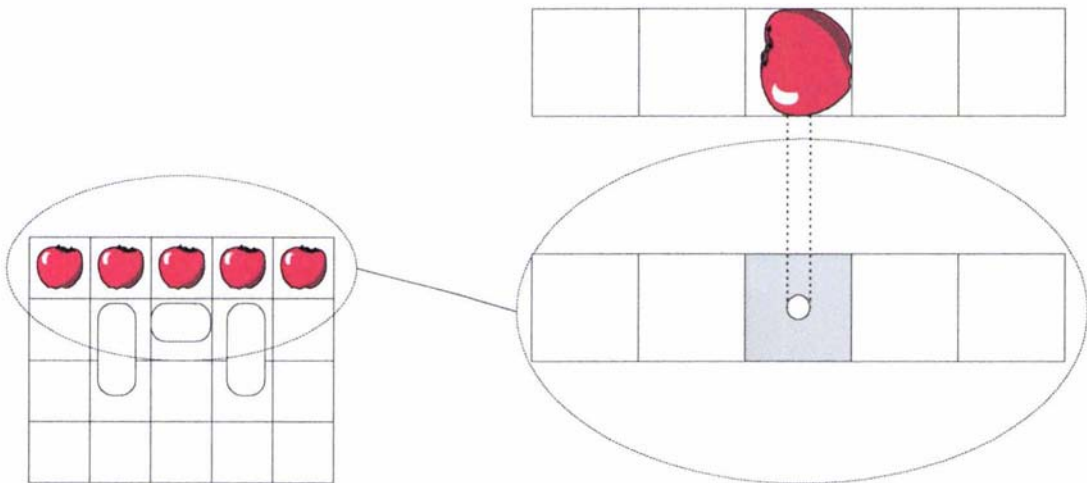


Figure 6.8. Concept utilised for measurement of actual fluid-fluid boundary areas (the shaded region indicates $A_{i,ff}$ for an individual position).

$$A_{i,flfl} = A_i - (A_{i,prpr} + A_{i,prfl} + A_{i,flpr} + A_{i,flpkfl} + A_{i,flpkpr} + A_{i,prpkfl} + A_{i,prpkpr}) \quad (6.6)$$

where A_i	=	total area of the i^{th} zone boundary (m^2).
$A_{i,prpr}$	=	area of product-product boundary for zone at position i (m^2).
$A_{i,prfl}$	=	area of product-fluid boundary at position i (m^2).
$A_{i,flpr}$	=	area of fluid-product boundary at position i (m^2).
$A_{i,flpkfl}$	=	area of fluid-packaging-fluid boundary at position i (m^2).
$A_{i,flpkpr}$	=	area of fluid-packaging-product boundary at position i (m^2).
$A_{i,prpkfl}$	=	area of product-packaging-fluid boundary at position i (m^2).
$A_{i,prpkpr}$	=	area of product-packaging-product boundary at position i (m^2).

These area values can be directly related to $A_{i,j}$ values for the various transfer modes ($j = 1$ to 25) discussed in Chapter 5.

6.3. EXPERIMENTAL WORK UNDERTAKEN ON APPLE PACKAGING

Velocity patterns in apple cartons (provided by ENZAFRUIT New Zealand (International)) were characterised. Experimental trials were completed for both the pre - 1996 ‘Standard’ apple packaging (with 125 count fruit, packed in five layers and 150 count fruit, packed in six layers) as well as the 1996 ‘Zeus’ (or Z-Pack) packaging (with 100 count fruit, packed in four layers). These configurations are explained separately.

Both cartons use alternatively aligning ‘Friday’ trays for placement of fruit, resulting in two possible complete package configurations (a plan view of these orientations is shown as Figure 6.9). Experimental velocity characterisation of both tray orientations showed that there was little effect due to Friday tray orientation on the observed profiles (Figure 6.10).

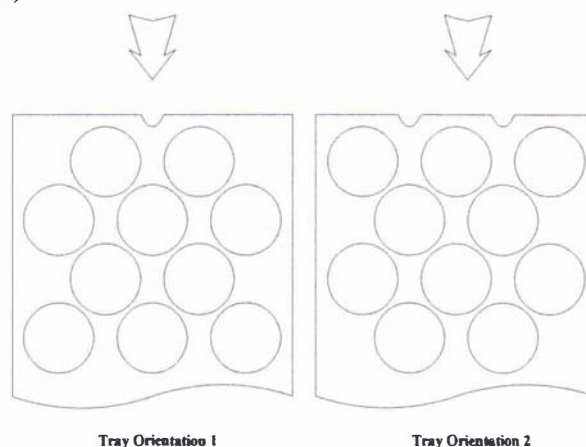


Figure 6.9. Plan view of two possible ‘Friday’ tray orientations in complete package configurations (**NB** these are for the top layer of the package).

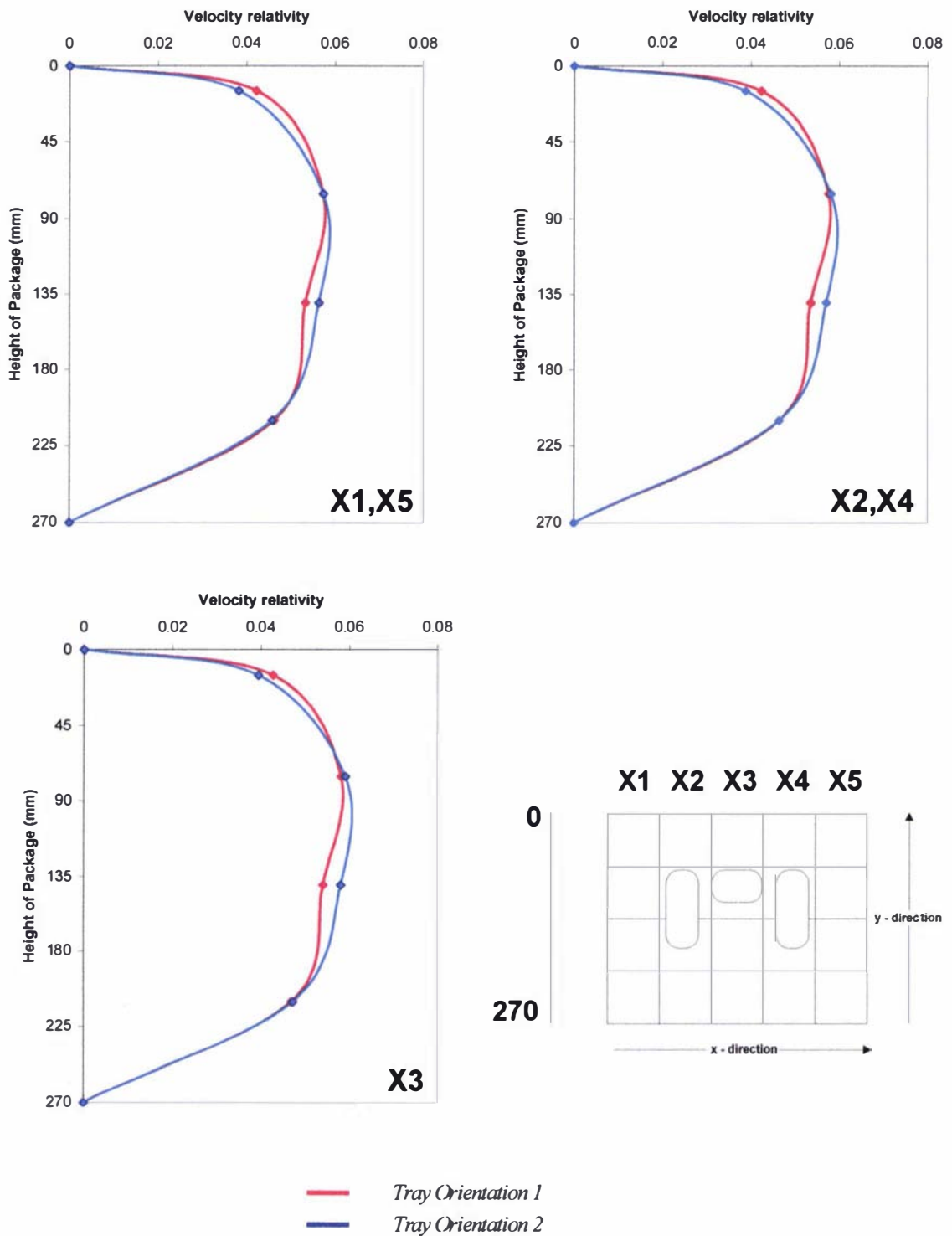


Figure 6.10. Velocity relativity data and visualisation curves for planes down the height (or y direction) at three positions across the width (x direction) in an apple package, with different 'Friday' tray orientations. The data are assumed to be valid for all positions in the direction of the flow into the system, in this case the z direction (into the page).

6.3.1. Pre - 1996 'Standard' Apple Packaging

This package (Figure 6.11) was assembled in two configurations: 1) with 125 count apples (var. 'Fuji'), packed onto five 'Friday' trays, and 2) with 150 count apples (var. 'Fuji'), packed onto six 'Friday' trays. The first configuration was characterised for five positions across the width (or x direction) and five positions down the height (or y direction), whilst the second was characterised for five positions across the width (or x direction) and six positions down the height (or y direction).



Figure 6.11. The 'Standard' apple packaging used in the determination of velocity relativity coefficients.

Both package configurations were assumed to have no cross-mixing with respect to the major flow down the length or z direction. Figures 6.12 and 6.13 present velocity relativity curves for both the width and height of the 5-layer package, whilst Figures 6.14 and 6.15 present curves for the 6-layer configuration. Air short-circuiting along the carton sides and relatively low flow towards the carton bottom are indicated. Smoke test visualisations confirmed these observations.

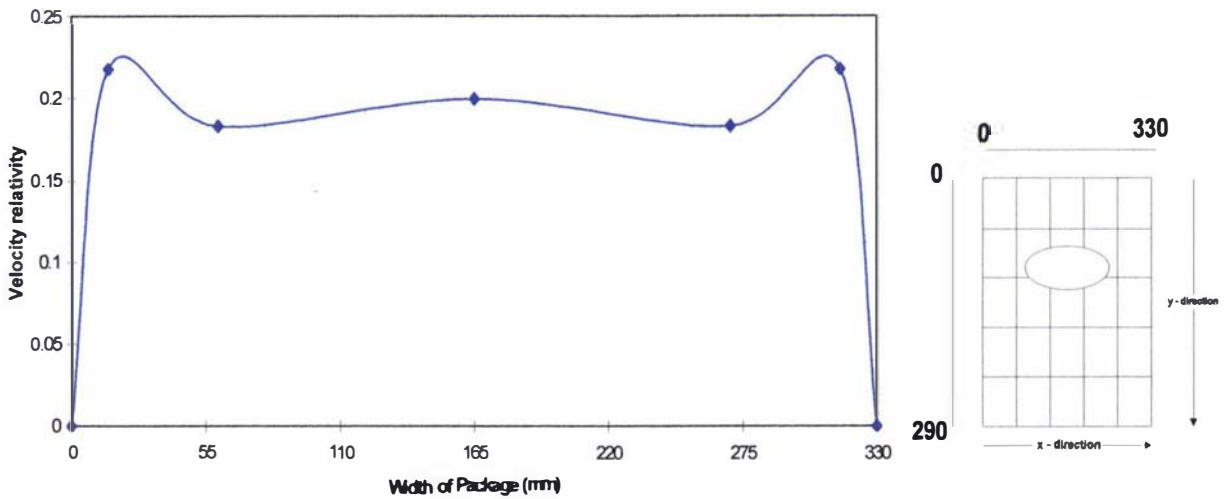


Figure 6.12. Velocity relativeity data and visualisation curve for positions across the width (or x direction) in a 5-layer 'Standard' apple package. The data are assumed to be valid for all positions down the height (or y direction) of the system.

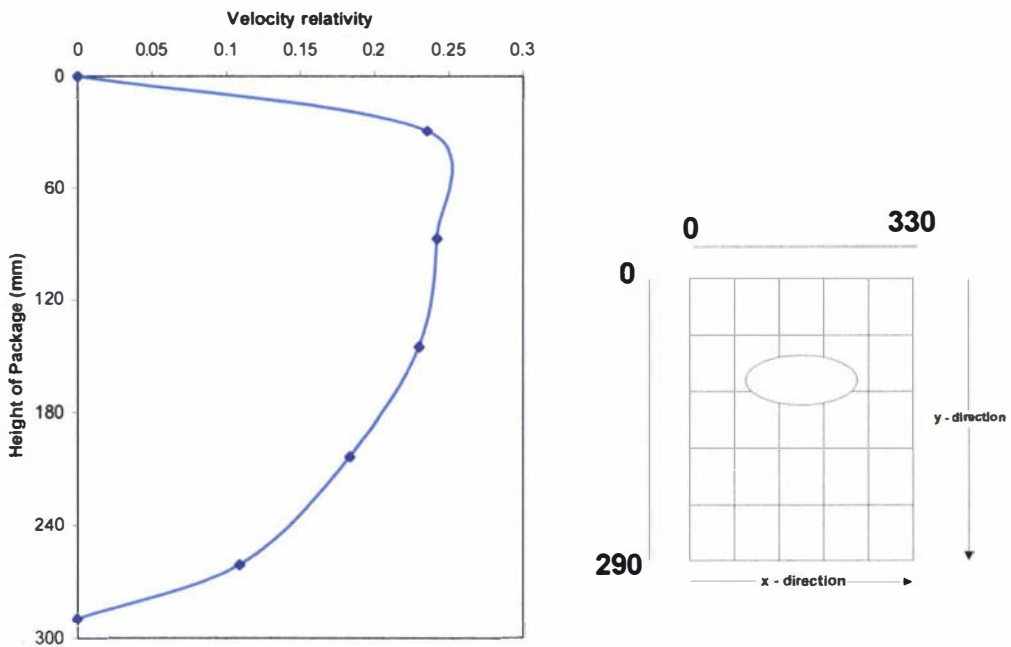


Figure 6.13. Velocity relativeity data and visualisation curve for positions down the height (or y direction) in a 5-layer 'Standard' apple package. The data are assumed to be valid for all positions in the direction of the flow into the system, in this case the z direction (into the page).

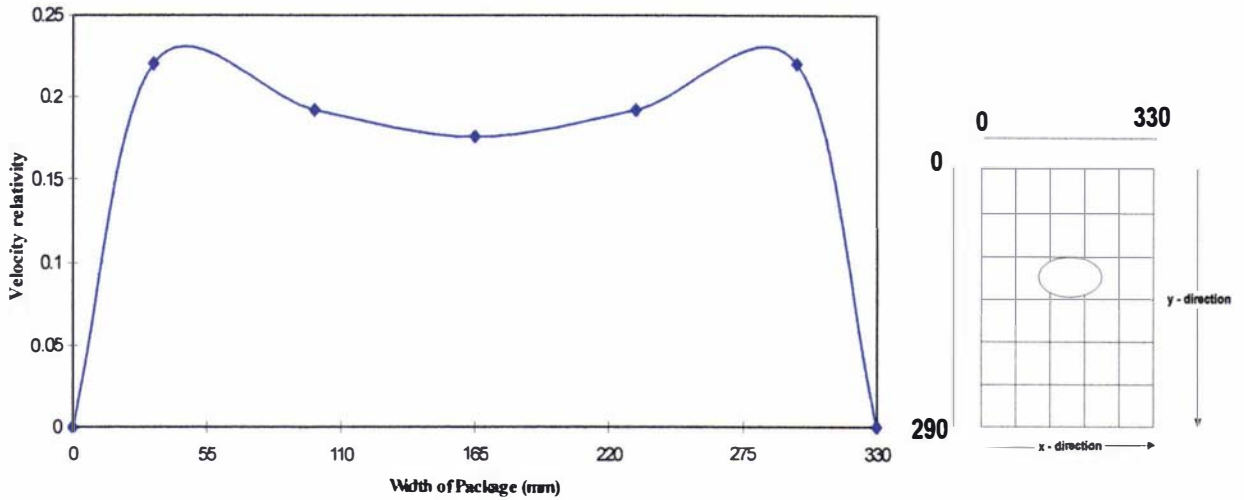


Figure 6.14. Velocity relativeity data and visualisation curve for positions across the width (or x direction) in a 6-layer 'Standard' apple package. The data are assumed to be valid for all positions down the height (or y direction) of the system.

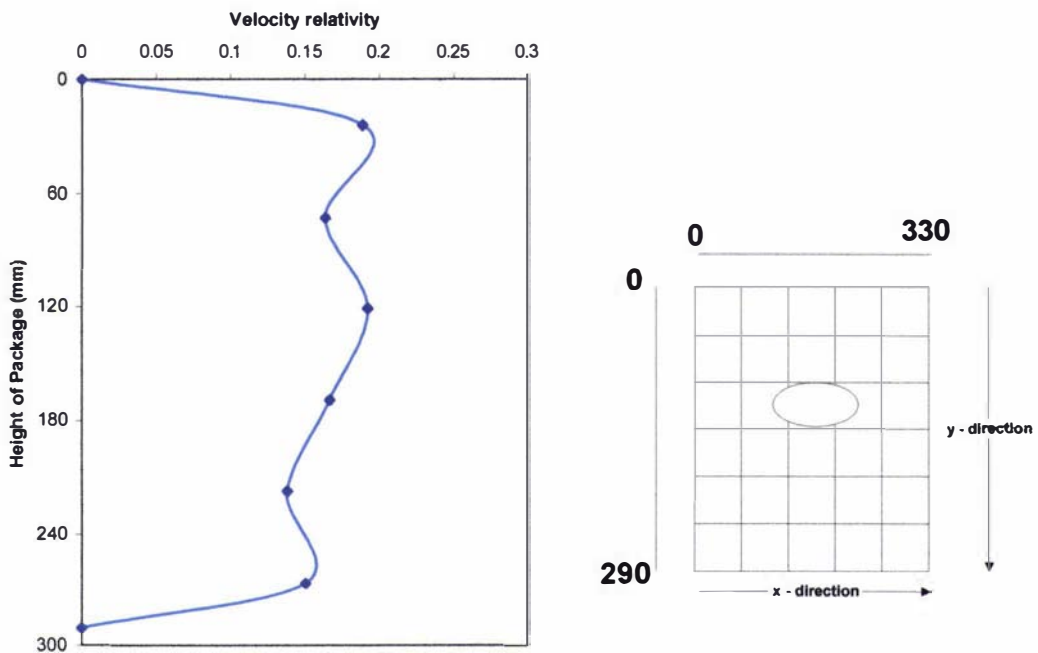


Figure 6.15. Velocity relativeity data and visualisation curve for positions down the height (or y direction) in a 6-layer 'Standard' apple package. The data are assumed to be valid for all positions in the direction of the flow into the system, in this case the z direction (into the page).

The velocity relativity curves for both configurations were combined into two-dimensional velocity relativity curves to produce a profile for each package configuration (Tables 6.2 and 6.3). These profiles assume that the width (*x* direction) of both configurations is divided into 5 zones (to represent the 5 lines of fruit on the ‘Friday’ tray), whilst the height (*y* direction) is divided into 5 zones, for the 5-layer package, and 6 zones, for the 6-layer package. The two-dimensional velocity relativity curves for these configurations are illustrated in Figures 6.16 and 6.17.

Table 6.2.

The two-dimensional velocity relativity profile for the pre-1996, 5-layered ‘Standard’ apple package. The *x* and *y* coordinates are shown in Figure 6.16.

	2DVRC				
	X1	X2	X3	X4	X5
Y1	0.0518	0.0452	0.0414	0.0452	0.518
Y2	0.0532	0.0465	0.0426	0.0465	0.532
Y3	0.0506	0.0442	0.0404	0.0442	0.506
Y4	0.0403	0.0352	0.0322	0.0352	0.403
Y5	0.0241	0.0210	0.0193	0.0210	0.241

Table 6.3.

The two-dimensional velocity relativity profile for the pre-1996, 6-layered ‘Standard’ apple package. The *x* and *y* coordinates are shown in Figure 6.17.

	2DVRC				
	X1	X2	X3	X4	X5
Y1	0.0415	0.0363	0.0332	0.0363	0.0415
Y2	0.0360	0.0314	0.0288	0.0314	0.0360
Y3	0.0423	0.0369	0.0388	0.0369	0.0423
Y4	0.0366	0.0320	0.0293	0.0320	0.0366
Y5	0.0304	0.0265	0.0243	0.0265	0.0304
Y6	0.0331	0.0289	0.0265	0.0289	0.0331

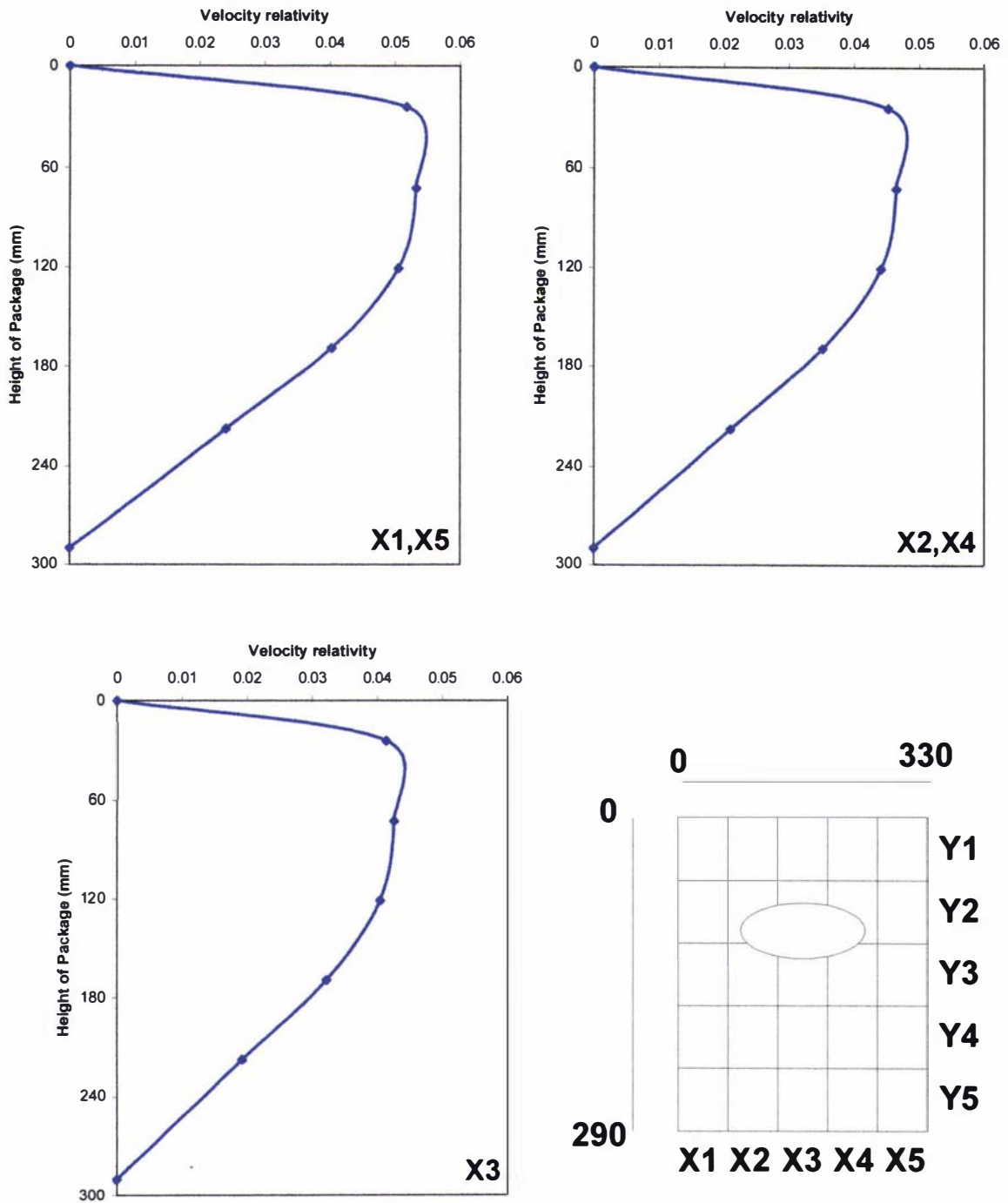


Figure 6.16. Velocity relativeity data and visualisation curves for planes down the height (or y direction) at three positions across the width (x direction) in a 5-layer 'Standard' apple package. The data are assumed to be valid for all positions in the direction of the flow into the system, in this case the z direction (into the page).

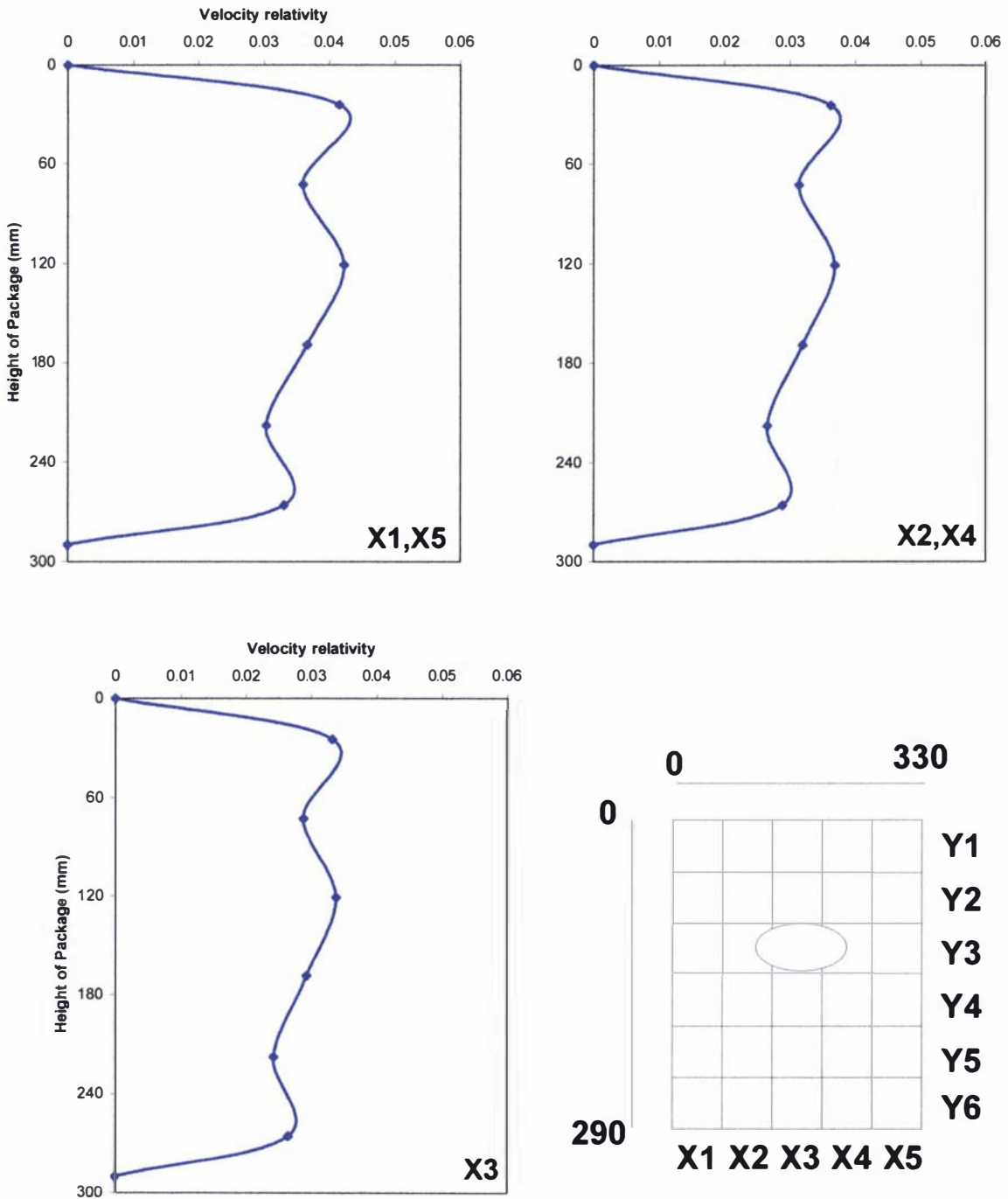


Figure 6.17. Velocity relativeity data and visualisation curves for planes down the height (or y direction) at three positions across the width (x direction) in a 6-layer 'Standard' apple package. The data are assumed to be valid for all positions in the direction of the flow into the system, in this case the z direction (into the page).

6.3.2. 1996 'Zeus' Apple Packaging

This package (Figure 6.18) was assembled with 100 count apples (var. 'Royal Gala'), packed onto four 'Friday' trays. This package was characterised for five positions across the width (or x direction) and four positions down the height (or y direction). This package configuration is used commercially for packaging of export apples by ENZAFRUIT New Zealand (International).

Figures 6.19 and 6.20 present velocity relativity curves for both the width and height of the package with forced flow down the length (or z direction). Velocity relativity curves are also presented for forced flow across the width (or x direction) of the package (Figures 6.21 and 6.22). Both were deemed necessary as palletisation of the 'Zeus' packaging configuration allows for airflow in both z and x directions. During measurement of flows in each of these directions, the vents in the opposing direction were covered to simulate more closely, the flow characteristics experienced in a commercial cooling operation.



Figure 6.18. The 'Zeus' apple packaging used in the determination of velocity relativity coefficients.

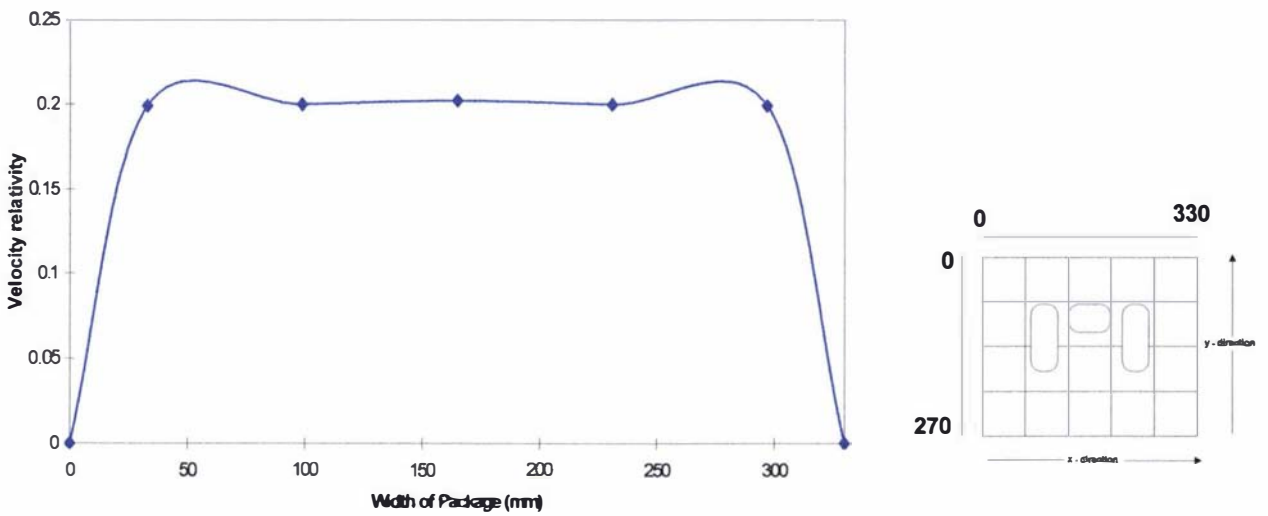


Figure 6.19. Velocity relativity data and visualisation curve for positions across the width (or x direction) in a 4-layer 'Zeus' apple package. The data are assumed to be valid for all positions down the height (or y direction) of the system.

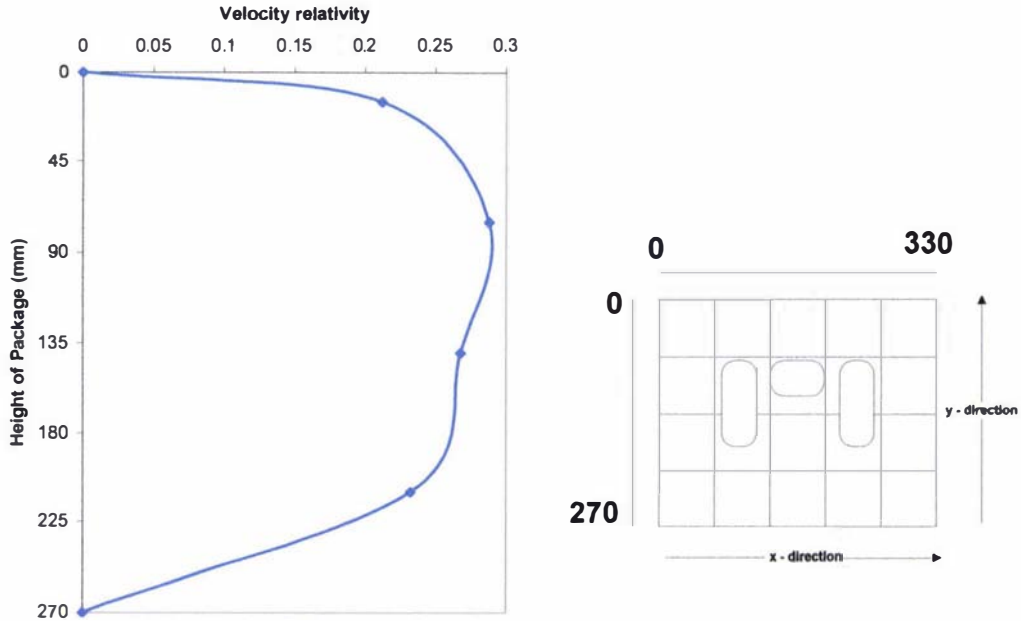


Figure 6.20. Velocity relativity data and visualisation curve for positions down the height (or y direction) in a 4-layer 'Zeus' apple package. The data are assumed to be valid for all positions in the direction of the flow into the system, in this case the z direction (into the page).

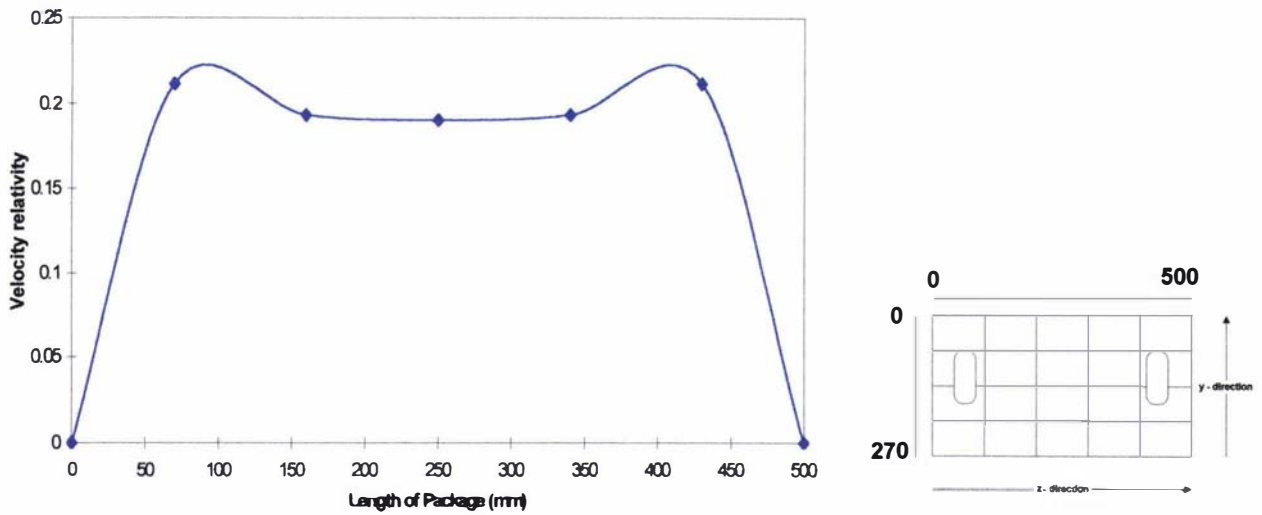


Figure 6.21. Velocity relativeity data and visualisation curve for positions along the length (or z direction) of a 4-layer 'Zeus' apple package. The data are assumed to be valid for all positions down the height (or y direction) of the system.

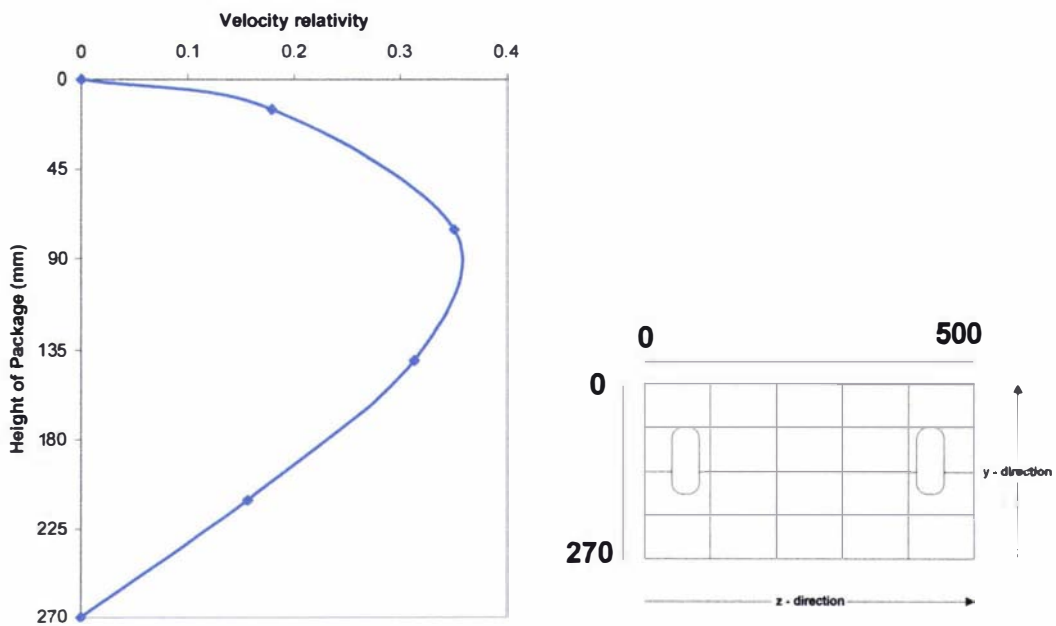


Figure 6.22. Velocity relativeity data and visualisation curve for positions down the height (or y direction) in a 4-layer 'Zeus' apple package. The data are assumed to be valid for all positions in the direction of the flow into the system, in this case the x direction (into the page).

These velocity relativity curves were combined into two-dimensional velocity relativity curves to produce a velocity relativity profile for the package configuration (Tables 6.6 and 6.7). The profile presented in Table 6.4 assumes that the width (x direction) of the package is divided into 5 zones (to represent the 5 lines of fruit on the ‘Friday’ tray), whilst the height (y direction) is divided into 4 zones (to represent the 4 layers in the package). The profile presented in Table 6.5 assumes that the length (z direction) of the package is divided into 5 zones (to represent the 5 lines of fruit in this direction on the ‘Friday’ tray), whilst the height (y direction) is, again, divided into 4 zones. The two-dimensional flow-relativity curves for the z directional flow are visualised in Figure 6.23, whilst for y directional flow, they are visualised in Figure 6.24.

Table 6.4.

Two-dimensional velocity relativity profile for the ‘Zeus’ apple package (flow in the z direction). The x and y coordinates are shown in Figure 6.23.

	2DVRC				
	X1	X2	X3	X4	X5
Y1	0.0422	0.0424	0.0428	0.0424	0.0422
Y2	0.0573	0.0576	0.0581	0.0576	0.0573
Y3	0.0533	0.0535	0.0541	0.0535	0.0533
Y4	0.0463	0.0465	0.0469	0.0465	0.0463

Table 6.5.

Two-dimensional velocity relativity profile for the ‘Zeus’ apple package (flow in the x direction). The y and z coordinates are shown in Figure 6.24.

	2DVRC				
	Z1	Z2	Z3	Z4	Z5
Y1	0.0379	0.0346	0.0341	0.0346	0.0379
Y2	0.0743	0.0678	0.0667	0.0678	0.0743
Y3	0.0663	0.0605	0.0596	0.0605	0.0663
Y4	0.0332	0.0303	0.0298	0.0303	0.0332

6.3.3. A Pallet Layer of 1997 ‘Zeus’ Apple Packages

A commercially utilised pallet-layer-packaging configuration was assembled using seven ‘Zeus’ packages filled with Count 100 apples (*var.* ‘Braeburn’). Flow was separately directed through two opposite faces to give both possible flow patterns in a commercial situation (Figure 6.25). During flow measurement, all vents on the outer boundaries of the pallet layer parallel to the inlet flow were covered to simulate stacking in the pre-cooler (as shown by the – symbols in Figure 6.26). All flow measurements were conducted at ambient conditions (approx. 15°C and 70% RH) with inlet air velocity through the vents set at $\approx 1.5 \text{ m.s}^{-1}$ to reflect common commercial practice.

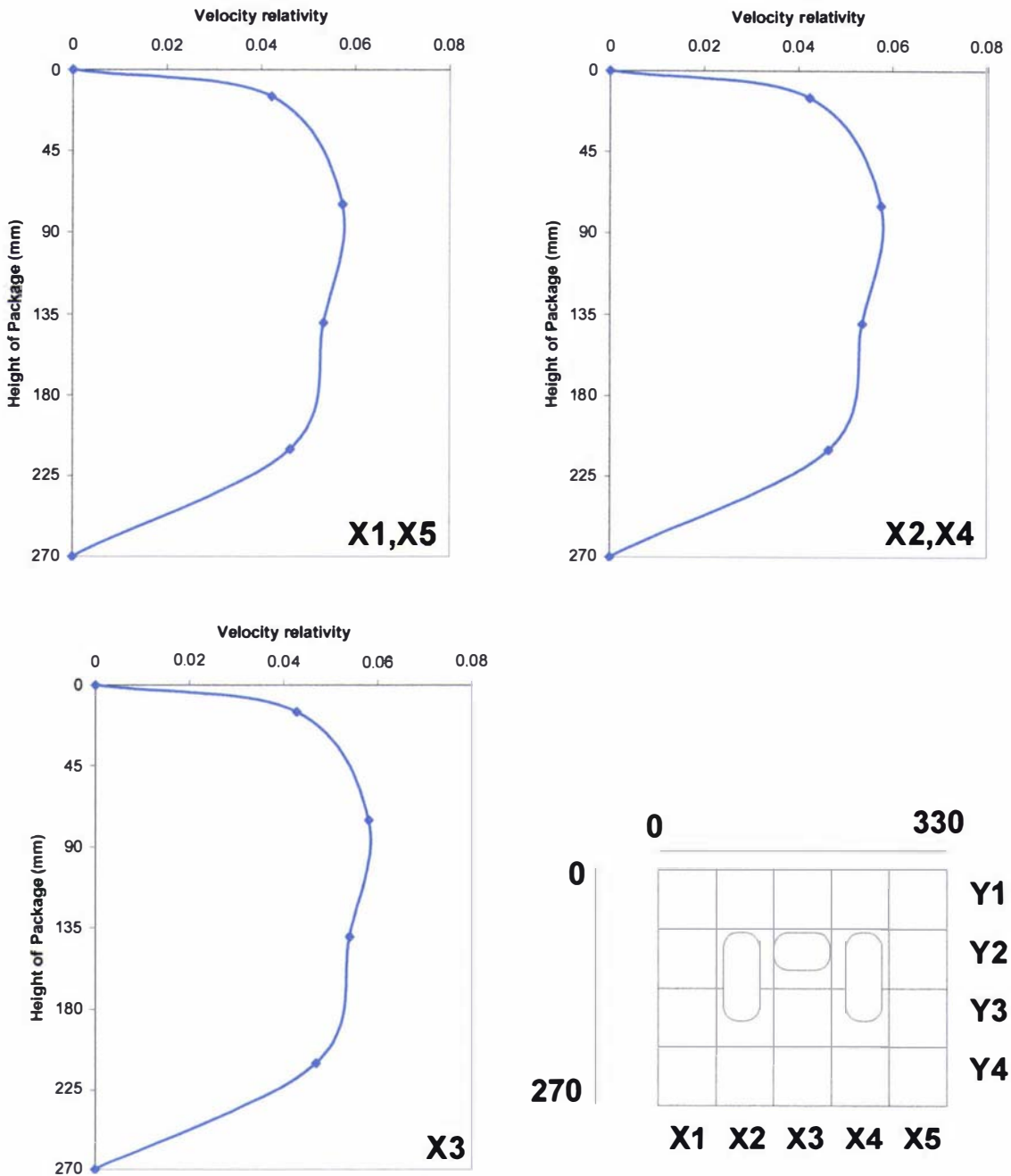


Figure 6.23. Velocity relativeity data and visualisation curves for planes down the height (or y direction) at three positions across the width (x direction) in a 4-layer 'Zeus' apple package. The data are assumed to be valid for all positions in the direction of the flow into the system, in this case the z direction (into the page).

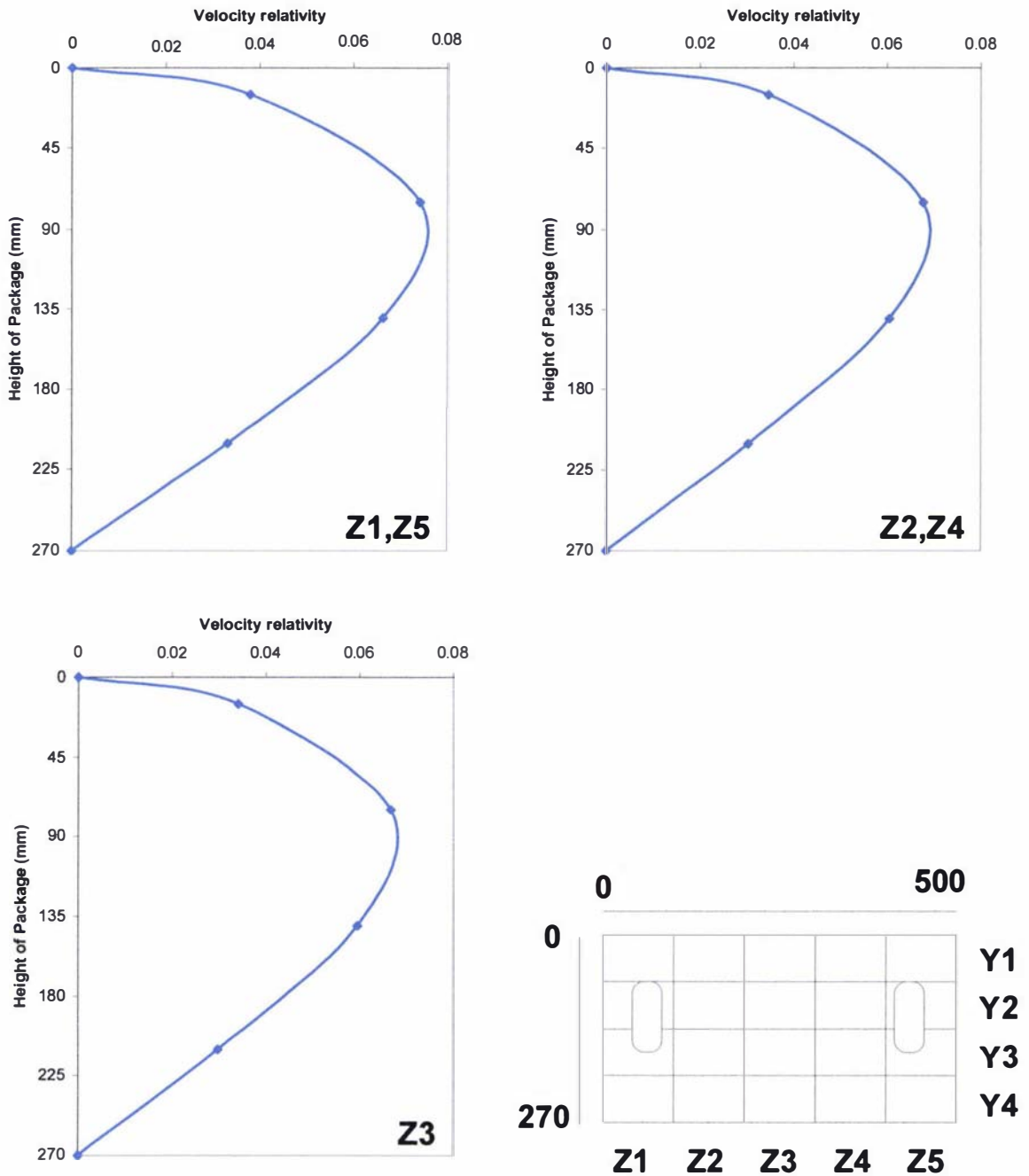


Figure 6.24. Velocity relativeity data and visualisation curves for planes down the height (or y direction) at three positions along the length (z direction) of a 4-layer 'Zeus' apple package. The data are assumed to be valid for all positions in the direction of the flow into the system, in this case the x direction (into the page).



Figure 6.25. The pallet layer configuration of 'Zeus' apple packaging used in the determination of velocity relativity coefficients (left - top view, right (top and bottom) - the two possible package orientations).

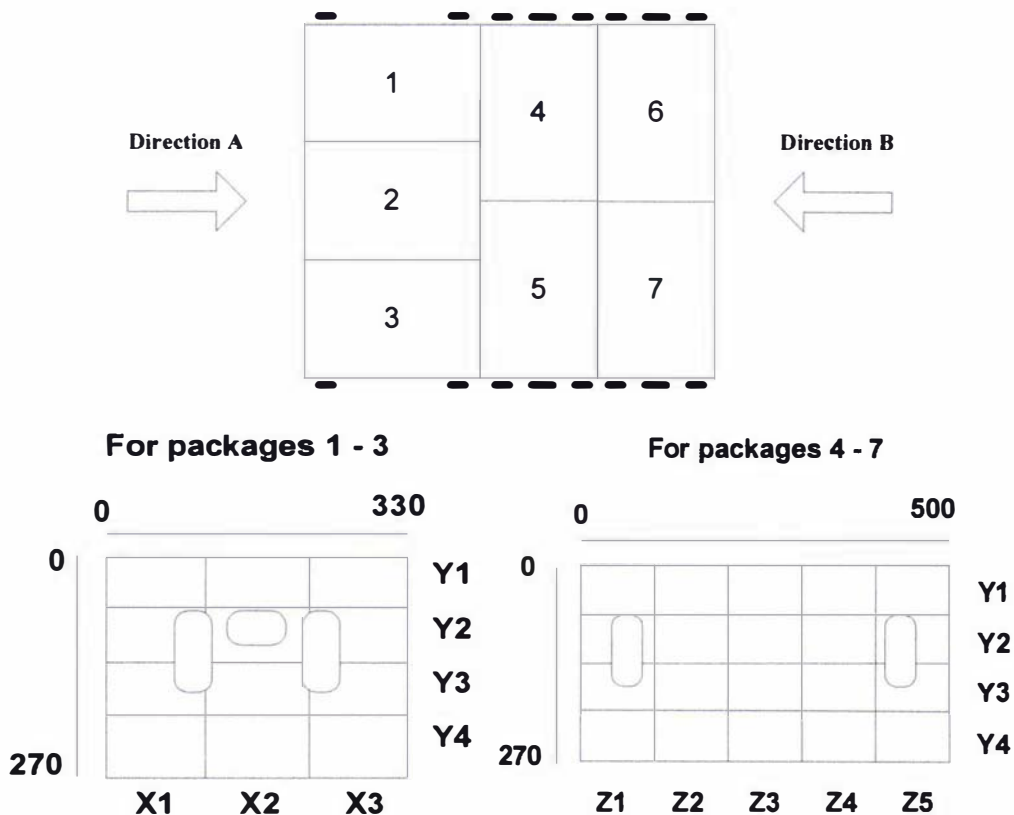


Figure 6.26. Numbering system and flow directions used (top) in CO₂ tracer studies for the 'Zeus' apple pallet layer. (– denotes vent blockage to simulate pre-cooler stacking). The zone coordinates in the x, y and z directions are also illustrated (bottom).

The flow visualisation profile across the pallet layer is shown in Figure 6.27. There were lower velocities through the centre of packages 4, 5, 6 and 7 in direction a due to the uneven spacing of vents across the side face of these packages, and their lack of alignment with some vents on packages 1, 2 and 3. The numerical data for each flow direction are shown in Tables 6.6 and 6.7.

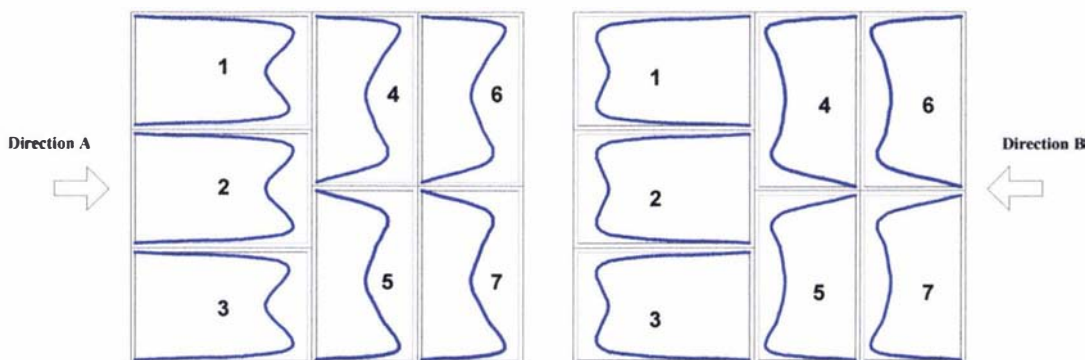


Figure 6.27. Example flow patterns for both directions across a pallet layer of “Zeus” apple packages.

Table 6.6.

Two-dimensional velocity relativity profile for the ‘Zeus’ apple package (flow in Direction A). The y and z coordinates are shown in Figure 6.26. Note that each package’s internal velocity profile is independent of others in the pallet configuration.

	2DVRC			2DVRC			2DVRC				
	Package 1 and 3			Package 2			Packages 4, 5, 6 and 7				
	X1	X2	X3	X1	X2	X3	Z1	Z2	Z3	Z4	Z5
Y1	0.086	0.074	0.086	0.086	0.074	0.086	0.059	0.047	0.036	0.043	0.049
Y2	0.089	0.090	0.089	0.089	0.090	0.089	0.062	0.059	0.056	0.056	0.056
Y3	0.084	0.085	0.084	0.083	0.085	0.083	0.058	0.056	0.053	0.053	0.053
Y4	0.081	0.069	0.081	0.081	0.070	0.081	0.051	0.041	0.031	0.037	0.043

Table 6.7.

Two-dimensional velocity relativity profile for the ‘Zeus’ apple package (flow in Direction B). The y and z coordinates are shown in Figure 6.26. Note that each package’s internal velocity profile is independent of others in the pallet configuration.

	2DVRC			2DVRC			2DVRC				
	Package 1 and 3			Package 2			Packages 4, 5, 6 and 7				
	X1	X2	X3	X1	X2	X3	Z1	Z2	Z3	Z4	Z5
Y1	0.083	0.082	0.083	0.083	0.081	0.083	0.054	0.049	0.044	0.047	0.050
Y2	0.100	0.101	0.094	0.099	0.105	0.099	0.058	0.058	0.056	0.054	0.053
Y3	0.079	0.084	0.074	0.078	0.083	0.078	0.054	0.053	0.052	0.050	0.049
Y4	0.072	0.070	0.072	0.071	0.070	0.071	0.049	0.044	0.040	0.042	0.045

6.4. OTHER PACKAGING CONFIGURATIONS

Velocity distribution data for the other packaging configurations used in testing of the heat and mass transfer simulation models are discussed below individually, and the assumed two-dimensional velocity relativity coefficients presented. These configurations were not quantified by the CO₂ tracer methodology because either the forced flow within the configuration was negligible, the flow distribution could reasonably be assumed to be uniform, or the equipment to measure the flows could not be assembled within the project budget.

6.4.1. Wooden Bin filled with Pears

Time-temperature pre-cooling data were collected by research staff at the University of California - Davis in a study of pear cooling in bins using airflow via vertical venting for cooling. A wooden bin of 1.2m by 1.2m by 0.6m high contained 75mm diameter pears. The slot configuration in the base of the bin was poorly described (personal communication with the experimenters yielded only a suggestion that the slot area was about 10% of the area of the base of the bin and evenly distributed). The velocity relativity profile (Table 6.8) assumed that the bin was divided into a 3 x 3 x 3 (x, y, z) grid of zones, and the flow was uniformly distributed with no cross-mixing.

Table 6.8.

Assumed two-dimensional velocity relativity profile for a wooden bin filled with pears.

	2DVRC		
	X1	X2	X3
Y1	0.111	0.111	0.111
Y2	0.111	0.111	0.111
Y3	0.111	0.111	0.111

6.4.2. Packed Bed of Apples

Data were collected for cooling of apples in a packed bed situation using both air and water as the cooling medium. The objective of this work was to collect reliable data for model testing, as well as define the benefits of using an alternative cooling-medium. Given that the bed had significant depth, and therefore pressure drop, it was reasonable to assume uniform air distribution. The assumed velocity relativity profile (Table 6.9) for the 0.24m x 0.24m x 0.32m package was for a 3 x 3 x 5 (x, y, z) grid of zones, with no cross-mixing.

Table 6.9.

Assumed two-dimensional velocity relativity profile for a packed bed of apples.

	2DVRC		
	X1	X2	X3
Y1	0.111	0.111	0.111
Y2	0.111	0.111	0.111
Y3	0.111	0.111	0.111

6.4.3. Further Apple Packaging Configurations assessed for Mass Transfer

Mass transfer model testing included variations to two apple packaging configurations, the 'Zeus' package and the Retail Display Tray (RDT). Neither configuration required velocity profile characterisation, as both types of test had no forced airflow through the package.

6.4.4. Tomato Packages

Mass transfer model testing also used two tomato packaging configurations. As with the apple packaging configurations described in Section 6.4.3, these configurations did not require velocity profile characterisation as they were assumed to have no net forced airflow through the package.

6.5. CONCLUDING REMARKS

The CO₂ pulsing technique proved to be a viable alternative to more advanced techniques (such as computational fluid dynamics) for quantifying airflow distribution in packages. It is quick, relatively simple, and requires only a modest amount of specialised equipment. It is also possible to use a similar apparatus for visualisation of flow patterns, with the addition of perspex packaging walls and smoke in place of CO₂. The flow-relativity coefficients provide necessary data for using the mathematical model of heat transfer in horticultural packaging. The data presented are more comprehensive than those previously available for apple packages. Flow profiles were not required for testing of the mass transfer model, as forced flow within the packaging configurations used was negligible.

CHAPTER 7

HEAT TRANSFER (PRE-COOLING) MODEL TESTING

7.1. INTRODUCTION

This chapter outlines the approach taken to test and validate the pre-cooling simulation model. The primary validation against experimentally measured data was supplemented by some theoretically based testing. A sensitivity analysis is presented to illustrate the effect of data uncertainties on prediction accuracy.

7.2. ANALYTICAL AND NUMERICAL INTEGRITY TESTING

Comparisons to predictions by an analytical solution to a relevant heat transfer problem were made. The physical situation consisted of a single, cuboid zone, with flow across two boundaries only. This zone did not contain product, and the boundary walls did not contain thermal capacity. Whilst a full model was applied in making numerical predictions, many data items were set to zero, thereby reducing the active component of the model to:

$$Mc \frac{\partial \theta_{int}}{\partial t} = vA\rho(c\theta_{ext}) - vA\rho(c\theta_{int}) \quad (7.1)$$

where M	=	mass of fluid in zone (kg).
c	=	specific heat capacity of fluid ($\text{J.kg}^{-1}\text{K}$).
θ_{int}	=	temperature within the zone ($^{\circ}\text{C}$ or K).
θ_{ext}	=	temperature external to the zone ($^{\circ}\text{C}$ or K).
v	=	velocity of fluid into the zone (m.s^{-1}).
A	=	area of boundary across which fluid flow occurs (m^2).

There is a well-known analytical solution to this equation with fixed boundary and initial conditions. Testing was performed using both properties for air and water as

the cooling fluid the maximum differences between analytically and numerically predicted cooling times was <0.05%.

As both a simulation integrity check and to enable the user to assess the accuracy of model predictions, a running energy balance was incorporated in the simulation software. Upon completion of each simulation, the energy balance result is reported at the base of the 'results' file. This compares the integral of heat flow over system boundaries with the nett internal energy change from initial to final conditions. The balance should be equal to 1 (within acceptable rounding error) if energy has been conserved during the simulation. In all simulations conducted across a wide range of conditions, the maximum inaccuracy was less than 0.01%.

7.3. EXPERIMENTAL DATA COLLECTION AND TESTING.

For testing of the pre-cooling simulation model, previously measured data were gathered from various sources to prevent duplication of work, and also to show relevance to the widest possible range of packaging situations.

7.3.1. Data collected and presented by Amos (1995)

Amos (1995) presented both experimental and predicted apple fruit cooling data for one apple packaging configuration undergoing different cooling conditions. These data were deemed suitable for use and thus pre-cooling model simulation datafiles were developed. The 3 conditions tested were: 'conduction only' cooling - in which a non-ventilated apple package was placed in a forced-draft cooling (FDC) unit; suppressed heat transfer cooling - in which a ventilated 'standard' apple package was encased in polystyrene except for the handholes through which ventilation occurred; and a normally cooled package - where a 'standard' ventilated package was placed in a FDC unit with all faces exposed to the airflow.

All predictions related to Amos' (1995) data were made using 150 Zone model datafiles. Each of the six layers was divided into 25 zones (5×5), which coincided with the five lines of fruit in the x direction across the package, and 5 planes of fruit in the z direction down the length of the package. This configuration is shown in Figure 7.1.

Relevant data for fruit and packaging materials for this packaging configuration were sourced via the methods in Appendix 2. Amos (1995) used a small number of

measured velocity values to estimate the flow profile through the pack. These were replaced by measured data collected according to the methods of Chapter 6.

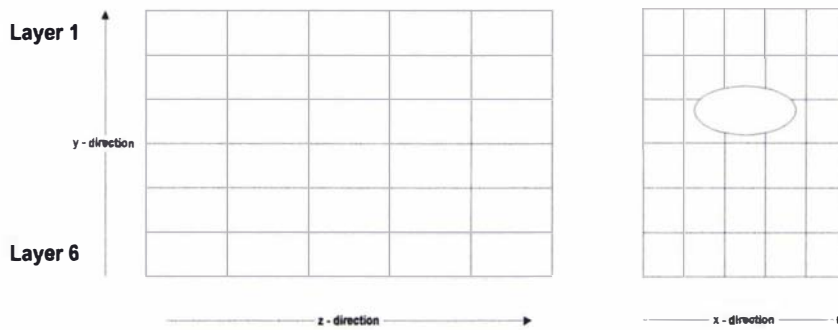


Figure 7.1. Configuration used in the model datafiles constructed for comparison of Amos (1995) data.

The major data used in development of the pre-cooling simulation datafile for temperature prediction in the ‘conduction-only’ package are shown in Table 7.1. Much of the data used by Amos (1995) were still appropriate (with the exception of any velocity data and calculated heat transfer coefficients). Predictions of both fruit and fluid temperatures were compared to Amos’ experimentally collected data. Examples are shown in Figures 7.2 and 7.3. Respiration was included in the modelling for this, the slowest cooling of Amos’ datasets to provide a test of this sub-model.

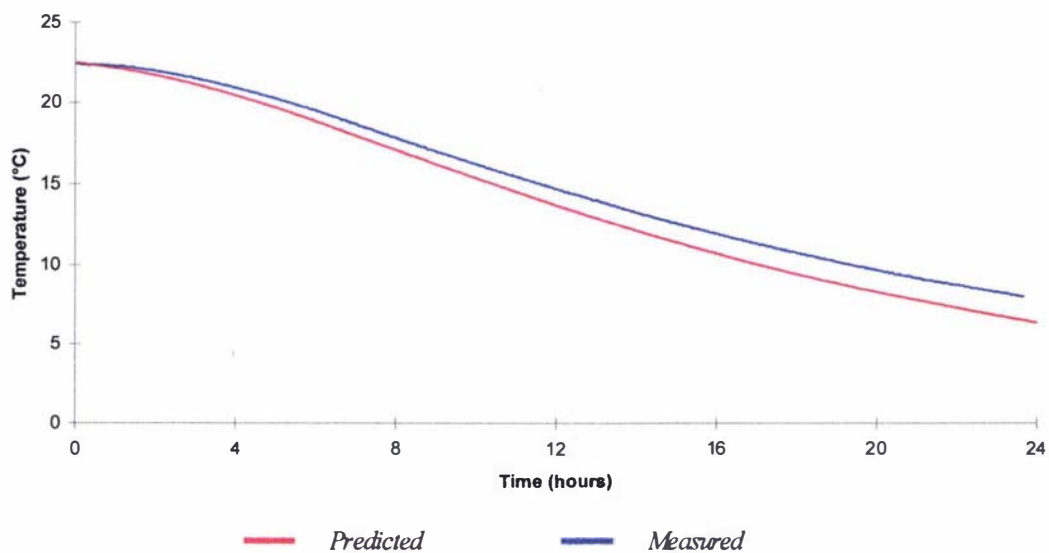


Figure 7.2. Predicted and measured air temperatures vs time for the centre of layer 3 of a ‘standard’ apple package undergoing ‘conduction-only’ cooling – Experimental data from Amos (1995).

Table 7.1.

Major data used for construction of a 150 zone, pre-cooling simulation model datafile for 'conduction-only' cooling of a 'standard' apple package. These data are sourced from physical measurement and Appendix 2. As there is no flow through this configuration, a velocity profile is not required.

Variable	Value	Units	Variable	Value	Units
Physical System Data			Fluid Data		
Width of package (x)	0.32	m	Specific heat capacity	1005	J.kg ⁻¹ K ⁻¹
Height of package (y)	0.29	m	Thermal conductivity	0.026	W.m ⁻¹ K ⁻¹
Length of package (z)	0.515	m	Density	1.28	kg.m ⁻³
Porosity of package	0.567	fraction	Convection factor	1	
Fluid velocity into package	N/A		External Environment Data		
Ventilation area in package	0.0	m ²	External fluid temperature	0	°C
Package Properties			External fluid velocity	2	m.s ⁻¹
Zones in x - direction	5		Packaging Material Data		
Zones in y - direction	6		'Friday' Trays		
Zones in z - direction	5		Specific heat capacity	1700	J.kg ⁻¹ K ⁻¹
Number of V boundaries	175		Thermal conductivity	0.048	W.m ⁻¹ K ⁻¹
Number of H boundaries	180		Density	260	kg.m ⁻³
Number of P boundaries	180		Thickness	0.003	m
Total internal zones	150		Package Lid and Base		
Total external zones	1		Specific heat capacity	1700	J.kg ⁻¹ K ⁻¹
Number of pack materials	3		Thermal conductivity	0.048	W.m ⁻¹ K ⁻¹
Active package surfaces	6		Density	220	kg.m ⁻³
Product Data			Thickness	0.0038	m
Specific heat capacity	3650	J.kg ⁻¹ K ⁻¹	Package Side Wall		
Thermal conductivity	0.42	W.m ⁻¹ K ⁻¹	Specific heat capacity	1700	J.kg ⁻¹ K ⁻¹
Total mass of product	18.6	kg	Thermal conductivity	0.048	W.m ⁻¹ K ⁻¹
Radius of each product item	0.027	m	Density	220	kg.m ⁻³
Number of products in pack	150		Thickness	0.0076	m
Is respiration considered?	Yes				
Respiration coefficient a	4.59e ⁻⁶				
Respiration coefficient b	2.66				

NB: Dynamic datafile located in 'Pre-cooling Input Files' directory ('Packaging Simulation for Design' software - Appendix 5), entitled: 'Conduction-only Standard Apple Package - 150 Zones.prn'.

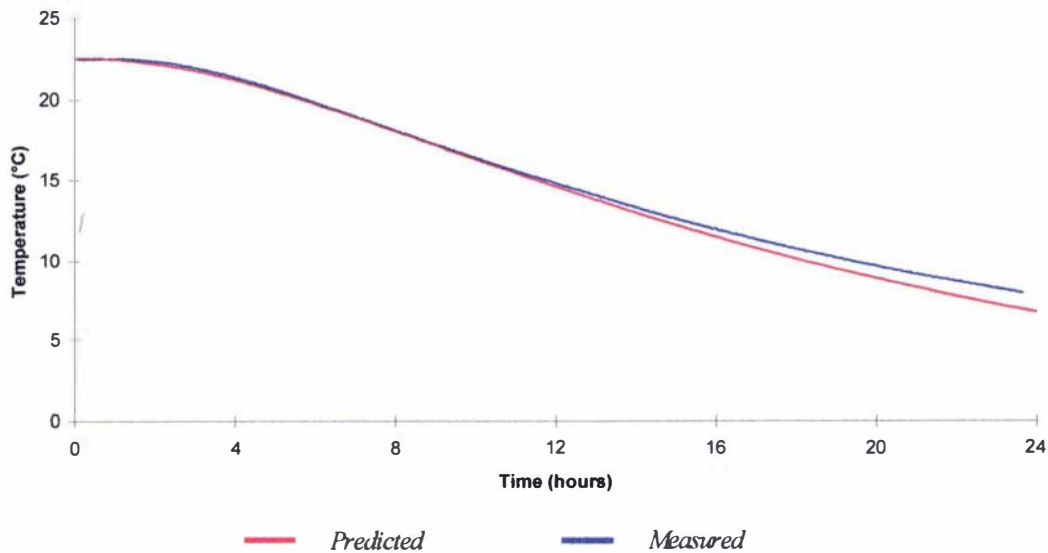


Figure 7.3. Predicted and measured fruit temperature vs time for the centre of layer 3 in a ‘standard’ apple package undergoing ‘conduction-only’ cooling – Experimental data from Amos (1995).

The suppressed heat transfer cooling situation was modelled using a datafile configuration similar to that for the ‘conduction only’ cooling scenario. The major data used in development of the suppressed heat transfer datafile were predominantly those presented in Table 7.1 with the substitution of the data presented in Table 7.2. These data were sourced from physical measurement and Appendix 2, and the velocity relativity profile presented in Table 6.3. Respiration was not included.

Table 7.2.

Amended data (to those of Table 7.1) for development of a 150-zone, pre-cooling simulation model datafile for a ‘suppressed’ heat transfer ‘standard’ apple package.

Variable	Value	Units	Variable	Value	Units
Physical System Data			Product Data		
Fluid velocity into package	1.4	m.s ⁻¹	Is respiration considered?	No	
Ventilation area in package	0.00388	m ²	External Environment Data		
Package Properties			External fluid temperature	0.4	°C
Active package surfaces	2		External fluid velocity	1.4	m.s ⁻¹

NB: Dynamic datafile located in ‘Pre-cooling Input Files’ directory (‘Packaging Simulation for Design’ software - Appendix 5), entitled: ‘Suppressed Heat Transfer Standard Apple Package – 150 Zones.prn’.

Predictions of both fruit and air temperature were compared with experimentally collected data (from experiments performed by Amos, 1995). An example is shown in Figure 7.4.

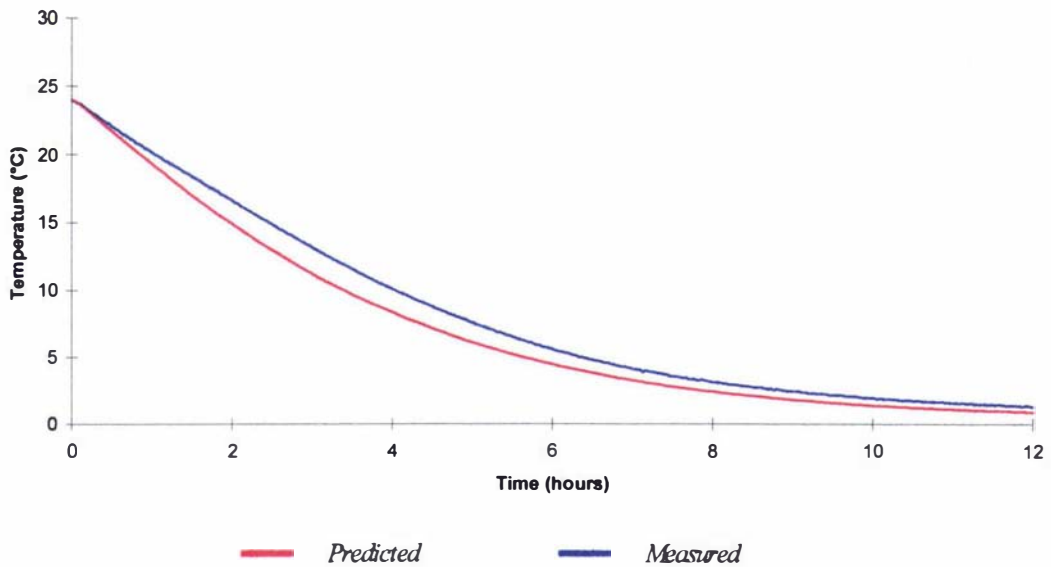


Figure 7.4. Predicted and measured product temperature vs time for the centre fruit in layer 4 in a ‘standard’ apple package undergoing ‘suppressed’ heat transfer – Experimental data from Amos (1995).

Forced-draft cooling of the ‘standard’ apple carton was also modelled. The data used were predominantly those presented in Table 7.1 with the substitution of the data presented in Table 7.3. These data were sourced from physical measurement and Appendix 2, and the velocity relativity profile presented in Table 6.3.

Table 7.3.

Amended data (to those of Table 7.1) for development of a 150-zone, pre-cooling simulation model datafile for an unmodified ‘standard’ apple package.

Variable	Value	Units	Variable	Value	Units
Physical System Data			Product Data		
Fluid velocity into package	1.4	m.s ⁻¹	Is respiration considered?	No	
Ventilation area in package	0.00388	m ²	External Environment Data		
Package Properties			External fluid temperature	0	°C
Active package surfaces	6		External fluid velocity	1.4	m.s ⁻¹

NB: Dynamic datafile located in ‘Pre-cooling Input Files’ directory (‘Packaging Simulation for Design’ software - Appendix 5), entitled: ‘Unmodified Standard Apple Package – 150 Zones.prn’.

As with the ‘suppressed’ heat transfer scenario, model predictions were compared with experimental data measured by Amos (1995). An example is shown in Figure 7.5.

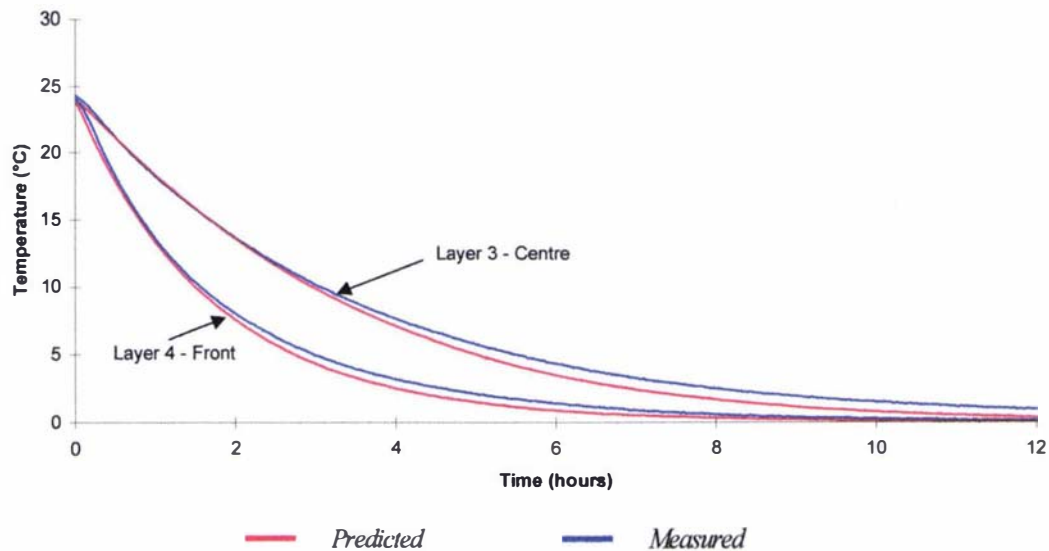


Figure 7.5. Predicted and measured product temperatures vs time for positions in 2 layers of a 'standard' apple package undergoing forced draft cooling – Experimental data from Amos (1995).

Overall, for the three tests, and for up to eight positions within each test, the predictions had at least the same levels of accuracy, and in some cases were better, than those presented by Amos (1995). The three sets of data are for circumstances in which quite different heat transfer pathways and hence sub-models are most important. The 'conduction-only' data provides a test of the 'through packaging' sub-models, whereas the 'suppressed heat transfer' data tests mainly the models for ventilation and fluid-product heat transfer. The 'standard' data allows for a more comprehensive test.

Amos (1995) stated that during replicated experimental work performed to measure temperature profiles, much of the variation in experimental data was due to differences in airflow through the carton configuration. Thermocouple positioning inaccuracies were also claimed to be responsible for some of the differences between measured and predicted temperatures. The author concluded that these factors largely explained the lack of fit by his model. The present model performed at least as well for all testing.

It was convenient to use the cooling situations examined by Amos to establish sensitivity of simulations to model assumptions and data inputs for the most contributory pathways/ sub-models. Assessment was undertaken to investigate sensitivity of simulations to the following:

- inclusion / exclusion of the natural convection model (most important in ‘conduction-only’),
- lumping of packaging thermal capacity with air thermal capacity,
- sensitivity to variation in inlet air velocity and,
- inclusion of a respiratory heat generation model (most important in ‘conduction-only’).

(i) *Assessment of the natural convection model*

Simulations for the ‘conduction-only’ apple package and forced-draft cooled apple package allowed the modelling of inter-zone natural convection to be assessed. Figures 7.6 to 7.9 show the effect of modelling natural convection at 3 levels – that expected theoretically ($CF = 1$), totally suppressed ($CF = 0$), and arbitrarily enhanced ($CF = 2$).

Figures 7.6 and 7.7 show that CF is a critical factor if forced convection is negligible, whereas Figures 7.8 and 7.9 show how forced convection dominates where there is flow through the package. Results such as Figures 7.2 and 7.3 were achieved with $CF = 1$, adding confidence to the approach taken for modelling inter-zone natural convection.

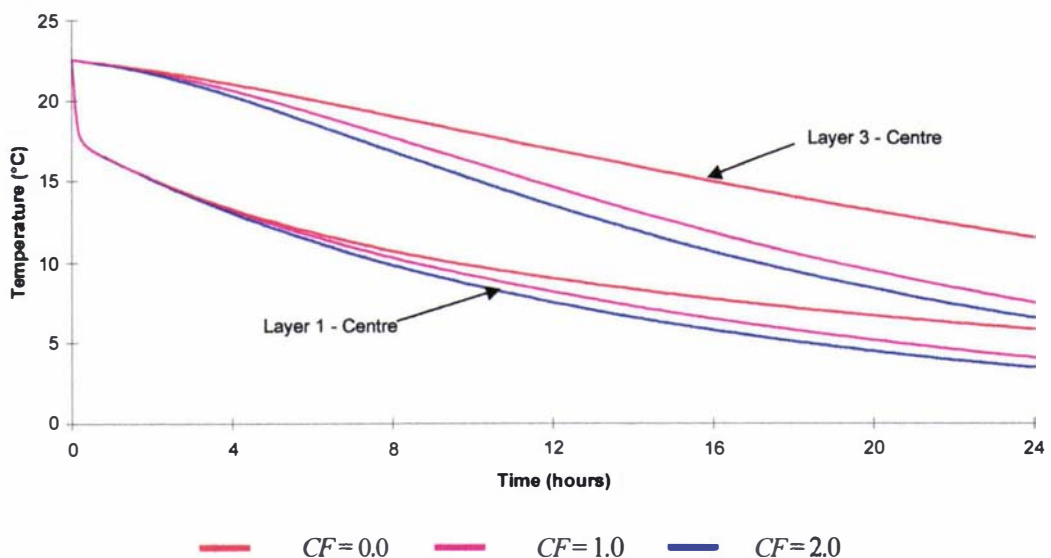


Figure 7.6. Air temperatures for two positions in a ‘conduction-only’ apple package for 3 levels of inter-zone natural convection.

Figures 7.6 and 7.7 show that the sensitivity to the appropriateness of the natural convection model changes with position within a ‘conduction-only’ apple package.

Overall there is strong evidence that the pathway must be included ($CF = 0$ gives results quite different to experimental values), and once it is there the only remaining question is whether $CF > 1$. As stated in Chapter 5, theoretically it should not be, and Figures 7.2 and 7.3 support this. Nevertheless, Figures 7.6 and 7.7 show that a change in CF between 1.0 and 2.0 would not be highly influential on model accuracy.

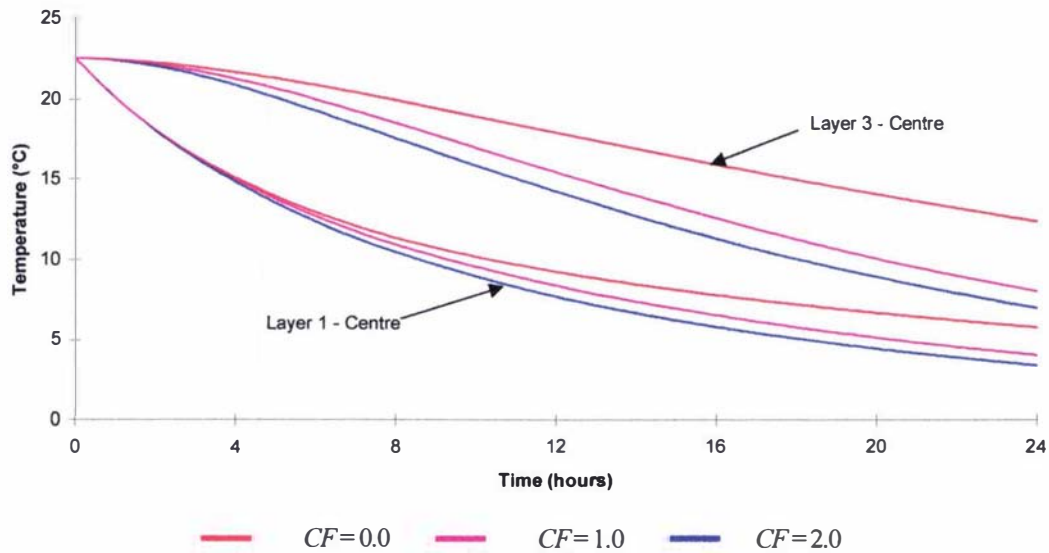


Figure 7.7. Product temperatures for two positions in a 'conduction-only' apple package layer for 3 levels of inter-zone natural convection.

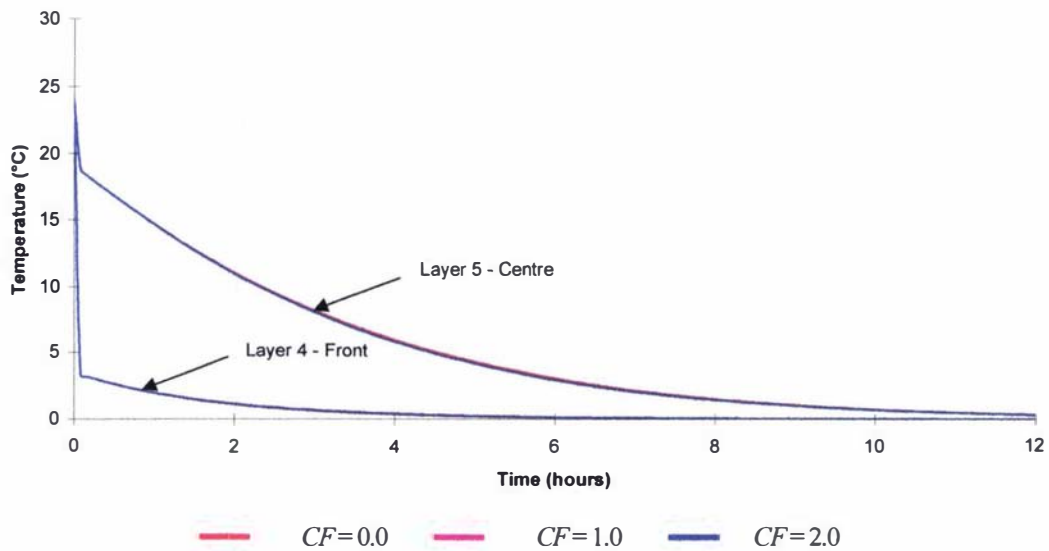


Figure 7.8. Air temperatures for two positions in a force-draft cooled apple package for 3 levels of inter-zone natural convection.

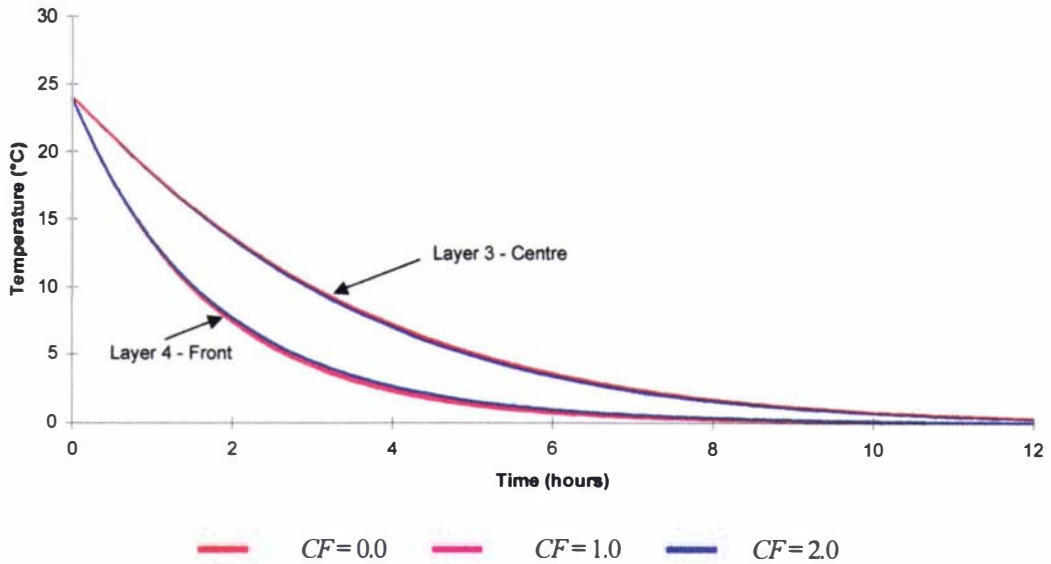


Figure 7.9. Product temperatures for two positions in a force-draft cooled apple package for 3 levels of inter-zone natural convection.

(ii) *Assessment of the packaging thermal capacity model*

An assumption made during model development was the lumping of packaging material thermal capacity with the air thermal capacity. It was convenient to test this assumption using the cooling situations examined by Amos (1995). Predictions considering packaging thermal capacity lumped with the air thermal capacity and ignoring packaging thermal capacity are presented in Figures 7.10 - 7.11.

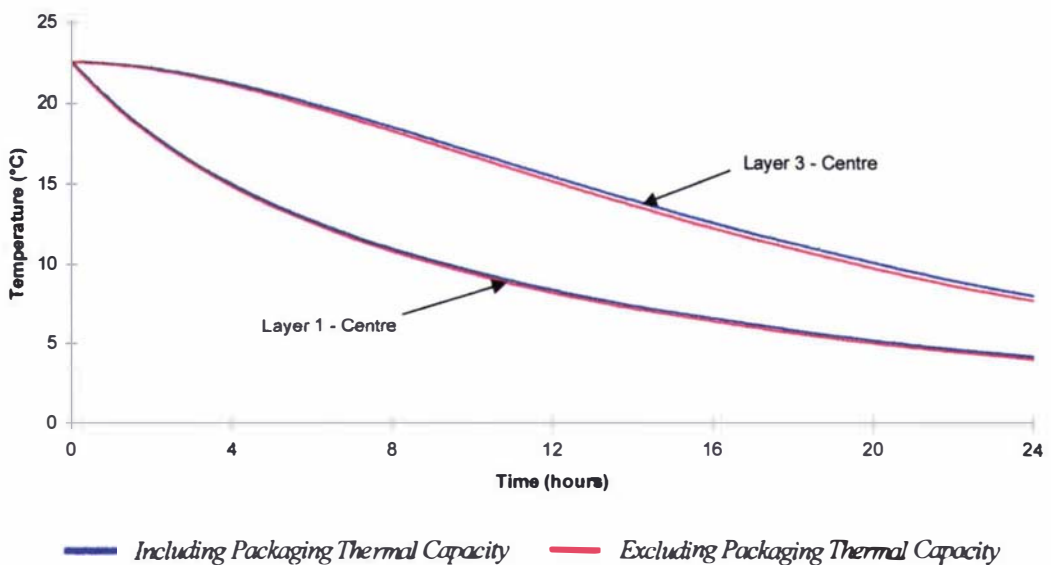


Figure 7.10. Product temperatures vs time for simulations both including and excluding packaging thermal capacity in a 'conduction-only' apple package.

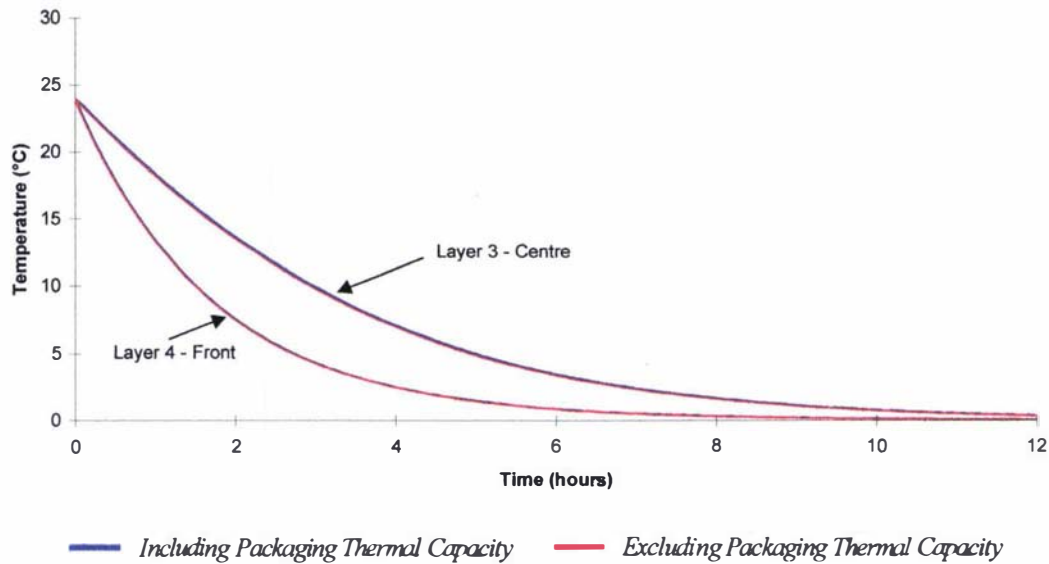


Figure 7.11. Product temperatures vs time for simulations both including and excluding packaging thermal capacity in a forced-draft cooled apple package.

In the ‘conduction only’ cooling scenario, there were small differences in both fluid and product temperature predictions, whilst in the forced-draft cooled situation, the effect of ignoring packaging thermal capacity had little or no effect on both fluid and product temperature predictions. It was however noted that when both the conduction and forced-draft simulations were computed, the necessary computational time was up to 10 times longer for conditions where packaging thermal capacity was ignored. Amos (1995) also encountered this problem, which is a result of the small volume of air (with little thermal capacity) requiring shortening of the simulation timestep. Amos (1995) overcame this problem by arbitrarily increasing the air thermal capacity 10-fold to shorten computation time. For the present simulation modelling methodology, it is recommended that packaging thermal capacity be lumped with that of the zone fluid and arbitrary scaling of air thermal capacity avoided.

(iii) *Assessment of the sensitivity to measurement of inlet air velocity*

In-pack velocity, which is directly proportional to inlet air velocity, has a direct bearing on the values of the heat transfer coefficient between the product and the cooling fluid, and on the air temperature profile through a package. Amos’ experimental forced-draft cooling situation was conveniently used to assess the effect of in-pack velocity on model predictions. The inlet air velocity near the package vent was 1.4 m.s^{-1} . The accuracy of the instruments used was stated by the manufacturers to be $\pm 0.02 \text{ m.s}^{-1}$ (Amos, 1995). However, the flow of air from a fan is rarely

constant with time, and uniformity across the full vent hole was unlikely. Hence, a sensitivity investigation range of $\pm 10\%$ was considered realistic (Figure 7.12).

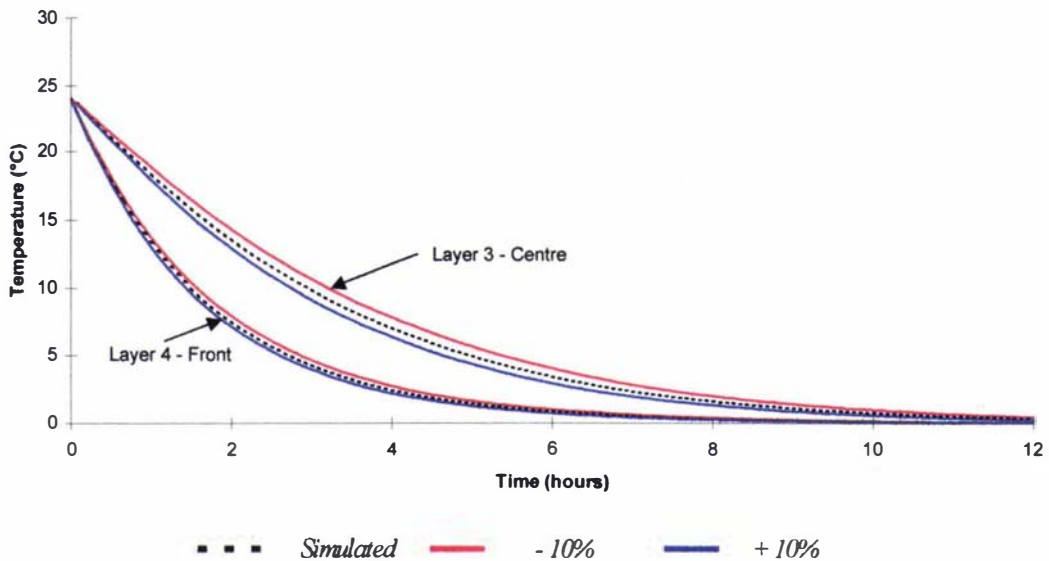


Figure 7.12. Assessment of sensitivity of predictions to the uncertainty in the inlet air velocity (for the apple forced-draft cooling scenario, 1.4 m.s^{-1}) using two positions in a force-draft cooled apple package.

The results of Figure 7.12 show that for both model testing and model application, it is vital that sufficient effort is put into characterising the mean air velocity through ventilation holes.

(iv) *Assessment of the respiratory heat generation model*

The benefit of including respiratory heat generation in the model was assessed for both forced-draft cooling and ‘conduction-only’ cooling situations, because it is in situations where the airflow velocity through the packaging configuration is very low, or non-existent (‘conduction-only’ cooling) that respiration might be important (Figures 7.13 and 7.14).

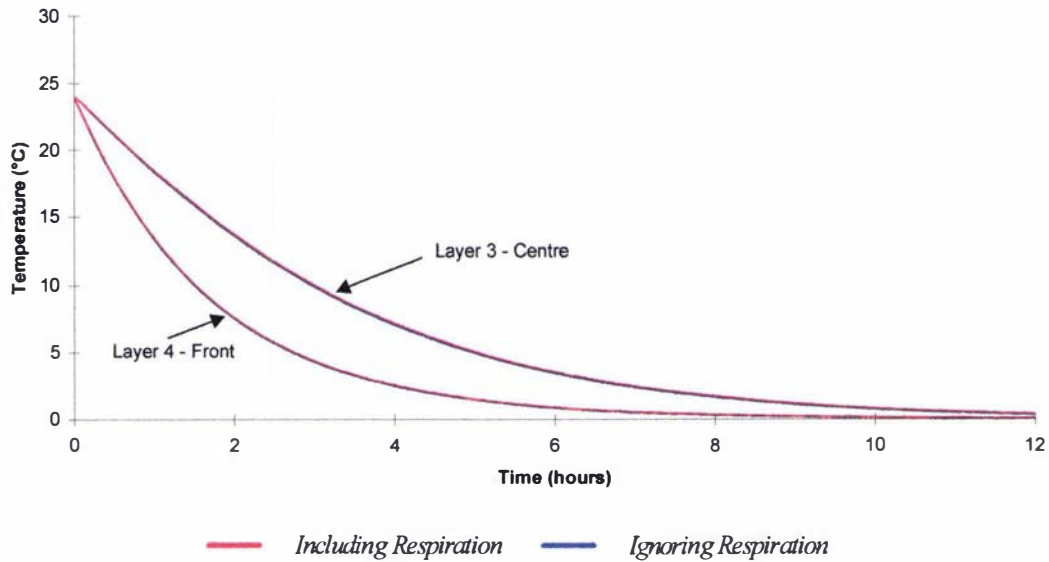


Figure 7.13. Assessment of the importance of inclusion of respiratory heat generation to prediction of product temperatures for two positions in a forced-draft cooling scenario (for apples, the respiratory coefficients for inclusion in the model of Gaffney *et al.* (1985b) are $a= 4.59 \times 10^{-6}$ and $b= 2.66$).

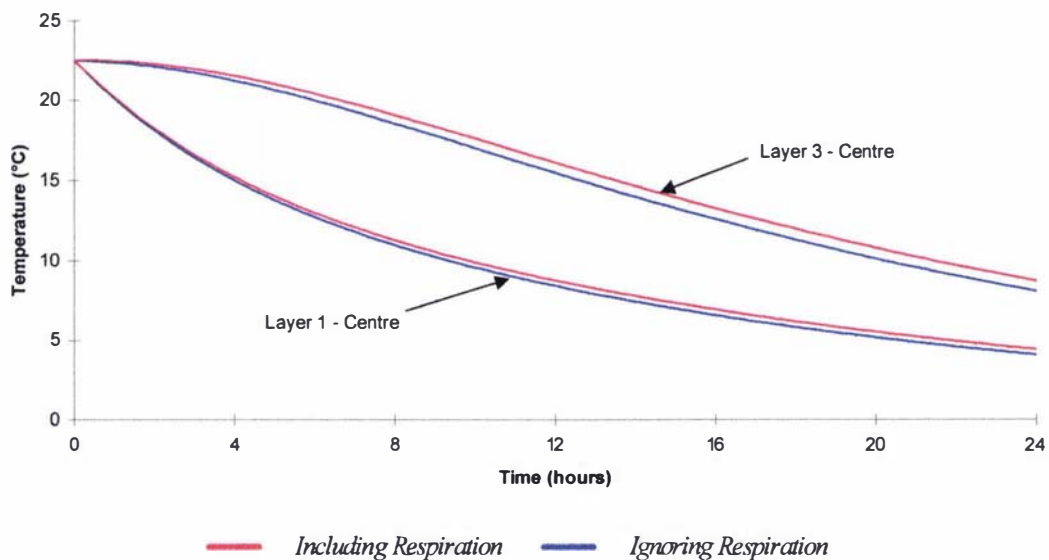


Figure 7.14. Assessment of the importance of inclusion of respiratory heat generation to prediction of product temperatures for two positions in a 'conduction-only' cooling scenario (for apples, the respiratory coefficients for inclusion in the model of Gaffney *et al.* (1985b) are $a= 4.59 \times 10^{-6}$ and $b= 2.66$).

The influence of respiratory heat generation in a 'conduction-only' situation was of the same order of magnitude as the temperature measurement error, implying that the

facility of having this model term available to ‘turn on’ was worthwhile, especially for products with high rates of respiration, but for forced-draft cooling (Figure 7.13) it is acceptable to neglect it.

7.3.2. Data collected and presented by Falconer (1995a).

The pre-cooling model was further tested using Z-Pack cooling data collected by Falconer (1995a), in experiments designed to characterise half-cooling times for apples in different packaging configurations.

The model of a single Z-Pack consisted of 100 zones (as shown in Figure 7.15) in a $5 \times 4 \times 5$ configuration, which coincided with the five lines of fruit in the x direction, four layers of fruit in the y direction and five planes of fruit in the z direction. The major data used in development of the single Z-Pack datafile are presented in Table 7.4. These data were sourced from physical measurement and Appendix 2, whilst the velocity relativity profile for the single Z-Pack is presented in Table 6.4.

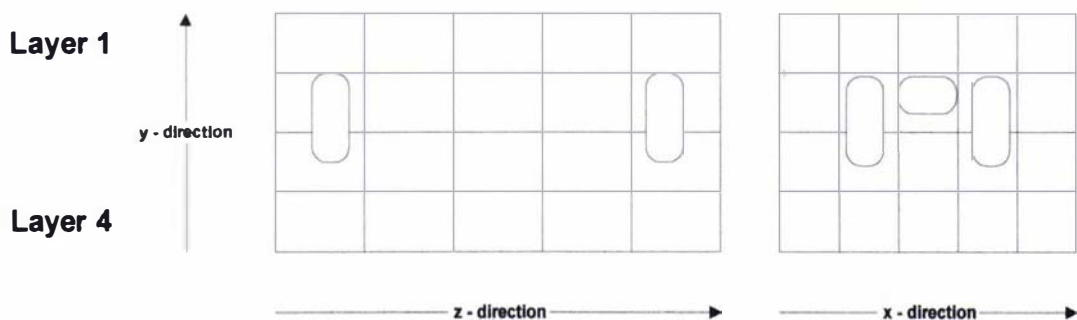


Figure 7.15. Configuration used in the model datafiles development for comparison of Falconer (1995a) data for the single Z-Pack.

Model predictions in comparison with experimental data are presented for the single package in Figure 7.16. These predictions show generally good agreement with measured temperature profiles. The greatest difference in prediction occurs in the bottom layer. Lack of fit may be contributed to by; inaccurate positioning of thermocouples, imprecision in measurement of flow velocity (or mass flow rate) into the package configuration, or inaccurate characterisation of the flow profile within the package. The bottom layer probably has the lowest flow rate and least-well characterised airflow pattern, so greatest differences between measured and predicted values were not unexpected.

Table 7.4.

Major data used for construction of a 100 zone, pre-cooling simulation model datafile for forced-draft cooling of an unmodified apple Z-Pack. These data are sourced from physical measurement and Appendix 2, whilst the velocity relativity profile is presented in Table 6.4.

Variable	Value	Units	Variable	Value	Units
Physical System Data			Fluid Data		
Width of package (x)	0.33	m	Specific heat capacity	1005	J.kg ⁻¹ K ⁻¹
Height of package (y)	0.26	m	Thermal conductivity	0.026	W.m ⁻¹ K ⁻¹
Length of package (z)	0.5	m	Density	1.28	kg.m ⁻³
Porosity of package	0.509	fraction	Convection factor	1	
Fluid velocity into package	1.95	m.s ⁻¹	External Environment Data		
Ventilation area in package	0.00472	m ²	External fluid temperature	-1	°C
Package Properties			External fluid velocity	1.95	m.s ⁻¹
Zones in x - direction	5		Packaging Material Data		
Zones in y - direction	4		'Friday' Trays		
Zones in z - direction	5		Specific heat capacity	1700	J.kg ⁻¹ K ⁻¹
Number of V boundaries	125		Thermal conductivity	0.048	W.m ⁻¹ K ⁻¹
Number of H boundaries	120		Density	260	kg.m ⁻³
Number of P boundaries	120		Thickness	0.002	m
Total internal zones	100		Package Lid and Base		
Total external zones	1		Specific heat capacity	1700	J.kg ⁻¹ K ⁻¹
Number of pack materials	3		Thermal conductivity	0.048	W.m ⁻¹ K ⁻¹
Active package surfaces	6		Density	220	kg.m ⁻³
Specific heat capacity	3650	J.kg ⁻¹ K ⁻¹	Thickness	0.0038	m
Thermal conductivity	0.42	W.m ⁻¹ K ⁻¹	Package Side Wall		
Total mass of product	18.6	kg	Specific heat capacity	1700	J.kg ⁻¹ K ⁻¹
Radius of each product item	0.035	m	Thermal conductivity	0.048	W.m ⁻¹ K ⁻¹
Number of products in pack	100		Density	220	kg.m ⁻³
Is respiration considered?	No		Thickness	0.0076	m

NB: Dynamic datafile located in 'Pre-cooling Input Files' directory ('Packaging Simulation for Design' software - Appendix 5), entitled: 'Unmodified Apple Z-Pack - 100 Zones.prn'.

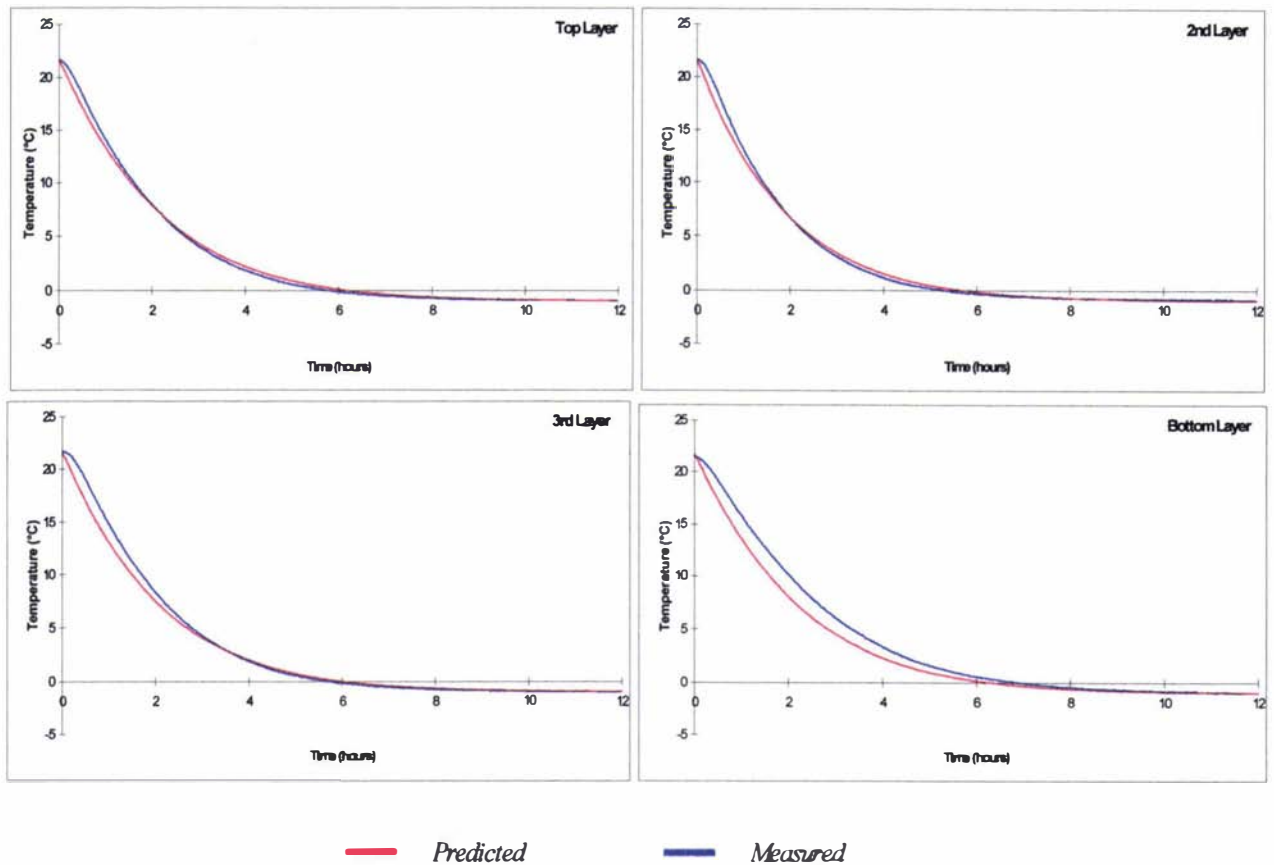


Figure 7.16. Predicted and measured fruit temperatures vs time located at the centre of layers 1 - 4 for the 1996 'Zeus' apple package – Experimental data from Falconer (1995a).

The modelling of an entire pallet layer of Z-Packs was simplified using symmetry considerations in the pallet-stacking configuration (as shown in Figure 7.17). This reduced model computation time and model complexity dramatically, without reducing model accuracy. The half-pallet configuration was modelled using a $2 \times 8 \times 9$ zone structure, which coincided with the one full and one half packages in the x direction (Packages 1 and 2), eight layers of fruit (as two pallet layers were modelled to better simulate centre of pallet conditions) in the y direction and three planes of fruit in the z direction down the length of each package. This configuration was implemented with perfectly insulated boundaries on the top and bottom faces of the system as this was deemed physically realistic for a central pallet layer within a larger pallet system.

The data used in development of this datafile were predominantly those presented in Table 7.4 with the substitution of the data presented in Table 7.5. These data were sourced from physical measurement and Appendix 2, whilst the velocity relativity profile for the pallet layer of Z-Packs is presented in Table 6.6.

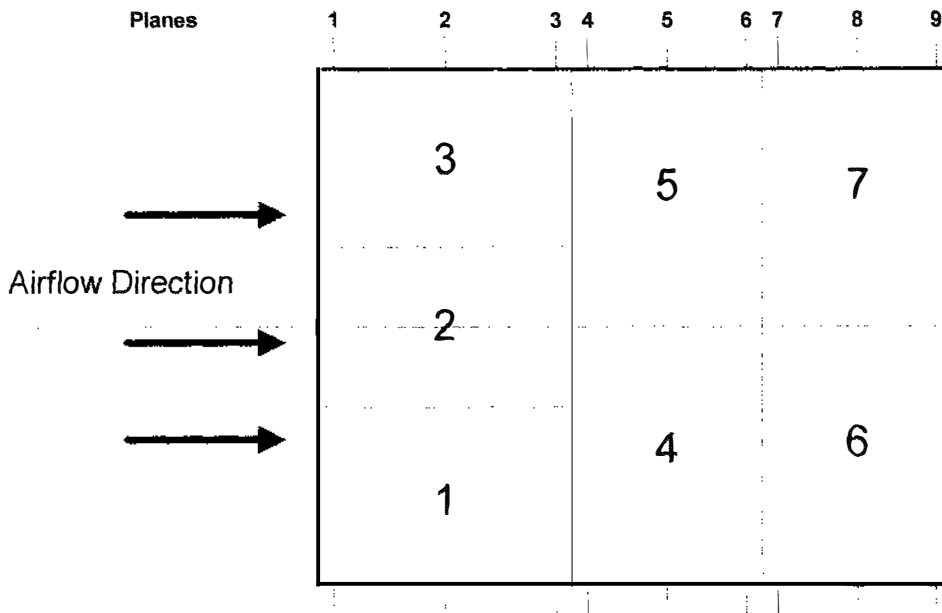


Figure 7.17. Pallet Layer configuration of the 1996 'Zeus' Apple Packaging - Modified from Falconer (1995a).

Table 7.5.

Amended major data (to those of Table 7.4) for development of a 144-zone, pre-cooling simulation model datafile for a pallet layer of apple Z-Packs.

Variable	Value	Units	Variable	Value	Units
Physical System Data			Package Properties cont.		
Width of package (x)	0.495	m	Total external zones	1	
Height of package (y)	0.52	m	Number of pack materials	4	
Length of package (z)	1.16	m	Active package surfaces	4	
Porosity of package	0.509	fraction	Product Data		
Package Properties			Total mass of product	130.2	kg
Zones in x - direction	2		Number of products in pack	700	
Zones in y - direction	8		Packaging Material Data		
Zones in z - direction	9		Double Package Layer		
Number of V boundaries	162		Specific heat capacity	1700	J.kg ⁻¹ K ⁻¹
Number of H boundaries	216		Thermal conductivity	0.048	W.m ⁻¹ K ⁻¹
Number of P boundaries	160		Density	220	kg.m ⁻³
Total internal zones	144		Thickness	0.0152	m

NB: Dynamic datafile located in 'Pre-cooling Input Files' directory ('Packaging Simulation for Design' software - Appendix 5), entitled: 'Pallet layer of Apple Z-Packs - 144 Zones.prn'.

Model predictions were compared with measured data (from Falconer, 1995a) in Figures 7.18 and 7.19.

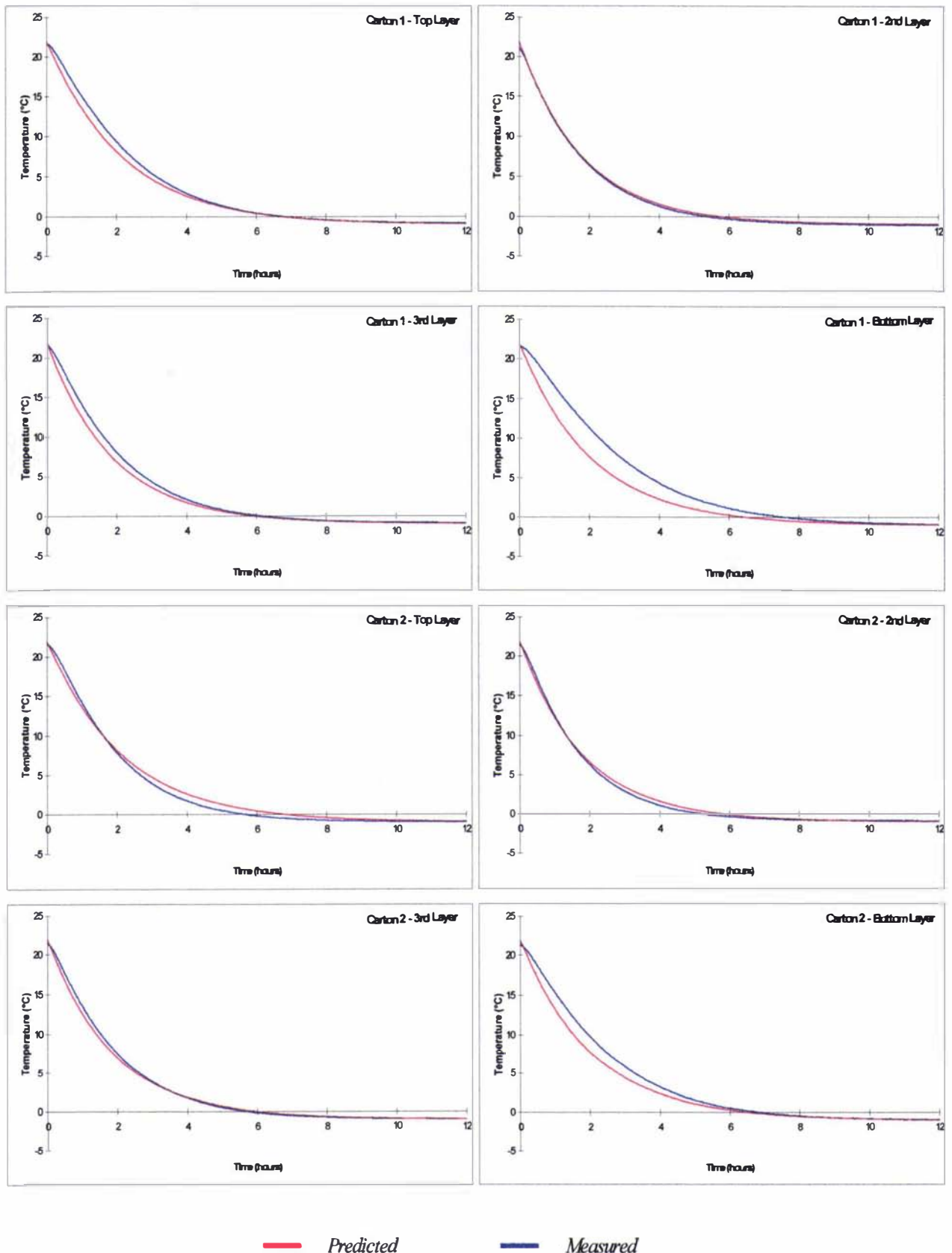


Figure 7.18. Predicted and measured fruit temperatures vs time for 'Zeus' apple packages in a pallet layer configuration (Cartons 1, and 2 - as shown in Figure 7.17) – Experimental data from Falconer (1995a).

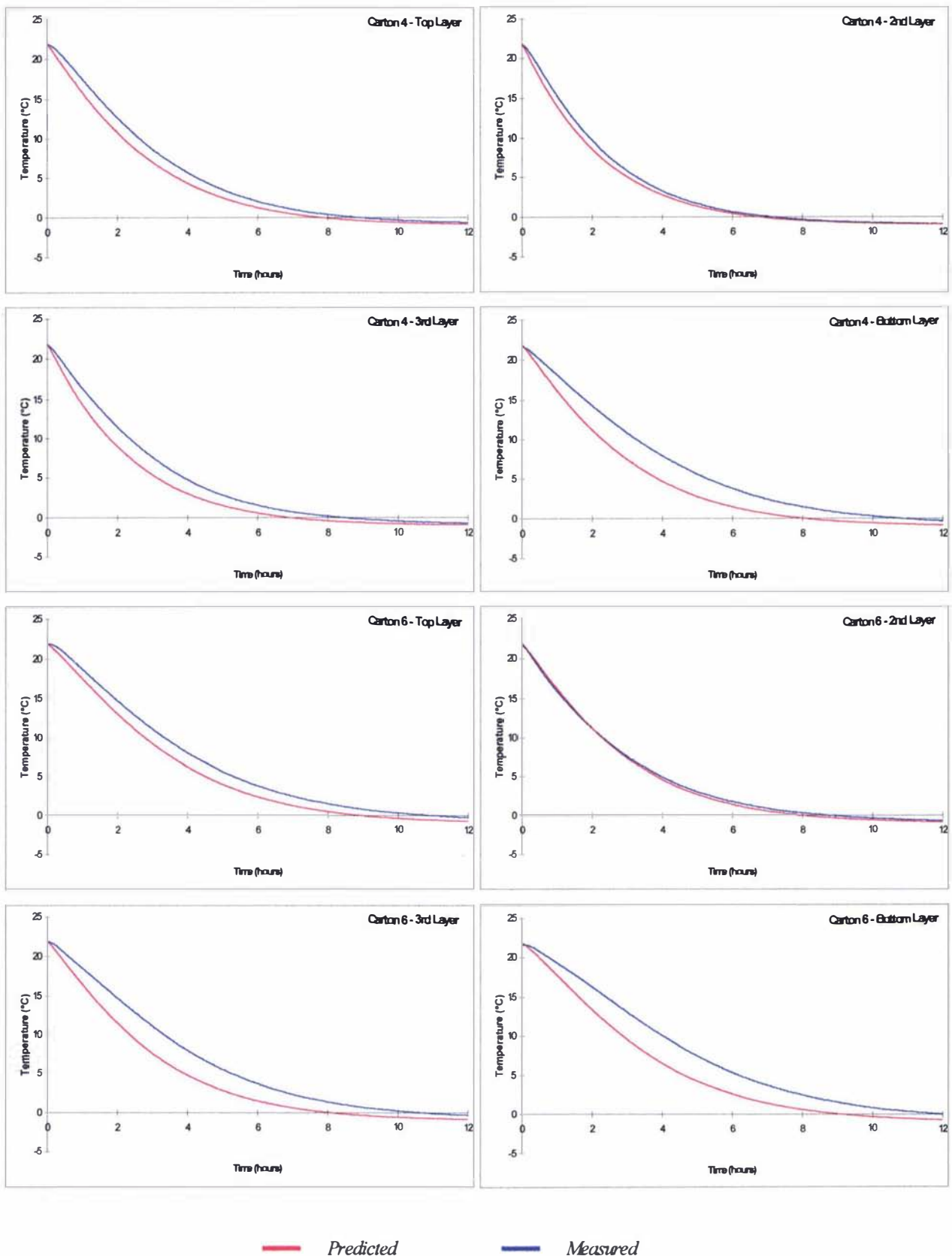


Figure 7.19. Predicted and measured fruit temperatures vs time for 'Zeus' apple packages in a pallet layer configuration (Cartons 4 and 6 - as shown in Figure 7.17) – Experimental data from Falconer (1995a).

The predicted fruit temperatures show generally good agreement with measured data, especially in packages 1 and 2, but progressively disagree more along the direction of airflow through the pallet configuration. Generally, the largest temperature differences were observed in the 4th or bottom layer of each of the cartons in the pallet configuration. This is consistent with the single Z-Pack situation.

Analysis of model predictions for the pallet layer shows that all predictions overestimated the measured rate of product cooling. This may be due to inaccuracy in measurement of the velocity of flow into the pallet layer resulting in an over-estimated mean velocity or over-estimation of fluid-product heat transfer coefficients. A plot of predicted and measured air outlet temperature versus time is presented in Figure 7.20. The observed difference is not easily explained.

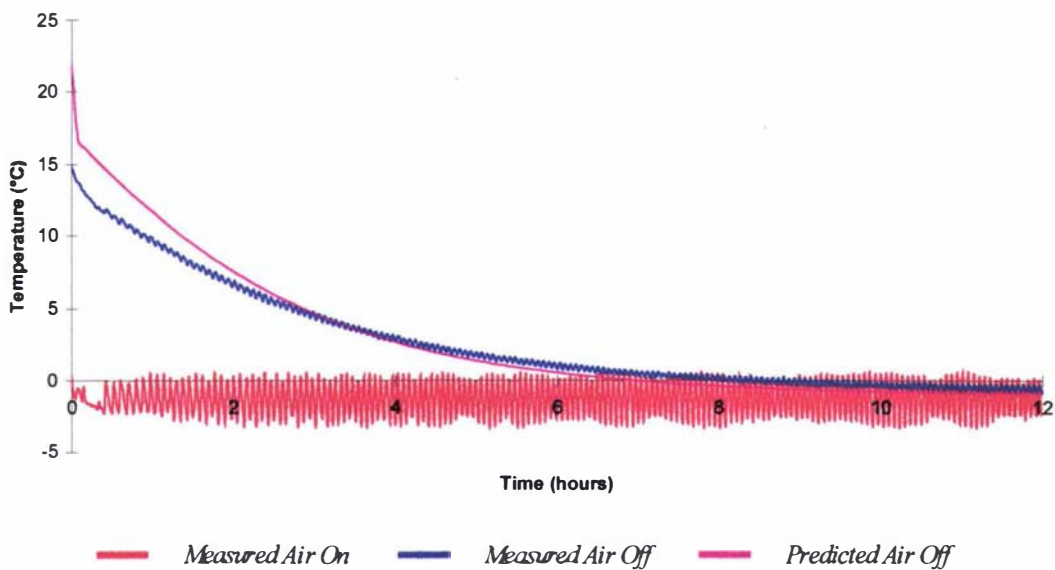


Figure 7.20. Predicted and measured air outlet temperature vs time for 'Zeus' apple packages in a pallet layer configuration - Modified from Falconer (1995a).

7.3.3. Packed Bed Experiment.

This experiment was performed to test the model in a packed bed situation using both air and water as the cooling medium. The objective was to collect reliable data for model testing, as well as define the benefits of using an alternative to air as the cooling medium. A forced-draft cooling experiment was undertaken using a 0.24m × 0.24m × 0.32m plastic package randomly packed with 'Braeburn' variety apples (the package was constructed with coarse wire mesh on each end face to retain the apples). Fruit and air temperature probes (24-gauge Type-T thermocouples attached to a Grant

Squirrel 16-channel datalogger) were placed at various positions within the package. Total measurement imprecision for temperature, accounting for thermocouple and datalogger inaccuracies, was expected to be approximately $\pm 0.2^\circ\text{C}$. The package was equilibrated in a constant temperature facility ($27^\circ\text{C} \pm 0.5^\circ\text{C}$) for 24 hours prior to movement to an experimental forced-draft cooling facility. The package was cooled for 3 hours. Superficial air velocity through the bed was controlled at $0.5\text{m}\cdot\text{s}^{-1}$ (measured using a Dantec Low Velocity Flow Analyser, Model 54N50; rated to $0.02\text{m}\cdot\text{s}^{-1}$ by the manufacturer) and inlet air temperature at $-1^\circ\text{C} \pm 0.5^\circ\text{C}$. Total measurement imprecision for mean velocity, accounting for flow analyser and fan delivery inaccuracies, was assessed to be at worst $\pm 0.1\text{m}\cdot\text{s}^{-1}$, but possibly much better.

Modeling was conducted using a $3\times 3\times 5$ zone configuration (giving a 45 zone datafile). The data used in development of the packed bed datafile were those presented in Table 7.6. These data are sourced from physical measurement and Appendix 2, whilst the velocity relativity profile, assuming evenly proportioned airflow across the z-face of the package configuration, is presented in Table 6.9. Figure 7.21 shows model predictions and measured data versus time. The model predictions for this cooling scenario showed good agreement with measured data, furthering the argument that the lack of fit to Falconer's data (Section 7.3.2) was more likely due to data uncertainty than model shortcoming.

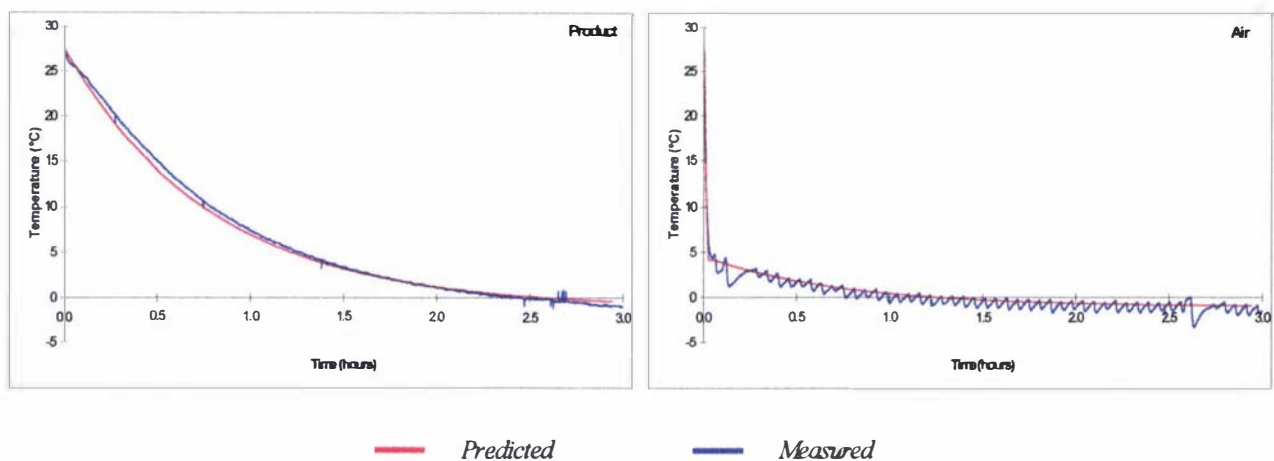


Figure 7.21. Predicted and measured product and air temperature vs time at the centre position of a packed bed container of apples – undergoing forced-air cooling.

Table 7.6.

Major data used for construction of a 45 zone, simulation model datafile for forced-draft cooling of a packed bed. These data are sourced from physical measurement and Appendix 2, whilst the velocity relativity profile is presented in Table 6.9.

Variable	Value	Units	Variable	Value	Units
Physical System Data			Product Data cont.		
Width of package (x)	0.24	m	Total mass of product	8.74	kg
Height of package (y)	0.24	m	Radius of each product item	0.035	m
Length of package (z)	0.32	m	Number of products in pack	47	
Porosity of package	0.463	fraction	Is respiration considered?	No	
Fluid velocity into package	0.5	m.s ⁻¹	Fluid Data		
Ventilation area in package	0.0576	m ²	Specific heat capacity	1005	J.kg ⁻¹ K ⁻¹
Package Properties			Thermal conductivity	0.026	W.m ⁻¹ K ⁻¹
Zones in x - direction	3		Density	1.28	kg.m ⁻³
Zones in y - direction	3		Convection factor	1	
Zones in z - direction	5		External Environment Data		
Number of V boundaries	60		External fluid temperature	-1	°C
Number of H boundaries	60		External fluid velocity	0.5	m.s ⁻¹
Number of P boundaries	54		Packaging Material Data		
Total internal zones	45		Plastic Construction		
Total external zones	1		Specific heat capacity	1800	J.kg ⁻¹ K ⁻¹
Number of pack materials	1		Thermal conductivity	0.12	W.m ⁻¹ K ⁻¹
Active package surfaces	6		Density	540	kg.m ⁻³
Product Data			Thickness	0.004	m
Specific heat capacity	3650	J.kg ⁻¹ K ⁻¹			
Thermal conductivity	0.42	W.m ⁻¹ K ⁻¹			

NB: Dynamic datafile located in 'Pre-cooling Input Files' directory ('Packaging Simulation for Design' software - Appendix 5), entitled: 'Air-cooled Packed Bed of Apples - 45 Zones.prn'.

Using the same experimental package as for air cooling, a hydro-cooling experiment was conducted. Fruit and air temperature probes (24-gauge Type-T thermocouples attached to a Grant Squirrel 16-channel datalogger) were placed at various positions within the package. This package was then equilibrated in a constant temperature facility (27°C ± 0.5°C) for 24 hours prior to movement to an experimental hydro-cooling facility. The package was cooled for 45 minutes. Using a recirculating system, water flow was directed through the package (velocity measured at 0.5m.s⁻¹ using an Electronic Measurement Technologies 'Testovent' 4000 flow meter), with initial water temperature of 15.8°C. Total measurement imprecision for velocity, accounting for flow meter and pump flow inaccuracies, was assessed to be no more than ± 0.1m.s⁻¹.

The data used in development of the modelling datafile were predominantly those presented in Table 7.6 with the substitution of the data presented in Table 7.7. These data are sourced from physical measurement and Appendix 2, whilst the velocity relativity profiles for packed bed configuration are presented in Table 6.9.

Table 7.7.

Amended major data (to those of Table 7.6) for development of a 45-zone, pre-cooling simulation model datafile for a hydro-cooled packed bed of apples.

Variable	Value	Units	Variable	Value	Units
Fluid Data			External Environment Data		
Specific heat capacity	4180	J.kg ⁻¹ K ⁻¹	Initial ext. fluid temperature	15.8	°C
Thermal conductivity	0.588	W.m ⁻¹ K ⁻¹	Final ext. fluid temperature	16.1	°C
Density	999.1	kg.m ⁻³			

NB: Dynamic datafile located in 'Pre-cooling Input Files' directory ('Packaging Simulation for Design' software - Appendix 5), entitled: 'Hydro-cooled Packed Bed of Apples – 45 Zones.prn'.

The prediction of the hydro-cooling scenario was excellent (Figure 7.22). Measured data agreed well with predicted data for all positions in the packaging configuration. This scenario also shows the effectiveness of using water as a cooling medium, as the heat transfer characteristics of this flow medium are far superior to those of air. Again, the quality of fit supports the contention that the lack of fit in Section 7.3.2 is as a result of data inaccuracy rather than model-caused.

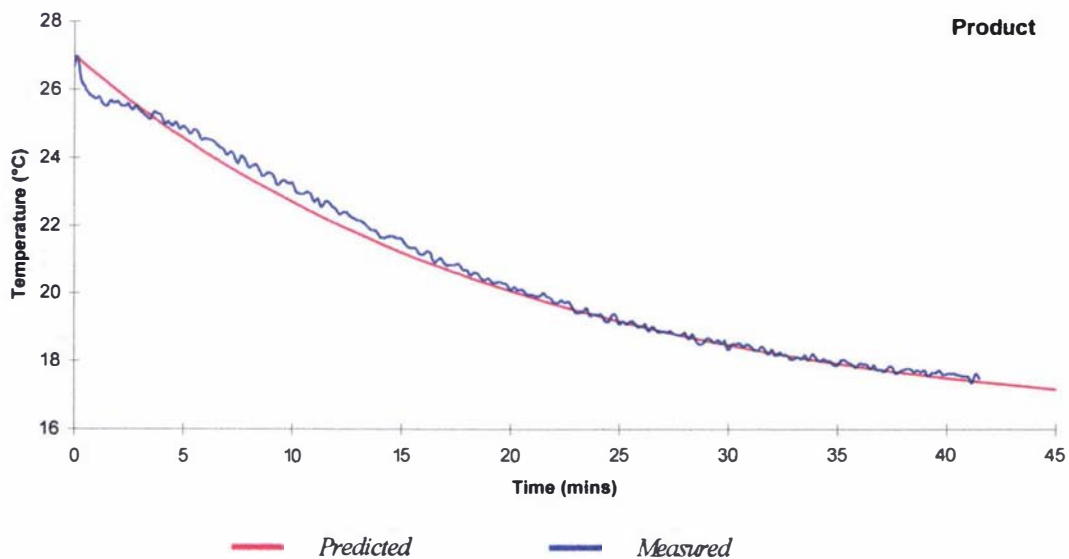


Figure 7.22. Predicted and measured fruit temperature vs time for the centre position of the packed bed container of apples – undergoing hydro-cooling.

7.3.4. Data collected by staff at UC - Davis (1996).

Research staff at the University of California – Davis, undertook a study of pear cooling in bins using air as the cooling medium. A wooden bin of 1.2m × 1.2m × 0.6m high was used to contain 75mm diameter pears. The data used in development of the simulation model datafile are presented in Table 7.8.

Table 7.8.

Major data used for construction of a 27 zone, pre-cooling simulation model datafile for forced-draft cooling of a bin of pears. These data are sourced from physical measurement and Appendix 2, whilst the velocity relativity profile is presented in Table 6.8.

Variable	Value	Units	Variable	Value	Units
Physical System Data			Product Data cont.		
Width of package (x)	1.2	m	Total mass of product	640	kg
Height of package (y)	0.6	m	Radius of each product item	0.0375	m
Length of package (z)	1.2	m	Number of products in pack	3200	
Porosity of package	0.463	fraction	Is respiration considered?	No	
Fluid velocity into package	2.17	m.s ⁻¹	Fluid Data		
Ventilation area in package	0.144	m ²	Specific heat capacity	1005	J.kg ⁻¹ K ⁻¹
Package Properties			Thermal conductivity	0.026	W.m ⁻¹ K ⁻¹
Zones in x - direction	3		Density	1.28	kg.m ⁻³
Zones in y – direction	3		Convection factor	1	
Zones in z – direction	3		External Environment Data		
Number of <i>V</i> boundaries	36		External fluid temperature	0.95→1.3	°C
Number of <i>H</i> boundaries	36		External fluid velocity	2.17	m.s ⁻¹
Number of <i>P</i> boundaries	36		Packaging Material Data		
Total internal zones	27		Wooden bin		
Total external zones	1		Specific heat capacity	2500	J.kg ⁻¹ K ⁻¹
Number of pack materials	1		Thermal conductivity	0.12	W.m ⁻¹ K ⁻¹
Active package surfaces	6		Density	700	kg.m ⁻³
Product Data			Thickness	0.015	m
Specific heat capacity	3750	J.kg ⁻¹ K ⁻¹			
Thermal conductivity	0.51	W.m ⁻¹ K ⁻¹			

NB: Dynamic datafile located in ‘Pre-cooling Input Files’ directory (‘Packaging Simulation for Design’ software - Appendix 5), entitled: ‘Air-cooled Bin of Pears – 27 Zones.prn’.

There is always potential difficulty in using data collected by other researchers or research teams because some of the necessary data needed for new purposes (ie. testing of the modelling methodology) were not directly available. Research team members are therefore often required to recall the details of aspects of their experiment, such as pear diameter and ventilation area, or the assumptions made. This leads to some loss of input data accuracy. Model predictions are shown in Figure 7.23.

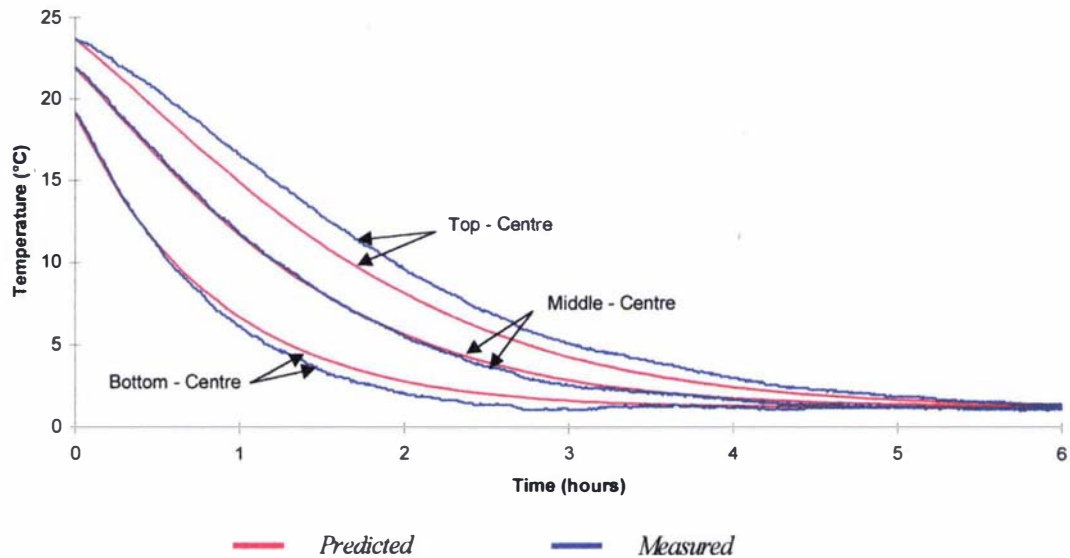


Figure 7.23. Predicted and measured fruit temperatures vs time for three positions in a bin of pears using airflow of $0.313\text{m}^3\cdot\text{s}^{-1}$.

The lack of fit shown in some regions (predominantly top and bottom of the bin) might be explained by the positioning of the fruit into which thermocouples were inserted (Figure 7.24). The probed fruit in the bottom of the bin was the lowermost fruit in the package whereas the simulated fruit temperature for the ‘bottom’ of the bin is a mass average temperature for the lower 1/3 of the package. In reality, fruit at position E_B will cool faster than those at position S_B . Likewise, the ‘top’ position is for a fruit in the top layer of the bin, whereas the modelling geometry predicts a mass average for the top 1/3 of the package, which will be a lower temperature.

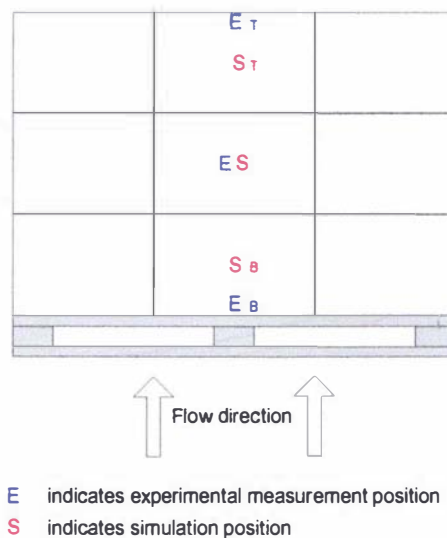


Figure 7.24. Positions where measurements were taken within the pear bin by UC – Davis Research Staff, and simulation positions in a 27-zone pear bin model datafile.

Increasing the number of zones in the simulation would increase the accuracy of the predictions. Disadvantages are increased simulation time and increased datafile complexity. Taking this into account and noting that only in the central position is a quantitative comparison possible agreement was considered satisfactory. This quality of fit adds support to the argument that the lack of fit in Section 7.3.2 is due to input data inaccuracy.

Earlier, the use of Amos' experimental cooling situations to investigate model validity and sensitivity of results to input data uncertainties was reported. Further sources of variation were conveniently investigated by sensitivity analyses of the 27 zone pear bin predictions. The sensitivity to variation of the following model input data were assessed:

- product specific heat capacity,
- product thermal conductivity,
- fluid specific heat capacity,
- fluid density, and
- fluid thermal conductivity.

(i) *Sensitivity to variation in product specific heat capacity*

In themselves, fruit are variable, and there is no certainty that a published value, no matter how precisely measured, will accurately represent actual fruit present in an experiment or industrial application. For simplicity, the sensitivity to variation was demonstrated in Figure 7.25 using $\pm 10\%$ changes in the published value for pears.

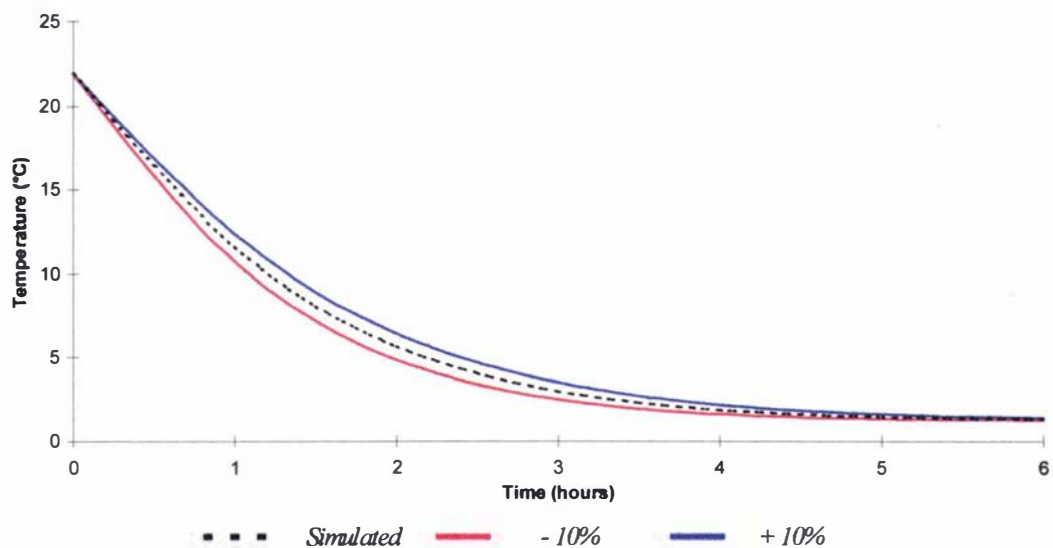


Figure 7.25. Assessment of sensitivity to variation in of product specific heat capacity (simulated value for pears: $3750 \text{ J.kg}^{-1}\text{K}^{-1}$) of $\pm 10\%$. The position used is the middle (centre) zone of the 27-zone pear bin.

It was concluded that inaccuracy in specific heat capacity had a small, but noticeable effect on the prediction accuracy. This model-input variable, which is always subject to an imprecision of a few percent, may therefore have contributed to some of the differences between measured and predicted temperatures in all test cases.

(ii) *Sensitivity to variation in product thermal conductivity*

Product thermal conductivity was assessed similarly. There are differing values in the literature for the same product and the various theoretical methods available for calculation of this parameter do not give the same predictions. The effect of inaccuracy in this parameter was also assessed using $\pm 10\%$ variations in the published value for pears (Figure 7.26).

The predictions proved to be insensitive to changes in product thermal conductivity (which was the expected case in cooling situations where the Biot number, Bi tends to 0).

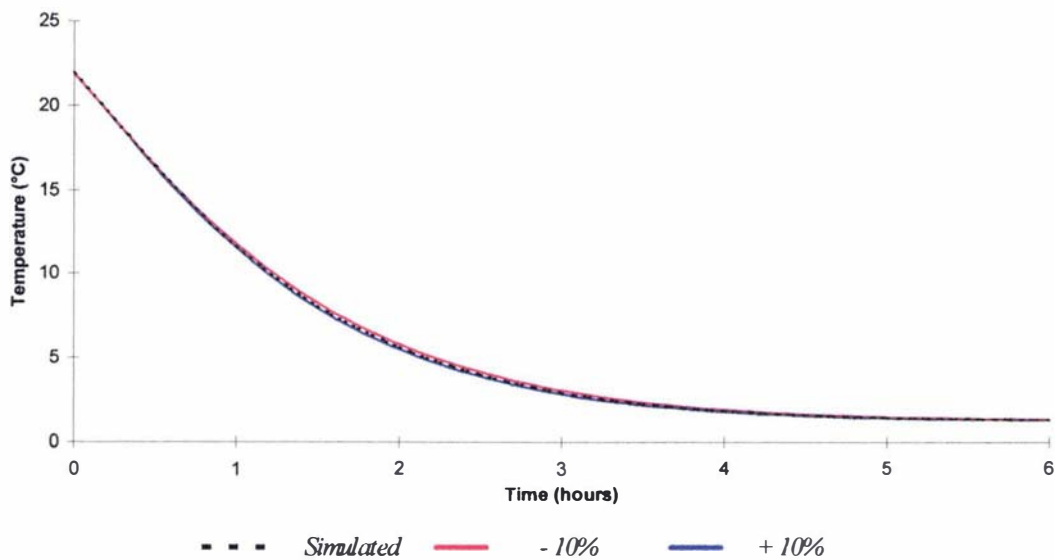


Figure 7.26. Assessment of sensitivity to variation in product thermal conductivity (simulated value for pears: $0.51 \text{ W.m}^{-1}\text{K}^{-1}$) of $\pm 10\%$.

(iii) *Sensitivity to variation in fluid specific heat capacity*

As with the product thermo-physical properties, the potential for inaccurate knowledge of fluid component properties to effect model predictions was assessed. For convenience, a $\pm 10\%$ change was considered (Figure 7.27), even though most commonly used fluids have been characterised to well within $\pm 1\%$.

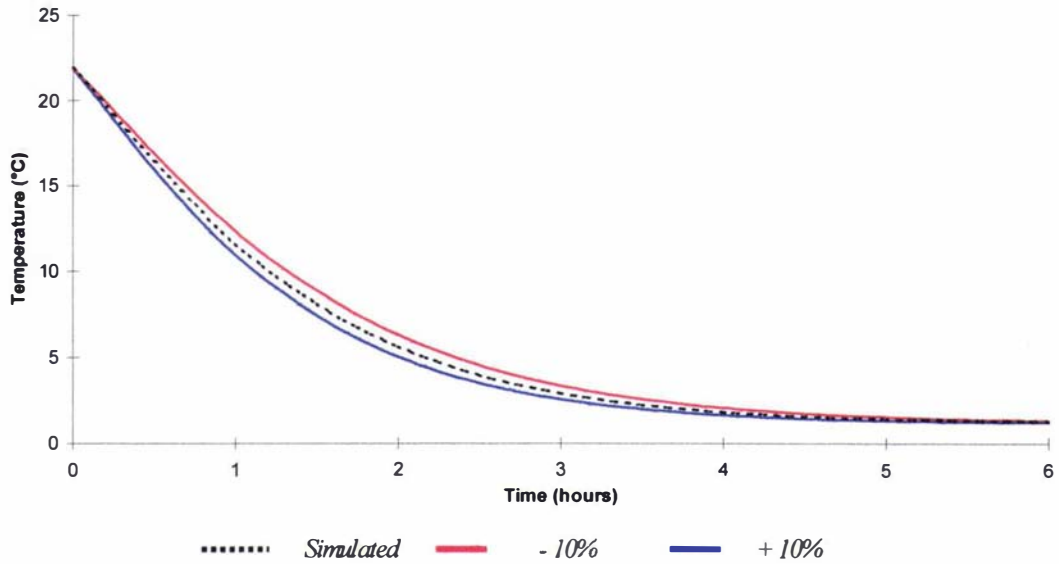


Figure 7.27. Assessment of sensitivity to variation in fluid specific heat capacity (simulated value for air: $1005 \text{ J.kg}^{-1}\text{K}^{-1}$) of $\pm 10\%$.

It was concluded that for common fluids, lack of fit was unlikely to arise from this source.

(iv) *Sensitivity to variation in fluid density*

The fluid density was similarly assessed (Figure 7.28). Density of the fluid is normally very well known so lack of fit through this source is unlikely.

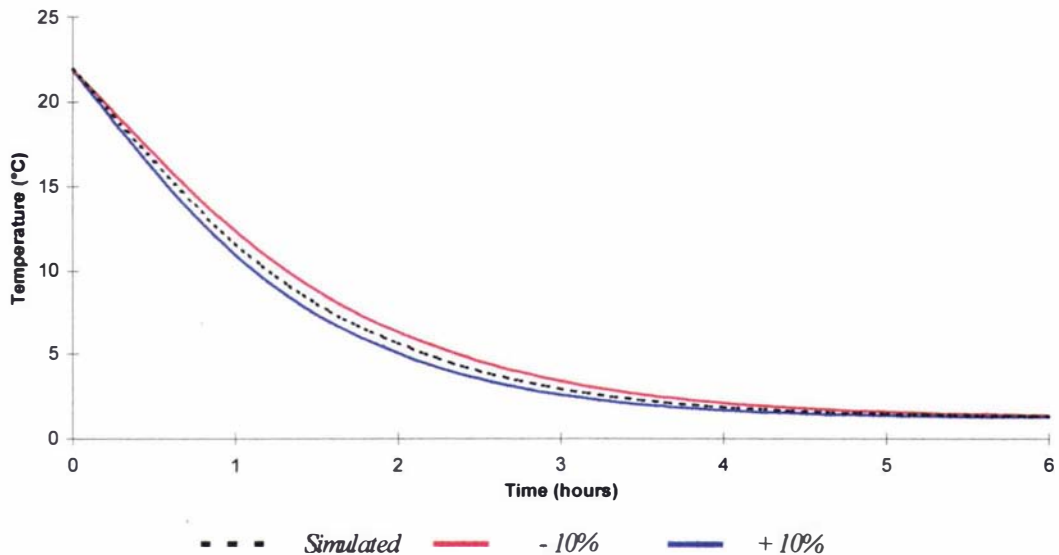


Figure 7.28. Assessment of sensitivity to variation in fluid density (simulated value for air: 1.28 kg.m^{-3}) of $\pm 10\%$.

(v) Sensitivity to fluid thermal conductivity

The fluid thermal conductivity was assessed similarly (results not shown). The model was insensitive.

7.4. DISCUSSION OF MODEL PERFORMANCE

Assessment of model performance would ideally be undertaken using statistical, or other quantitative techniques. Such an approach was not possible for those data sets obtained from other researchers, as in these cases, data for spread of replicates were not available. For those systems where measurement was undertaken at Massey University (as part of this work), replication of cooling trials was not possible due to scheduling of the work outside the apple season. There were insufficient similar fruit in good enough condition to withstand reheating and equilibration at 20 - 25°C to allow independent replication of trials. When fruit in good condition were available, the mass transfer experimentation was given precedence at the wishes of the project sponsor.

Thus, the evaluation of model predictions, from multiple independent data sources, involved careful visual inspection of measured and predicted temperatures, sensitivity analysis, and assessment of the impact of uncertainty sources by engineering judgement alone. The graphical representations showed that model predictions were in agreement with experimental results, and generally any disagreement between experimental data and predictions was probably more caused by uncertainties in input data than it was by model shortcomings. Only Figure 7.20 gave a substantial lack of agreement in the shape of the profile.

It is considered that the nine inter-zonal and one intra-zonal heat transfer pathways included in the model simulate all those mechanisms likely to be significant in industrial practice for a range of products and packages. Not all heat transfer pathways were significant contributors to temperature change in every package tested, so it was not possible to make an absolute claim of accuracy for all the heat transfer sub-models in all circumstances. However, the successful testing using eight types of package and data from four independent sources, plus the results of the sensitivity analysis, suggests that the model can be used with confidence for simulation of pre-cooling of commonly occurring package designs.

Further, the overall quality of fit to experimental data builds confidence in the use of the velocity profile characterisation system, explained in Chapter 6, for immediate industrial application in the New Zealand horticultural industry.

Overall, whilst the level of proof is not absolute (and never is for any mathematical model), there is confidence that accurate predictions can be expected if good quality model-input data are available.

Further, the envisaged use of this prediction system was not assessment of measured data (although this is necessary to understand the likely level of accuracy), but assessment of the relative effect of different packaging configuration design on product heat transfer. Investigation would probably be undertaken by ‘fixing’ those data which would remain constant in a cooling situation, whilst varying the key parameters. The relative effects of such changes may be more accurately predicted than the absolute cooling rate.

7.5. RECOMMENDATIONS FOR FUTURE WORK

The testing and validation of the heat transfer simulation model has shown that the generality built-in during formulation of the mathematical models, was a key contributor to successful prediction of temperature profiles of products and fluids in different horticultural packages. Future improvements may be possible by diversifying the simulation model to include food products other than those horticultural. These could include:

- meat chilling, including two-stage cooling regimes;
- chilling of processed foods, such as canned goods; and
- cooling, and heat generation, in powdered goods.

CHAPTER 8

MASS TRANSFER (BULK STORAGE) MODEL TESTING

8.1. INTRODUCTION

This chapter outlines the approach taken to test and validate the mass transfer (bulk storage) component of the computer-based “Packaging Simulation for Design” model, as well as the steady-state ‘Weight Loss Simulator’ model. An experimental programme was conducted in conjunction with ENZAFRUIT New Zealand (International), to provide both model testing data for both mass transfer models, as well as immediately useable data for packaging development by the apple industry. Results from this experimental programme are compared with model predictions.

8.2. EXPERIMENTAL DATA COLLECTION

Previous research into mass loss in a range of apple packaging configurations had been conducted by ENZAFRUIT New Zealand (International) and contracted parties. These programmes, their results, and their limitations are explained below.

8.2.1. Previous Data Collected for Apple Package Configurations

Bartholomew (1990) reviewed all ‘in house’ mass loss research work conducted by ENZAFRUIT New Zealand (International) up until that time. Data were presented for different varieties stored under standard conditions (specified for each variety) with some varieties stored in polyliners while others were not. These data are shown in Tables 8.1 and 8.2.

Table 8.1.

Assessment of mass loss as a result of storage regime and variety for the 1986 apple season - After Bartholomew (1990).

Variety	Storage Conditions	Time in Storage	% Mass Loss
Gala	0.5°C, no polyliner	10 weeks	3.16
Red Delicious	0.5°C, no polyliner	8 weeks	3.05 - 3.12
Braeburn	0.5°C, no polyliner	12 weeks + 1 week ambient	3.10 - 3.44
Cox Orange Pippin	3°C, polylined	13 weeks	1.6

Table 8.2.

Assessment of mass loss as a result of polyliner use for 'Braeburn' apples in the 1985 season - After Bartholomew (1990).

Variety	Storage Conditions	Time in Storage	% Mass Loss
Braeburn	0.5°C, no polyliner	12 weeks + 1 week ambient	3.72
	0.5°C, unperforated ¹ polyliner	12 weeks + 1 week ambient	0.62
	0.5°C, standard ² polyliner	12 weeks + 1 week ambient	0.74
	0.5°C, microperforated ³ polyliner	12 weeks + 1 week ambient	0.65

¹ The unperforated polyliner had no holes.

² The standard polyliner had 16 holes (diameter not given).

³ The micro-perforated polyliner was not described.

Additional data for Cox Orange Pippin in both polylined and un-polylined cartons were also presented which showed that fruit in un-polylined cartons lost on average 66% more weight than those placed in polylined cartons. However, no data were presented to indicate what proportion of the reduction in mass loss was as result of suppressed respiration rate due to atmospheric modification, and therefore reduced rate of carbon loss and what proportion was due to a decrease in the partial pressure driving force (rise in relative humidity within the liner). Coolstore relative humidity conditions were not measured.

Frampton *et al.* (1994) investigated the mass loss of apples during storage and shipping. The rate of mass loss from a carton of fruit was approx. 9.5×10^{-8} kg.s⁻¹ for 'Royal Gala' and 'Braeburn'. The storage temperature and relative humidity were not stated in the report.

Frampton and Ahlborn (1994) presented data for the effect of different cooling regimes on the long-term rate of Royal Gala mass loss (Table 8.3, Figure 8.1). Room-cooled fruit had a mean rate of approx. $9.4 \times 10^{-8} \text{ kg.s}^{-1}$ while forced draft-cooled fruit had a mean rate of approx. $6.5 \times 10^{-8} \text{ kg.s}^{-1}$.

Table 8.3.
Mass changes in a carton of Royal Gala apples after 13 weeks coolstorage (g) - After Frampton and Ahlborn (1994).

	Mass change after 13 weeks of coolstorage (g)		Mass change after 7 days at ambient (g)	
	Room Cooled	Force Draft	Room Cooled	Force Draft
Fruit	-619 ± 57	-431 ± 28	-150 ± 49	-133 ± 30
Packaging	+131 ± 24	+111 ± 21	+96 ± 34	+92 ± 40
Gross	-486 ± 49	-337 ± 24	-241 ± 55	-241 ± 62

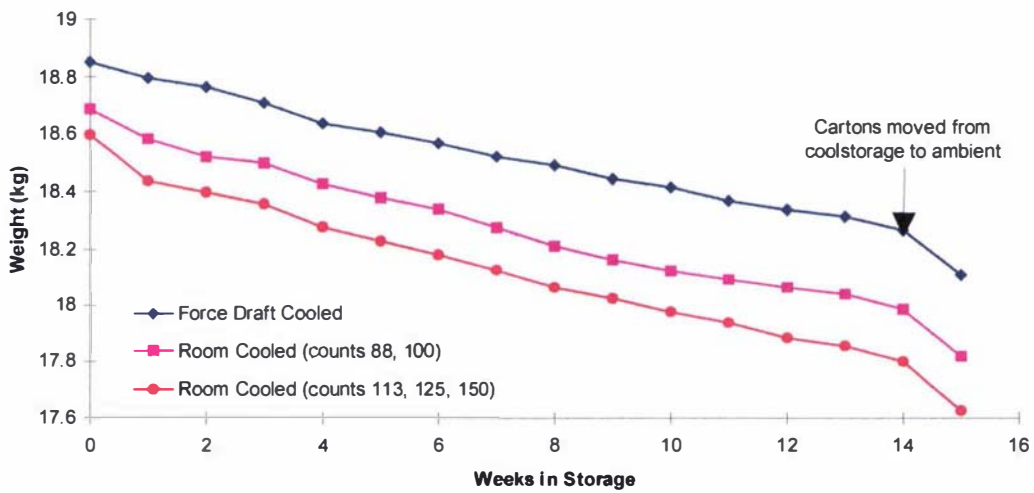


Figure 8.1. Royal Gala weekly fruit weights during 13 weeks coolstorage (After Frampton and Ahlborn, 1994).

Frampton (1995) presented further results for mass loss in 4 apple carton configurations (Standard, '60 x 40 Retail Display Trays' (RDT), 'Zeus' un-vented and 'Zeus'-vented) after storage and shipping to the United Kingdom. One carton from each of two positions (outside centre of pallet and top corner) were removed from a pallet stack, disassembled and the components weighed. This work showed that the carton configuration had no effect on fruit mass loss as fruit packed in all carton types lost 1.2 - 1.3% over an 8 week storage period. This trial was performed on only a small sample (approx. 400 fruit).

Burmeister *et al.* (1996) measured apple mass loss in different packaging configurations; 'Zeus' packages, RDT's as well as 'Standard' apple cartons, with the treatments being as follows; polylined, taped over side vents and normal storage. It was found that fruit in the 'Zeus' pack lost more mass than in the standard pack. Relative humidity measurements were not conducted during this work.

Burmeister *et al.* (1997) investigated the influence of increased time between harvest and placement in a forced draft cooler on mass loss and visual shrivel. Two fruit treatments were assessed:

1. After forced-draft cooling in bins, fruit were hand-packed into Zeus packages, either with or without polyliners, and placed in static coolstorage, or
2. After forced-draft cooling in bins, fruit were held in static coolstorage for 9-11 weeks before being repacked into Zeus packages either with or without polyliners.

Results indicated that delaying cooling increased total mass loss and visual shrivel. Inclusion of a polyliner reduced mass loss and visual shrivel in both fruit treatments, but storage in bins increased the mass loss and shrivel of fruit. Important environmental conditions, such as in-package relative humidity, were not presented.

Whilst all these experimental programmes provided useful data for package assessment, they had insufficient or inappropriate data for testing of the mass transfer model for apple-packaging systems. As a consequence, a new experimental programme was initiated in a commercial coolstorage facility in Hastings, New Zealand, to gather mass loss and associated system data for apple packaging systems. In addition, an experimental programme, conducted in controlled laboratory conditions, was carried out at Massey University for two tomato packaging configurations.

8.2.2. Mass Loss Data Collection

Specific objectives of this work were to:

1. Quantify the influence of pack type and configuration on fruit mass loss.
2. Measure the levels of relative humidity modification within packaging systems.
3. Measure packaging material water uptake.

Experiments designed to meet these objectives would provide information directly to the project sponsor on the effects of relative humidity modification, packaging system atmospheric modification and packaging materials on product mass loss. By

conducting a wide variety of experiments, the data would also provide a fair test of the validity of the proposed models.

8.2.2.1. Experimental Methodologies

Apple Mass Loss

This research programme was undertaken in an ENZAFRUIT coolstorage facility (Whakatu, Hastings). The trial consisted of the two commercially used packaging configurations (the 0.313m × 0.257m × 0.482m ‘Zeus’ or ‘Z-Pack’ and the 0.4m × 0.151m × 0.6m ‘Retail Display Tray’ or ‘RDT’) each with at least four treatments as shown in Table 8.4.

Table 8.4.
Package configurations and their modifications tested in the mass loss trial.

Pack Type	Treatments				
	Unmodified	No Ventilation	Vented Polyliner	24 Hole Vented Polyliner	Pallet Cling Wrap
Z-Pack	✓	✓	✓	✓	✓
RDT	✓	✓	×	✓	✓

Eighteen pallets (each pallet consisting of 49 cartons) of apples were used in this experiment. These fruit were delivered to the storage facility from two growing regions, Hawke’s Bay (Grower No. D183) and Waikato (Grower No. B134), after packing. These two regions were used, as Waikato fruit are often considered more susceptible to mass loss than Hawkes Bay fruit. Use of fruit from a single grower in each region was desirable for minimising variability sources beyond the store. Both consignments of fruit were stored at ambient conditions for a similar length of time (approx. 24 hours) prior to a forced-draft cooling regime of 12 hours. After forced-draft cooling, fruit were placed in static storage for up to 3 days prior to assembly in the package configurations.

The following procedures and materials were used:

- Experimental package and pallet assembly and initial weighing took place within the coolstore.
- Control pallets were assembled according to standard commercial storage practice.
- Standard polylined Z-Packs used a high-density polyethylene gauge, 18 µm, 24 × 6mm hole, liner for encasing fruit (Source: Chequer Systems Ltd.).

- Vented polylined Z-Packs used a 3-layer laminate, ~25 μm prototype polyliner (as shown in Figure 8.2.) for encasing fruit (Source: Chequer Systems Ltd.). This polyliner system was developed to allow airflow through the packaging system during forced-draft cooling, and the vents would close during bulk-storage (low flow) conditions.
- Polylined RDT's used a 'standard' high-density polyethylene gauge, 18 μm , holeless, liner for encasing fruit (Source: Chequer Systems Ltd.).
- Cling wrapped samples were palletised as normal before the addition of a single layer (with minimal overlap) of SM570Y micro-perforated cling wrap with a "100" perforation pattern and 15 micron thickness (Source: WR Grace Cryovac Ltd.) around the entire pallet. The perforation area of this film was 3.2%.

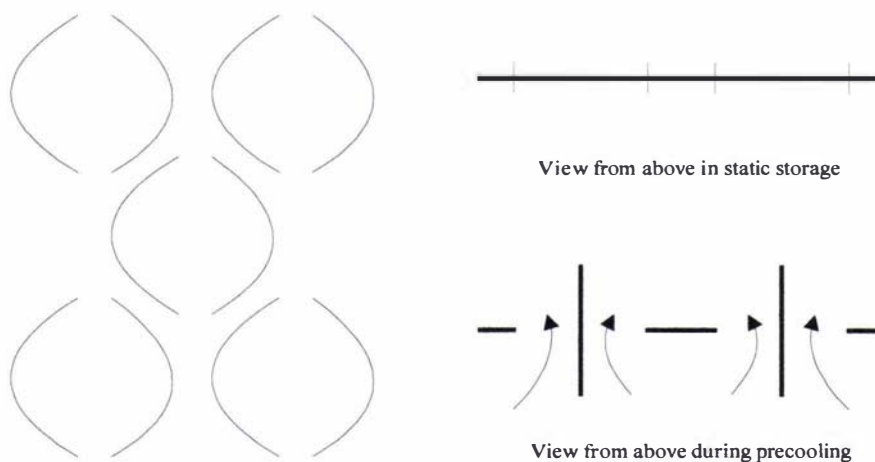


Figure 8.2. Outline of the construction (left) of the ventilation holes in the prototype ENZA vented polyliner. Dark lines indicate die cuts in the polyliner material. The mode of action is also presented (right).

After assembly, pallets were moved to the storage area. All packages on a pallet were used for data collection. Up to 16 packages per pallet were fitted with temperature (24-gauge Type-T thermocouples attached to a Grant Squirrel 16-channel datalogger) and relative humidity (Vaisala HMP 130Y Series Humidity and Temperature Transmitters - calibrated at 0°C and 80-96% RH, also attached to a Grant Squirrel 16-channel datalogger) sensors. These packages were used to assess atmospheric modification, whereas all others were used in mass measurements. Total temperature measurement imprecision, accounting for the thermocouples and datalogger inaccuracies, was expected to be approximately $\pm 0.2 - 0.3^\circ\text{C}$. Total measurement imprecision for relative humidity, accounting for probe and datalogger inaccuracies, was expected to be approximately $\pm 2\%$.

Destructive mass measurements were performed on both the fruit and packaging materials from 10 cartons per pallet of Z-Packs after each of 4 and 8 weeks in storage (using a Mettler PM30000 balance; resolution of 0.0001kg). After 12 weeks, all remaining cartons were assessed. Spacer cartons were used at each 4 weekly destructive test to replace those cartons removed during testing. Measurements were also taken of localised store air relative humidity, temperature and air velocity in the storage facility at seven-day intervals.

Destructive measurements at 4 and 8 weeks were not performed on RDT configurations as it was judged that dismantling of the pallet would result in atmosphere loss in all trays, which may have affected the measured mass loss.

Unlike many previous measurements by ENZAFRUIT, the measurements of product mass loss were carried out inside the coolstore environment. This avoided error arising from changes in cold fruit mass due to condensation under ambient conditions (as demonstrated in Figure 8.3). The increases observed are reversible, as condensate will evaporate from the rewarming surface, as shown for the single fruit and layer of fruit in Figure 8.3. Reversal would also be expected to occur from the complete package after further time at ambient conditions.

Skin mass transfer coefficients for a sample of 100 'Braeburn' fruit were calculated by controlled weight loss characterisation. These fruit were weighed (using a Mettler PM1206 Balance; resolution of 0.001g) then placed in a dedicated transpiration cabinet, with moderate velocity airflow ($> 2 \text{ m.s}^{-1}$), for 24 hours under strict temperature and humidity control. Fruit were re-weighed upon removal. A random sample of 24 fruit was used to characterise respiration rate, thus determining the proportion of mass loss that was respiratory carbon loss. This latter was measured by placement of individual product items in a flushed, sealed jar for 20 minutes after which a sample of the gas atmosphere was analysed for CO₂ composition. Using the weight loss, relative humidity and product and air temperature data, the mass transfer coefficient was calculated, using standard mass conservation and mass transfer equations.

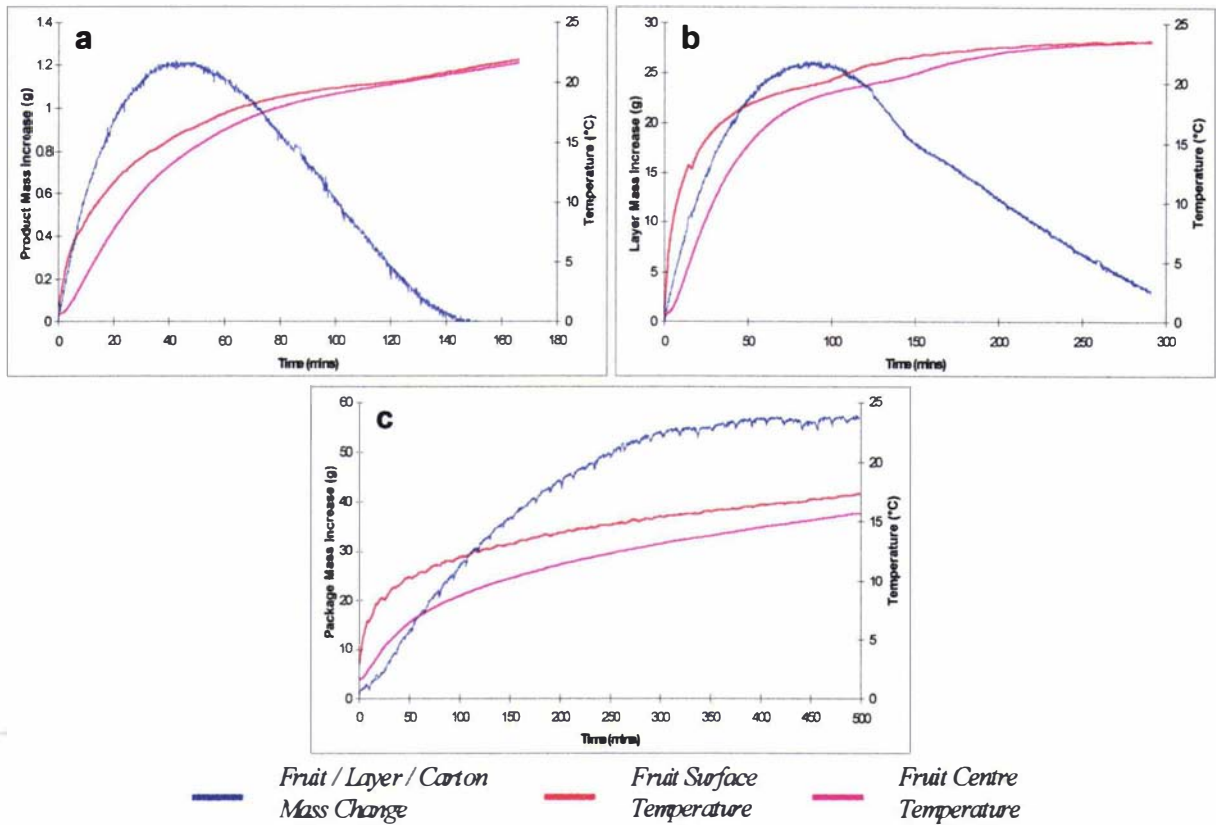


Figure 8.3. Measured mass changes vs time in (a) a single apple fruit, (b) a layer of fruit within a package and (c) a complete apple package, after removal from coolstorage conditions to laboratory-controlled ambient conditions (23°C and 65% RH) for mass loss measurements.

Tomato Mass Loss

Mass loss was measured in two package configurations (Figure 8.4) for hothouse tomatoes (early blush, size 60-70) in a laboratory controlled storage situation (15°C and 78% RH). The first configuration assessed was a 10kg corrugated paperboard (62623 CB - 623 C composite) package, used for local market packaging of hothouse tomatoes in New Zealand. This 0.3m × 0.38m × 0.185m carton contained 4.3% ventilation area, predominantly on the top face. The second package configuration assessed was a 15kg, 0.335m × 0.335m × 0.28m plastic package with 2.6% ventilation area when stacked (as the open top is covered).

The experimental programme was undertaken in controlled temperature and humidity rooms in the Centre for Post-harvest and Refrigeration Research at Massey University. This facility allowed control of temperature at 14.0 ± 0.5°C and 75 - 78% RH for a 4-5 day period for measurement of ‘Hothouse’ tomato mass loss.



Figure 8.4. The two package configurations used to assess tomato fruit mass loss (left - 10kg corrugated paperboard carton used for local market packaging; right - 15kg plastic cube crate used to reduce water vapour transport pathways).

Three 10kg cartons of tomato fruit (25% blush) were purchased from a local wholesale distributor, and equilibrated at 20°C for 5 hours. All fruit were removed from packaging, labelled and weighed. Measurements to evaluate proportions of mass loss attributable to both respiration and water loss were conducted using the same methods as those for apple fruit (described earlier). All fruit were then placed in the storage facility for 6 hours to allow equilibration to the storage temperature.

Empty packages were placed in storage for 24 hours prior to fruit packing to allow the materials to reach equilibrium temperature and moisture content (the latter was important in only the paperboard package). Fruit were then placed in each package, along with fruit and air temperature probes (24-gauge Type-T thermocouples attached to a Grant Squirrel 16-channel datalogger) and relative humidity sensors (Vaisala HMP 130Y Series Humidity and Temperature Transmitters attached to a Grant Squirrel 16-channel datalogger). All measurements of product mass were carried out in the storage environment to avoid changes in fruit mass associated with condensation in ambient conditions. The configured package was placed on a balance (Mettler PM30000; resolution of 0.0001kg) and logged continuously for 4-5 days. Fruit and packaging material weights were re-measured upon completion of each mass loss experiment. Relative humidity and temperature in the storage facility were measured continuously over the duration of the experiment, whilst air velocity (using a Dantec Low Velocity Flow Analyser) in the storage facility was measured prior to, and during the experiment.

8.2.2.2. Results and Other Observations

Apple Mass Loss

Table 8.5 summarises results and Figure 8.5 shows trends for three of the fourteen configurations. Table 8.6 shows the mean in-package conditions.

Key observations were:

- The unmodified, non-ventilated and cling-wrapped Z-Packs lost more mass than the two polylined-carton configurations. The measured relative humidity was higher in these polylined configurations (Table 8.6).
- Fruit in both the top and bottom layers of all pallets, irrespective of base configuration, lost more weight than those in any other region in the pallet. This effect was more pronounced with pallets stored at floor level in a two pallet storage situation, probably due to an increase in temperature in these packages, brought about by the heat flow through the un-insulated concrete floor. Evidence for this explanation is provided by Amos (1995), who observed a 0.5°C increase in air temperature around the bottom pallet in an un-insulated apple storage room at the ENZAFRUIT Whakatu coolstorage facility.

Table 8.5.

Fruit mass loss results from all package configurations measured after \approx 4, 8 and 12 weeks (mean \pm 95% confidence limits, assuming replicates are normally distributed).

Package Configuration	Mean Mass Loss (%) \approx 4 weeks	Mean Mass Loss (%) \approx 8 weeks	Mean Mass Loss (%) \approx 12 weeks
Waikato Fruit:	after 27 days	after 57 days	after 85 days
Unmodified Z-Pack	0.64 (\pm 0.17)	1.27 (\pm 0.31)	1.60 (\pm 0.31)
Non ventilated Z-Pack	0.68 (\pm 0.24)	1.22 (\pm 0.31)	1.51 (\pm 0.35)
Vented ¹ polylined Z-Pack	0.17 (\pm 0.12)	0.57 (\pm 0.19)	0.89 (\pm 0.19)
Unmodified RDT	--	--	2.26 (\pm 0.42)
Standard unperforated polylined RDT	--	--	0.84 (\pm 0.17)
Hawke's Bay Fruit:	after 30 days	after 60 days	after 88 days
Unmodified Z-Pack	0.70 (\pm 0.12)	1.23 (\pm 0.12)	1.47 (\pm 0.16)
Non ventilated Z-Pack	0.74 (\pm 0.18)	1.16 (\pm 0.19)	1.48 (\pm 0.21)
Cling-wrapped Z-Pack	0.71 (\pm 0.14)	1.13 (\pm 0.17)	1.51 (\pm 0.16)
Standard 24 \times 6mm hole polylined Z-Pack	0.39 (\pm 0.16)	0.49 (\pm 0.19)	0.65 (\pm 0.15)
Vented ¹ polyliner Z-Pack	0.44 (\pm 0.15)	0.78 (\pm 0.20)	0.97 (\pm 0.18)
Unmodified RDT	--	--	1.87 (\pm 0.31)
Non ventilated RDT	--	--	1.52 (\pm 0.30)
Cling-wrapped RDT	--	--	1.78 (\pm 0.29)
Standard ² polyliner RDT	--	--	0.96 (\pm 0.19)

NB: ¹ = ventilated polyliner with slots corresponding to pack vents (Figure 8.2).

- Fruit in the top layer of the polylined Z-Packs lost 15 - 20% less mass than fruit in all other layers. This may be due to either or both a reduction in air volume in this layer resulting from folding of the polyliner over the fruit prior to placement of the 'capper' tray or this layer being bounded by only one 'Friday' tray (where all other layers are bounded on two surfaces by a water-absorbing 'Friday' tray).
- In >70% of cases, fruit in the top layer of polylined RDTs lost appreciably more mass than fruit in the bottom layer of the same tray. This may have been partly or completely explained by the observation that polyliners were possibly too small for the package configuration, and thus did not have sufficient overlap for adequate sealing in all trays.

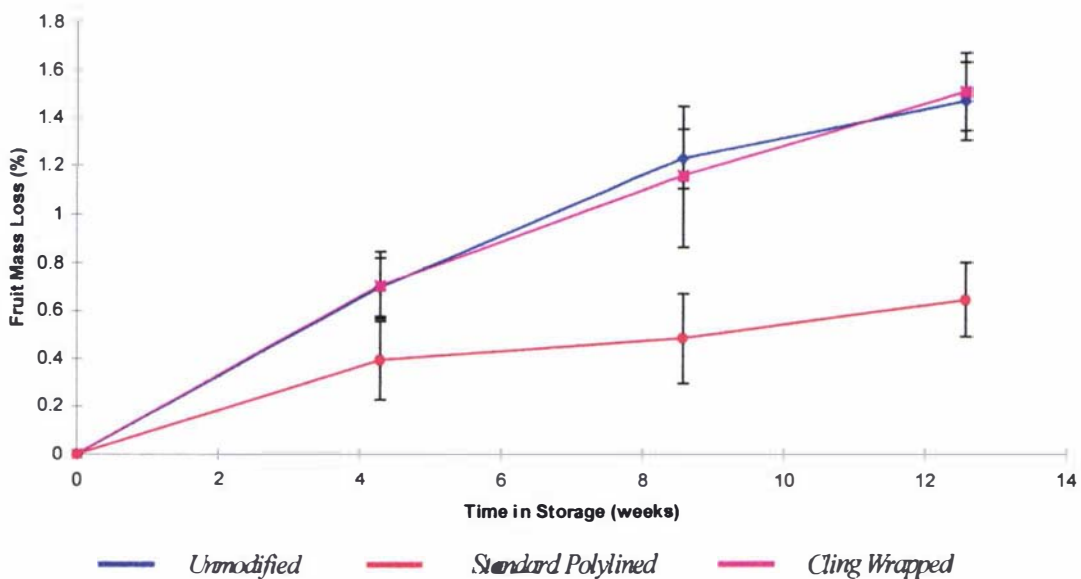


Figure 8.5. Mass loss vs time from three Hawke's Bay Z-Pack configurations during storage (with 95% confidence interval bars).

- Single layer cling-wrapping of pallets did not significantly reduce fruit mass loss. This was probably due to a larger than optimal perforation area on the provided wrap (3.2%), which resulted in a low relative humidity (RH) increase within the palletised units and therefore higher than anticipated mass loss. This over-perforation could have been overcome by use of a commercial wrapping method, in which overlapping of layers of wrap is common. King (pers. comm.) used a less perforated wrap (1.2%) in a separate on-shore / off shore pallet trial and found a 70 - 80% reduction in visual shrivel from susceptible fruit grown in the Waikato region. This was presumably due to a significant increase in RH inside the wrapped pallet with subsequent reduction in fruit mass loss. It is suggested that other materials (with perforation areas < 1.5%) and/or overlap wrapping be tested and the effects on in-package relative humidity and product mass loss be

measured. The resultant moisture contents of packaging materials and subsequent strength characteristics may need to be assessed also.

- Laboratory testing at 20°C and 50% RH indicated that at those conditions, respiratory mass loss was only 4.7% and 6.2% of total mass loss for the Waikato and Hawke's Bay fruit respectively. The carbon loss was similar in magnitude to values predicted using a temperature-dependant respiration model presented by Dadzie (1992) for 'Braeburn' apples. This model was used to estimate the contribution of carbon loss to total mass loss at actual storage conditions (Table 8.6). The common assumption that carbon loss is insignificant is wrong for this product-storage environment combination.

The degree of relative humidity modification developed in different packaging configurations is also shown in Table 8.6. Even though RH measurement accuracy was only $\pm 2\%$, the means are based on many measurements, so data are shown to 1 decimal place. The unmodified RDT gave an unexpectedly high result. The measured package air temperature was appreciably lower than all other packaging configurations.

Table 8.6.

Mean temperature and in-package relative humidity conditions (in comparison with mean coolstore conditions of 90% RH and 0.1°C). The contribution of carbon loss to mass loss is also presented.

Package Configuration	Fruit temperature	Package air temperature	In-package relative humidity	Contribution of carbon loss to mass loss
Unmodified Z-Pack	0.69°C	0.68°C	92.9%	17%
Non ventilated Z-Pack	0.81°C	0.80°C	95.2%	17%
Cling-wrapped Z-Pack	1.01°C	0.82°C	92.9%	16%
Standard polyliner Z-Pack	0.72°C	0.61°C	99.2%	39%
New vented polyliner Z-Pack	0.73°C	0.47°C	98.4%	24%
Unmodified RDT	0.48°C	0.38°C	96.0%	17%
Non ventilated RDT	0.64°C	0.51°C	95.0%	20%
Cling-wrapped RDT	0.70°C	0.51°C	95.9%	20%
Standard polyliner RDT	0.64°C	0.55°C	96.3%	29%

In the coolstore facility where the trial was conducted, staff took coolstore air relative humidity measurements at weekly intervals. Logistical difficulties meant that the calibration accuracy of the measurement equipment could not be checked, but a trend of increasing RH, between 86% and 90%, over the 12-week storage period was evident. Amos *et al.* (1993b) indicated that over the storage season, the relative humidity of a New Zealand apple coolstore increased by up to 15% when pre-cooling

was taking place in the store. There is also anecdotal evidence suggesting that in a bulk storage only facility, relative humidity will rise over the storage season. This rise is probably due to a reduction in ambient air temperatures outside the coolstore and an increase in stored product volume within the coolstore, leading to a changed Sensible Heat Ratio.

Gas atmosphere composition was measured from all package configurations. In no case, was appreciable CO₂ or O₂ modification found. Fruit quality was also assessed, with the incidence of visual shrivel found to be greater in non-polylined configurations, and greater in Waikato-grown fruit than in Hawkes Bay-grown fruit.

Packaging moisture content was analysed after 12 weeks in storage by drying a sample at 105°C for 48 hours (Table 8.7). Key observations were:

- Outer packaging reached a higher equilibrium moisture content (*emc*) in configurations without polyliners. This was due to this packaging being exposed to a higher, modified relative humidity inside the package. In contrast, the outer package of the polylined samples was directly exposed to only the bulk store relative humidity and hence the material had a lower *emc*.
- 'Friday' trays in polylined configurations absorbed more water than in non-polylined configurations due to the higher in-carton relative humidity. This moisture uptake was predominantly from the fruit (as this was the only water source in the package environment).

Table 8.7.

Mean moisture content of packaging materials at the conclusion of the mass loss trial.

Package Configuration	Moisture Content					
	Inner		Outer		'Friday' Tray	
	%	g	%	g	%	g
Unmodified Z-Pack	23.8	143	22.2	122	26.5	24
Non ventilated Z-Pack	22.8	137	23.2	128	26.4	24
Cling-wrapped Z-Pack	23.7	142	22.6	124	24.5	22
Standard polyliner Z-Pack	15.5	93	17.2	95	34.9	31
Vented polyliner Z-Pack	18.2	109	17.1	94	31.9	29

NB: Inner = Brown inner box - constructed of 626 (290/160/290 g.m⁻²) C flute.

Outer = White outer lid - constructed of 626 (290/160/290 g.m⁻²) B flute.

Tomato Mass Loss

Mass loss profiles from the two package configurations are presented in Figures 8.6 and 8.7. Key observations were:

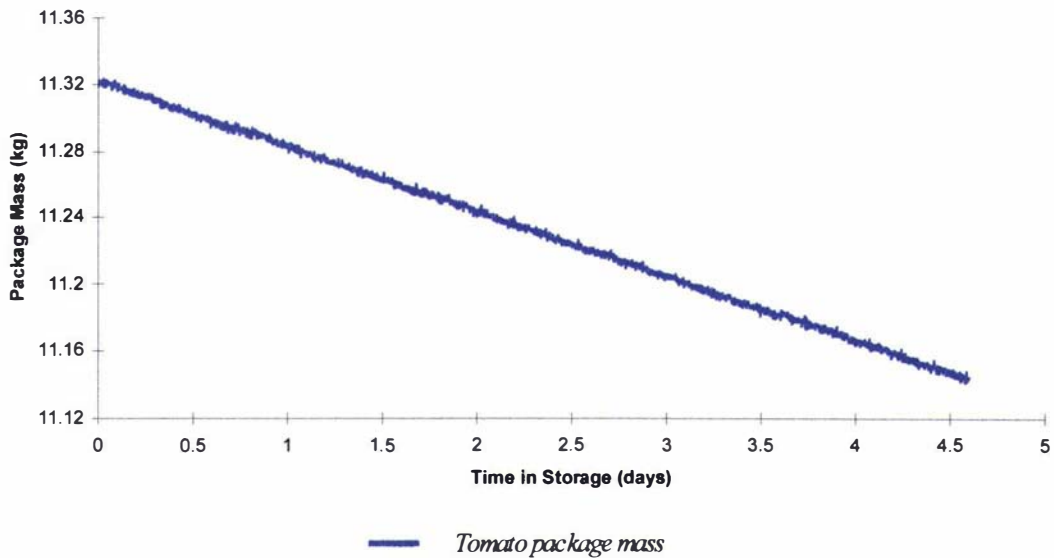


Figure 8.6. Plot of tomato package mass vs time in the mass loss trial (paperboard configuration - shown in Figure 8.5).

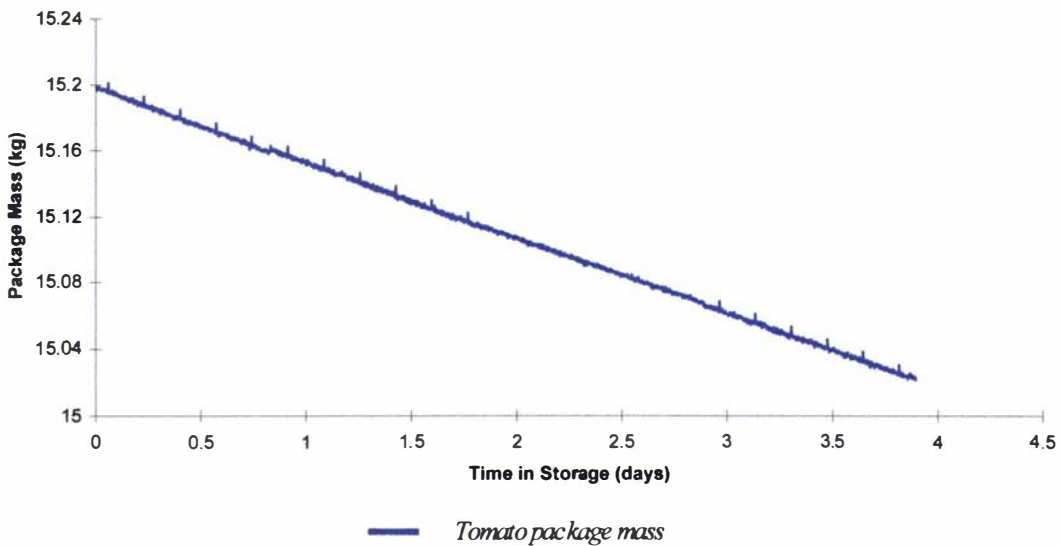


Figure 8.7. Plot of tomato package mass vs time in mass loss trial (plastic cube configuration - shown in Figure 8.5).

- The paperboard packaging configuration lost mass approx. 30% faster over this period in comparison with the plastic cube package.
- For the paperboard configuration, the measured steady-state relative humidity was found to be 88% (external conditions of 78% RH) with the paperboard packaging adsorbing approximately 3.6g of water.

- The plastic packaging configuration developed a steady-state relative humidity of 91% (external conditions of 75% RH). Within the measurement precision, the plastic packaging materials did not adsorb any moisture.

8.2.2.3. Summary of Experimental Observations and Discussion

Apple Mass Loss

The unmodified, non-ventilated and cling-wrapped packages lost more mass than polylined package configurations. In polylined Z-Pack cartons, the mass loss in the top layer was significantly lower than that from the other three layers.

There was no significant difference in total mass loss from fruit sourced from growers in the Waikato and Hawke's Bay regions although there was a difference in the proportion of fruit from these regions showing visual shrivel.

Single layer cling-wrapping of pallets performed poorly as a packaging strategy for reducing mass loss due to over-perforation of the wrap used, and the wrapping method used.

Use of polylined carton configurations resulted in reduced moisture uptake by the outer packaging (i.e. box and lid for Z-Pack and tray for RDT) in comparison to un-polylined configurations. The 'Friday' trays in the polylined configurations absorbed more water than those in un-polylined packages. There may be higher pallet strength for polylined cartons, reducing the incidence of pallet lean after long-term storage.

Those configurations with polyliners had a higher relative humidity in the airspace around the fruit (approx. 8% greater than the coolstore air) whereas non-polylined package configurations had a lower level of modification (3-5%). Gas atmosphere modification was found to be negligible within all package configurations, thus eliminating the possibility that mass loss reductions in polylined configurations were due to gas composition-induced respiration rate reductions.

Tomato Mass Loss

The observed 30% higher rate of mass loss in the paperboard packaging configuration suggests that the transmission of water vapour through the paperboard was significant. A higher relative humidity developed in the plastic package. Addition of a barrier layer on the paperboard materials, or a polyliner within the package configuration, may reduce the rate of mass loss significantly for paperboard packages.

8.3. MODEL TESTING - APPLE PACKAGING SYSTEMS

8.3.1. Mass Loss from Palletised, Unmodified, 1997 'Zeus' Apple Packages

Model testing using data for the 1997 Z-Pack apple-packaging configuration, in commercial bulk storage, was undertaken in two ways.

(a) *Modelling the 'Z-Pack' as a single, mixed zone*

A single, 'average' Z-Pack in a palletised situation (as shown in Figure 8.8) was modelled assuming no water vapour transport across four faces of the carton. The major data for the development of the 1-zone datafile used for simulation are presented in Table 8.8. A key assumption used in modelling this packaging configuration was that the flow velocity through the package ventilation holes was assumed to be 0 m.s^{-1} , due to both the nature of the storage facility, in which only low velocity forced airflow was occurring, and the high pressure-drop across the densely-packed carton.

To approximate the observed behaviour, it was assumed that the coolstore relative humidity changed 1% per 18 days in a stepwise fashion with time from an initial RH of 86% to 90% over the 3-month storage period.

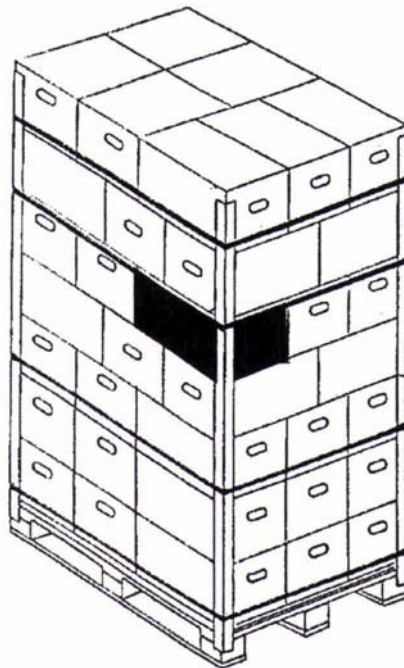


Figure 8.8. The positioning of an 'average' palletised Z-Pack (as shown in black).

Table 8.8.

Major data used for development of a single zone, bulk-storage simulation model datafile for an ‘average’ palletised Z-Pack. These data were sourced from physical measurement and Appendix 2.

Variable	Value	Units	Variable	Value	Units
Physical System Data			External Environment Data		
Width of package (x)	0.313	m	External fluid temperature	0.1	°C
Height of package (y)	0.257	m	Ext. fluid relative humidity	86→90	%
Length of package (z)	0.482	m	Packaging Material Data		
Porosity of package	0.457	fraction	'Friday' Trays		
Fluid velocity into package	0.0	m.s ⁻¹	GAB coefficient mc_0	6.537	g.100g ⁻¹
Ventilation area in package	0.00472	m ²	GAB coefficient ϕ_l	54900	
Package Properties			GAB coefficient γ_l	0.733	
Zones in x - direction	1		Material thickness	0.002	m
Zones in y - direction	1		MTC, K_{pkfl}	1.0e ⁻⁸	kg.m ⁻² .s ⁻¹ .Pa ⁻¹
Zones in z - direction	1		Packaging Resistance Factor	N/A	
Number of V boundaries	2		626 C Corrugated Board		
Number of H boundaries	2		GAB coefficient mc_0	6.022	g.100g ⁻¹
Number of P boundaries	2		GAB coefficient ϕ_l	80000	
Total internal zones	1		GAB coefficient γ_l	0.7	
Total external zones	1		Material thickness	0.0034	m
Number of pack materials	4		MTC, K_{pkfl}	1.0e ⁻⁸	kg.m ⁻² .s ⁻¹ .Pa ⁻¹
Active package surfaces	2		Packaging Resistance Factor	0.09	
Product Data			626 B Corrugated Board		
Product temperature	0.69	°C	GAB coefficient mc_0	5.848	g.100g ⁻¹
Product water activity	0.995	fraction	GAB coefficient ϕ_l	58400	
MTC, K_{flpr}	3.51e ⁻¹⁰	kg.m ⁻² .s ⁻¹ .Pa ⁻¹	GAB coefficient γ_l	0.729	
Respiration rate	2.53e ⁻¹¹	kg.m ⁻² .s ⁻¹ .Pa ⁻¹	Material thickness	0.0044	m
Product items in pack	100		MTC, K_{pkfl}	1.0e ⁻⁸	kg.m ⁻² .s ⁻¹ .Pa ⁻¹
Mass of individual item	0.186	kg	Packaging Resistance Factor	0.11	
Volume of individual item	2.1e ⁻⁴	m ³	626 C and 626 B Combined		
Surface area of individual item	0.0185	m ²	GAB coefficient mc_0	6.022 ^a	g.100g ⁻¹
Fluid Data			GAB coefficient ϕ_l	80000 ^a	
Internal fluid temperature	0.68	°C	GAB coefficient γ_l	0.7 ^a	
Atmospheric pressure	101325	Pa	Material thickness	0.0078	m
Fluid density	1.29	kg.m ⁻³	MTC, K_{pkfl}	1.0e ⁻⁸	kg.m ⁻² .s ⁻¹ .Pa ⁻¹
			Packaging Resistance Factor	0.13	

^a = there are no GAB coefficients for this paperboard, so data for 626C board were used.

NB: Dynamic datafile located in ‘Bulk Storage Input Files’ directory (‘Packaging Simulation for Design’ software - Appendix 5), entitled: ‘Unmodified Z-Pack - 1 Zone.prn’.

As stated in Chapter 5, the steady-state ‘Weight Loss Simulator’ assumes, by default, that the entire package configuration under investigation is a single, perfectly mixed zone. Predictions using both the steady-state simulation model and the dynamic simulator ‘Packaging Simulation for Design’ are presented in Figure 8.9.

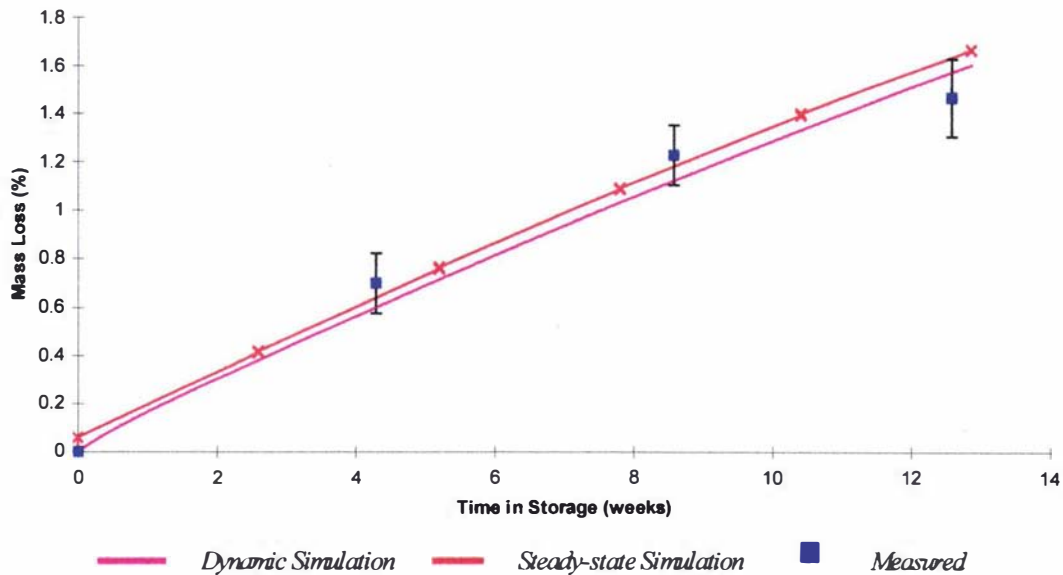


Figure 8.9. Predicted and measured fruit mass loss vs time for a single palletised apple Z-Pack in commercial storage (95% confidence bounds are shown). This configuration was modelled as a single zone, using both the dynamic, and steady state, simulation systems.

A decreasing rate of mass loss with time is evident in the experimental data in Figure 8.9. In part, this reflects the rising coolstore relative humidity (which is why the predictions also curve), but by itself this does not fully explain the curvature. It is postulated that the decreasing mass loss rate is possible due to biological aging of the fruit. As a result, the permeance to water vapour may significantly decrease (Maguire, 1998) and/or the local water activity under the fruit skin may decrease (because soluble solids levels rise in the cell sap). Nevertheless, the predictions by the dynamic model were within the 95% confidence bounds of the measurements, and the quasi-steady-state model predictions were just outside.

The quasi-steady-state in-pack relative humidity that was predicted by both models for the Z-Pack configuration was 92.7%. This compared favourably with the 92.9% mean measurement. The predicted moisture uptake by the packaging materials over the storage period was 17g by the 'Weight Loss Simulator' and 19g using 'Packaging Simulation for Design'. These values were both less than that measured during experimentation (24g).

The rates of relative humidity modification and packaging material moisture uptake were also predicted using the dynamic simulation system. The predictions are shown in Figure 8.10. There are no corresponding measured data to validate these predictions.

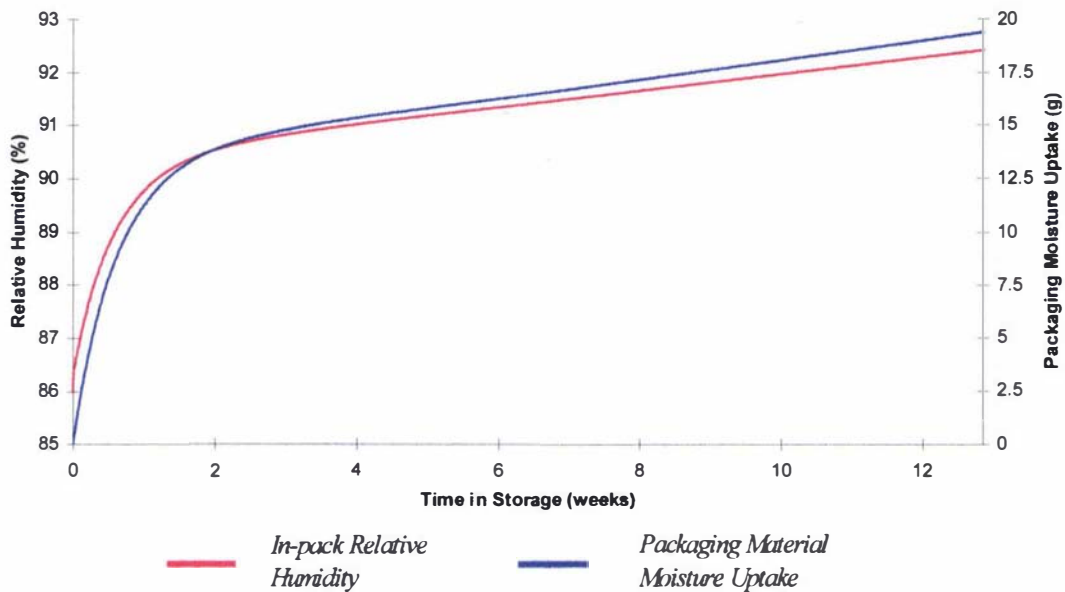


Figure 8.10. Predicted relative humidity and packaging material moisture uptake vs time for an 'average' palletised apple Z-Pack in commercial storage, modelled as a single zone, using the dynamic simulation system.

In the models it was assumed that packaging material water to air interaction was by adsorption only. In practice, both adsorption and desorption may occur due to cycling of the temperature and relative humidity. Using the desorption coefficients for the G.A.B model (as presented by Eagleton and Marcondes, 1994), the quasi-steady-state model predicted packaging material water uptake for the unmodified Z-Pack to be 45g; an amount much greater than that measured. The observed system behaviour is thus bounded by the extremes of totally adsorption and desorption behaviour. The most likely system behaviour in horticultural food storage situations is to approach equilibrium moisture content by adsorption, rather than desorption. Thus, the adsorption coefficients are more likely to lead to accurate predictions than the desorption coefficients, justifying the decision made.

The difference between the predictions of product mass loss by the two prediction systems results from the time-integrated partial pressure driving force for mass transfer out of the system in the quasi-steady-state simulation being greater than that for the dynamic system (and this is the case for all model testing presented). This occurs because the quasi-steady-state condition is assumed to be instantaneous in its formation, thereby immediately creating a greater partial pressure driving force than in the dynamic simulation (Figure 8.11). Therefore, the mass loss from the product is predicted differently by both systems, although values for quasi-steady-state relative humidity and rate of mass loss will be the same from both systems.

The lower prediction of packaging material water uptake by the quasi-steady-state model may result from the assumption in this model that packaging materials and product do not interact. Hence, packaging is predicted to reach a steady state with the fluid only, even though a proportion of the packaging is touching the fruit. In the dynamic model, the interaction between packaging materials and product is modelled, and the packaging material is predicted to reach a higher mean steady-state moisture content due to some contact with the product's higher water activity.

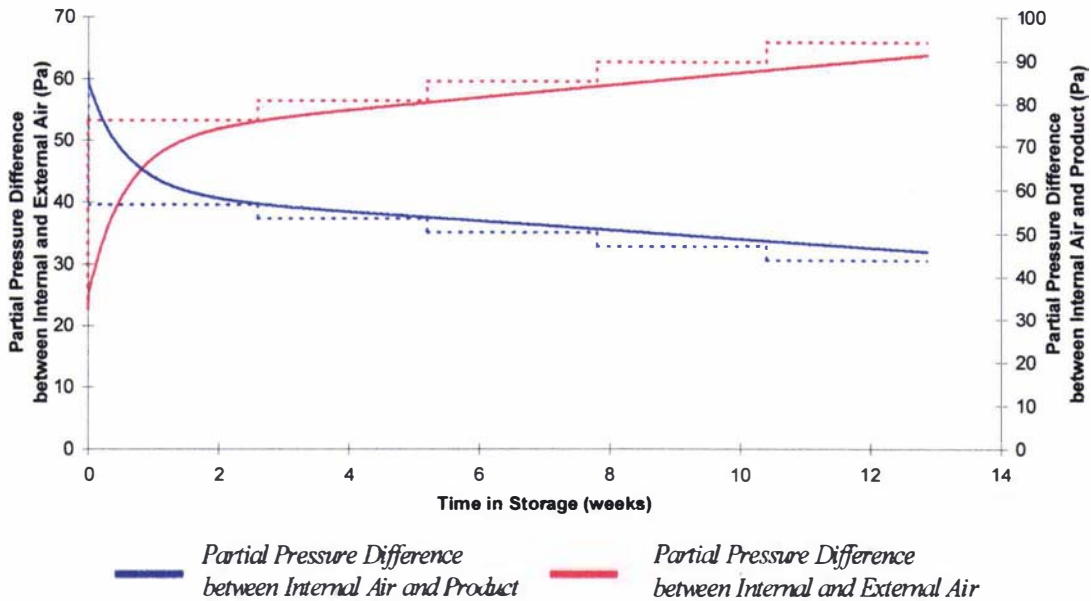


Figure 8.11. Example of differences in partial pressure driving force as simulated by the dynamic simulation system, 'Packaging Simulation for Design' (solid lines) and the steady-state 'Weight Loss Simulator' (dashed lines).

(b) *Modelling the 'Z-Pack' as 4 mixed zones*

The second approach for this package configuration considered spatial variation in the package assessed in (a) above, by modelling fruit mass loss, relative humidity and package material moisture content in each of the 4 individual package layers. Major data for development of the model datafiles are presented in Table 8.8 with the substitution of the data presented in Table 8.9 as appropriate.

Table 8.9.

Amended data (to those of Table 8.8) for development of a 4-zone, bulk-storage simulation model datafile for an ‘average’ palletised Z-Pack. These data were sourced from physical measurement and Appendix 2.

Variable	Value	Units	Variable	Value	Units
<i>Package Properties</i>			<i>Package Properties cont.</i>		
Zones in x - direction	1		Total internal zones	4	
Zones in y - direction	4		Total external zones	1	
Zones in z - direction	1		Number of pack materials	4	
Number of <i>V</i> boundaries	5		<i>Packaging Material Data</i>		
Number of <i>H</i> boundaries	8		<i>'Friday' Trays</i>		
Number of <i>P</i> boundaries	8		Packaging Resistance Factor	0.16	

NB: Dynamic datafile located in ‘Bulk Storage Input Files’ directory (‘Packaging Simulation for Design’ software – Appendix 5), entitled: ‘Unmodified Z-Pack - 4 Zoned.prn’.

The predictions for the spatial variation in this packaging configuration suggested marginally greater mass loss in the middle two layers (Figure 8.12), with final relative humidity in these layers predicted to be approximately 0.06% lower than the top and bottom layers. Spatial variation in relative humidity was not measured during experimentation, and a 0.06% difference would have been undetectable anyway.

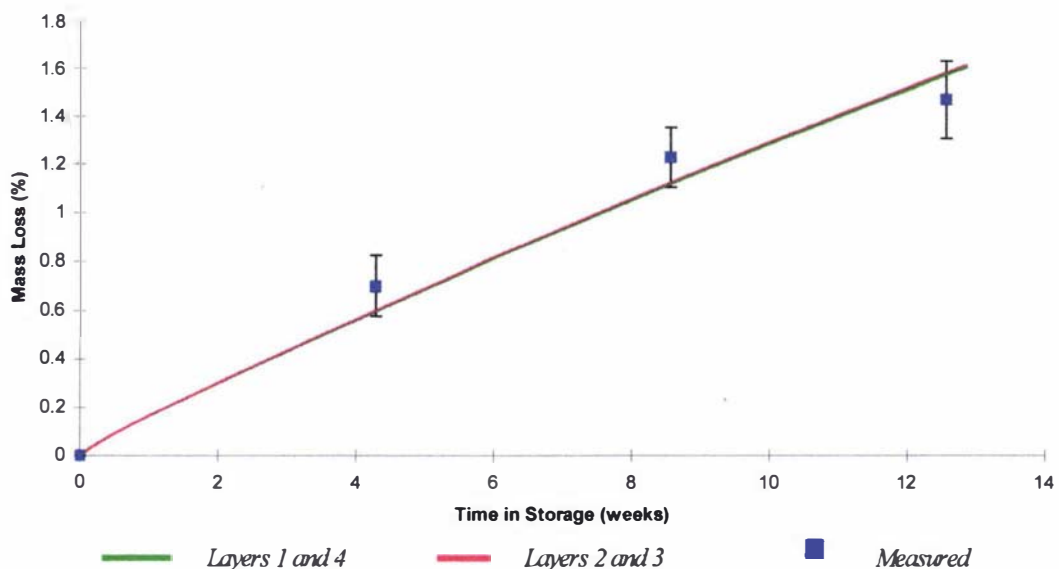


Figure 8.12. Predicted and measured fruit mass loss vs time for individual layers of an ‘average’ palletised apple Z-Pack in commercial storage, modelled as 4 zones, using the dynamic simulation system (95% confidence bounds are shown).

The predicted packaging material moisture uptake was essentially the same as that predicted for a single zone 'Z-Pack' investigated in Section 8.3.1(a).

8.3.2. Mass Loss from Palletised, Cling-wrapped, 1997 'Zeus' Apple Packages

The physical system was similar to that presented in Section 8.3.1 except that the entire pallet was wrapped in a micro-perforated cling film (as discussed in Section 8.2.2.1). The cling wrap reduced the water vapour transport through the 2 exposed carton faces. Major data for development of the single-zone, model datafile are presented in Table 8.8 with the substitution of the data presented in Table 8.10 as appropriate.

Table 8.10.

Amended data (to those of Table 8.8) for development of a single zone, bulk-storage simulation model datafile for an 'average' palletised cling-wrapped Z-Pack. These data were sourced from physical measurement and Appendix 2.

Variable	Value	Units	Variable	Value	Units
<i>Fluid Data</i>			<i>Packaging Material Data</i>		
Internal fluid temperature	0.82	°C	626 C and 626 B Combined + Cling		
<i>Product Data</i>			Packaging Resistance Factor	0.12	
Product Temperature	1.01	°C			

NB: Dynamic datafile located in 'Bulk Storage Input Files' directory ('PackSim' software – Appendix 5), entitled: 'Cling-wrapped Z-Pack - 1 Zone.prn'.

Predicted fruit mass loss from this packaging configuration was compared with mean fruit mass loss for a palletised, cling-wrapped package (Figure 8.13). These measured data were predicted satisfactorily by both the dynamic simulation system and the quasi-steady-state simulator, except for the latter at 12-13 weeks. The quasi-steady-state relative humidity, predicted for this packaging configuration after 12-13 weeks in storage, was 93.8%, comparing favourably with the 92.9% mean measurement. The predicted moisture uptake by the packaging materials in this configuration was 21g by the 'Weight Loss Simulator' and 23g using 'Packaging Simulation for Design'. These values were both less than that measured during experimentation (30g). The under-prediction is consistent with that observed in Section 8.3.1(a). Use of desorption coefficients would have led to significant over-prediction.

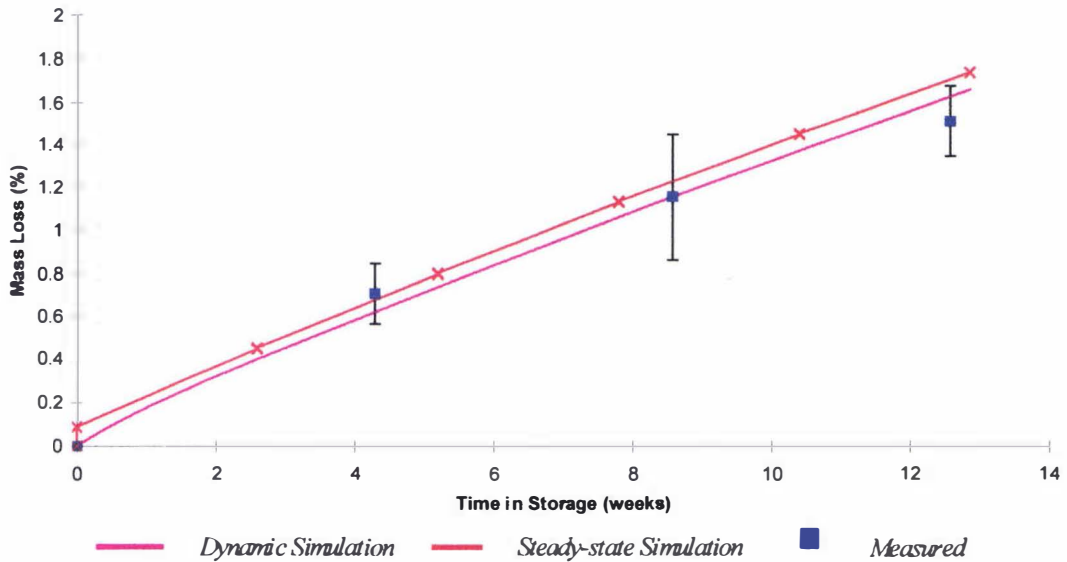


Figure 8.13. Predicted and measured fruit mass loss vs time for an ‘average’ palletised apple Z-Pack, wrapped in cling-film, in commercial storage (95% confidence bounds are shown). This package was modelled as a single zone, using both the dynamic, and steady state models.

8.3.3. Mass Loss from Palletised, Non-ventilated, 1997 ‘Zeus’ Apple Packages

The physical system was also similar to that presented in Section 8.3.1 for an unmodified ‘Z-Pack’. The configuration was constructed of a lid-and-box corrugated paperboard ‘Z-Pack’ without ventilation. Major data for development of the single-zone, model datafile are presented in Table 8.8 with the substitution of the data presented in Table 8.11 as appropriate.

Table 8.11.

Amended data (to those of Table 8.8) for development of a single zone, bulk-storage simulation model datafile for an ‘average’ palletised Z-Pack, with no ventilation. These data were sourced from physical measurement and Appendix 2.

Variable	Value	Units	Variable	Value	Units
Physical System Data			Product Data		
Area of ventilation in package	0.0	m ²	Product Temperature	0.81	°C
Fluid Data					
Internal fluid temperature	0.80	°C			

NB: Datafile located in ‘Bulk Storage Input Files’ directory (‘Packaging Simulation for Design’ software – Appendix 5), entitled: ‘Non-ventilated Z-Pack - 1 Zone.prn’.

Predicted fruit mass loss agreed well with measured data for both the steady-state simulator and dynamic modelling system (Figure 8.14).

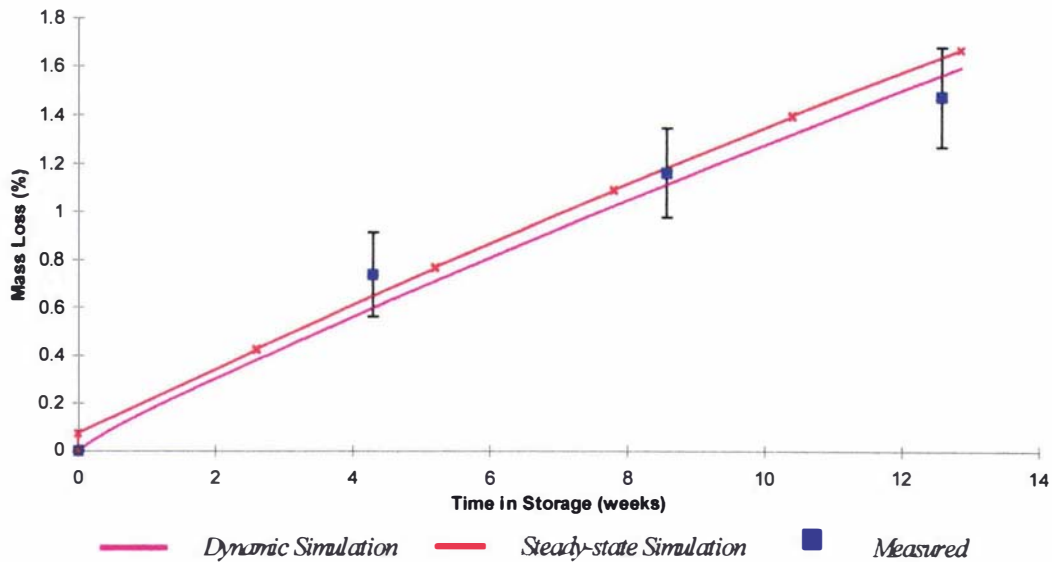


Figure 8.14. Predicted and measured fruit mass loss vs time for an ‘average’ palletised apple Z-Pack, with no ventilation, in commercial storage (95% confidence bounds are shown). This configuration was modelled as a single zone, using both the dynamic, and steady state, simulation systems.

The predicted relative humidity of this configuration was found to be 92.8%, which did not compare favourably with the mean measured value of 95.2%. The lack of agreement is not easily explained.

The predicted moisture uptake by the packaging materials in this configuration was 17g by the ‘Weight Loss Simulator’ and 20g using ‘Packaging Simulation for Design’. These values were both less than that measured during experimentation (36g), a result consistent with all previous configurations. The measured value was less than the predictions made using desorption G.A.B coefficients.

8.3.4. Mass Loss from Palletised, Polylined, 1997 ‘Zeus’ Apple Packages

The physical system was the ‘standard’ 24 hole polyethylene lined Z-Pack, used by the export pipfruit industry to minimise apple mass loss (commonly for the ‘Cox Orange Pippin’ and ‘Braeburn’ apple varieties). In this packaging configuration, the box-and-lid packaging were not considered to be within the packaging system, but rather the polyliner was considered the exterior boundary. Due to a lack of G.A.B isotherm data for the polyliner material, water vapour adsorption into it was not considered. Summary data for development of the modelling datafile is presented in Table 8.12. Figure 8.15 shows both predicted and measured data vs time.

Table 8.12.

Major data used for development of a single zone, bulk-storage simulation model datafile for an ‘average’ palletised Z-Pack, with a polyliner. These data were sourced from physical measurement and Appendix 2.

Variable	Value	Units	Variable	Value	Units
Physical System Data			Fluid Data		
Width of package (x)	0.313	m	Internal fluid temperature	0.61	°C
Height of package (y)	0.257	m	Atmospheric pressure	101325	Pa
Length of package (z)	0.482	m	Fluid density	1.29	kg.m ⁻³
Porosity of package	0.457	fraction	External Environment Data		
Fluid velocity into package	0.0	m.s ⁻¹	External fluid temperature	0.1	°C
Ventilation area in package	0.00068	m ²	Ext. fluid relative humidity	86→90	%
Package Properties			Packaging Material Data		
Zones in x - direction	1		<i>‘Friday’ Trays</i>		
Zones in y - direction	1		GAB coefficient mc_0	6.537	g.100g ⁻¹
Zones in z - direction	1		GAB coefficient ϕ_l	54900	
Number of V boundaries	2		GAB coefficient γ_l	0.733	
Number of H boundaries	2		Material thickness	0.002	m
Number of P boundaries	2		MTC, K_{pkt}	1.0e ⁻⁸	kg.m ⁻² .s ⁻¹ .Pa ⁻¹
Total internal zones	1		Packaging Resistance Factor	N/A	
Total external zones	1		<i>High density polyethylene liner</i>		
Number of pack materials	2		GAB coefficient mc_0	0 ^a	g.100g ⁻¹
Active package surfaces	6		GAB coefficient ϕ_l	0 ^a	
Product Data			GAB coefficient γ_l	0 ^a	
Product temperature	0.72	°C	Material thickness	1.8e ⁻⁵	m
Product water activity	0.995	fraction	MTC, K_{pkt}	N/A	kg.m ⁻² .s ⁻¹ .Pa ⁻¹
MTC, K_{fpr}	3.51e ⁻¹⁰	kg.m ⁻² .s ⁻¹ .Pa ⁻¹	Packaging Resistance Factor	3.75e ⁻⁷	
Respiration rate	2.53e ⁻¹¹	kg.m ⁻² .s ⁻¹ .Pa ⁻¹			
Product items in pack	100				
Mass of individual item	0.186	kg			
Volume of individual item	2.1e ⁻⁴	m ³			
Surface area of individual item	0.0185	m ²			

^a = there are no GAB coefficients for this packaging material, so it was assumed that this material did not adsorb/desorb moisture.

NB: Dynamic datafile located in ‘Bulk Storage Input Files’ directory (‘Packaging Simulation for Design’ software - Appendix 5), entitled: ‘Polylined Z-Pack – 1 Zone.prn’.

For this system, the packaging film mass transfer coefficient (permeance) was not measured, but rather, the measured permeance to water vapour of a similar film used by Merts (1996) was assumed to apply. The polyliner in this system was perforated with 6mm diameter holes so moisture movement through the perforated regions rather than the film is dominant, meaning that a precise value for permeability was not vital.

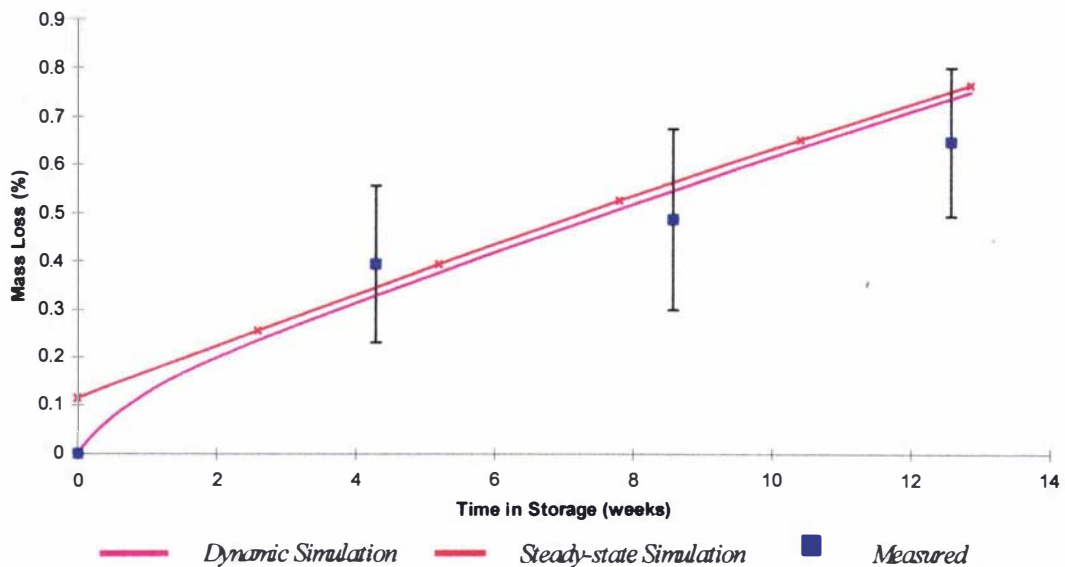


Figure 8.15. Predicted and measured fruit mass loss vs time for an ‘average’ palletised apple Z-Pack, with a polyliner, in commercial storage (95% confidence bounds are shown). This configuration was modelled as a single zone, using both the dynamic, and steady state, simulation systems.

The steady-state relative humidity, calculated for this packaging configuration after 12-13 weeks in storage, was 98.2%, comparing favourably with the mean measured value of 99.2%. The predicted moisture uptake by the packaging materials in this configuration was 21g by the ‘Weight Loss Simulator’ and 23g using ‘Packaging Simulation for Design’. Again, these values were both less than that measured during experimentation (32g), but the experimental value was less than the prediction using desorption coefficients in the G.A.B. isotherm model.

8.3.5. Mass Loss from Palletised, Vented Polylined, 1997 ‘Zeus’ Apple Packages

No attempt was made to model the vented polyliner (explained in section 8.2.2.1), because characterisation of the exact perforation area of the liner was not carried out.

8.3.6. Mass Loss from Different Configurations of the 1997 Apple Retail Display Tray

In the experimental trial, conducted in commercial storage conditions and discussed in Section 8.2.2, four configurations of the ‘Retail Display Tray’ were assessed for their effect on apple mass loss. These configurations were not assessed at 4 weekly intervals (as in the ‘Z-Pack’ configurations) as it was deemed that destructive testing would inhibit water vapour equilibrium attainment. Predictions of fruit mass loss and final relative humidity after 12 weeks are presented in Table 8.13.

Table 8.13.

Model predictions of fruit mass loss and relative humidity for four Retail Display Tray packaging configurations after 12 weeks in commercial storage.

Package Configuration	Measured		Predicted	
	Mass Loss	Relative Humidity	Mass Loss	Relative Humidity
Unmodified RDT	1.87± 0.31%	96.0%	1.73%	93.2%
RDT without ventilation	1.52± 0.30%	95.0%	1.48%	94.8%
Cling-wrapped RDT	1.78± 0.29%	95.9%	1.44%	95.5%
Polylined RDT	0.96± 0.19%	96.3%	0.98%	96.8%

In the unmodified RDT packaging configuration, the relative humidity measurement does not compare favourably with the predicted value. However, the other three predicted values for relative humidity, and three of the four mass loss predictions compare favourably with measured values. The fourth mass loss figure is just outside the 95% confidence bound.

8.4. MODEL TESTING - TOMATO PACKAGING SYSTEMS

Model testing against experimental data collected for two tomato packaging systems was performed using the dynamic mass transfer simulation model in 'Packaging Simulation for Design', and the steady-state 'Weight Loss Simulator'.

8.4.1. Mass loss from a 10kg Paperboard Tomato Package

Modelling for this packaging configuration was undertaken using a single, mixed zone model, with water vapour transport assumed to occur across all faces of the package (data used for development of the modelling datafile are presented in Table 8.14). In the absence of better information, the packaging equilibrium moisture content coefficients used were those measured by Eagleton and Marcondes (1994) for similar packaging materials. Predicted fruit mass loss was compared with measured fruit mass loss for a corrugated paperboard packaging configuration (Figure 8.16).

Table 8.14.

Major data used for development of a single zone, bulk-storage simulation model datafile for a corrugated paperboard tomato pack. These data were sourced from physical measurement and Appendix 2.

Variable	Value	Units	Variable	Value	Units
Physical System Data			Fluid Data		
Width of package (x)	0.3	m	Internal fluid temperature	14.4	°C
Height of package (y)	0.185	m	Atmospheric pressure	101325	Pa
Length of package (z)	0.38	m	Fluid density	1.24	kg.m ⁻³
Porosity of package	0.507	fraction	External Environment Data		
Fluid velocity into package	0.0	m.s ⁻¹	External fluid temperature	14.1	°C
Ventilation area in package	0.021	m ²	Ext. fluid relative humidity	78	%
Package Properties			Packaging Material Data		
Zones in x - direction	1		623 C Corrugated Board		
Zones in y - direction	1		GAB coefficient mc_0	5.336 ^a	g.100g ⁻¹
Zones in z - direction	1		GAB coefficient φ_1	103000 ^a	
Number of <i>V</i> boundaries	2		GAB coefficient γ_1	0.768 ^a	
Number of <i>H</i> boundaries	2		Material thickness	0.003	m
Number of <i>P</i> boundaries	2		MTC, K_{pktl}	1.0e ⁻⁸	kg.m ⁻² .s ⁻¹ .Pa ⁻¹
Total internal zones	1		Packaging Resistance Factor	0.07	
Total external zones	1		62623 CB Corrugated Board		
Number of pack materials	2		GAB coefficient mc_0	5.336 ^a	g.100g ⁻¹
Active package surfaces	6		GAB coefficient φ_1	103000 ^a	
Product Data			GAB coefficient γ_1	0.768 ^a	
Product temperature	14.2	°C	Material thickness	0.005	m
Product water activity	0.995	fraction	MTC, K_{pktl}	1.0e ⁻⁸	kg.m ⁻² .s ⁻¹ .Pa ⁻¹
MTC, K_{fpr}	1.81e ⁻⁹	kg.m ⁻² .s ⁻¹ .Pa ⁻¹	Packaging Resistance Factor	0.08	
Respiration rate	1.63e ⁻¹⁰	kg.m ⁻² .s ⁻¹ .Pa ⁻¹			
Product items in pack	92				
Mass of individual item	0.123	kg			
Volume of individual item	1.1e ⁻⁴	m ³			
Surface area of individual item	0.01133	m ²			

^a = GAB coefficients for apple packaging materials.

NB: Dynamic datafile located in 'Bulk Storage Input Files' directory ('Packaging Simulation for Design' software - Appendix 5), entitled: 'Corrugated Paperboard Tomato Pack - 1 Zone.pm'.

The predicted steady-state relative humidity for this configuration was 85.1%, which is broadly similar to the mean measured value of 87.8%. The predicted moisture uptake, using both 'Weight Loss Simulator' and 'Packaging Simulation for Design', by the packaging materials (3.4g) was similar to that which was measured during experimentation (3.6g).

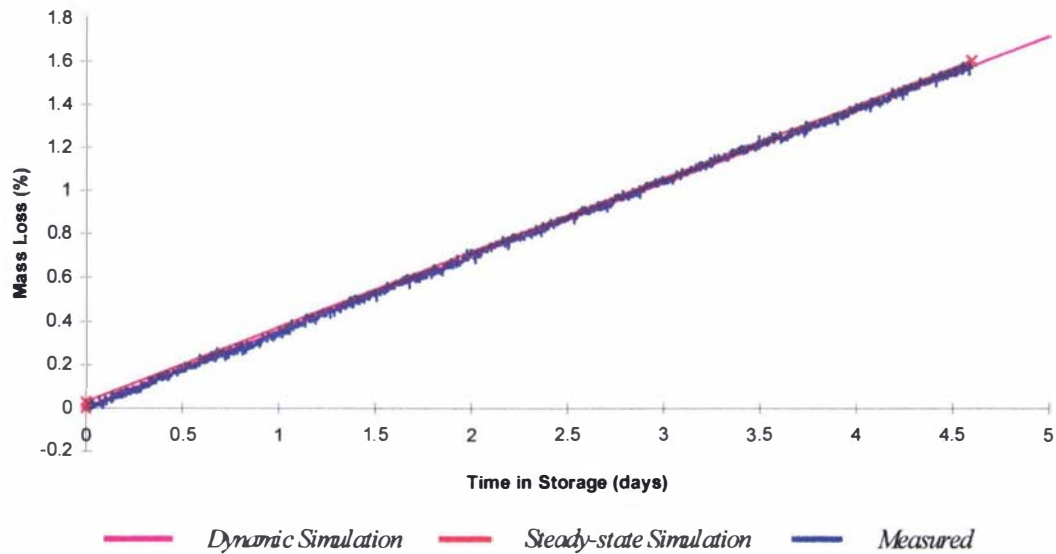


Figure 8.16. Predicted and measured fruit mass loss vs time for a 10kg corrugated paperboard tomato package in controlled laboratory storage. This configuration was modelled as a single zone, using both the dynamic, and steady state, simulation systems.

8.4.2. Mass Loss from a 15kg Plastic Tomato Package

Simulation for this packaging configuration was undertaken using a single, perfectly mixed zone, but with water vapour transport assumed to only occur across the ventilation slots in the package (data used in development of the modelling datafile are presented in Table 8.15). The packaging materials were assumed to be impermeable to water vapour movement and moisture uptake. The fruit mass loss predictions and measurements are shown in Figure 8.17.

The predicted steady-state relative humidity for this configuration was 92.1%, which is similar to the mean measured value of 91.1%. This higher in-pack relative humidity than for the paperboard package reduced the rate of product mass loss by more than 13% (in comparison to that of the paperboard package).

Table 8.15.

Major data used for development of a single zone, bulk-storage simulation model datafile for a plastic tomato pack. These data were sourced from physical measurement and Appendix 2.

Variable	Value	Units	Variable	Value	Units
Physical System Data			Product Data cont.		
Width of package (x)	0.335	m	Product items in pack	120	
Height of package (y)	0.28	m	Mass of individual item	0.1266	kg
Length of package (z)	0.335	m	Volume of individual item	1.1e ⁻⁴	m ³
Porosity of package	0.568	fraction	Surface area of individual item	0.01154	m ²
Fluid velocity into package	0.0	m.s ⁻¹	Fluid Data		
Ventilation area in package	0.0156	m ²	Internal fluid temperature	14.3	°C
Package Properties			Atmospheric pressure	101325	Pa
Zones in x - direction	1		Fluid density	1.24	kg.m ⁻³
Zones in y - direction	1		External Environment Data		
Zones in z - direction	1		External fluid temperature	13.8	°C
Number of V boundaries	2		Ext. fluid relative humidity	75	%
Number of H boundaries	2		Packaging Material Data		
Number of P boundaries	2		Plastic material		
Total internal zones	1		GAB coefficient mc_0	0 ^a	g.100g ⁻¹
Total external zones	1		GAB coefficient ϕ_l	0 ^a	
Number of pack materials	1		GAB coefficient γ_l	0 ^a	
Active package surfaces	6		Material thickness	0.0018	m
Product Data			MTC, K_{pkfl}	0	
Product temperature	14.4	°C	Packaging Resistance Factor	0	
Product water activity	0.995	fraction			
MTC, K_{fpr}	2.71e ⁻⁹	kg.m ⁻² .s ⁻¹ .Pa ⁻¹			
Respiration rate	1.63e ⁻¹⁰	kg.m ⁻² .s ⁻¹ .Pa ⁻¹			

^a = there are no GAB coefficients for this packaging material, so it was assumed that this material did not adsorb/desorb moisture.

NB: Dynamic datafile located in 'Bulk Storage Input Files' directory ('Packaging Simulation for Design' software - Appendix 5), entitled: 'Plastic Tomato Pack - 1 Zone.prn'.

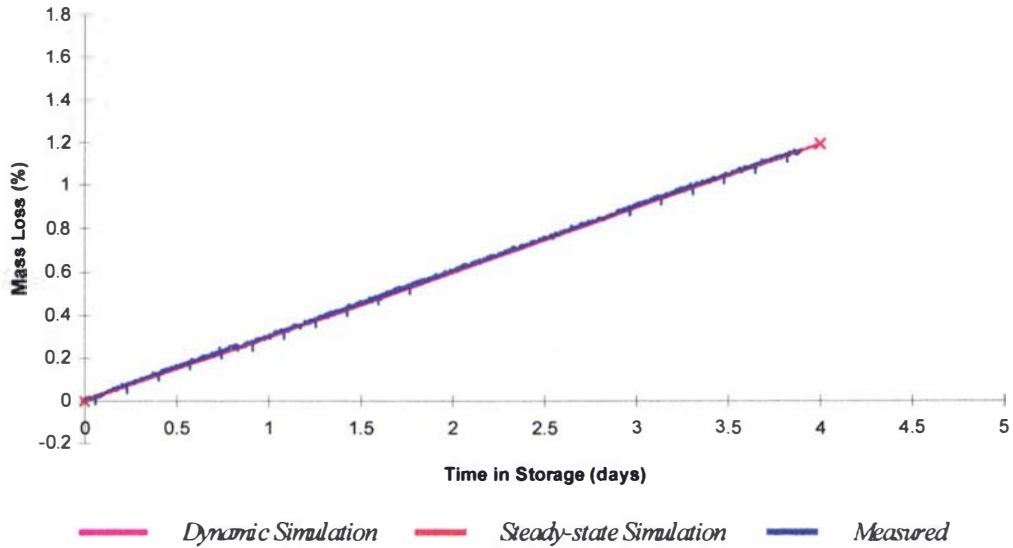


Figure 8.17. Predicted and measured fruit mass loss vs time for a 15kg plastic tomato package in controlled laboratory storage. This configuration was modelled as a single zone, using both the dynamic, and steady state, simulation systems.

8.5. SENSITIVITY ANALYSIS

A sensitivity analysis was performed to assess the sensitivity of predictions to variation (or inaccuracy) in key individual data needed for simulation of mass transfer. A single packaging configuration was used as the base case for this analysis (a single zone Z-Pack exposed on all sides to a controlled environment). Product water activity, initial coolstore relative humidity, product mass transfer coefficient and respiration rates were altered to establish the effect of data variability on the reliability of product mass and fluid relative humidity predictions. Table 8.16 outlines the major data used to develop the base datafile.

8.5.1. Sensitivity to Variation in Product Mass Transfer Coefficient, $K_{fpr} = K_{skin}$

The sensitivity of predictions to possible variability/inaccuracy in the mass transfer coefficient was assessed both to cover error that may have been introduced during measurement, and to establish the strength of the need to measure this product property accurately. Variations of $\pm 10\%$ of the measured value were arbitrarily chosen, leading to the results of Figure 8.18.

Table 8.16.

Major data used for development of a single zone, bulk-storage simulation model datafile as a control for sensitivity analysis. These data were sourced from physical measurement and Appendix 2.

Variable	Value	Units	Variable	Value	Units
Physical System Data			External Environment Data		
Width of package (x)	0.313	m	External fluid temperature	0.1	°C
Height of package (y)	0.257	m	Ext. fluid relative humidity	89	%
Length of package (z)	0.482	m	Packaging Material Data		
Porosity of package	0.457	fraction	<i>Friday Trays</i>		
Fluid velocity into package	0.0	m.s ⁻¹	GAB coefficient mc_0	6.537	g.100g ⁻¹
Ventilation area in package	0.00472	m ²	GAB coefficient ϕ_1	54900	
Package Properties			GAB coefficient γ_1	0.733	
Zones in x - direction	1		Material thickness	0.002	m
Zones in y - direction	1		MTC, K_{pkfl}	1.0e ⁻⁸	kg.m ⁻² .s ⁻¹ .Pa ⁻¹
Zones in z - direction	1		Packaging Resistance Factor	N/A	
Number of V boundaries	2		626 C Corrugated Board		
Number of H boundaries	2		GAB coefficient mc_0	6.022	g.100g ⁻¹
Number of P boundaries	2		GAB coefficient ϕ_1	80000	
Total internal zones	1		GAB coefficient γ_1	0.7	
Total external zones	1		Material thickness	0.0034	m
Number of pack materials	4		MTC, K_{pkfl}	1.0e ⁻⁸	kg.m ⁻² .s ⁻¹ .Pa ⁻¹
Active package surfaces	6		Packaging Resistance Factor	0.09	
Product Data			626 B Corrugated Board		
Product temperature	0.55	°C	GAB coefficient mc_0	5.848	g.100g ⁻¹
Product water activity	0.995	fraction	GAB coefficient ϕ_1	58400	
MTC, K_{fpr}	3.51e ⁻¹⁰	kg.m ⁻² .s ⁻¹ .Pa ⁻¹	GAB coefficient γ_1	0.729	
Respiration rate	2.53e ⁻¹¹	kg.m ⁻² .s ⁻¹ .Pa ⁻¹	Material thickness	0.0044	m
Product items in pack	100		MTC, K_{pkfl}	1.0e ⁻⁸	kg.m ⁻² .s ⁻¹ .Pa ⁻¹
Mass of individual item	0.186	kg	Packaging Resistance Factor	0.11	
Volume of individual item	2.1e ⁻⁴	m ³	626 C and 626 B Combined		
Surface area of individual item	0.0185	m ²	GAB coefficient mc_0	6.022 ^a	g.100g ⁻¹
Fluid Data			GAB coefficient ϕ_1	80000 ^a	
Internal fluid temperature	0.5	°C	GAB coefficient γ_1	0.7 ^a	
Atmospheric pressure	101325	Pa	Material thickness	0.0078	m
Fluid density	1.29	kg.m ⁻³	MTC, K_{pkfl}	1.0e ⁻⁸	kg.m ⁻² .s ⁻¹ .Pa ⁻¹
			Packaging Resistance Factor	0.13	

^a = there are no GAB coefficients for this paperboard, so data for 626C board were used.

NB: Dynamic datafile located in 'Bulk Storage Input Files' directory ('Packaging Simulation for Design' software - Appendix 5), entitled: 'Sensitivity Analysis Control - 1 Zone.prn'.

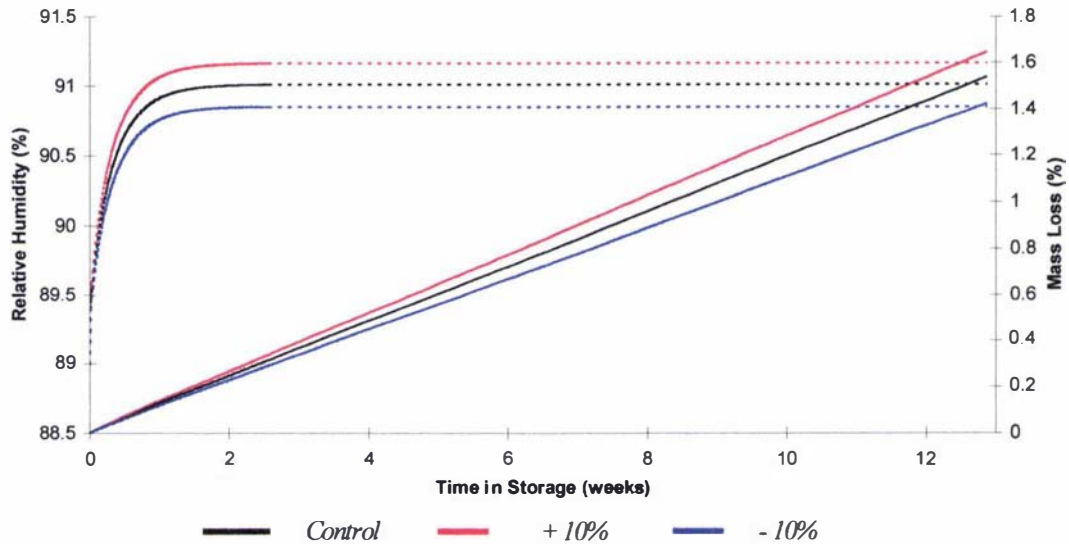


Figure 8.18. Assessment of the effect of variation/inaccuracy in the product mass transfer coefficient on predictions of product mass loss and packaging internal air relative humidity (control for apples was $3.51 \times 10^{-10} \text{ kg.s}^{-1}.\text{m}^{-2}.\text{Pa}^{-1}$). The dashed lines are the relative humidity predictions whilst the solid lines predict mass loss.

For a 10% change in K_{skin} , the resulting product mass loss changed $\pm 7.4\%$ in comparison with the control mass loss after a storage period of 90 days. This variation in prediction highlights the need for accurate measurement (or prediction methods) for product mass transfer coefficients, especially if these are time-variable.

8.5.2. Sensitivity to Variation in Product Respiration Rate

Respiration rates were measured for samples of these fruit in controlled laboratory conditions whilst mass loss measurements were being undertaken. Sensitivity to variability/inaccuracy was assessed using $\pm 10\%$ variations (Figure 8.19). Respiratory mass loss is generally considered to contribute less to total product mass loss than water loss (except in high relative humidity conditions). This was backed by the experimental data (in Section 8.2.2.2) which showed that the respiratory contribution to mass loss was generally less than 20%, except in polylined cartons, where the contribution of respiratory mass loss rose to approximately 40%.

Caution must be applied in using the model for packages in which carbon loss is such a significant contributor. The model, whilst potentially able to, does not yet calculate any effect of CO_2/O_2 atmospheric modification to the carbon loss rate. Thus, for gas-tight packages, there is potential for predictions to lose accuracy.

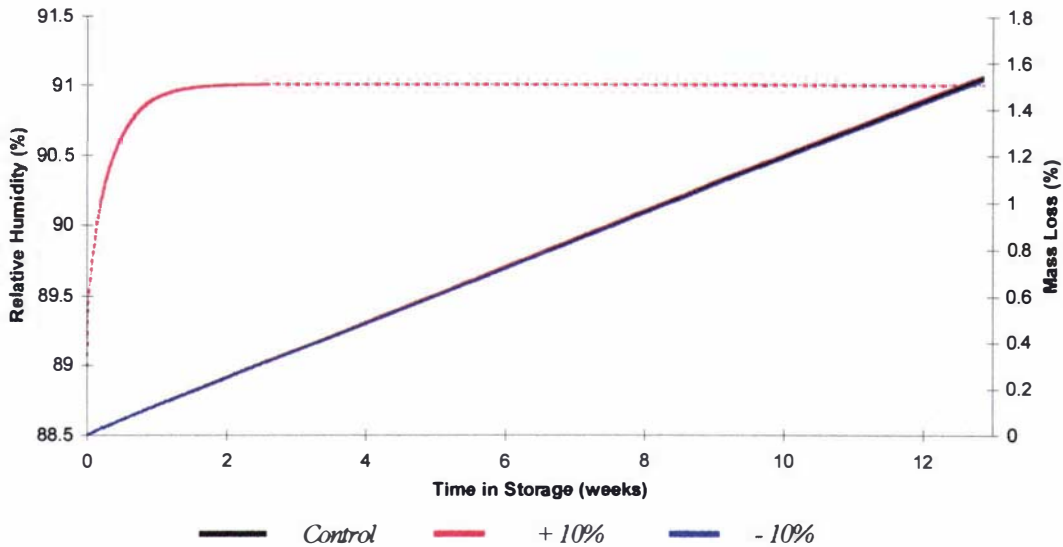


Figure 8.19. Assessment of the effect of variation/inaccuracy in the product respiration rate on total mass loss and relative humidity prediction (control for apples: $2.53 \times 10^{-11} \text{ kgmol.kg}^{-1}.\text{s}^{-1}$). The dashed lines are the relative humidity predictions whilst the solid lines predict mass loss.

Neither inaccurate data nor variation in respiration rate has a significant effect on product mass loss for the base case, and it has no effect on relative humidity modification (as no moisture transport pathways are recognised in the modelling of respiratory mass loss - this is considered to be only carbon loss).

8.5.3. Effect of Poor Knowledge of Fruit Temperature - Package Air Temperature Difference

In the base modelling datafile, the product to internal package air temperature difference was assumed to be 0.05°C . Sensitivity of predictions to variation/inaccuracy in this parameter was assessed by assuming the difference was both decreased to 0°C and increased to 0.1°C , which results in a change in the partial pressure driving force between the product and the air (the dominant driving force for product mass loss). The predictions are shown in Figure 8.20.

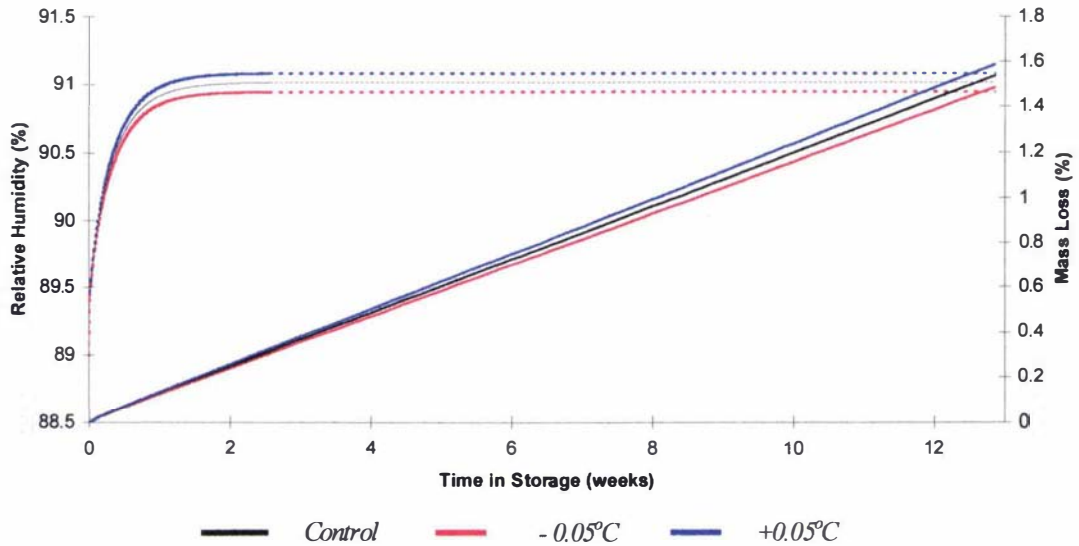


Figure 8.20. Assessment of the effect of variation/inaccuracy in the product-package air temperature difference on predictions of product mass loss and packaging internal air relative humidity (control for apples: $+0.05^{\circ}\text{C}$). The dashed lines are the relative humidity predictions whilst the solid lines predict mass loss.

The predictions of sensitivity to changes in the product-package air temperature difference are moderately sensitive to inaccuracy/variation. The resulting product mass loss changed $\pm 3.3\%$ in comparison with the control mass loss after a storage period of 90 days. This highlights the need for accurate measurement for this system-input parameter.

8.5.4. Sensitivity to Variation in Product Water Activity

The product water activity was assumed to be 0.995. Sensitivity to imprecision in this parameter was assessed by assuming the fraction decreased by 0.005 and increased by 0.005 (Figure 8.21), thus causing a change in the partial pressure driving force between the product and the air (a dominant driver in product mass loss prediction).

The predictions were moderately sensitive to variation/inaccuracy. The resulting change in prediction of product mass loss was $\pm 4.6\%$ in comparison with the control mass loss after a storage period of 90 days. This highlights the need for accurate evaluation or prediction of this system-input parameter.

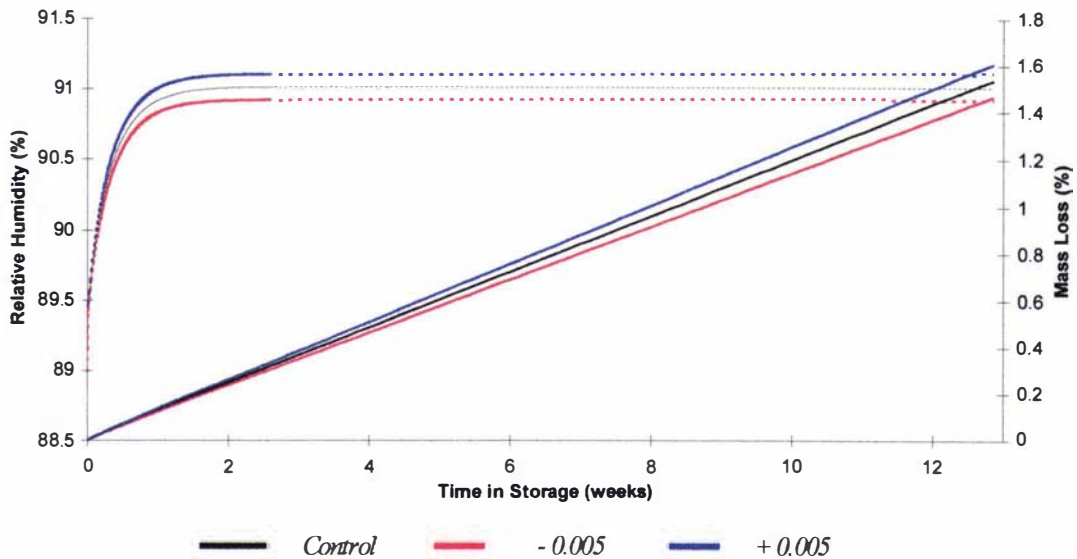


Figure 8.21. Assessment of the effect of variation/inaccuracy in the product water activity on predictions of product mass loss and packaging internal air relative humidity (control for apples, 0.995). The dashed lines are the relative humidity predictions whilst the solid lines predict mass loss.

8.5.5. Sensitivity to Variation in Effective Packaging Material Mass Transfer Coefficient, $K_{eff,pk}$

This parameter describes the rate of water vapour transport across the packaging material boundary (excluding transport through ventilation slots). It can be modified by increasing / decreasing the resistance of the material. The transmission rate was both increased to twice the control rate, and decreased to half the control rate, because such changes are realistically achievable by packaging designers. For example, work performed at Massey University by Lewis *et al.* (1997) highlighted four packaging material barrier coatings which reduced the effective mass transfer coefficient by > 70%. Reduction in paper grades for packaging materials or use of more porous materials will increase the rate of water vapour transport. The sensitivity of predictions is shown in Figure 8.22.

In spite of doubling or halving the rate of water vapour transport across packaging materials, the predicted product mass loss in the base case changed only $\pm 12.9\%$ in comparison with the control mass loss after a storage period of 90 days. However, if ventilation slots were significantly reduced, or removed, a more dramatic sensitivity would have been shown. The conclusion reached was that this parameter must be accurately known if the packaging system has a low ventilation area.

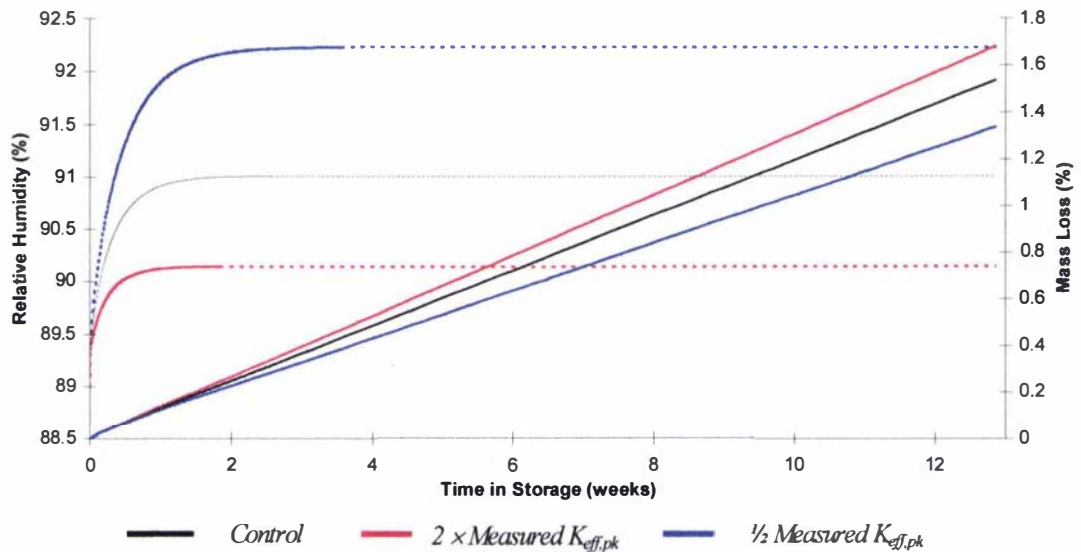


Figure 8.22. Assessment of the effect of variation/inaccuracy in the effective packaging material mass transfer coefficient on predictions of product mass loss and packaging internal air relative humidity (control for corrugated material, $2.95 \times 10^{-9} \text{ kg.s}^{-1}.\text{m}^{-2}.\text{Pa}^{-1}$). The dashed lines are the relative humidity predictions whilst the solid lines predict mass loss.

8.5.6. Sensitivity to Variation in the External Fluid Relative Humidity

In theory, measurement of the storage environment (termed the external environment) relative humidity is not difficult in large horticultural storage facilities. The accuracy of the equipment for this measurement is, however, questionable, with many manufacturers stating accuracy to only $\pm 2\%$ at best. Further, re-calibration of sensors may be infrequent. Figure 8.23 shows that changing the external relative humidity by $\pm 1\%$ has a significant effect on product mass loss predictions. The resulting product mass loss changed $\pm 9.2\%$ in comparison with the control mass loss after a storage period of 90 days. This analysis indicates the need for accurate measurement of this system-input parameter.

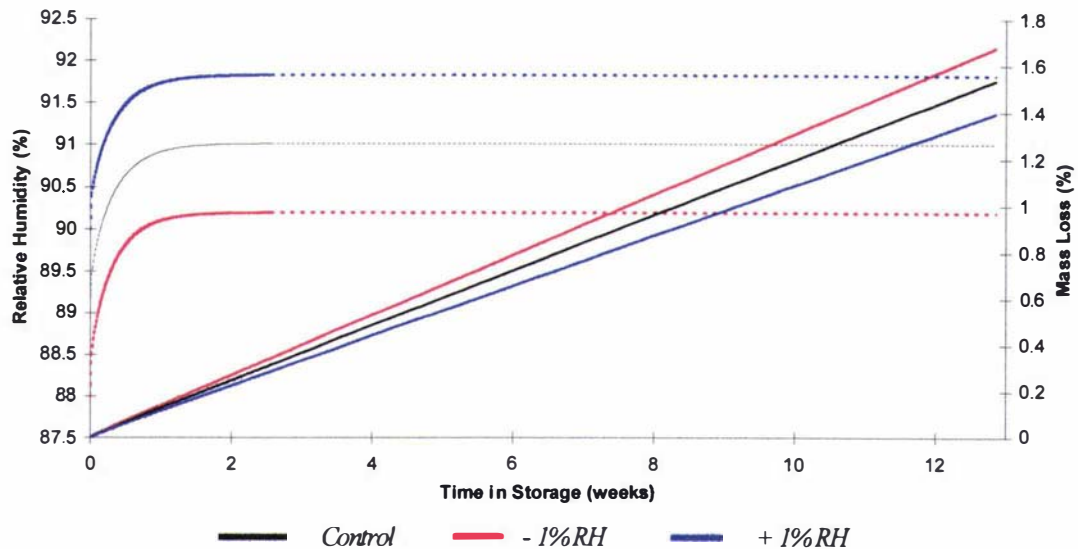


Figure 8.23. Assessment of the effect of variation/inaccuracy in the external relative humidity on predictions of product mass loss and packaging internal air relative humidity (control for this configuration was 89%). The dashed lines are the relative humidity predictions whilst the solid lines predict mass loss.

8.5.7. Effect of Variation in the In-package Air - Coolstore Air Temperature Difference

The in-package air to external coolstore air temperature difference was also assessed for its effect on product mass loss and steady-state RH prediction. This temperature difference is increased by inadequate pre-cooling, resulting in excessive heat (and possibly further heat generation) within the package. The sensitivity of predictions to variation/inaccuracy in this parameter is shown in Figure 8.24.

The predictions were moderately sensitive to the increasing of the product-coolstore air temperature difference by 0.1°C and 0.2°C . The resulting product mass loss was +5.8% and +11.5% respectively in comparison with the control mass loss after a storage period of 90 days. This also highlights the need for accurate measurement of this system-input parameter.

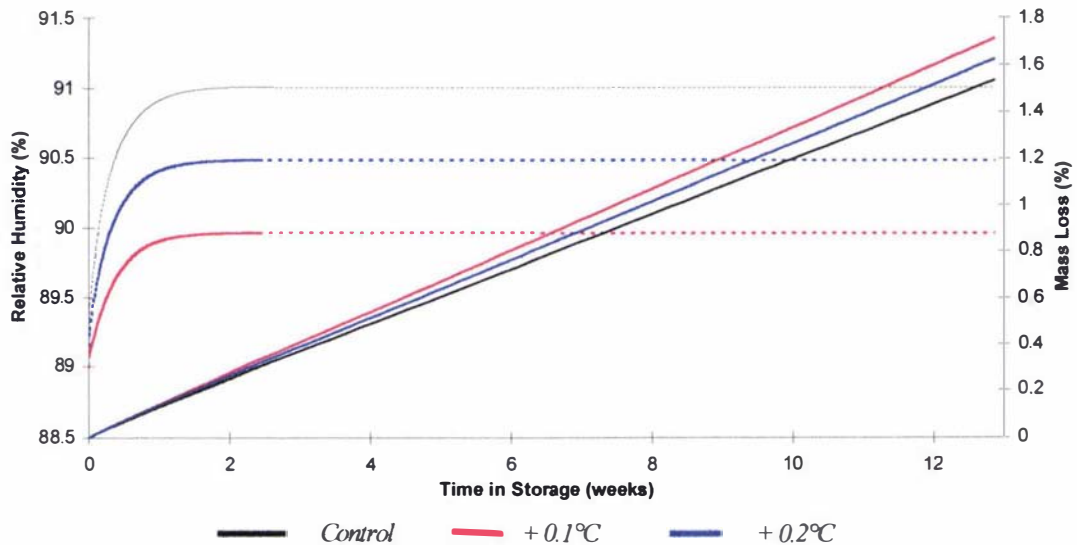


Figure 8.24. Assessment of effect of variation/inaccuracy in the package - coolstore air temperature difference on predictions of product mass loss and packaging internal air relative humidity (control for this configuration was a 0°C temperature difference). The dashed lines are the relative humidity predictions whilst the solid lines predict mass loss.

8.5.8. Sensitivity to Variation in the Lower Limit for Packaging Thickness, x_{pk}

As discussed by Merts (1996), the success of modelling water vapour diffusion through perforations or ventilation slots in packaging configurations is dependant on the method used for calculation of the thickness of the still air gap through which water vapour diffusion occurs. In the present work, the thickness of the still air layer was assumed to be the thickness of the packaging material. An empirically derived lower limit was placed on this thickness of 1mm (as discussed in Chapter 5).

Sensitivity to the selection of the lower limit for packaging thickness was assessed using the packaging scenario presented in Section 8.3.4. The major data were presented in Table 8.12 with the exception of external relative humidity, which was fixed at 89%. In the case presented in Section 8.3.4, the lower limit for packaging thickness had been set at 1mm, even though the actual thickness of the polyliner material was 18 μ m. The lower limit was both halved and doubled (Figure 8.25).

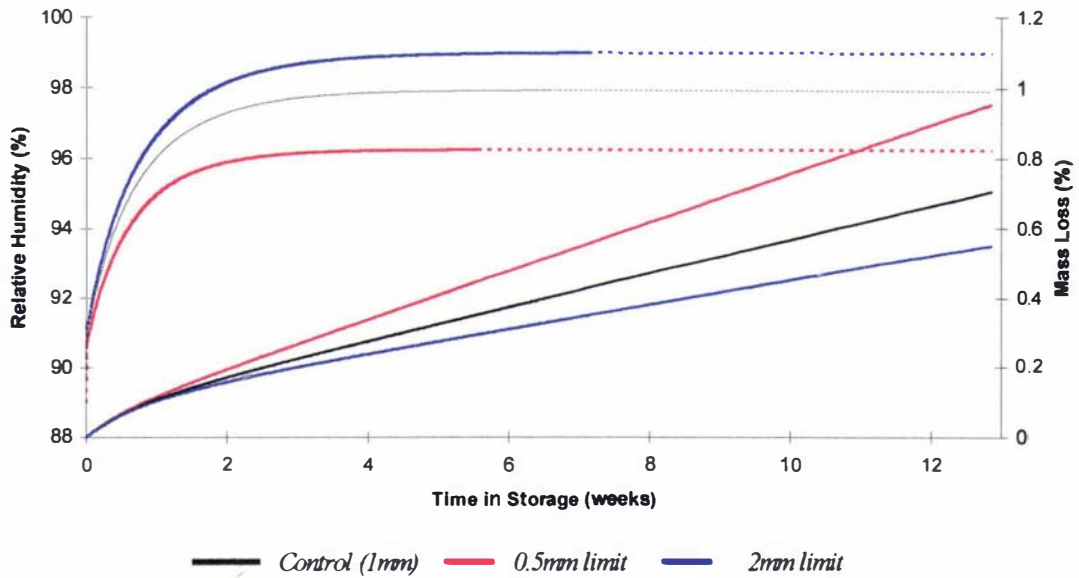


Figure 8.25. Assessment of effect of variation in the packaging thickness lower limit on predictions of product mass loss and relative humidity (control for this configuration was a 1mm lower limit). The dashed lines are the relative humidity predictions whilst the solid lines predict mass loss.

The predictions were very sensitive to variation in the packaging material lower limit. The resulting product mass loss percentage, when the lower limit was halved or doubled, was 35% higher and 22% lower respectively in comparison with the control mass loss after a storage period of 90 days. In the cases examined, the 1mm lower limit had given physically realistic mass transfer coefficients (in comparison to others in the complete system), and led to predictions that matched experimental data.

The 1mm lower limit is consistent with, but not exactly equivalent to, the curve-fitted empirical correlation factors used by previous researchers (Emond *et al.*, 1991; Merts, 1996). Merts used a range of empirical factors, ξ , depending on the hole diameter:film thickness ratio. The value of ξ decreased as hole diameter:film thickness ratio increased (eg. $\xi = 1$ for a ratio of 3.25, and $\xi = 0.01$ for a ratio of 200). For the 18 μm liner used, the ratio for 6mm perforations was 333 indicating that an appropriate value of ξ would be about 0.01. A value of 0.018 corresponds to 1mm.

Further work investigating development of a model for water vapour movement through holes in thin packaging materials where boundary layer effects are significant is justified.

8.6. DISCUSSION OF MODEL PERFORMANCE

Testing against experimental data was undertaken on ten product/package systems. Analysis of the accuracy of these predictions was undertaken using graphical comparisons. However, sensitivity analyses indicate that much of the disagreement was likely to be attributable to imprecision in model-input data.

The models consistently underestimated packaging material water uptake. This was considered a minor concern, as the effect on overall mass loss predictions was low. However, there may well be benefits in seeking a model that is more applicable than the G.A.B adsorption-only isotherm for cyclic relative humidity conditions and relative humidity conditions of $> 90\%$ (the region of most interest in horticultural storage but least accuracy for this moisture sorption isotherm).

The quasi-steady-state model, which included those mass transfer pathways necessary for prediction of the steady-state mass loss within a chosen packaging design, yielded very similar predictions, to those of the dynamic model, for long storage times. The two models predict the same long-term quasi-steady-state rate of mass loss, but differ in their predictions for the period preceding establishment of the quasi-steady-state.

Small differences were found for predictions of product mass loss by the two models as a result of the time-integrated partial pressure driving force for mass transfer out of the system in the quasi-steady-state simulation being greater than that for the dynamic system. This occurred because the quasi-steady-state condition was assumed to be instantaneous in its formation, thereby immediately creating a greater partial pressure driving force than in the dynamic simulation. Therefore, the mass loss from the product was predicted differently by both systems, although values for quasi-steady-state relative humidity and rate of mass loss were the same from both systems.

The three intra-zonal and three inter-zonal mass transfer pathways included in the dynamic mass transfer model covered all those expected to be significant in industrial practice for a range of products and package systems. Not all mass transfer pathways were significant contributors to water vapour transport in each package tested, so it was not possible to claim accuracy for all the pathway sub-models in all circumstances. However, the testing was sufficiently broad that the model can be used with confidence for simulation of bulk-storage product mass loss from commonly occurring product-package designs. Nevertheless, it may over-predict at long storage

times if biological aging of the product changes its water activity and/or skin mass transfer coefficient (permeance). More study of these effects is warranted.

For long-term storage, the quasi-steady-state model, due to its lower data requirement, is recommended for industrial practitioners, whereas the dynamic model yields valuable insights to the packaging or horticultural industry researcher.

Overall, the models developed in this work are significantly more advanced than the tools previously available to the horticultural industry for design of packaging systems. These models predicted fruit mass loss, packaging material moisture uptake and in-package relative humidity for a range of packaging systems with sufficient accuracy for most industrial applications. Although only tested for two horticultural products, the model is designed to be general, requiring a small number of product specific data for prediction. It is not envisaged that extension of the model to further products and packaging configurations will present any significant difficulties.

8.7. RECOMMENDATIONS FOR FUTURE WORK

These models have proven useful in prediction of mass transport pathways within packaging systems. Further investigation of the lower bound on vent hole mass transfer coefficients, a replacement for the G.A.B adsorption-only isotherm, the effect of biological aging and reduction of input-data inaccuracy is justified. Additionally, model extension to predict gas atmosphere and fruit quality (for which sound sub-models exist) could be undertaken. Thus, further steps could initially include:

- experimental characterisation and testing of all mass transfer pathways included in the modelling methodology.
- improvement of estimation methods for mass transfer coefficients.
- investigation or development of an improved model for water vapour movement through perforations in thin packaging materials.
- collection of reliable moisture sorption isotherm data for $RH > 90\%$ (the isotherm model need not be limited to the G.A.B model) for packaging materials.
- incorporation of heat transfer modelling with mass transport modelling to better model long-term temperature differences in packaging systems.
- incorporating modification of other gases in the package atmosphere (such as CO_2 and O_2).
- incorporation of product quality models, including the effects of heat and mass transfer.

CHAPTER 9

CONCLUSIONS

The proposed generalised methodology allows simulation of widely varying packages by changing only input data for each package design; thereby overcoming system specificity which limited application of previous models.

The zone definition methodology provided an effective technique for relating the geometry of the wide variety of packages investigated to specific model input data. Placement of the fluid at the same level in the modelling hierarchy as packaging and product was instrumental in achieving the sought-after flexibility and improved alignment of the model with physical reality.

The experimental technique developed for characterisation of airflow distributions, using CO₂ as a tracer enabled rapid estimation of in-package air velocities, for use as model input data. Whilst, the technique did not enable precise determination of fluid velocity, all indications are that it gave reliable flow-relativity coefficients.

The nine inter-zonal and one intra-zonal heat transfer pathways included in the model simulate all those mechanisms likely to be significant in industrial practice for a range of products and packages. Analysis of eight types of package showed that the model predictions were broadly in agreement with experimental results, and any disagreement was probably more the result of uncertainties in input data than of model shortcomings.

Not all heat transfer pathways were significant contributors to temperature change in the packages tested, so it was not possible to claim confidence in the accuracy of all the heat transfer sub-models in all circumstances. However, the testing was sufficiently broad that the overall model can be used with confidence for simulation of pre-cooling of commonly occurring package designs.

The three intra-zonal and three inter-zonal mass transfer pathways included in the dynamic mass transfer model cover all those expected to be significant in industrial practice for a range of products and package systems. Most of the disagreement between experimental data and predictions for the ten product/package systems investigated was attributed to imprecision in model input data and not shortcomings in the model itself. At long storage times, the assumptions of constant product water activity and skin mass transfer resistance may break down due to biological change in the product, leading to slight over-prediction. The quasi-steady-state model, which included those mass transfer pathways necessary for prediction of the steady-state mass loss within a chosen packaging design, yielded very similar predictions, to those of the dynamic model, for long storage times. The two models differ in their predictions for the period preceding establishment of the quasi-steady-state. The quasi-steady-state model, due to its lower data requirement, is recommended for industrial users, whereas the dynamic model yields valuable insights to the packaging or horticultural industry researcher.

The potential for wider application of the models for design of horticultural packaging and prediction of heat and mass transfer characteristics in horticultural packaging systems is significant. Improvements that could be investigated further include:

- replacement of the G.A.B adsorption-only isotherm for packaging materials with a model better suited to adsorption/desorption processes at $RH > 90\%$.
- improved heat and mass transfer coefficient estimation methods, especially for water vapour movement through perforations in thin packaging materials.
- combination of heat and mass transfer into a single model.
- incorporation of gas atmosphere models.
- incorporation of prediction of product quality attributes.

Overall, the generalised simulation systems developed, and tested in this research have advanced the ability to predict heat and mass transfer in a range of horticultural packaging systems. Their generality is sufficient to suggest that these models need not be limited to only horticultural commodities, but might have wider food industry applications.

REFERENCES.

- Adre, N. and Hellickson, M.L. (1989). Simulation of the transient refrigeration load in a cold storage for apples and pears. *Trans. ASAE*. **32 (2)**: 1038-1048.
- Amos, N.D. (1995). *Mathematical modelling of heat and mass transfer and water vapour transport in apple coolstores*. Ph.D. Dissertation, Massey University, Palmerston North, New Zealand.
- Amos, N.D., Cleland, D.J. and Banks, N.H. (1993a). Effect of pallet stacking arrangement on fruit cooling rates within forced-air precoolers. *Refrig. Sci and Technol*. **1993-3**: 232-241.
- Amos, N.D., Cleland, D.J., Banks, N.H. and Cleland, A.C. (1993b). A survey of air velocity, temperature and relative humidity in a large horticultural coolstore. *Refrig. Sci. and Technol*. **1993-3**: 414-422.
- Amos, N.D., Cleland, D.J., Cleland, A.C. and Banks, N.H. (1993c). The effect of coolstore design and operation on air relative humidity. *Proc. Int. Conf. Agricultural Machinery & Process Engng*, Seoul, October 1993, **1**: 433-442.
- Ansari, F.A., Charan, V. and Varma, H.K. (1984). Heat and mass transfer analysis in air-cooling of spherical food products. *Int. J. Refrig*. **7**: 194-197.
- Arifin, B.B. and Chau, K.V. (1988). Cooling of strawberries in cartons with new vent hole designs. *Trans. ASHRAE*. **94 (1)**: 1415-1419.
- ASHRAE. (1990). *ASHRAE Handbook - Refrigeration Systems and applications*. American Society of Refrigeration and Air Conditioning Engineers Publishers, Atlanta, GA.
- ASHRAE. (1993). *ASHRAE Handbook - Fundamentals*. American Society of Refrigeration and Air Conditioning Engineers Publishers, Atlanta, GA.
- ASHRAE. (1997). *ASHRAE Handbook - Fundamentals*. American Society of Refrigeration and Air Conditioning Engineers Publishers, Atlanta, GA.
- Awberry, J.H. (1927). The flow of heat in a body generating heat. *Phil. Mag*. **4 (7)**: 629-638.
- Baird, C.D., and Gaffney, J.J. (1976). A numerical procedure for calculating heat transfer in bulk loads of fruits and vegetables. *Trans ASHRAE* **82 (2)**: 525-540.

- Baleo, J.N., Guyonnaud, L. and Sollicec, C. (1995). Numerical simulation of air flow distribution in a refrigerated display case air curtain. *Proc. 19th Int. Congr. Refrig.* **Vol 2**: 681-688.
- Bartholomew, F.B. (1990). Weight Loss Review. Internal report for The New Zealand Apple and Pear Marketing Board.
- Bazan, T., Chau, K.V. and Baird, C.D. (1989). Heat transfer simulation of the bulk cooling of fruits. *ASAE Paper No. 896559*.
- Becker, B.R. and Fricke, B.A. (1996). Transpiration and Respiration of fruits and vegetables. *Refrig. Sci. and Technol.* **1996-6**: 110-121.
- Becker, B.R., Misra, A. and Fricke, B.A. (1994). *A computer algorithm for determining the moisture loss and latent heat load in the bulk storage of fruits and vegetables*. Final ASHRAE Report for project 777-RP.
- Bellagha, S. and Chau, K.V. (1985). Heat and mass transfer during the cooling of tomatoes individually and in bulk. *ASAE Paper No. 85-6002*.
- Bizot, H. (1983). Using the G.A.B. model to construct sorption isotherms. In: *Physical properties of foods* (R. Jowitt, Ed.). Elsevier Science Publishing, New York. pp. 43-54.
- Burmeister, D.M., Elgar, H.J., Brookfield, P.L. and Jackson, P.J. (1996). Shriveling in 'Braeburn'. Report for ENZA New Zealand (International) Project PH96/93. HortResearch Client Report **No. 96/197**.
- Burmeister, D.M., Marsh, K., Roughan, S., Rose, K., Madhikarmy, S. and Davy, M. (1997). Coolchain Protocol to prevent shrivel. Report for ENZA New Zealand (International) Project HR96P09-01. HortResearch Client Report **No. 97/288**.
- Campanone, L.A., Giner, S.A. and Mascheroni, R.H. (1995). The use of a simulation software to optimise cooling time and to lower weight losses in fruit refrigeration. *Proc. 19th Int. Congr. Refrig.* **Vol 1**: 121-128.
- Carslaw, H.S. and Jaeger, J.S. (1959). *Conduction of Heat in Solids* (2nd Ed). Clarendon Press, Oxford.
- Cengel, Y.A. (1997). *Introduction to Thermodynamics and Heat Transfer* (Int. Ed.) McGraw-Hill, New York.
- Chan, J.K.C. and Scott, D.R. (1988). A critical survey of mathematical models for predicting room air movement. *Institute of Environmental Engineering Res. Memo No. 109*.

- Chau, K.V. and Gaffney, J.J. (1990). A finite difference model for heat and mass transfer in products with internal heat generation and transpiration. *J. Food Sci.* **55**: 484-487.
- Chau, K.V., Gaffney, J.J. and Bellagha, S. (1984). Simulation of heat and mass transfer in products with internal heat generation and transpiration. *ASAE Paper No. 84-6513*.
- Chau, K.V., Romero, R.A., Baird, C.D. and Gaffney, J.J. (1987). Transpiration coefficients of fruits and vegetables in refrigerated storage. *ASHRAE Report* 370-RP.
- Chau, K.V., Gaffney, J.J. and Romero, R.A. (1988). A mathematical model for the transpiration from fruits and vegetables. *Trans ASHRAE.* **94 (1)**: 1541-1552.
- Cheng, Q., Banks, N.H., Nicholson, S.E., Kingsley, A.M. and MacKay, B.R. (1998). Effects of temperature on gas exchange of 'Braeburn' apples. (In Press).
- Chuntranuluck, S. (1995). *Prediction of chilling times of foods subject to both convective and evaporative cooling at the product surface*. Ph.D. Dissertation, Massey University, Palmerston North, New Zealand.
- Chuntranuluck, S. Serrallach, G.F. and Cleland, A.C. (1989). Shape factors for prediction of chilling times of irregular shapes. *Refrig. Sci. Technol.* **1989**: 215-222.
- C.I.B.S Guide (1980). Thermal properties of building structures. *The Chartered Institute of Building Services Vol. A3*: A3-31 - A3-42.
- Clary, B.L., Nelson, G.L. and Smith, R.E. (1971). The application of geometry analysis techniques in determining the heat transfer rates from biological materials. *Trans ASAE* **14**: 586-589.
- Clayton, M. (1995). *Mathematical modelling of bulk stored onions in transport containers*. M.Hort Dissertation, Massey University, Palmerston North, New Zealand.
- Clayton, M., Amos, N.D., Banks, N.H. and Morton, R.H. (1995). Estimation of apple fruit surface area. *NZ J. Crop Hort. Sci.* **23**: 345-349.
- Cleland, A.C. (1983). Simulation of industrial refrigeration plants under variable load conditions. *Int. J. Refrig.* **6**: 11-19.
- Cleland, A.C. (1990). *Food Refrigeration Processes - Analysis, Design and Simulation*. Elsevier Science Publishers, London. 284p.
- Cleland, A.C. and Cleland, D.J. (1992). *Cost Effective Refrigeration*. Dept. of Biotechnology, Massey University, Palmerston North, New Zealand.

- Cleland, A.C. and Earle, R.L. (1982). A simple method for prediction of heating and cooling rates in solids of various shapes. *Int. J. Refrig.* **5**: 98-106.
- Cleland, D.J. (1985). *Prediction of freezing and thawing times for foods*. Ph.D. Dissertation, Massey University, Palmerston North, New Zealand.
- Cleland, D.J. and Cleland, A.C. (1989a). Appropriate level of model complexity in dynamic simulation of refrigeration systems. *Refrig. Sci. and Technol.* **1989 - 1**: 261-268.
- Cleland, D.J. and Davey, L.M. (1995). Prediction of food chilling rates with time variable cooling medium temperature. *Proc 19th Int Congr. Refrig.* **Vol 2**:392-399.
- Cleland, D.J., Boyd, N.S. and Cleland, A.C. (1982). A model for fish freezing and storage on board small New Zealand fishing vessels. *Refrig. Sci. and Technol.* **1982 - 1**: 147-156.
- Cleland, D.J. and Valentas, K.J. (1997). Prediction of freezing time and design of food freezers. In: *Handbook of Food Engineering Practice*. CRC Press, Boca Raton, New York.
- Contreras-Medellin, R. (1980). *Estimation of moisture transfer rates through food packaging material under frozen storage conditions*. M.S. Dissertation, University of Minnesota, St Paul, MN.
- Cowell, N.D. and Namor, M.S.S. (1974). Heat transfer coefficients in plate freezing: the effect of packaging materials. *Refrig. Sci. and Technol.* **3**: 45-50.
- Creed, P.G. and James, S.J. (1985). Heat transfer during the freezing of liver in a plate freezer. *J. Food Sci.* **50**: 285-288,294.
- Dadzie, B.K. (1992). *Gas exchange characteristics and quality of apples*. PhD Dissertation, Massey University, Palmerston North, New Zealand.
- Devres, Y.O. and Bishop, C.F.H. (1992). A computer model for weight loss and energy conservation in a fresh produce refrigerated store. *Institute of Environmental Engineering Res. Memo No.* **134**.
- Dincer, I. (1995). Airflow precooling of individual grapes. *J. Food Engng.* **26**: 243-249.
- Dincer, I., Yildiz, M., Loker, M. and Gun, H. (1992). Process parameters for hydrocooling apricots, plums, and peaches. *Int. J. Food Sci. Technol.* **27**: 347-352.

- Eagleton, D.G. and Marcondes, J.A. (1994). Moisture-sorption isotherms for paper-based components of transport packaging for fresh produce. *TAPPI J.* **77** (7): 75-81.
- Earle, R.L. (1983). *Unit operations in food processing*. (2nd Ed.) Pergamon Press Ltd., Oxford, England.
- Edwards, D. and Hamson, M. (1989). *Guide to Mathematical Modelling*. MacMillan Education Ltd., Hong Kong.
- Emond, J.P., Castaigne, F., Toupin, C.J. and Desilets, D. (1991). Mathematical modelling of gas exchange in modified atmosphere packaging. *Trans ASAE*. **34**: 239-245.
- Falconer, R.M. (1995a). Experimental Forced-air cooling of apple cartons. IRL Report # 523. Confidential Report to the New Zealand Apple and Pear Marketing Board.
- Falconer, R.M. (1995b). Forced-air cooling of single layer cartons with different packaging. IRL Report # 522. Confidential Report to the New Zealand Apple and Pear Marketing Board.
- Falconer, R.M. and Billing, D.P. (1995). *Forced-air cooling of 'Zeus' ventilated cartons*. IRL Report # 527. Confidential Report to the New Zealand Apple and Pear Marketing Board.
- Faubion, D.F. and Kader A.A. (1997). Influence of place packing or tray packing on the cooling rate of palletised 'Anjou' pears. *HortTechnol.* **7** (4): 378-382.
- Fiikin, A.G. (1983). Investigating the factors for intensifying fruit and vegetable cooling. *Int. J. Refrig.* **6**: 176-181.
- Fiikin, A.G. and Fiikina, I. (1971). Calculation de la duree de refrigeration des produits alimentaires et des corps solides. *Proc. 13th Int. Congr. Refrig.* **Vol 2**: 411-414.
- Fletcher, C.A.J. (1991). *Computational Techniques for Fluid Dynamics 2: Specific techniques for different flow categories*. (2nd Ed.) Springer-Verlag, Berlin.
- Fockens, F.H. and Meffert, H.F.Th. (1972). Biophysical properties of horticultural products as related to loss of moisture during cooling down. *J. Sci. Fd. Agric.* **23**: 285-298.
- Foss, W. (1997). Postdoctoral Engineer, Paper, Physics and Mechanics R&D, Weyerhaeuser, Tacoma, Washington. Personal Communication.

- Foss, W.R., Bronkhorst, C.A., Bennett, K.A. and Riedemann, J.R. (1997). Transient moisture transport in paper in the hygroscopic range and its role in the mechano-sorptive effect. *Proc. 3rd Int. Symp. Moisture and Creep effects on Paper, Board and Containers*, Rotorua, New Zealand. Vol 1: 221-236.
- Frampton, L. (1995). Pear Cooling Options. HB/50. Internal Report for ENZA New Zealand (International).
- Frampton, L. (1996). Weight Loss and cooling rates of Z, RDT and Standard Packs. PH96/6. Internal Report for ENZA New Zealand (International).
- Frampton, L. and Ahlborn, G. (1994). *Cooling Rates of apples in ENZA New Zealand (International) coolstores*. PH94/8. Internal Report for ENZA New Zealand (International).
- Frampton, L., Cregoe, B., Timms, A., Clampin, G. and Ahlborn, G. (1994). Weight loss during shipping and storage in the UK. PH94/7/HB. Internal Report for ENZA New Zealand (International).
- Gaffney, J.J. (1978). Humidity: Basic principles and measurement techniques. *HortScience* **13**: 551-555.
- Gaffney, J.J., Baird, C.D. and Chau, K.V. (1985a). Methods for calculating heat and mass transfer in fruits and vegetables individually and in bulk. *Trans. ASHRAE*. **91 (2B)**: 333-352.
- Gaffney, J.J., Baird, C.D. and Chau, K.V. (1985b). Influence of Airflow rate, respiration, evaporative cooling, and other factors affecting weight loss calculations for fruits and vegetables. *Trans. ASHRAE* **91 (1B)**: 690-707.
- Gan, G. and Woods, J.L. (1989). A deep bed simulation of vegetable cooling. *Proc. 11th Int. Congr. Agric. Engng.* Vol. 4: 2301- 2308.
- Geankoplis, C.J. (1993). *Transport processes and unit operations*. (3rd Ed.) Allyn and Bacon, Boston.
- Gigiel, A.J., Swain, M.J. and James, S.J. (1994). The use of CFD modelling in air flow problems in the food industry. In: *Automatic control of food and biological processes* (J.J. Bimbenet, E. Dumoulin and G. Trystram eds.) Elsevier Science, B.V.
- Goodman, T.R. (1958). The heat balance integral and its application to problems involving a change of phase. *Trans. ASME* **80**: 335-342.
- Goodman, T.R. (1961). The heat balance integral - further considerations and refinements. *J. Heat Transfer* **83**: 83-86.

- Goodman, T.R. (1964). Application of integral methods to transient non-linear heat transfer. *Adv. Heat Transfer* **1**: 51-121.
- Gosman, A.D., Nielson, P.V., Restivo, A. and Whitelaw, J.H. (1980). The flow properties of rooms with small ventilated openings. *Trans. ASME* **102**: 316-323.
- Haas, E. and Felsenstein, G. (1985). Factors affecting the cooling rate of avocados packed in corrugated cartons. *Refriger. Sci. and Technol.* **1985-5**: 291-299.
- Haas, E., Felsenstein, G., Shitzer, A. and Manor, G. (1976). Factors affecting resistance to air flow through packed fresh fruit. *Trans. ASHRAE*. **82 (2)**: 548-554.
- Haghighi, K. and Segerlind, L.J. (1988). Modelling simultaneous heat and mass transfer in an isotropic sphere - A finite element approach. *Trans ASAE* **31 (2)**: 629-637.
- Hall, E.G. (1962). Cooling of apples and pears in cartons. *C.S.I.R.O. Food Pres. Quart.* **22**: 89-91.
- Hardenburg, R.E., Watada, A.E. and Wang, C.Y. (1986). *The commercial storage of fruits, vegetables, and florist and nursery stocks*. U.S. Dept. Agr. Handbook 66, Washington D.C.
- Harris, S. and McDonald, B. (1975). Physical data for kiwifruit (*Actinidia chinensis*). *N.Z. J. Sci.* **18**: 307-312.
- Hayakawa, K. (1978). Computerised simulation for heat transfer and moisture loss from an idealised fresh produce. *Trans ASAE* **21**: 1015-1024.
- Hayakawa, K. and Succar, J. (1982). Heat transfer and moisture loss of spherical fresh produce. *J. Food Sci.* **47**: 596-605.
- Hellickson, M.L. and Baskins, R.A. (1997). Effect of tight-stacking bins on fruit temperature reduction. *Wash. State Uni. Tree Fruit Postharv. J.* **8 (3)**: 16-20.
- Holdredge, R.M. and Wyse, R.E. (1982). Computer simulation of the forced convection cooling of sugarbeets. *Trans. ASAE* **25**: 1425-1430.
- Holman, J.P. (1986). *Heat Transfer*. (6th Ed.) McGraw - Hill Inc, United States of America.
- Holman, J.P. (1990). *Heat Transfer*. (7th Ed.) McGraw - Hill Inc, United States of America.
- Hood, C.E. (1964). *Temperature progression during cooling of pickling cucumbers*. PhD. Dissertation, North Carolina State University, Raleigh, NC.

- Incropera, F.P. and DeWitt, D.P. (1981). *Fundamentals of Heat Transfer* (1st Ed.). John Wiley and Sons Inc, United States of America.
- Incropera, F.P. and DeWitt, D.P. (1996). *Fundamentals of Heat Transfer* (4th Ed.). John Wiley and Sons Inc, United States of America.
- Jamieson, D.J., Cleland, D.J. and Falconer, R.M. (1993). Modelling of bulk-stacked cheese cooling in coolstores. *Refrig. Sci. and Technol.* **1993-3**: 268-276.
- Jiang, H., Thompson, D.R. and Morey, R.V. (1987). Finite element model of temperature distribution in broccoli stalks during forced-air precooling. *Trans. ASAE.* **30(5)**: 1473-1477.
- Karlekar, B.V. and Desmond, R.M. (1982). *Heat Transfer*. West Publishing Co. St. Paul, USA.
- Keey, R.B. (1972). *Drying Principles and Practice*. Pergamon Press, New York.
- Kelly, B.P., Magee, T.R.A. and Ahmad, M.N. (1995). Convective heat transfer in open channel flow; Effects of geometric shape and flow characteristics. *Trans. IChemE* **73**: 171-182.
- King, D. (1996). Research Manager, ENZAFRUIT New Zealand (International). Personal Communication.
- Kopelman, I.J. and Pflug, I.J. (1968). The relationship of the surface, mass average and geometric center temperatures in transient conduction heat flow. *Food Technol.* **22**: 141-144.
- Labuza, T.P. (1982). Moisture gain and loss in packaged foods. *Food Technol.* **36**: 92-97.
- Lee, D.S., Haggard, P.E., Lee, J. and Yam, K.L. (1991). Model for fresh produce respiration in modified atmospheres based on principles of enzyme kinetics. *J. Food Sci.* **56**: 1581-1585.
- Lewis, S., Iskander, S., Densem, R., Anthony, J. and Beswick, N. (1997). *Packaging that sucks!?!*. An Innovating with Industry CREST Report for ENZAFRUIT New Zealand (International).
- Liebenspacher, F. and Weisser, H. (1989). Sorption of water vapour and its kinetics in cellulosic packaging material for food. *Proc. 5th Int. Congr. Food Engng.* **Vol. 1**: 610-623.
- Lin, Z., Cleland, A.C., Serrallach, G.F. and Cleland, D.J. (1993). Prediction of chilling times for objects of regular multi-dimensional shapes using a general geometric factor. *Refrig. Sci. Technol.* **1993-3**: 259-267.

- Lin, Z., Cleland, A.C., Serrallach, G.F. and Cleland, D.J. (1994). *Practical application of a generally applicable method for chilling time prediction*. IRHACE Report, 17p.
- Lin, Z., Cleland, A.C., Cleland, D.J. and Serrallach, G.F. (1996a). A simple method for prediction of chilling times for objects of two-dimensional irregular shape. *Int. J. Refrig.* **19**: 95-106.
- Lin, Z., Cleland, A.C., Cleland, D.J. and Serrallach, G.F. (1996b). A simple method for prediction of chilling times: extension to three-dimensional irregular shapes. *Int. J. Refrig.* **19**: 107-114.
- Lin, Z., Cleland, A.C., Serrallach, G.F. and Cleland, D.J. (1997). Models of the thermal conductivity of a food (cheese) with voids during chilling. *Engng. And Food at ICEF 7* (R. Jowitt Ed.) **Part 2**: F13-F16.
- Lovatt, S.J. (1992). *A dynamic modelling methodology for the simulation of industrial refrigeration systems*. PhD Dissertation, Massey University, Palmerston North, New Zealand.
- Lovatt, S.J., Pham, Q.T., Cleland, A.C. and Loeffen, M.P.F. (1993a). A new method of predicting the time-variability of product heat load during food cooling - Part 1: Theoretical Considerations. *J. Food Engng.* **18**: 13-36.
- Lovatt, S.J., Pham, Q.T., Loeffen, M.P.F. and Cleland, A.C. (1993b). A new method of predicting the time-variability of product heat load during food cooling - Part 2: Experimental Testing. *J. Food Engng.* **18**: 37-62.
- Lovatt, S.J., Willix, J. and Pham, Q.T. (1993c). A physical model of air flow in beef chillers. *Refrig. Sci. and Technol.* **1993-3**: 199-206.
- MacKinnon, I.R. and Balinski, W.K. (1992). Heat and mass transfer characteristics of fruits and vegetables prior to shipment. *SAE Technical Paper Series* **921620**.
- Maguire, K.M. (1998). *Factors affecting mass loss of apples*. PhD Dissertation, Massey University, Palmerston North, New Zealand.
- Maguire, K., Banks, N.H., Lang, S. and Gordon, I. (1996). *FCU Report 1996 - Water Vapour Permeance of Apples*. Report to Fruit Crops Unit, Massey University.
- Marchant, A.N., Lidstone, P.H. and Davies, T.W. (1994). Artificial intelligence techniques for the control of refrigerated potato stores. Part 2: Heat and Mass transfer simulation. *J. Agric. Engng. Res.* **58**: 27-36.
- Marcondes, J.A. (1992a). Cushioning properties of corrugated fiberboard and the effects of moisture content. *Trans ASAE.* **35**: 1949-1953.

- Marcondes, J.A. (1992b). Effect of load history on the performance of corrugated fibreboard boxes. *Pack. Technol. Sci.* **5**: 179-187.
- Marcondes, J.A. (1996). Corrugated fibreboard in modified atmospheres: moisture sorption/desorption and shock cushioning. *Pack. Technol. Sci.* **9**: 87-98.
- Marshall, S.A. and James, R.W. (1975). Dynamic analysis of an industrial refrigeration system to investigate capacity control. *Proc. Inst. Mech. Engrs.* **189**: 437-444.
- McCabe, W.L., Smith, J.C. and Harriot, P. (1993). *Unit Operations of Chemical Engineering*. (5th Ed.) McGraw-Hill Book Co., Singapore.
- McDonald, B. (1990). Cooling of Apples. *DSIR Report No. 9022 (2)*.
- McDonald, B., Billing, D.P. and Wilks, B.G. (1993). Coolstore performance and specifications. *Refrig. Sci. and Technol.* **1993-3**: 390-398.
- Merts, I. (1996). *Mathematical modelling of modified atmosphere packaging systems for apples*. PhD Dissertation, Massey University, Palmerston North, New Zealand.
- Miles, C.A., Van Beek, G. and Veerkamp, C.H. (1983). Calculation of thermo-physical properties of foods. In: *Physical properties of foods*. (R. Jowitt Ed.) Applied Science Publishers, London.
- Mirams, M. (1996). Horticultural Export Earnings. *The Orchardist* **69 (10)**: 10-13.
- Moore, W.J. (1972). *Physical Chemistry*. Prentice-Hall Inc., New Jersey, USA.
- Mueller, T.J. (1983). Recent developments in smoke flow visualisation. In: *Flow Visualisation III*. (W.J. Yang Ed.) Hemisphere Publishing Company, New York. pp 30-40.
- Nakayama, Y. (1993). *Fantasy of flow*. (Y. Nakayama *et al.* Eds.) Visualisation Society of Japan, Ohmsha, Tokyo, Japan.
- Newman, A.B. (1936). Heating and cooling rectangular and cylindrical solids. *Indust. Engng. Chem.* **28**: 545-548.
- Nielson, P.V., Restivo, A. and Whitelaw, J.H. (1978). The velocity characteristics of ventilated rooms. *J. Fluid Engng.* **100**: 291-298.
- Nilsson, L., Wilhelmsson, B. and Stenstrom, S. (1993). The diffusion of water vapour through pulp and paper. *Drying Technol.* **11**: 1205-1225.
- Pala, M. and Devres, Y.O. (1988). Computer simulated model for power consumption and weight loss in a cold store. *Refrig. Sci. and Technol.* **1988-1**: 233-241.

- Pan, J.C. and Bhowmik, S.R. (1991). The finite element analysis of transient heat transfer in fresh tomatoes during cooling. *Trans. ASAE*. **34**: 972-976.
- Parsons, R.A., Mitchell, F.G. and Mayer, G. (1972). Forced-air cooling of palletised fresh fruit. *Trans ASAE* **15**: 729-731.
- Patankar, S.V. (1980). *Numerical heat transfer and fluid flow*. Hemisphere Publishing Corporation, New York.
- Patankar, S.V. and Spalding, D.B. (1972). A calculation procedure for heat, mass and momentum transfer in three-dimensional parabolic flows. *Int. J. Heat Mass Trans.* **15**: 1787-1806.
- Patel, P.N. and Sastry, S.K. (1988). Effects of temperature fluctuation on transpiration of selected perishables: Mathematical models and experimental studies. *Trans. ASHRAE* **94** (1): 1588-1601.
- Perry, R.H. (1973). *Chemical engineers handbook*. (5th Ed.) McGraw-Hill, New York.
- Pflug, I.J. and Blaisdell, J.L. (1963). Methods of analysis of precooling data. *ASHRAE J.* Reprint, 9p.
- Pham, Q.T. and Willix, J. (1989). Thermal conductivity of fresh lamb meat, offals and fat in the range -40°C to +30°C. *J. Food Sci.* **54**: 508-515.
- Pham, Q.T., Wee, H.K., Lovatt, S.J., Lindsay, D. and Kemp, R.M. (1993). A quasi-steady state approach to the design of meat plant refrigeration systems. *Refrig. Sci. and Technol.* **1993-3**: 215-223.
- Rahman, M.S. (1991). Evaluation of the precision of the modified fitch method for thermal conductivity measurement of foods. *J. Food Engng.* **14**: 71-82.
- Rahman, M.S. (1992). Thermal conductivity of four food materials as a single function of porosity and water content. *J. Food Engng.* **15**: 261-268.
- Rahman, M.S. (1995). *Food Properties Handbook*. CRC Press, Boca Raton, Florida, USA.
- Rahman, M.S. and Chen X.D. (1995). A general form of thermal conductivity equation as applied to an apple: effects of moisture, temperature and porosity. *Drying Technol.* **13**: 1-18.
- Rahman, M.S., Chen, X.D. and Perera, C.O. (1997). An improved thermal conductivity prediction model for fruits and vegetables as a function of temperature, water content and porosity. *J. Food Engng.* **31**: 163-170.

- Renault, P., Houal, L., Jacquemin, G. and Chambroy, Y. (1994a). Gas exchange in modified atmosphere packaging 2: Experimental results with strawberries. *Int. J. Food Sci. Technol.* **29**: 379-394.
- Renault, P., Souty, M. and Chambroy, Y. (1994b). Gas exchange in modified atmosphere packaging 1: A new theoretical approach for micro-perforated packs. *Int. J. Food Sci. Technol.* **29**: 365-378.
- Robertson, T.R. (1996). *Packaging Engineering Notes*. Massey University, Palmerston North, New Zealand.
- Robertson, T.R., Thompson, F.B. and Cleland, A.C. (1998). Dynamic measurement of thermal resistance of corrugated paperboard. (In Press.)
- Romero, R.A. and Chau, K.V. (1987). A mathematical simulation for transpiration from fruits and vegetables in bulk storage. *ASAE Paper No. 87-6007*.
- Salisbury, F.B. and Ross, C.W. (1992). *Plant Physiology*. (4th Ed.) Wadsworth Publishing Co. Belmont, California.
- Samaniego-Esguerra, C.M. and Robertson, G.L. (1991). Development of a mathematical model for the effect of temperature and relative humidity on the water vapour permeability of plastic films. *Pack. Technol. Sci.* **4**: 61-68.
- Sastry, S.K. and Buffington, D.E. (1982). Transpiration rates of stored perishable commodities: a mathematical model and experiments on tomatoes. *ASHRAE Trans.* **88**: 159-184.
- Sastry, S.K. and Buffington, D.E. (1983). Transpiration rates of stored perishable commodities: a mathematical model and experiments on tomatoes. *Int. J. Refrig.* **6 (2)**: 84-96.
- Sastry, S.K., Baird, C.D. and Buffington, D.E. (1978). Transpiration rates of certain fruits and vegetables. *Trans ASHRAE* **84 (1)**: 237-255.
- Shah, D.J., Ramsey, J.W. and Wang, M. (1984). An experimental determination of the heat and mass transfer coefficients in moist, unsaturated soils. *Int. J. Heat Mass Transfer* **27**: 1075-1085.
- Smith, R.E., Nelson, G.L. and Henrickson R.L. (1967). Analyses on transient heat transfer from anomalous shapes, *Trans. ASAE* **10**: 236-245.
- Sweat, V.E. (1974). Experimental values of thermal conductivity of selected fruits and vegetables. *J. Food Sci.* **39**: 1080-1083.
- Talbot, M.T., Oliver, C.C. and Gaffney, J.J. (1990). Pressure and velocity distribution for air flow through fruits packed in shipping containers using porous media flow analysis. *Trans ASHRAE.* **96 (1)**: 406-417.

- Tanner, D.J., Cleland, D.J. and Wake, G.C. (1995). Prediction of food chilling rates with time variable surface heat transfer coefficient. *Proc. 19th Int. Congr. Refrig.* Vol 2: 455-462.
- Thompson, J.F., Knutson, J. and Rumsey, T.R. (1996). Moisture loss during forced air cooling of fruits and vegetables. ASAE Paper No. 96-6081.
- Threlkeld, J.L. (1970). *Thermal Environmental Engineering*. Prentice-Hall Inc. New Jersey, USA.
- Touber, S. (1984). Principles and methods for mathematical modelling the steady-state and dynamic behaviour of refrigeration components and installations. *Refrig. Sci. and Technol.* 1984-2: 163-175.
- van Beek, G. (1985). Practical applications of transpiration coefficients of horticultural produce. *Trans ASHRAE.* 91 (1B): 708-725.
- van der Ree, H., Basting, W.J. and Nievergeld, P.G.M. (1974). Prediction of temperature distributions in cargoes with the aid of a computer program using the method of finite elements. *Refrig. Sci and Technol.* 1974-2: 195-220.
- van Gerwen, R.J.M. and van Oort, H. (1989). The use of fluid dynamics simulation models in cold store design. *Refrig. Sci and Technol.* 1989-1: 233-240.
- van Gerwen, R.J.M. and van Oort, H. (1990). Optimisation of cold store design using fluid dynamics models. *Refrig. Sci and Technol.* 1990-4: 473-478.
- Van Gerwen, R.J.M., Van der Sluis, S.M. and Van Oort, H. (1991). Computer modelling of carcass chilling processes. *Proc. 18th Int. Congr. Refrig.* Vol. 4: 1893-1897.
- Visser, F.R. and Burrows, J.K. (1983). *Composition of New Zealand Foods 1. Characteristic Fruits and Vegetables*. Science Information Publishing Centre, Wellington, New Zealand.
- Visser, F.R., Hannah, D.J. and Bailey, R.W. (1990). *Composition of New Zealand Foods 2. Export Fruits and Vegetables*. The Royal Society of New Zealand, Wellington, New Zealand.
- Wade, N.L. (1984). Estimation of the refrigeration capacity required to cool horticultural produce. *Int. J. Refrig.* 7: 358-366.
- Wang, H.W. (1991). *Modelling of a refrigerating system coupled with a refrigerated room*. PhD Dissertation, Delft University of Technology, The Netherlands.
- Wang, H. and Janssens, F.M. (1994). Modelling of precooling process of cut flowers. *Proc. Contrib. du froid.* May 1993: 349-364.

- Wang, H.W. and Touber, S. (1987). Prediction of air flow patterns in cold stores based on temperature measurements. *Proc. 17th Int. Congr. Refrig.* Vol. D: 52-60.
- Wang, H.W. and Touber, S. (1988). Simple non-steady state modelling of a refrigerated room accounting for air flow and temperature distributions. *Refrig. Sci. and Technol.* **1988-1**: 211-219.
- Wang, H.W. and Touber, S. (1990). Distributed dynamic modelling of a refrigerated room. *Int. J. Refrig.* **13**: 214-222.
- Wang, H. and Touber, S. (1991). Distributed and non-steady-state modelling of an air cooler. *Int. J. Refrig.* **14**: 98-111.
- Watkins, J.B. (1990). *Forced-air cooling*. (2nd Ed.) Queensland Department of Primary Industries, Brisbane.
- Wells, C.M. (1992). *Modelling the greenhouse environment and the growth of cucumbers (Cucumis sativus L.)*. PhD Dissertation, Massey University, Palmerston North, New Zealand.
- Wexler, A. and Greenspan, L. (1971). Vapour pressure equation for water in the range of 0 to 100°C. *NBS J. Res.* **75A**: 213-230.
- Whitaker, S. (1972). Forced convection heat transfer correlations for flow in pipes, past flat plates, single cylinders, single spheres, and for flow in packed beds and tube bundles. *AIChE Journal.* **18**: 361-371.
- Wilhelm, L.R. (1976). Numerical calculation of psychrometric properties in SI units. *Trans ASAE* **19**: 318-325.
- Willix, J. and Amos, N.D. (1995). *Thermal properties of foods*. MIRINZ Tech. Rep. No. 955, 11p.
- Willix, J., Lovatt, S.J. and Amos, N.D. (1998). Additional thermal conductivity values of foods measured by a guarded hot plate. *J. Food Engng.* In Press.
- Wink, W.A. (1961). The effect of relative humidity and temperature on paper properties. *TAPPI J.* **44**: 171-180.
- Wood Handbook (1955). *Handbook No. 72*. Forest Products Laboratory, U.S. Department of Agriculture.
- Yilmaz, T. (1995). Equations for heating and cooling of bodies of various shapes. *Int. J. Refrig.* **18**: 395-402.

APPENDIX 1

TABLE OF NOMENCLATURE

Symbol	Definition	Units
$\%WL$	Percent weight loss	%
δ	Diffusivity of water vapour through a material	$\text{kg.m.m}^{-2}.\text{s}^{-1}.\text{Pa}^{-1}$
α	Thermal diffusivity of material	$\text{m}^2.\text{s}^{-1}$
ψ	Volume coefficient of expansion of air	K^{-1}
ρ	Density of material	kg.m^{-3}
θ	Temperature of material	K or $^{\circ}\text{C}$
β	Root of the transcendental equation	dimensionless
ϕ	Heat removal from a material	W
ε	Volume fraction of air voids, or porosity	fraction
μ	Kinematic viscosity	$\text{kg.m}^{-1}.\text{s}^{-1}$
τ	Characteristic of Clayton <i>et al.</i> (1995) correlation	kg or m^3
δ'	Diffusivity of water vapour through a material	$\text{m}^2.\text{s}^{-1}$
φ_1	Guggenheim constant	dimensionless
γ_1	Factor correcting properties of the multi-layer molecules with respect to the bulk liquid	dimensionless
χ_1, χ_2, χ_3	Guggenheim-Anderson-De Boer coefficients for a packaging material	dimensionless
A	Area of material	m^2
a	Product specific respiratory constant, or Commodity specific are coefficient	dimensionless dimensionless
a_w	Water activity of material	fraction
b	Product specific respiratory constant, or Commodity specific are coefficient	dimensionless dimensionless
Bi	Biot number	dimensionless
c	Specific heat capacity of material	$\text{J.kg}^{-1}.\text{K}^{-1}$
CF	Mixing coefficient proportioning factor	dimensionless

d	Product diameter	m
D_t	Shortest dimension of material	m
E	Shape factor from Cleland and Earle (1982)	dimensionless
e	Thermal conductivity correlation parameter, or Commodity specific area coefficient	dimensionless dimensionless
emc	Equilibrium moisture content of material	$g_{H_2O} \cdot 100g_{dry \text{ pkg}}$
f	Commodity specific area coefficient	dimensionless
F	Fat mass fraction of material	fraction
Fo	Fourier number	dimensionless
g	Acceleration due to gravity	$m \cdot s^{-2}$
G	Shape factor from Smith <i>et al.</i> (1967)	dimensionless
Gr	Grashof number	dimensionless
H	Absolute humidity of air	$kg_{water} \cdot kg_{dry \text{ air}}^{-1}$
h	Surface heat transfer coefficient	$W \cdot m^{-2} \cdot K^{-1}$
H_R	Relative humidity	fraction
H_{No}	Horizontal boundary numbering syntax	dimensionless
i	Modelling boundary number (max. of six)	dimensionless
j	Heat transfer mode	dimensionless
j	Function of β and geometry	dimensionless
K	Mass transfer coefficient	$kg \cdot m^{-2} \cdot s^{-1} \cdot Pa^{-1}$
k	Thermal conductivity of material	$W \cdot m^{-1} \cdot K^{-1}$
K_t	Mass transfer coefficient	$m \cdot s^{-1}$
k_e	Effective thermal conductivity of material	$W \cdot m^{-1} \cdot K^{-1}$
K_{fl}	Fluid film mass transfer coefficient	$kg \cdot m^{-2} \cdot s^{-1} \cdot Pa^{-1}$
k_g	Thermal conductivity of gas phase	$W \cdot m^{-1} \cdot K^{-1}$
K_i	Inhibition constant for Carbon Dioxide	% CO ₂
K_m	Michaelis-Menton constant for Oxygen	% O ₂
k_{mc}	Rate constant for water adsorption / desorption	s^{-1}
K_{pk}	Packaging film mass transfer coefficient	$kg \cdot m^{-2} \cdot s^{-1} \cdot Pa^{-1}$
k_s	Thermal conductivity of solid phase	$W \cdot m^{-1} \cdot K^{-1}$
K_{skin}	Skin mass transfer coefficient	$kg \cdot m^{-2} \cdot s^{-1} \cdot Pa^{-1}$
K_t	Total mass transfer coefficient	$kg \cdot m^{-2} \cdot s^{-1} \cdot Pa^{-1}$
KA	Mass transfer coefficient \times area term	$kg \cdot s^{-1} \cdot Pa^{-1}$
L	Length of flow path in velocity characterisation	M
M	Mass of material	kg
m	Mass flow rate	$kg \cdot s^{-1}$
mc	Moisture content of material	$g_{H_2O} \cdot 100g_{dry \text{ pkg}}$

mc_0	Moisture content corresponding to saturation of all primary adsorption sites by one water molecule	$g_{H_2O} \cdot 100 g_{dry\ pk}$
m_{CO_2}	Carbon Dioxide production per unit mass of product	$mg \cdot kg^{-1} \cdot hr^{-1}$
n	Molar mass of element	$kg \cdot kmol^{-1}$
Nu	Nussult number	dimensionless
o	Product specific respiratory constant	dimensionless
p	Product specific respiratory constant	dimensionless
p_a	Partial pressure of water vapour in ambient air	Pa
P_f	Packaging protection factor	dimensionless
Pr	Prandtl number	dimensionless
P_{No}	Perpendicular boundary numbering syntax	dimensionless
p_s	Partial pressure of water vapour in boundary layer at product surface	Pa
$p_{sat,amb}$	Saturated partial pressure of water vapour at the ambient air temperature	Pa
$p_{sat,surf}$	Saturated partial pressure of water vapour at the product surface temperature	Pa
Q	Respiratory heat generation	W
q	Respiratory heat generation rate	$J \cdot kg^{-1} \cdot s^{-1}$
R	Characteristic dimension of material	m
Re	Reynolds number	dimensionless
R_g	Universal gas constant	$kJ \cdot mol^{-1} \cdot K^{-1}$
R_{pk}	Empirical resistance factor for packaging	dimensionless
RH	Relative humidity	%
rr	Respiration rate	$kmol \cdot kg^{-1} \cdot s^{-1}$
S	Solids, other than fat, mass fraction of material	fraction
SA	Surface area of material	m^2
Sc	Schmidt number	dimensionless
Sh	Sherwood number	dimensionless
t	Time	s
v	Velocity	$m \cdot s^{-1}$
UA	Heat transfer coefficient \times area term	$W \cdot K^{-1}$
V	Volume of solid	m^3
V_m	Maximum respiration rate	$kmol \cdot kg^{-1} \cdot s^{-1}$
VRC	Velocity relativity coefficient	dimensionless
V_{No}	Vertical boundary numbering syntax	dimensionless
W	Water mass fraction of material	fraction
wc	Water content (wet basis) of material	%

w_{pkd}	Moisture loss from packed product	kg.s^{-1}
w_{unpkd}	Moisture loss from unpacked product	kg.s^{-1}
X	Number of packaging materials in a zone	dimensionless
x	Thickness, or distance, through material	m
Y	Dimensionless temperature ratio as a function of time and position within a material	dimensionless
Z	Space saving variable	dimensionless

Specific Subscripts not already defined

act	Actual property
air	Air property
atm	Atmospheric property
av	Average
c	Convection
$carbon$	Carbon ₁₂
d	Dry
eff	Effective property
ext	External condition
f	Freezing property
fl	Fluid property
i	Modelling boundary number (max. of six)
int	Internal condition
j	Heat transfer mode
pk	Packaging material property
pr	Product property
r	Space position within a material relative to its centre
$resp$	Respiration property
$skin$	Product skin property
tot	Total
$uptake$	Uptake of water vapour
v	Ventilation property
w	Water property
wv	Water vapour property
x,y,z	Space position within material

APPENDIX 2

DETERMINATION OF MODEL INPUT DATA

A2.1. INTRODUCTION

The use of the modelling systems requires input of system specific data. This Appendix covers the important data for the products, packaging materials and fluids, describing how or where the data were obtained and issues pertaining to the accuracy of the data. Some data were calculated from fundamental equations, others were calculated using empirical equations, while others were measured experimentally. In each area, a brief summary of literature is presented, but then specific data used in this work are identified. Ultimately, selection of data requires judgement by the engineer. It is acknowledged that other users may choose their data differently and the summary of literature is therefore intended to aid them.

A2.2. THERMO-PHYSICAL PROPERTIES

A2.2.1. Thermal Conductivity

Thermal conductivity is a measure of the resistance to heat transfer by conduction through a material. Thermal conductivity depends on many factors: including the kind of substance (metal, solid liquid); composition (impurities, mixtures); structure and structural orientation; temperature; and pressure (ASHRAE, 1993). Some experimental data are available, and there are prediction methods, which are sufficiently accurate for many food materials.

A2.2.1.1. Prediction Methods for Thermal Conductivity

Empirical relationships have been presented in the literature for predicting thermal conductivity of unfrozen materials. Sweat (1974) presented a correlation, which was applicable for predicting thermal conductivity for fruits and vegetables (except those with significantly lower densities than that of water). This linear model was based on water content and, although no statistical bounds were given, was stated to predict measured values to within $\pm 15\%$:

$$k = 0.148 + (0.00493wc) \quad (A2.1)$$

where k = thermal conductivity of the material ($\text{W}\cdot\text{m}^{-1}\cdot\text{K}^{-1}$).
 wc = water content as a percent, wet basis (%).

Pham and Willix (1989) and Willix *et al.* (1998) stated that above freezing point, the conductivity of food with a high water content is close to linear with temperature, thus:

$$k = k_f + d(\theta - \theta_f) \quad (\text{A2.2})$$

where k_f = thermal conductivity of food material at θ_f ($\text{W}\cdot\text{m}^{-1}\cdot\text{K}^{-1}$).
 d = correlation parameter (Pham and Willix, 1989; Willix *et al.*, 1998).
 θ = food material temperature ($^{\circ}\text{C}$).
 θ_f = freezing temperature for the food material (also presented in Pham and Willix, 1989; Willix *et al.*, 1998) ($^{\circ}\text{C}$).

Rahman (1991, 1992), Rahman and Chen (1995) and Rahman *et al.* (1997) have presented a range of generalised correlations including temperature and porosity effects, which were stated to agree well with measured data.

Air voids within products have a substantial effect on its heat transfer properties. Cleland and Cleland (1992) stated that if the voids occur at the product surface, then adjustment of the surface heat transfer coefficient is an effective approach for more accurate prediction. However, if the voids are dispersed more randomly through the product, or group of products (such as within a horticultural package), calculation of effective thermal properties is a more satisfactory approach. For this, calculation of the volume fraction of the voids (ε) is necessary, and the following methodology (Eqn. A2.3) was suggested.

$$\varepsilon = \frac{V_{fl}}{V_{pr} + V_{fl}} \quad (\text{A2.3})$$

where ε = volume fraction of air voids.
 V_{fl} = volume of fluid in package (m^3).
 V_{pr} = volume of product in package (m^3).

A number of approaches for calculating effective thermal conductivity have been proposed in the literature, and many of these were reviewed extensively by Lin *et al.* (1997). The authors evaluated eight estimation methods for chilling of products with air voids and found that the method proposed by Keey (1972) gave the most accurate predictions. Keey (1972) stated that the conductivity of a porous material could be correlated by reference to two models. The proposed method combined both parallel and series thermal conductivity models using a distribution factor (which determined the proportion of the heat transfer pathway that is in series).

$$\frac{1}{k_e} = \frac{1-f}{(1-\varepsilon)k_s + \varepsilon k_g} + f \left(\frac{1-\varepsilon}{k_s} + \frac{\varepsilon}{k_g} \right) \quad (\text{A2.4})$$

where k_e = effective thermal conductivity ($\text{W}\cdot\text{m}^{-1}\cdot\text{K}^{-1}$).
 f = a distribution factor which is the fraction of the pathway that is in series mode ($0 < f < 0.25$).
 k_s = thermal conductivity of the solid phase ($\text{W}\cdot\text{m}^{-1}\cdot\text{K}^{-1}$).
 k_g = thermal conductivity of the gas phase ($\text{W}\cdot\text{m}^{-1}\cdot\text{K}^{-1}$).

Lin *et al.* (1997) found the model proposed by Keey gave the best predictions of effective thermal conductivity for one porous food when $f = 0.16$.

According to ASHRAE (1993), the thermal conductivity of moist air is approximately identical to that of dry air within the temperature range -40°C to 120°C . Karlekar and Desmond (1982) presented the following correlation between dry air thermal conductivity and temperature (correlation coefficient not stated):

$$k_{air} = 0.02397 + (7.59 \times 10^{-5} \theta_{air}) \quad (\text{A2.5})$$

where k_{air} = thermal conductivity of air ($\text{W}\cdot\text{m}^{-1}\cdot\text{K}^{-1}$).
 θ_{air} = air temperature ($^{\circ}\text{C}$).

Using data presented by McCabe *et al.* (1993) for thermal conductivity of water in the temperature range $0 - 150^{\circ}\text{C}$, a polynomial relationship (correlation coefficient of 0.99) was developed:

$$k_w = 0.5536 + 0.00245\theta_w - 1.44 \times 10^{-5}\theta_w^2 + 2.61 \times 10^{-8}\theta_w^3 \quad (\text{A2.6})$$

where k_w = thermal conductivity of water ($\text{W}\cdot\text{m}^{-1}\cdot\text{K}^{-1}$).
 θ_w = water temperature ($^{\circ}\text{C}$).

A2.2.1.2. Experimental Values of Thermal Conductivity

Experimentally determined values of thermal conductivity of horticultural commodities are widely available in the literature, but data for packaging materials are sparse. Data are summarised in Table A2.1 for a range of horticultural products and known packaging materials. The accuracy is dependent on the measurement method.

McCabe *et al.* (1993) present measured data for thermal conductivity of air over the temperature range $0 - 100^{\circ}\text{C}$, and of water over the temperature range $0 - 150^{\circ}\text{C}$. The change in thermal conductivity of air with temperature, over the given range, was linear. These data are summarised in Table A2.2.

A2.2.1.3. Data Used

Data for thermal conductivity of products used in the present work were selected from Table A2.1, whilst fluid thermal conductivity was calculated using either Eqn. (A2.5) or (A2.6). Almost all model testing carried out was for $Bi < 1$ conditions. As $Bi \rightarrow 0$, the influence of error in the product thermal conductivity diminishes. Hence the influence of data error was not expected to be large. It was considered unlikely that any of the prediction methods would yield more accurate information. Data for thermal conductivity of packaging materials used in the present work were also selected from Table A2.1.

Table A2.1.

Experimental values of thermal conductivity for a range of horticultural products and packaging materials.

Product	Thermal Conductivity (W.m ⁻¹ K ⁻¹)	Product	Thermal Conductivity (W.m ⁻¹ K ⁻¹)
<i>Horticultural Product</i>			
Apple var. 'Red Delicious'	0.42 ¹	Grapefruit	0.54 ¹
Apple var. 'Braeburn'	0.42 ¹	Kiwifruit var. 'Hayward'	0.427 ⁴
Apple var. 'Royal Gala'	0.456 ²	Nectarine	0.585 ³
Apple var. 'Fiesta'	0.428 ²	Orange	0.469 ⁵
Apple var. 'Cox's Orange'	0.448 ²	Peach	0.581 ³
Apple - green	0.422 ³	Pear	0.595 ³
Apple - red	0.513 ³	Plum	0.551 ³
Avocado	0.429 ³	Tomato	0.57 ¹
Banana	0.481 ³		
<i>Packaging Materials</i>			
Corrugated Cardboard	0.065 ⁶	Polystyrene foam	0.035 ⁷
Hardwoods	0.15 ⁷	Rigid Polystyrene	0.027 ⁹
Natural Kraft Paper	0.079 ⁸	PET (500µm)	0.115 ⁸
Polycarbonate Plastic	0.23 ⁷	Rigid PVC Plastic	0.16 ⁷
Polyethylene, High Density	0.48 ⁶	Solid Cardboard	0.07 ¹⁰
Polyethylene, Low Density	0.33 ⁶	Wood - pine, white	0.11 ¹¹

- | | |
|---------------------------------|------------------------------------|
| 1. Lin <i>et al.</i> (1994). | 7. C.I.B.S Guide (1980). |
| 2. Willix <i>et al.</i> (1998). | 8. Robertson <i>et al.</i> (1998). |
| 3. Sweat (1974). | 9. ASHRAE (1997). |
| 4. Harris and McDonald (1975). | 10. Perry (1973). |
| 5. Romero and Chau (1987). | 11. Wood Handbook (1955). |
| 6. ASHRAE (1993). | |

Table A2.2.

Values for thermal conductivity of air and water (After McCabe *et al.*, 1993).

Temperature (°C)	Thermal Conductivity (W.m ⁻¹ K ⁻¹)	Temperature (°C)	Thermal Conductivity (W.m ⁻¹ K ⁻¹)
<i>Air</i>			
0	0.0242	100	0.0318
<i>Water</i>			
0	0.554	60	0.654
4	0.564	71	0.665
10	0.576	82	0.672
16	0.588	93	0.678
21	0.599	104	0.682
27	0.609	116	0.685
32	0.620	127	0.685
38	0.627	138	0.685
49	0.642	149	0.685

A2.2.2. Specific Heat Capacity

The specific heat capacity of a material (units of $\text{J.kg}^{-1}.\text{K}^{-1}$) is defined as the amount of heat necessary to raise the temperature of a unit mass of the material by a unit degree.

A2.2.2.1. Prediction Methods for Specific Heat Capacity

The specific heat capacity of foods is widely modelled as a function of a product's constituents, most often the water content. Hardenburg *et al.* (1986) presented a correlation for specific heat capacity of horticultural commodities as a function of product moisture content:

$$c_{pr} = 33.5wc + 837 \quad (\text{A2.7})$$

where c_{pr} = product specific heat capacity ($\text{J.kg}^{-1}.\text{K}^{-1}$).
 wc = percent water content (%).

Cleland and Cleland (1992) presented an empirical correlation for materials above their freezing temperature. This correlation (Eqn. A2.8) takes into account the product's water, solid and fat fractions. Tabulated composition data that might be used with any composition-based method are presented Table A2.3.

$$c_{unfrozen} = 4180W + 1400S + 1900F \quad (\text{A2.8})$$

where W = water mass fraction of material.
 F = fat mass fraction of material.
 S = solids other than fat mass fraction of material.

The specific heat capacity of moist air can be calculated from the linear relationship (correlation coefficient for relationship not stated) given by Threlkeld, (1970):

$$c_{air} = 1000 + 1880H \quad (\text{A2.9})$$

where;

$$H = \frac{18P_{fl}}{29(P_{atm} - P_{fl})} \quad (\text{A2.10})$$

and

$$P_{fl} = H_R P_{sat,amb} \quad (\text{A2.11})$$

where, using an Antoine equation (Cleland and Cleland, 1992) for water:

$$P_{sat,amb} = e^{\left[\frac{23.4795 - \frac{3990.56}{\theta_{ar} + 233.833}}{\theta_{ar} + 233.833} \right]} \quad (\text{A2.12})$$

where c_{air} = air specific heat capacity ($\text{J.kg}^{-1}.\text{K}^{-1}$).
 H = humidity ratio of the air ($\text{kg.kg}_{\text{dry air}}^{-1}$).
 P_{fl} = partial pressure of water vapour in ambient air (Pa).
 H_R = relative humidity (fraction).
 $P_{sat,amb}$ = vapour pressure of water at ambient air temperature (Pa).

θ_{air} = air temperature ($^{\circ}\text{C}$).

Using data presented by Incropera and DeWitt, (1981) for specific heat capacity of water over the temperature range 0 - 100 $^{\circ}\text{C}$, a polynomial relationship (correlation coefficient of 0.99) was developed:

$$c_w = 4213.9 - 2.168\theta_w + 0.036\theta_w^2 - 1.47 \times 10^{-4}\theta_w^3 \quad (\text{A2.13})$$

where c_w = specific heat capacity of water ($\text{J.kg}^{-1}.\text{K}^{-1}$).
 θ_w = water temperature ($^{\circ}\text{C}$).

A2.2.2.2. *Experimental Values of Specific Heat Capacity*

Table A2.3 shows specific heat capacity values from literature for packaging materials whilst Table A2.4 shows the available horticultural product composition data and either measured or calculated values for specific heat capacity for these products.

Table A2.3.
Values for specific heat capacity of packaging materials.

Packaging Material	Specific Heat ($\text{J.kg}^{-1}.\text{K}^{-1}$)	Packaging Material	Specific Heat ($\text{J.kg}^{-1}.\text{K}^{-1}$)
Corrugated board	1700 ¹	Polyethylene - High density	2300 ⁴
Moulded pulp 'Friday' tray	1340 ²	Rigid PVC Plastic	1300 ⁵
Paper	1300 ³	Softwoods	1630 ³
Polystyrene	1210 ³	Solid Cardboard	1260 ⁶
Polyethylene - Low density	2300 ⁴		

1. Amos (1995).

2. Merts (1996).

3. ASHRAE (1997).

4. ASHRAE (1993).

5. Robertson (1996).

6. Earle (1983).

Table A2.5 shows specific heat capacity data for both air and water over the temperature range 0 - 100 $^{\circ}\text{C}$.

A2.2.2.3. *Data Used*

Data for specific heat capacity of packaging materials used in the present work were selected from Table A2.3. For products, data were selected from Table A2.4 as it was considered unlikely that any of the prediction methods would yield more accurate information, whilst fluid specific heat capacity was calculated using either Eqn. (A2.9) or (A2.13).

Table A2.4.
Experimentally determined values for horticultural product composition and measured or calculated specific heat capacity.

Product	Composition (%)			Specific Heat (J.kg ⁻¹ K ⁻¹)
	Water Content	Solid Content	Fat Content	
Apple var. 'Braeburn'	-----	-----	-----	3800 ¹
Apple var. 'Cox's Orange'	87.3 ²	12.67	0.03	3827 ³
Apple var. 'Fiesta'	87.1 ²	12.55	0.35	3823 ³
Apple var. 'Gala'	86.0 ⁴	13.60	0.4	3793 ³
Apple var. 'Granny Smith'	86.0 ⁴	13.40	0.6	3794 ³
Apple var. 'Red Delicious'	85.2 ⁵	14.40	0.4	3682 ⁶
Apple var. 'Royal Gala'	87.6 ²	12.36	0.04	3834 ³
Apple - green	88.5 ⁷	-----	-----	3802 ⁸
Apple - red	84.9 ⁷	-----	-----	3681 ⁸
Apricot var. 'Moorpark'	86.0 ⁴	13.60	0.4	3793 ³
Avocado var. 'Hass'	63.0 ⁴	11.00	26.0	3281 ³
Banana	75.7 ⁷	-----	-----	3373 ⁸
Feijoa var. 'Mammoth'	85.0 ⁹	14.60	0.4	3765 ³
Feijoa var. 'Triumph'	85.0 ⁹	14.70	0.3	3765 ³
Grapefruit var. 'Marsh'	-----	-----	-----	3703 ⁶
Kiwifruit var. 'Hayward'	85.7 ⁵	13.90	0.4	3650 ¹⁰
Nectarine var. 'Fantasia'	88.0 ⁴	11.70	0.3	3848 ³
Orange var. 'Valencia'	-----	-----	-----	3515 ⁶
Peach var. 'Red Haven'	87.0 ⁴	12.60	0.4	3821 ³
Pear var. 'Packham's'	84.0 ⁴	15.60	0.4	3737 ³
Pear var. 'Bartlett'	83.8 ¹¹	-----	-----	3730 ¹¹
Plum var. 'Black Doris'	87.0 ⁴	12.50	0.5	3514 ⁶
Tomato	94.7 ¹²	-----	-----	4005 ⁸

- | | |
|---|---|
| <ol style="list-style-type: none"> 1. Lin <i>et al.</i> (1994). 2. Willix and Amos (1995). 3. Calculated using Eqn. (A2.8) (Cleland and Cleland, 1992). 4. Visser <i>et al.</i> (1990). 5. Willix <i>et al.</i> (1998). 6. Rahman (1995). | <ol style="list-style-type: none"> 7. Sweat (1974). 8. Calculated using Eqn. (A2.7) (Hardenburg <i>et al.</i>, 1986). 9. Visser and Burrows (1983) 10. Harris and McDonald (1975). 11. ASHRAE (1993). 12. Bellagha and Chau (1985). |
|---|---|

Table A2.5.

Literature presented values for specific heat capacity of air and water.

Temperature (°C)	Specific Heat (J.kg ⁻¹ .K ⁻¹)	Temperature (°C)	Specific Heat (J.kg ⁻¹ .K ⁻¹)
<i>Air</i> ¹			
0	1005	100	1009
<i>Water</i> ²			
0	4217	57	4184
7	4198	67	4188
17	4184	77	4195
27	4179	87	4203
37	4178	97	4214
47	4180	100	4217

1. Geankoplis (1993).

2. Incropera and DeWitt (1981).

A2.2.3. Density

A2.2.3.1. Prediction Methods for Density

Cleland and Cleland (1992) presented a correlation for food product density as a function of the compositional properties of materials (tabulated in Table A2.4). This prediction method is useful where experimentally measured data are unavailable.

$$\rho = \frac{1}{\frac{W}{1000} + \frac{S}{1300} + \frac{F}{850}} \quad (\text{A2.14})$$

where W = water mass fraction of material.
 F = fat mass fraction of material.
 S = solids other than fat mass fraction of material.

The dry air density can be calculated from ideal gas considerations as a function of the air temperature and the humidity ratio of the air:

$$\rho_{air} = \frac{273.15}{22.4(273.15 + \theta_{air}) \left(\frac{1}{29} + \frac{H}{18} \right)} \quad (\text{A2.15})$$

where ρ_{air} = dry air density (kg.m⁻³).
 H = absolute humidity of the air - calculated using Eqn. (A2.10)
 (kg.kg_{dry air}⁻¹).
 θ_{air} = air temperature (°C).

Using data presented by McCabe *et al.* (1993) for density of water as a function of temperature (over the range 0 - 150°C), a quadratic relationship (correlation coefficient of 0.99) was developed:

$$\rho_w = 1001.36 - 0.128\theta_w - 0.0029\theta_w^2 \quad (\text{A2.16})$$

where ρ_w = density of water (kg.m^{-3}).
 θ_w = water temperature ($^{\circ}\text{C}$).

A2.2.3.2. Experimental Values of Density

As with thermal conductivity and specific heat capacity, various data have been presented in the literature for density of horticultural and packaging products. These are tabulated in Table A2.6.

Table A2.6.

Experimental values of density for a range of horticultural and packaging products.

Product	Density (kg.m^{-3})	Product	Density (kg.m^{-3})
<i>Horticultural Commodity</i>			
Apple var. 'Red Delicious'	840 ¹	Kiwifruit var. 'Hayward'	1045 ⁴
Apple var. 'Braeburn'	870 ²	Nectarine	990 ³
Apple - green	790 ³	Orange	880 ²
Apple - red	840 ³	Peach	930 ³
Avocado	1060 ³	Pear	1000 ³
Banana	980 ³	Plum	1130 ³
Grapefruit	1060 ²	Tomato	962 ⁵
<i>Packaging Materials</i>			
626 ^a B - Corrugated board	250 ⁶	Rigid PVC Plastic	1350 ⁷
626 ^a C - Corrugated board	195 ⁶	Solid Cardboard	802 ⁸
6226 ^b B - Corrugated Board	250 ⁶	Unbleached Liner - Grade 1	706 ⁹
Moulded pulp 'Friday' tray	260 ⁶	Unbleached Liner - Grade 2	695 ⁹
Polycarbonate Plastic	1150 ⁷	Unbleached Liner - Grade 3	688 ⁹
Polyethylene - High density	960 ¹	Unbleached Liner - Grade 6	659 ⁹
Polyethylene - Low density	930 ¹	Wood - pine, white	430 ⁸

- | | |
|---|---|
| <ol style="list-style-type: none"> 1. ASHRAE (1993). 2. Lin <i>et al.</i> (1994). 3. Sweat (1974). 4. Harris and McDonald (1975). 5. Bellagha and Chau (1985). | <ol style="list-style-type: none"> 6. Experimentally measured as part of this research. 7. C.I.B.S Guide (1980). 8. Wood Handbook (1955). 9. From Carter Holt Harvey (Pulp and Paper) - Kinleith Mill Specifications. |
|---|---|

Note:

- | | | |
|---|---|---|
| a | - | 290 / 160 / 290 g.m^{-2} paper grades. |
| b | - | 290 / 160 / 160 / 290 g.m^{-2} paper grades. |

Measured data for density of dry air over the temperature range, 17.8 - 93.3 $^{\circ}\text{C}$, has been presented by Geankoplis (1993) and for water over the temperature range, 0 - 150 $^{\circ}\text{C}$, by McCabe *et al.* (1993). These data are summarised in Table A2.7.

Table A2.7.
Values of density of air and water.

Temperature (°C)	Density (kg.m ⁻³)	Temperature (°C)	Density (kg.m ⁻³)
<i>Dry Air</i> ¹			
-17.8	1.379	37.8	1.137
0	1.293	65.6	1.043
10	1.246	93.3	0.964
<i>Water</i> ²			
0	999.9	60	983.2
4	1000.0	71	977.1
10	999.9	82	970.4
16	999.1	93	963.2
21	998.0	104	955.2
27	996.7	116	946.7
32	995.0	127	937.6
38	993.1	138	928.1
49	988.5	149	918.0

1. Geankoplis (1993).

2. McCabe *et al.* (1993).

A2.2.3.3. Data Used

Data for density of products and packaging materials used in the present work were selected from Table A2.7, whilst fluid density was calculated using either Eqn. (A2.15) or (A2.16).

A2.2.4. Fluid Kinematic Viscosity

ASHRAE (1997) states that the kinematic viscosity is the ratio of absolute viscosity to density. Geankoplis (1993) presented data for the kinematic viscosity of both dry air and water over the temperature range 0 - 100°C. The data for dry air is approximately linear with temperature (correlation coefficient for relationship of 0.99) (Eqn. A2.17) whilst the water data was fitted with a reciprocal quadratic (correlation coefficient of 0.99) (Eqn. A2.18) and both were used in all the present work:

$$\mu_{air} = 1.781 \times 10^{-5} + 4.71 \times 10^{-8} \theta_{air} \quad (\text{A2.17})$$

$$\mu_w = \frac{1}{557.81 + 19.71\theta_w + 0.11\theta_w^2} \quad (\text{A2.18})$$

where μ_{air} = kinematic viscosity of air (kg.m⁻¹.s⁻¹).
 θ_{air} = air temperature (°C).
 μ_w = kinematic viscosity of water (kg.m⁻¹.s⁻¹).
 θ_w = water temperature (°C).

A2.2.5. Product Surface Area

In calculating product heat transfer, it is necessary to calculate the surface area of the product. Given that natural products are inherently variable, simplifications are possible, such as assuming pseudo-spherical objects to be spherical and pseudo-ellipsoidal objects to have the same surface area as that of an ellipsoid. Correlations have been developed for a number of fruits and vegetables, giving measures of true product surface area.

Chau *et al.* (1987) determined experimentally a linear correlation (correlation coefficient not stated) between a single commodity's surface area and its mass, which is expressed as:

$$A = a + b(M_{pr} \times 1000) \quad (\text{A2.19})$$

where A = surface area of the product (m²).
 a, b = commodity specific area coefficients (dimensionless).
 M_{pr} = mass of product (kg).

Table A2.8.
Parameter values for linear regression models relating product mass to product surface area (Chau *et al.*, 1987).

Product	Area Coefficients	
	<i>a</i>	<i>b</i>
Apples	7.23×10^{-3}	6.02×10^{-5}
Grapefruit	1.3×10^{-2}	4.16×10^{-5}
Lemons	4.08×10^{-3}	6.36×10^{-5}
Limes	2.38×10^{-3}	6.4×10^{-5}
Oranges	-4.73×10^{-4}	7.98×10^{-5}
Peaches	6.12×10^{-3}	5.1×10^{-5}
Pears	2.52×10^{-3}	7.16×10^{-5}
Tomatoes	4.29×10^{-3}	6.21×10^{-5}

Clayton *et al.* (1995) presented non-linear regression models for predicting the surface area of four varieties of apple fruit, correlated with both fruit mass and fruit volume. These models were tested against assumptions of spherical and ellipsoidal properties with actual surface area being underestimated by 15% and 18% respectively by the spherical and ellipsoidal model in these cases. A finite element method was also found to inaccurately predict surface area, overestimating except in the case of small apple fruit. The non-linear model and parameters determined by Clayton *et al.* (1995), with a correlation coefficient of 0.99 in all cases, are presented in Eqn. (A2.20) and Table A2.9.

$$A = e\tau^f \quad (\text{A2.20})$$

where e, f = cultivar-specific mass or volume parameters (dimensionless).
 τ = mass (kg) or volume (m^3) of product.

Table A2.9.

Parameter values for non-linear regression models relating apple surface area to fruit mass and fruit volume for four apple cultivars and the combined dataset (Clayton *et al.*, 1995).

Variety	Mass (kg)		Volume (m^3)	
	e	f	e	f
'Royal Gala'	0.0583	0.688	4.52	0.653
'Braeburn'	0.0575	0.687	4.88	0.661
'Red Delicious'	0.0593	0.689	4.88	0.661
'Granny Smith'	0.0590	0.693	4.87	0.663
Combined	0.0581	0.685	4.77	0.659

A2.2.5.1. Data used

In the present work, surface area correlations for apples utilised either the specific variety parameters (if available) or the combined data of Clayton *et al.* (1995). Model predictions for other products, such as pears and tomatoes, utilised the surface area correlations of Chau *et al.* (1987).

A2.2.6. Energy Release by Product Respiration

Respiration rates for specific products are largely dependent on temperature and atmospheric environment. Experimental values are generally presented for specified temperature ranges and standard atmosphere conditions.

A2.2.6.1. Prediction of Respiration Phenomena

Empirical equations for respiration as a function of temperature have been developed for a range of fresh horticultural products (Hayakawa and Succar, 1982; Gaffney *et al.*, 1985b; Wang, 1991).

The empirical equation used by Gaffney *et al.* (1985b) has a correlation coefficient of 0.99 for a range of products across the temperature range of 0 - 27°C and so is widely used to calculate the heat of respiration as a function of product temperature:

$$q = a[\theta_{pr} + 17.8]^b \quad (\text{A2.21})$$

where q = heat generation rate due to respiration ($\text{J.kg}^{-1}\text{s}^{-1}$).
 θ_{pr} = product temperature ($^{\circ}\text{C}$).
 a, b = product specific constants.

The product-specific constants obtained by Gaffney *et al.* (1985b) using regression of data from USDA Handbook 66 (edited by Hardenburg *et al.*, 1986) are:

Apples:	$a = 4.59 \times 10^{-6}$	and	$b = 2.66$
Peaches:	$a = 1.37 \times 10^{-7}$	and	$b = 3.88$

Both had a correlation coefficient of 0.99. Using the additional data presented by Hardenburg *et al.* (1986), the following constants were calculated for a greater range of products for use in the model presented by Gaffney *et al.* (1985b). Correlation coefficients for these data were greater than 0.98 in all cases.

Apricots:	$a = 3.77 \times 10^{-6}$	and	$b = 2.77$
Avocados:	$a = 1.70 \times 10^{-5}$	and	$b = 2.64$
Grapefruit:	$a = 1.87 \times 10^{-6}$	and	$b = 2.86$
Grapes:	$a = 8.31 \times 10^{-7}$	and	$b = 3.17$
Kiwifruit:	$a = 8.97 \times 10^{-5}$	and	$b = 1.74$
Lemons:	$a = 1.58 \times 10^{-4}$	and	$b = 1.64$
Limes:	$a = 1.02 \times 10^{-10}$	and	$b = 5.47$
Oranges:	$a = 3.73 \times 10^{-6}$	and	$b = 2.73$
Pears:	$a = 5.64 \times 10^{-8}$	and	$b = 3.92$
Plums:	$a = 6.19 \times 10^{-7}$	and	$b = 3.14$
Tomatoes:	$a = 4.40 \times 10^{-6}$	and	$b = 2.69$

Becker and Fricke (1996) presented the equivalent correlation calculating the heat of respiration as a function of the respiration rate, m_{CO_2} . This correlation was based on the Hardenburg *et al.* (1986) assertion that for every one milligram of CO_2 produced, 10.7 joules of heat is generated. The rate of respiratory heat generation thus becomes:

$$q = \frac{10.7m_{CO_2}}{3600} \quad (A2.22)$$

where:

$$m_{CO_2} = o \left(\frac{9}{5} \theta_{prod} + 32 \right)^p \quad (A2.23)$$

where m_{CO_2} = carbon dioxide production per unit mass of product ($mg.kg^{-1}.hr^{-1}$).
 θ_{prod} = mass average product temperature ($^{\circ}C$).
 o,p = product specific respiratory coefficients (presented in Table A2.10).

The weight loss due to respiratory carbon loss is then:

$$m_{resp} = rr_{pr} M_{pr} n_{carbon} \quad (A2.24)$$

where:

$$rr_{pr} = \frac{\left(\frac{m_{C_{O_2}}}{1 \times 10^6} \right)}{3600} \times \frac{1}{n_{carbon}} \quad (A2.25)$$

where m_{resp} = mass flow due to respiratory carbon loss (kg.s⁻¹).
 rr_{pr} = respiration rate of the product (kmol.kg⁻¹.s⁻¹).
 M_{pr} = mass of product in zone (kg).
 n_{carbon} = molar mass of carbon (kg.kmol⁻¹).

Table A2.10.

Respiration coefficients for Eqn. (A2.20) for a range of horticultural products, based on data presented by Hardenburg *et al.* (1986). All cases yielded a correlation coefficient greater than 0.98.

Product	Respiration coefficients	
	θ	p
Apples	5.69×10^{-4}	2.60
Grapefruit	3.58×10^{-3}	2.00
Lemons	1.12×10^{-2}	1.78
Limes	2.99×10^{-8}	4.73
Oranges	2.81×10^{-4}	2.68
Peaches	1.3×10^{-5}	3.64
Pears	6.36×10^{-5}	3.20
Plums	8.61×10^{-5}	2.97
Tomatoes	2.01×10^{-4}	2.84

A2.2.6.2. Cultivar-specific Respiration Data

Data for respiration rates for a range of horticultural commodities has been experimentally collected and tabulated by many researchers. Dadzie (1992) presented correlations for fruit respiration rate in response to storage temperature for a range of apple cultivars.

$$rr_{pr} = \left((a + b\theta_{pr} + c\theta_{pr}^2) \times \frac{12187.27}{(\theta_{pr} + 273.15)} \times \frac{1}{3600} \right) \times 10^{-9} \quad (A2.26)$$

where a, b, c = respiratory equation parameters.
 θ_{pr} = temperature of product (°C).

Table A2.11 presents the correlation parameters for each cultivar (with a correlation coefficient greater than 0.96 in all cases). This equation assumes standard atmospheric pressure (101325 Pa). Cheng *et al.* (1998) developed a further correlation for respiration of 'Braeburn' variety apples in response to temperature (correlation coefficient greater than 0.99):

$$rr_{pr} = (20.8 + 2.3\theta_{pr} + 0.131\theta_{pr}^2) \times 10^{-12} \quad (A2.27)$$

Table A2.11.

Parameter values for non-linear regression models relating apple cultivar respiration rate to temperature (Dadzie, 1992).

Apple Cultivar	Respiration coefficients		
	<i>a</i>	<i>b</i>	<i>c</i>
'Braeburn'	0.94	0.3554	0.0033
'Cox Orange Pippen'	2.75	0.0455	0.0244
'Red Delicious'	2.33	0.1780	0.0182
'Granny Smith'	1.81	0.2105	0.0082
'Royal Gala'	1.33	0.4512	0.0015
'Gala'	2.07	0.3186	0.0057
'Golden Delicious'	3.17	0.3771	0.0068
'Splendor'	1.49	0.1786	0.0049

A2.2.6.3. Measured Data

Hardenburg *et al.* (1986) summarise respiration rate data (reproduced in Table A2.12) for fruit and vegetables at different temperature ranges. Many further data are available in the literature.

Table A2.12.

Respiration rates for a range of horticultural products (After Hardenburg *et al.*, 1986).

Product	Rate of respiration at a given temperature (x 10 ⁻¹¹ kmol.kg ⁻¹ .s ⁻¹)					
	0°C	4 - 5°C	10°C	15-16°C	20-21°C	25-27°C
Apple	2.53	4.73	10.73	15.78	19.57	-
Apricot	3.47	4.73	9.47	17.05	25.57	-
Avocado	-	15.78	-	69.13	132.89	172.35
Banana	-	-	18.94	31.57	55.24	93.12
Lemon	-	-	6.94	10.73	14.52	15.15
Lime	-	-	-	5.05	8.21	18.94
Kiwifruit	1.89	3.79	7.58	-	11.99	-
Orange	2.21	3.47	4.73	11.68	17.68	20.52
Peach	3.16	4.73	10.10	23.67	50.82	64.07
Pear var 'Bartlett'	3.16	4.73	9.15	23.67	31.57	-
Plum	1.58	4.10	5.68	7.58	13.89	31.25
Tomato	-	-	9.15	16.73	21.46	25.88

A2.2.6.4. Data used

In the limited number of cases requiring respiration heat data, and noting that respiratory heat generation is a minor effect in the pre-cooling model, only a simple model was required. Thus, the correlation of Gaffney *et al.* (1985b) was utilised (and built into the dynamic heat transfer simulation system, 'Packaging Simulation for Design'), along with the constants adapted from Hardenburg *et al.* (1986).

For respiration rate modelling (in the mass transfer models), where a better model and/or data were justified, measured data values were utilised where appropriate. If the product was not covered by measured data, as is the case with specific varieties of apple, Eqns. A2.26 or A2.27 are recommended.

A2.3. HYDRO-PHYSICAL PROPERTIES OF PRODUCTS

A2.3.1. Product Water Activity

Water present within horticultural produce tends to contain dissolved substances such as sugars, which lower the water activity at the product surface.

A2.3.1.1. Theoretical Determination of Product Water Activity

This effect could be accurately quantified if the molar concentrations of the substances dissolved in the water near the product surface could be determined. As quantification of the molar concentrations of the dissolved substances is extremely difficult, product water activity can be approximated using (Moore, 1972):

$$a_w = \frac{1}{1 + \frac{0.018\Delta\theta_f}{1.86}} \quad (\text{A2.28})$$

or (Campanone *et al.*, 1995):

$$\ln a_w = -182wc^{-0.696} + 0.232wc^{0.0411} e^{-43.943wc} \ln\left(100e^{\left[\frac{72.74 - 8.2 \ln \theta + 0.00571\theta - \frac{7235.4}{\theta_x}}{\theta_x}\right]}\right) \quad (\text{A2.29})$$

where a_w = water activity of product (fraction).
 $\Delta\theta_f$ = freezing point depression at the product surface ($^{\circ}\text{C}$).
 wc = water content on a wet basis ($\text{kg}_{\text{H}_2\text{O}} \cdot \text{kg}^{-1}$).
 $\Delta\theta_f$ = product surface temperature ($^{\circ}\text{C}$).

The correlation coefficients for Eqns. A2.28 and A2.29 were not given, though both were claimed 'to fit very well' to literature data over a wide temperature range.

A2.3.1.2. Experimental Determination of Product Water Activity

Chau *et al.* (1987) performed a number of experiments to determine the freezing point depression for various fruits and vegetables. From these, commodity surface water activities were calculated. Chau *et al.* (1988) stated that the water activity for most horticultural products was about 0.98 or 0.99. Their values are presented in Table A2.13.

Table A2.13.
Commodity surface water activities (Chau *et al.*, 1988).

Product	Water Activity	Product	Water Activity
'Red Delicious' Apple	0.98	'Valencia' Orange	0.98
'Marsh' Grapefruit	0.99	'Red Globe' Peach	0.99
'Eureka' Lemon	0.98	'D'Anjou' Pear	0.98
'Persian' Lime	0.98	'Sunny' Tomato	0.99

A2.3.1.3. Data Used

For 'Braeburn' apples, the water activity in the present work was taken as 0.995, thereby matching previous work on this cultivar by Merts (1996) and Maguire (1998). The same value was applied for tomatoes in the absence of specific data for the particular cultivar.

A2.3.2. Effective Diffusivity of Water Vapour in Air

To account for water vapour movement within a still air region in a horticultural package, the diffusivity of water vapour in still air was required. Shah *et al.* (1984) presented a linear correlation (correlation coefficient unstated) for the effective diffusivity of water vapour in air:

$$\delta'_{wv} = \frac{1.7255 \times 10^{-3}(\theta_{air} + 273) - 0.2552}{1 \times 10^4} \quad (A2.30)$$

where δ'_{wv} = effective diffusivity of water vapour in air ($m^2 \cdot s^{-1}$).
 θ_{air} = air temperature ($^{\circ}C$).

To convert the effective diffusivity to units used in the modelling methodology, Eqn. (A2.31) was used.

$$\delta_{wv} = \left(\frac{\delta'_{wv}}{(\theta_{air} + 273)R_g} \right) n_w \quad (A2.31)$$

where δ_{wv} = effective diffusivity of water vapour in air ($kg \cdot m \cdot m^{-2} \cdot s^{-1} \cdot Pa^{-1}$).
 R_g = Universal gas constant ($kJ \cdot mol^{-1} \cdot K^{-1}$).
 n_w = molar mass of water ($kg \cdot kmol^{-1}$).

Values for air temperatures between $0^{\circ}C$ and $42^{\circ}C$ from literature are summarised in Table A2.14. Calculation of effective diffusivity of water vapour in air in all presented work utilised Eqn. A2.30.

Table A2.15.

Commodity skin mass transfer coefficients (Chau *et al.*, 1987;
Gan and Woods, 1989; and Becker *et al.*, 1994).

Product	Skin Mass Transfer Coefficient ($\text{kg}\cdot\text{m}^{-2}\cdot\text{s}^{-1}\cdot\text{Pa}^{-1}$)			
	Low	Mean	High	Std. Dev.
Apple var. 'Red Delicious'	1.11×10^{-9}	1.67×10^{-9}	2.27×10^{-9}	3×10^{-10}
Grapefruit var. 'Marsh'	1.09×10^{-8}	1.68×10^{-8}	2.22×10^{-8}	6.4×10^{-9}
Orange var. 'Valencia'	1.38×10^{-8}	1.72×10^{-8}	2.14×10^{-8}	2.1×10^{-9}
Peach var. 'Red Globe'	1.36×10^{-8}	1.42×10^{-7}	4.59×10^{-7}	5.2×10^{-8}
Pear var. 'D'Anjou'	5.23×10^{-9}	6.86×10^{-9}	1.20×10^{-8}	1.49×10^{-9}
Tomato var. 'Sunny'	2.17×10^{-9}	1.10×10^{-8}	2.43×10^{-8}	6.7×10^{-9}

Maguire *et al.* (1996) presented transpiration coefficient data for a range of apple varieties. These coefficients included mass loss as a result of respiratory carbon loss, as part of the water loss process, and are presented in Table A2.16.

Table A2.16.

Apple variety mass transfer coefficients (Maguire *et al.*, 1996).

Apple variety	Mass Transfer Coefficient ($\text{kg}\cdot\text{s}^{-1}\cdot\text{m}^{-2}\cdot\text{Pa}^{-1}$)	Apple variety	Mass Transfer Coefficient ($\text{kg}\cdot\text{s}^{-1}\cdot\text{m}^{-2}\cdot\text{Pa}^{-1}$)
'Cox's Orange Pippin' ¹	1.10×10^{-9}	'Braeburn' ²	7.92×10^{-10}
'Golden Delicious' ¹	6.12×10^{-10}	'Pacific Rose' ²	6.30×10^{-10}
'Fiesta' ¹	4.50×10^{-10}	'Granny Smith' ²	3.06×10^{-10}
'Royal Gala' ¹	5.04×10^{-10}	'Cripps Pink' ^{2,3}	3.78×10^{-10}

where ¹ = Values averaged over a 6 week harvest period.
² = Values averaged over a 12 week harvest period.
³ = Also known as 'Pink LadyTM' in Australia.

In the experimental work performed as part of this research, transpiration rates were measured for the specific samples of 'Braeburn' apples from two New Zealand growing regions (Hawke's Bay and Waikato) used in this work, using the method of Maguire (1998). The values measured for these fruit were $3.51 \times 10^{-10} \text{ kg}\cdot\text{s}^{-1}\cdot\text{m}^{-2}\cdot\text{Pa}^{-1}$ and $4.48 \times 10^{-10} \text{ kg}\cdot\text{s}^{-1}\cdot\text{m}^{-2}\cdot\text{Pa}^{-1}$ respectively. As these products are inherently variable, values can have up to a 10-fold spread across a population, depending on growing conditions, harvest time and year.

A2.3.3.2. Data Used

This work utilised measured values where possible. If these are not available for the line of fruit under examination, a typical value can be sourced from that tabulated here or in other literature.

A2.3.4. 'Effective' Mass Transfer Coefficients for Packaging Materials

The 'effective' mass transfer coefficient of water vapour through packaging materials, $K_{pk,eff}$, describes the resistance of the material to transport across it. Again, experimental values should be used where possible although these values may be difficult to find for the full range of packaging materials, especially for corrugated fibreboards, which are commonly in use in the horticultural industry.

Determination of $K_{pk,eff}$, required development of a conceptual model. A mathematical model used for corrugated paperboard (Foss, pers. comm.), for which the conceptual model was diffusion of water vapour through a still air layer (in the fluted region), slowed by the presence of slightly porous paper-based materials, was used:

$$K_{pk,eff} = R_{pk} \frac{\delta_{fl}}{x_{pk}} \quad (A2.34)$$

where:

$$R_{pk} = \frac{\delta_{pk}}{\delta_{fl}} \quad (A2.35)$$

where $K_{pk,eff}$ = 'effective' mass transfer coefficient for water vapour through a packaging material boundary ($\text{kg.m}^{-2}.\text{s}^{-1}.\text{Pa}^{-1}$).
 R_{pk} = empirical resistance factor for packaging materials.
 δ_{fl} = effective diffusivity of water vapour through still air ($\text{kg.m.m}^{-2}.\text{s}^{-1}.\text{Pa}^{-1}$).
 δ_{pk} = effective diffusivity of water vapour through a packaging material ($\text{kg.m.m}^{-2}.\text{s}^{-1}.\text{Pa}^{-1}$).
 x_{pk} = thickness of the packaging material (m).

To calculate empirical resistance factors for packaging materials, characterisation of the effective diffusivity of water vapour through packaging materials is required. Nilsson *et al.* (1993) presented data indicating that the effective diffusivity of a solid paper product was correlated to its density (the data did not include corrugated cardboard samples). This data has been fitted by the following model, with a correlation coefficient of 0.99:

$$\delta'_{pk} = 1.8797 \times 10^{-5} e^{-0.00445\rho} \quad (A2.36)$$

$$\delta_{pk} = \left(\frac{\delta'_{pk}}{(\theta_{pk} + 273)R_g} \right) n_w \quad (\text{A2.37})$$

where δ'_{pk} = effective diffusivity of water vapour through a packaging material ($\text{m}^2 \cdot \text{s}^{-1}$).

ρ = density of packaging material ($\text{kg} \cdot \text{m}^{-3}$).

θ_{pk} = temperature of packaging material ($^{\circ}\text{C}$).

R_g = Universal gas constant ($\text{kJ} \cdot \text{mol}^{-1} \cdot \text{K}^{-1}$).

n_w = molar mass of water ($\text{kg} \cdot \text{mol}^{-1}$).

Nilsson *et al.* (1993) also showed that the effective diffusivity was relatively constant over the relative humidity range examined (10 - 60%).

In experimental work performed as part of this research, a correlation with density was fitted to effective diffusivity data measured for a range of corrugated packaging materials (Eqn. A2.38). This relationship had a lower correlation coefficient than that of the Nilsson *et al.* (1993) data of 0.91.

$$\delta'_{pk} = 6.1214 \times 10^{-6} e^{-0.00403\rho} \quad (\text{A2.38})$$

A2.3.4.1. Measurement of 'effective' mass transfer coefficients for packaging materials

Water vapour transmission is normally measured as the rate of water vapour passing through a barrier, once the barrier has reached equilibrium moisture content. Two processes occur (Figure A2.1); equilibrium moisture content attainment and water vapour transmission. The portion of interest in measurement of the effective mass transfer coefficient is the linear portion of the curve (the slope of this relationship is proportional to the 'effective' mass transfer coefficient across a packaging material, also termed *water vapour transmission rate, WVTR*).

The measurement system was a sealed plastic container, containing pure water, with a packaging sample, of known area, sealed to the container lid. The system was allowed to stand in a temperature controlled room for at least 24 hours to ensure the equilibration of the packaging material, after which it was placed on a Mettler PM balance (PM6100; resolution of 0.01g) and weight logged for a further 24 hours. External relative humidity of approximately 50% RH was measured continuously (using a Hycal relative humidity sensor; resolution of 0.05% RH), whilst the internal container relative humidity was, by nature of the closed system, maintained near 100% (also measured continuously). The total imprecision in measurement of relative humidity was taken to be <2%. At least three replicates were measured for each material, with differences being <5% in all cases. Measured values for a range of horticultural packaging materials are presented in Table A2.17.

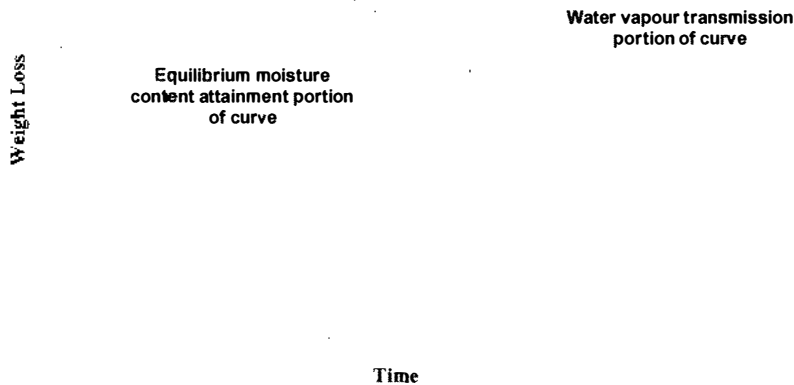


Figure A2.1. Graph showing the two portions of the water vapour transport into and through packaging materials.

Table A2.17.

‘Effective’ mass transfer coefficients for packaging materials, including percentage of rate relative to rate through a still air gap of the same thickness (at 0°C).

Packaging Material	Thickness (mm)	$K_{pk,eff}$ ($\text{kg}\cdot\text{s}^{-1}\cdot\text{m}^{-2}\cdot\text{Pa}^{-1}$)	Empirical factor (R_{pk})
626 C Corrugated board	≈ 3.4	4.30×10^{-9}	0.09
626 ^a B Corrugated board	≈ 4.4	4.32×10^{-9}	0.11
626 ^a C + 626 B Combined	≈ 7.8	2.95×10^{-9}	0.13
623 ^b C Corrugated board	≈ 5.0	5.17×10^{-9}	0.15
313 ^c C Corrugated board	≈ 5.0	5.78×10^{-9}	0.17
623 ^b C + 313 C Combined	≈ 10.0	3.47×10^{-9}	0.20
6226 ^d C Corrugated board	≈ 4.5	4.46×10^{-9}	0.12
2 Layers of 6226 C Corrugated board	≈ 9.0	2.23×10^{-9}	0.12
Moulded pulp “Friday Tray”	≈ 2.0	1.36×10^{-8}	0.16
Solidwall Fibreboard ($\rho = 635 \text{ kg}\cdot\text{m}^{-3}$)	≈ 0.75	3.80×10^{-9}	0.02

NB:

- a - 290 / 160 / 290 $\text{g}\cdot\text{m}^{-2}$ paper grades.
- b - 290 / 160 / 220 $\text{g}\cdot\text{m}^{-2}$ paper grades.
- c - 220 / 120 / 220 $\text{g}\cdot\text{m}^{-2}$ paper grades.
- d - 290 / 160 / 160 / 290 $\text{g}\cdot\text{m}^{-2}$ paper grades.

In comparison to these figures and for reference, a ‘Braeburn’ apple has an ‘effective’ mass transfer coefficient of $7.34 \times 10^{-10} \text{ kg}\cdot\text{s}^{-1}\cdot\text{m}^{-2}\cdot\text{Pa}^{-1}$, therefore packaging is approximately 5 times more permeable.

In this work, measured data were used where possible. In the absence of measured values, it is recommended that Eqns. A2.36 and A2.38 be used with caution, as these are not extensively tested.

A2.3.5. Mass Transfer Coefficients for Fluid - Packaging Material Contact

The rate of water vapour uptake (as distinct from transmission) by a packaging material is predominantly governed by the mass transfer coefficient between the packaging material and the bulk storage cooling fluid, normally air. The research undertaken in this project did not include measurement of these rates. Instead, these values from previous literature were used.

Amos (1995) included a similar mass transfer pathway in a coolstore model to take account of the adsorption / desorption that occurs as the relative humidity changes in horticultural product storage. The first order rate constants presented by Amos (1995) were $7.83 \times 10^{-5} \text{ s}^{-1}$ for pre-cooling and ranged from $7.83 \times 10^{-5} \text{ s}^{-1}$ - $1.3 \times 10^{-4} \text{ s}^{-1}$ for bulk storage.

Merts (1996) also used a similar approach to estimate the rate of adsorption / desorption of water vapour by moulded pulp 'Friday' trays in a Modified Atmosphere Packaging (MAP) model. This researcher assumed a rate of $1.0 \times 10^{-8} \text{ kg.m}^{-2}.\text{s}^{-1}.\text{Pa}^{-1}$ (accuracy not reported). The work undertaken in the research reported here also used this value.

A2.3.6. Guggenheim-Anderson-De Boor (G.A.B) Moisture Isotherm Coefficients

Eagleton and Marcondes (1994) applied the GAB moisture-sorption isotherm model to paper-based packaging materials used in construction of transport packaging for apples (previously presented in Chapter 5). This isotherm relates the equilibrium moisture content of the material to the relative humidity and temperature of the environment in which it occupies. These authors present GAB model coefficients for three apple packaging materials with respect to temperature for both sorption and desorption (Table A2.18).

As stated in Chapter 5, in the modelling methodology presented in this thesis, only the adsorption coefficients were utilised as packaging materials are generally placed in a high relative humidity storage environment from a lower, warmer storage environment.

The data presented by Eagleton and Marcondes (1994) were packaging material and temperature range specific, therefore a small error was created when isotherm data were used for temperatures other than those for which they were originally collected, and for materials other than those originally characterised. The temperature most closely corresponding to the measured data was utilised. When used at temperatures other than those for which they were measured, errors in water content estimates of <5% are expected. If packaging materials were vastly different to those characterised by presented data, predictions of equilibrium moisture content would be unreliable.

Table A2.18.

GAB moisture-sorption isotherm model equation coefficients for paper-based packaging materials used in construction of transport packaging for apples (After Eagleton and Marcondes, 1994).

Packaging Material	Sorption			
	Temp. (°C)	mc_0	ϕ_1	γ_1
Outer Corrugated Sleeve (Lid)	1	5.848	58400	0.729
	10	5.376	106000	0.771
	20	5.262	106000	0.773
	30	4.666	29400	0.791
	40	4.698	35200	0.758
Inner Corrugated Sleeve (Box)	1	6.022	80000	0.700
	10	5.336	103000	0.768
	20	5.260	212000	0.774
	30	4.879	25600	0.782
	40	4.668	22400	0.770
Moulded Pulp Tray	1	6.537	54900	0.733
	10	6.155	18600	0.764
	20	6.016	22600	0.769
	30	5.168	44600	0.792
	40	5.849	2690	0.686

A2.4. CONCLUDING REMARKS.

The information presented in this appendix was used in parameter estimation as part of development of the simulation model datafiles. Many of the equations presented here were built into a spreadsheet based datafile generator, or the individual computer-based simulation models themselves (these are discussed in Appendices 3 and 4).

APPENDIX 3

PRACTICAL GUIDE TO "PACKAGING SIMULATION FOR DESIGN"

A3.1. COMPUTER REQUIREMENTS

Computer: A 486, or Pentium equipped IBM or IBM compatible personal computer running Windows 95 (a Pentium is recommended). Time for simulation is ultimately dependent on the size of the computer's processor.

Disk Drives: A hard drive with at least 5 megabytes of available space and a 3 ½ inch floppy disk drive.

A3.2. INSTALLATION

To install the 'Packaging Simulation for Design' software on a IBM or IBM compatible personal computer, follow the instructions listed below.

1. From the A:\ drive, run the executable zip file 'PackSimSetup.exe'. This will copy all contents of Appendix 5 Disk 1 (found attached to the inside back cover of this manuscript) into a newly created directory ('Packaging Simulation for Design').
2. Run the executable file (PackSim.exe) to operate the software.

A3.3. RUNNING THE SOFTWARE

The user interface for this software has been developed using the Borland C++ Builder programming language, utilising the rapid application development (RAD) environment that this software provides. The initial screen for this software (shown as Figure A3.1) introduces the software, then 'evaporates' to expose the initial input screen for the simulation model software (shown as Figure A3.2). At this point, a user decision of which model (Pre-cooling Simulation or Bulk Storage Simulation) is required. This decision is made by simply clicking the speed button (either Pre-cooling Simulation or Bulk Storage Simulation) on the menu bar.

A3.3.1. Pre-cooling Simulation Model

Clicking on the 'Pre-cooling Simulation' button implements importation of the pre-configured datafile for the packaging configuration under investigation (Figure A3.3). This is followed by a request for information about the length of simulation, output frequency, solution timestep and an error parameter (Figure A3.4). The default values for the latter two are recommended unless the user has experience in changing of these.

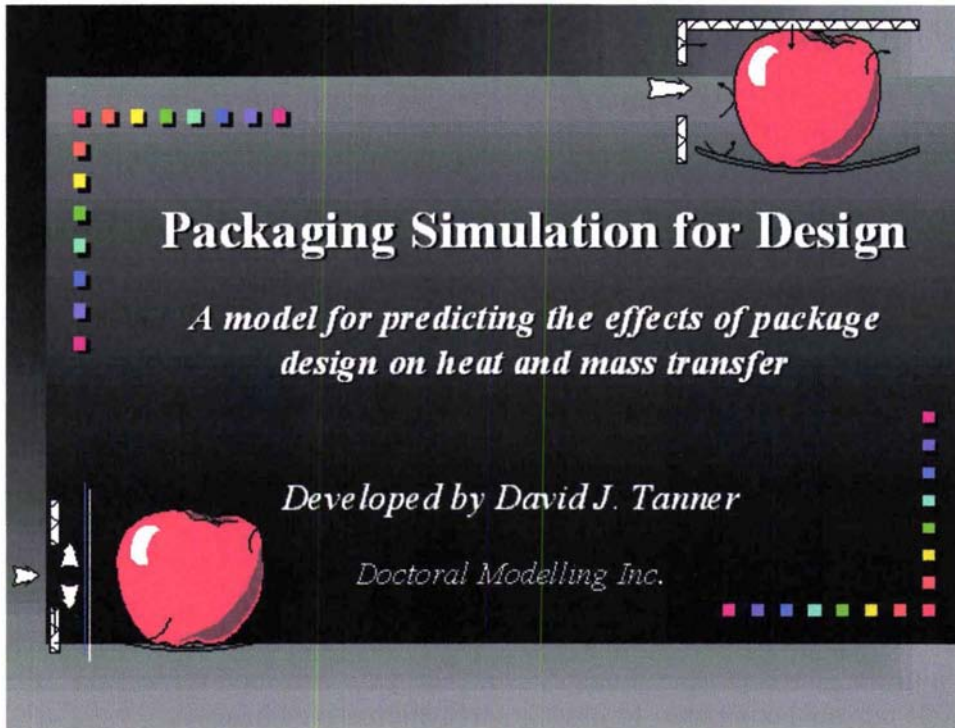


Figure A3.1. The initial 'splash' screen for the 'Packaging Simulation for Design' software.

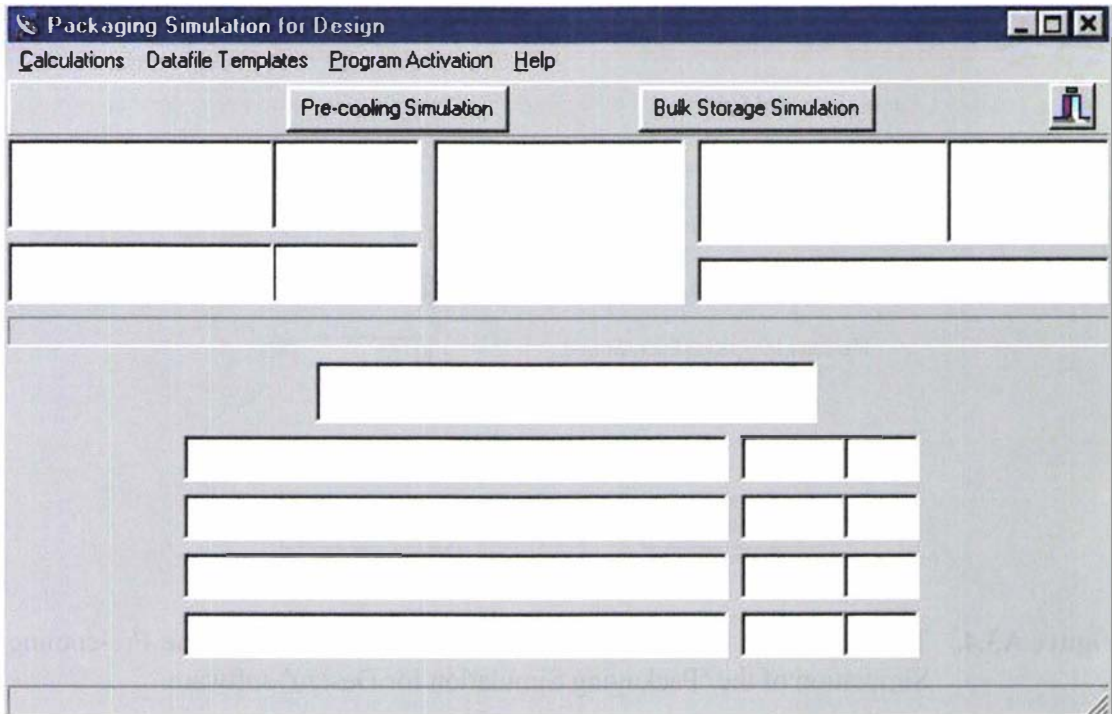


Figure A3.2. The main screen for the 'Packaging Simulation for Design' software - where the first decision, on which simulation model to activate, is required.

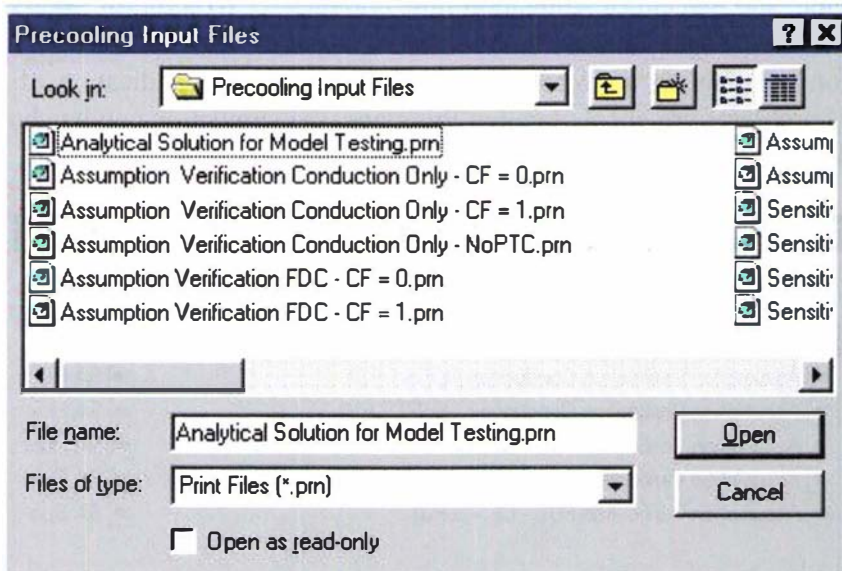


Figure A3.3. The first implementation screen for the Pre-cooling Simulation of the 'Packaging Simulation for Design' software.

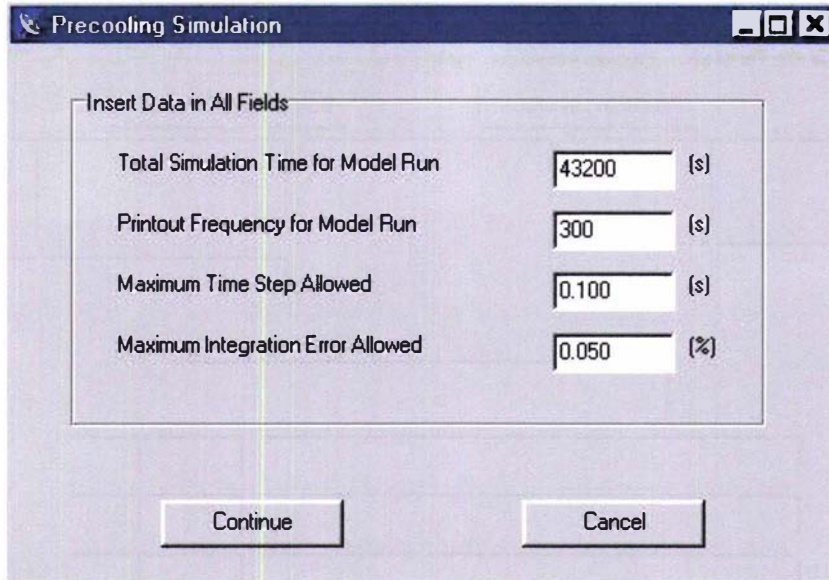


Figure A3.4. The simulation duration and output frequency screen for the Pre-cooling Simulation of the 'Packaging Simulation for Design' software.

Upon input of the simulation duration and frequency, the results filename is required for storage of simulation data (Figure A3.5). Once this is registered, the simulation will begin. The main screen updates the user as to the total time of the simulation, the current simulation time, and percent of simulation time completed. In addition, spot values for a single zone are shown (Figure A3.6). This allows the user to assess at a glance whether the simulation is behaving as expected, and provides an early indication of simulation problems. If problems are encountered at this stage, the simulation can be shutdown and problems addressed, without wasting valuable time.

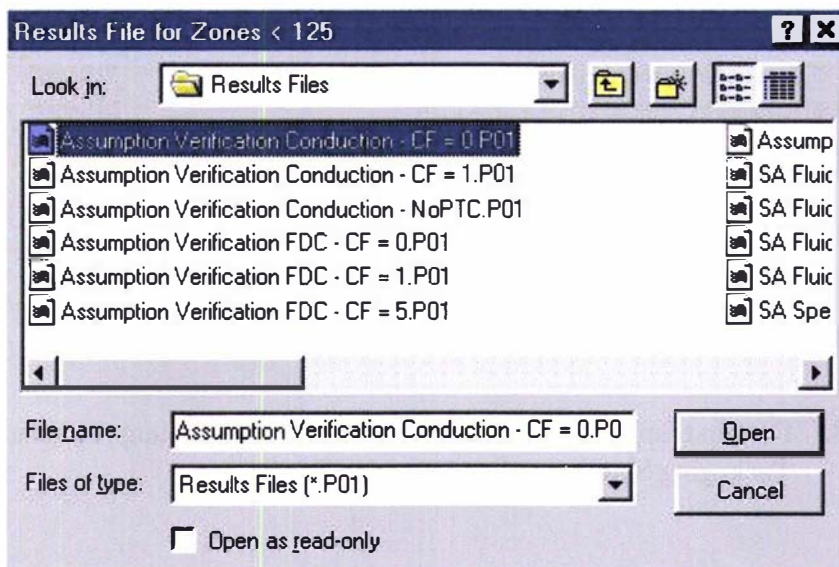


Figure A3.5. The dialog box requiring input of the results file for the Pre-cooling Simulation. Multiple results files will be required for modelling scenarios of greater than 125 zones.

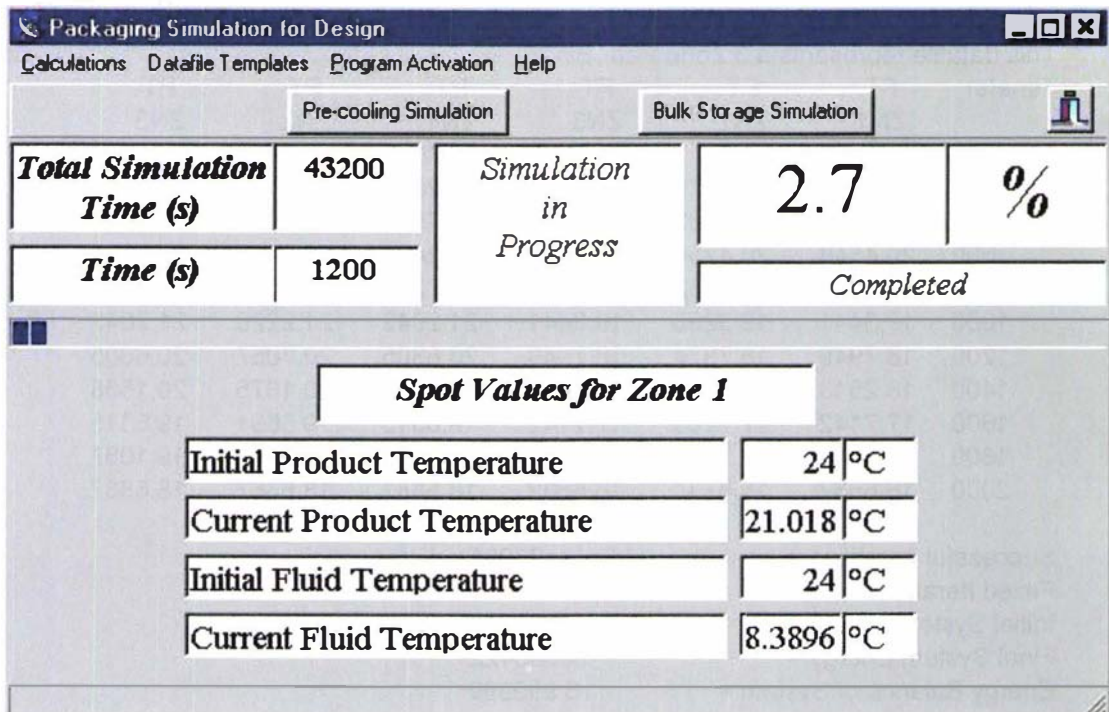


Figure A3.6. The main simulation screen which remains active throughout the duration of the Pre-cooling Simulation.

Upon completion of a simulation, the user is informed that the simulation is complete and upon checking of the Results directory, a file should exist with the data from the simulation. This data includes a zone-by-zone output of both product and fluid temperature, and at the base of this output, a summary of successful solver iterations, the initial system energy, final system energy and an energy balance. This final parameter indicates the success of the simulation (a value of approx. 1 indicates a successful simulation, values greater or less than 1, an unsuccessful simulation). If the value of the energy balance indicates a failed simulation, analysis of the datafile is required as it is possible that mass flows into the system are not balanced by flows out. A summary of a results datafile is shown in Figure A3.7.

A3.3.2. Bulk Storage Simulation Model

Clicking on the 'Bulk Storage Simulation' button also implements importation of a pre-configured datafile for the packaging configuration under investigation (as shown in Figure A3.3). This is also followed by a request for information about the length of simulation (in days), output frequency (in seconds), solution timestep and an error parameter (as shown in Figure A3.4). Again, the default values for the latter two are recommended unless the user has experience in changing of these.

This datafile represents a 3 Zone Pear Bin

Time(s)	FT ZN1	FT ZN2	FT ZN3	PT ZN1	PT ZN2	PT ZN3
0	23.7	23.7	23.7	23.7	23.7	23.7
200	21.5787	21.5275	21.5787	23.2631	23.2484	23.2631
400	21.0138	20.9762	21.0138	22.7567	22.7509	22.7567
600	20.4548	20.4254	20.4548	22.2437	22.2465	22.2437
800	19.8977	19.8762	19.8977	21.7258	21.7366	21.7258
1000	19.3441	19.3298	19.3441	21.2042	21.2226	21.2042
1200	18.7949	18.7874	18.7949	20.6805	20.7057	20.6805
1400	18.2513	18.2501	18.2513	20.1558	20.1875	20.1558
1600	17.7142	17.7189	17.7142	19.6315	19.6691	19.6315
1800	17.1846	17.1947	17.1846	19.1087	19.1518	19.1087
2000	16.6632	16.6784	16.6632	18.5887	18.6367	18.5887

Successful Iterations =	20001
Failed Iterations =	0
Initial System Energy =	53024686
Final System Energy =	36695422
Energy Balance of System =	0.999999

Figure A3.7. A summary of a 3 zone results file as produced by the ‘Packaging Simulation for Design’ software. This can be readily imported into a spread-sheeting package for data analysis and graphing.

Upon input of the simulation duration and frequency, the results filename is required for storage of simulation data (as shown in Figure A3.5). Once this is registered, the simulation will begin. The main screen for this simulation offers similar information as the pre-cooling model with spot values for a single zone initial and current product mass and initial and current fluid relative humidity (Figure A3.8).

Upon completion of a simulation, the user is, once again, informed that the simulation is complete and upon checking of the Results directory, a file should exist with the data from the simulation. This data includes a zone-by-zone output of product mass, fluid relative humidity, and packaging material water mass. At the base of this output, a summary of successful solver iterations, the initial system energy, final system energy and an energy balance. A summary of a results datafile for the Bulk Storage simulation is shown in Figure A3.9.

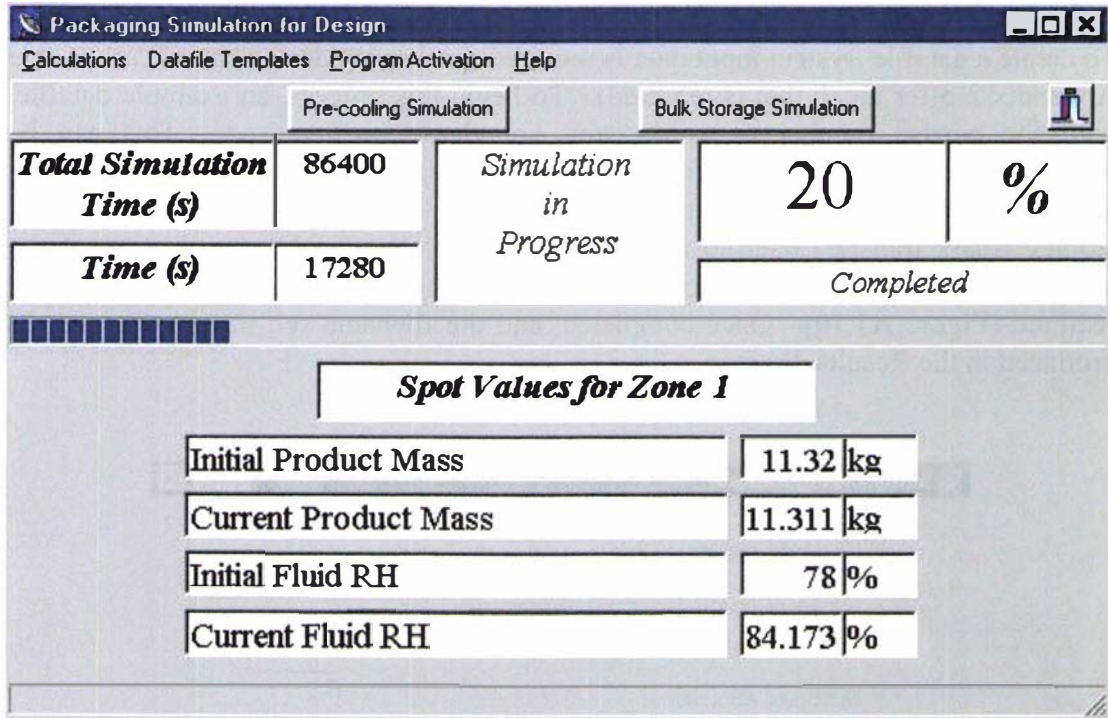


Figure A3.8. The main simulation screen which remains active throughout the duration of the Bulk Storage Simulation.

This datafile represents a 1 Zone Tomato Cardboard Carton

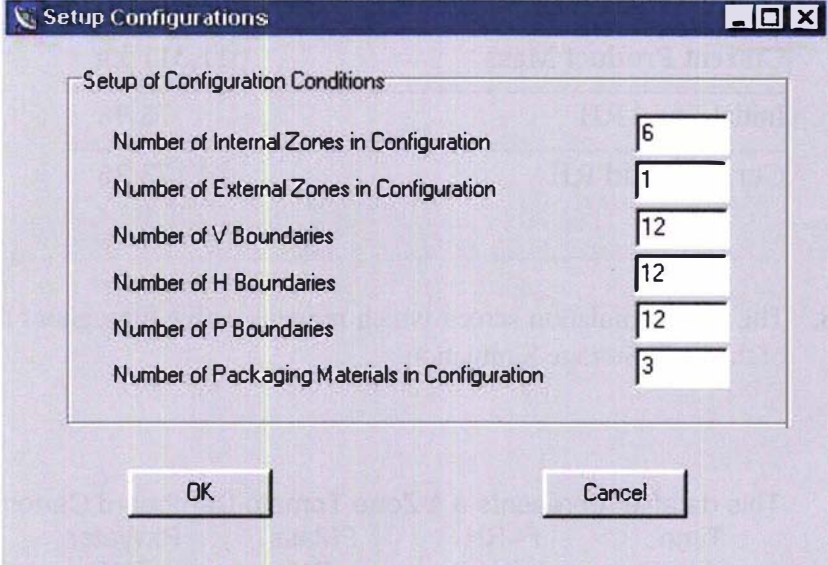
Time (days)	FI-RH ZN1	PMass ZN1	PkWater ZN1
0	0.7	11.313	0.022019
0.25	0.81081	11.29771	0.025876
0.5	0.815452	11.28381	0.026462
0.75	0.816356	11.27012	0.026596
1	0.816575	11.25647	0.02663

Successful Iterations =	86401
Failed Iterations =	0
Initial System Mass =	11.33512
Final System Mass =	11.28443
Total System % Weight Loss =	0.447254
Mass Balance of System =	0.999999

Figure A3.9. A summary of the results file as produced by the 'Bulk Storage Simulation' component of the 'Packaging Simulation for Design' software. This can also be readily imported into a spread-sheeting package for data analysis and graphing.

A3.4. CREATING HEAT AND MASS TRANSFER DATAFILES

To create a datafile, system input data is required (packaging design specifications and Appendix 2 offer much that is required). To begin this process, an example datafile, with the correct number of zones, and boundaries, is required. This can be implemented using the **Datafile Templates** drop down menu in 'Packaging Simulation for Design'. This utility allows both pre-cooling (heat transfer) and bulk storage (mass transfer) datafile templates to be developed. Upon selection of the appropriate datafile template, the user will be asked to input the size of the datafile required (Figure A3.10). Once completed, and the filename set, the datafile will be produced in the Results directory.



Configuration Condition	Value
Number of Internal Zones in Configuration	6
Number of External Zones in Configuration	1
Number of V Boundaries	12
Number of H Boundaries	12
Number of P Boundaries	12
Number of Packaging Materials in Configuration	3

Figure A3.10. The setup conditions required for generation of a datafile template, used to generate a heat transfer or mass transfer datafile.

These templates can then be imported into the Datafile Generator Worksheet (created for use in MS Excel), shown in Figure A3.11. This generator worksheet allows input of product, packaging and package material data, which is then placed in the imported datafile template. This process requires some specialist knowledge of the packaging system. The final output, a pre-cooling (Figure A3.12) or bulk storage datafile, can then be imported into the simulation model (as described in Sections A3.3.1 and A3.3.2).

	A	B	C	D	E
1	Rules for use of Datafile Generator				
2	1. All commands in BLUE are not to be edited				
3	2. All command in RED require editing				
4	3. All commands in PINK are calculations and are not to be edited				
5					
6	Data Used to Develop a Precooling Model Datafile				
7					
8	Physical System Data				
9	Length of package in X direction	1.2 m			
10	Height of package in Y direction	0.6 m			
11	Depth of package in Z direction	1.2 m			
12	Porosity of packaging system	0.220741	fraction of air in package		
13	Fluid flow rate into packaging system	2.174 m / s			
14	Fluid flow rate around packaging system	2.174 m / s			
15	Area of ventilation in packaging system	0.016 m ²			
16					
17	Flow Proportioning Coefficients				
18	For planes in the Z direction		X		
19	A 3 x 3 matrix	0.11	0.11	0.11	
20		0.11	0.11	0.11	
21		0.11	0.11	0.11	
22					
23	Configuration Data				
24	Number of Internal Zones	27			

Figure A3.11. The main screen in the datafile generator worksheet which is used to develop a pre-cooling simulation datafile for inclusion in the ‘Packaging Simulation for Design’ software.

This datafile represents a 1 Zone Apple Carton exposed to coolstore air on all faces.

PACKAGE CONFIGURATION DATA

Total Internal Zones	1
Total External Zones	1
Total V Boundaries	2
Total H Boundaries	2
Total P Boundaries	2
Total Packaging Material Types	4

PRODUCT DATA

Product Temperature	0.55
Product Water Activity	0.995
Transpiration Coefficient	3.51E-10
Respiration Rate	2.18E-11

FLUID DATA

Fluid Temperature	0.5
Fluid Dry Density	1.28543973
Fluid Atmosphere Pressure	101325

PACKAGING MATERIAL DATA

PK1	
Adsorption Coeff. M0	6.537
Adsorption Coeff. C	54900

Figure A3.12. An example of a portion of the input datafile as produced by the datafile generator worksheet. More examples of these can be seen in the Pre-cooling and Bulk Storage Input files directory.

A3.5. USING OTHER COMPONENTS OF THE SIMULATION SOFTWARE

The only other simulation component not already discussed is the convection factor calculator, built into the menu option 'Calculations'. This calculator provides an input screen for variables so that the convection factor (used in the pre-cooling simulation datafile) can be calculated. Upon clicking the Convection Factor item, an input screen (Figure A3.13) is revealed. Upon pressing the calculate button, an estimate of the convection factor is provided (Figure A3.14). This can then be placed in the datafile.

Insert Data in all Fields		
Average Fluid Temperature	273	(°K)
Zone 1 Product Temperature	273	(°K)
Zone 2 Product Temperature	273.5	(°K)
Distance between products (d)	0.010	(m)
Distance between horizontal surfaces (e.g. x)	0.050	(m)

Figure A3.13. The data input screen for the Convection Factor calculator.

The Convection Factor is

Convection Factor = 1.212

Finish

Figure A3.14. The output screen for the Convection Factor calculator.

A3.6. FUTURE MODIFICATIONS OF SOFTWARE

This software was developed as a prototype simulation tool, for research only. This is therefore a disclaimer - the developer does not accept any responsibility for software development downfalls. In addition, this developer does not accept responsibility for the software's wrongful or improper use.

Future modifications that are planned for this software include;

- moulding the heat and mass transfer into a single simulation system - without excessively increasing the simulation time.
- allowing for greater flexibility in storage conditions, such as step changes in external temperature and relative humidity.
- development of a more graphical user interface which provides graphical indicators of temperature and weight loss.

Future modifications to the underlying modelling methodology, such as incorporation of quality parameters, have already been discussed in Chapter 7.

A3.7. FILES INCLUDED FOR SOFTWARE OPERATION

A number of files have been included (as Appendix 5) for operation of the 'Packaging Simulation for Design' software. These files are outlined below in Table A3.1 - and their purpose briefly discussed where necessary.

Table A3.1.
Table of files included in Appendix 5
(Disk 1 attached to the back cover of this manuscript)

Filename	Description
In the PackSim Directory;	
<i>PackSim.exe</i>	The Executable file for running the 'Packaging Simulation for Design' software
In the Bulk Storage Input Files Directory;	
<i>All datafiles in this directory are self-explanatory. The sensitivity analysis files relate to the sensitivity analysis performed for, and discussed in Chapter 8.</i>	
In the Pre-cooling Input Files Directory;	
<i>All datafiles in this directory are self-explanatory. The sensitivity analysis files relate to the sensitivity analysis performed for, and discussed in Chapter 7.</i>	
In the Results Files Directory;	
<i>All datafiles in this directory are self-explanatory. The *.BO* files relate to Bulk Storage Simulation Results Files, whilst the *.PO* files relate to Pre-cooling Simulation Results Files.</i>	

APPENDIX 4

PRACTICAL GUIDE TO "WEIGHT LOSS SIMULATOR"

A4.1. COMPUTER REQUIREMENTS

- Computer: A 486, or Pentium equipped IBM or IBM compatible personal computer running Windows 95 (a Pentium is recommended).
- Disk Drives: A hard drive with at least 5 megabytes of available space and a 3 ½ inch floppy disk drive.
- Software: This software includes database applications. It requires the computer upon which it is to be run to have installed the Borland BDE. This is available with Borland Paradox 7 and Borland C++ Builder.

A4.2. INSTALLATION

To install the 'Weight Loss Simulator' software on an IBM or IBM compatible personal computer, follow the instructions listed below.

1. From the A:\ drive, run the executable zip file 'WLSSetup.exe'. This will copy all contents of Appendix 5 Disk 2 (found attached to the inside back cover of this manuscript) into a newly created directory ('Weight Loss Simulator').
2. Run the executable file (WeightLossSim.exe) to operate the software.

A4.3. RUNNING THE SOFTWARE

The user interface for this software has also been developed using the Borland C++ Builder programming language, utilising the rapid application development (RAD) environment that this software provides. The initial screen for this software (shown as Figure A4.1) introduces the software, then evaporates to expose the main screen for the simulation model software (shown as Figure A4.2). At this point, the user can run the simulator by simply clicking the speed button (Run WLS) on the menu bar.

Clicking on the 'Run WLS' Button implements importation of a dialogue box for input of product data. This dialogue box is fed by a database of products (Figure A4.3), which can be edited using the 'Edit Product DB' speed button on the Main form's menu bar (explained further in section A4.4.).

Once the product in the packaging system is decided upon, initiation of package storage conditions is required (implemented by clicking on 'Initiate Storage Conditions').

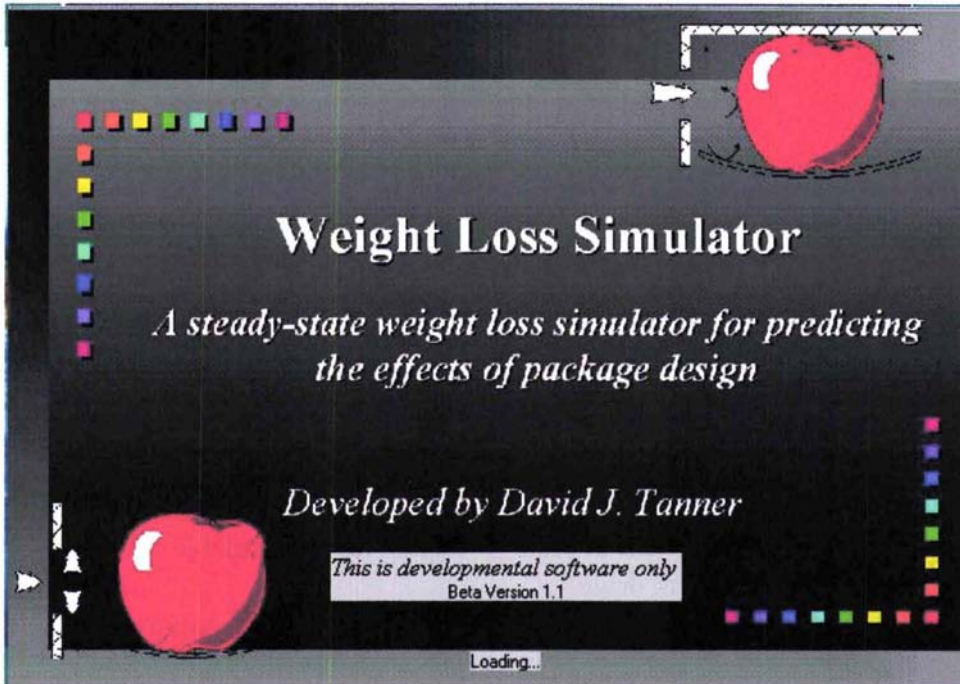


Figure A4.1. The initial 'splash' screen for the 'Weight Loss Simulator' software.

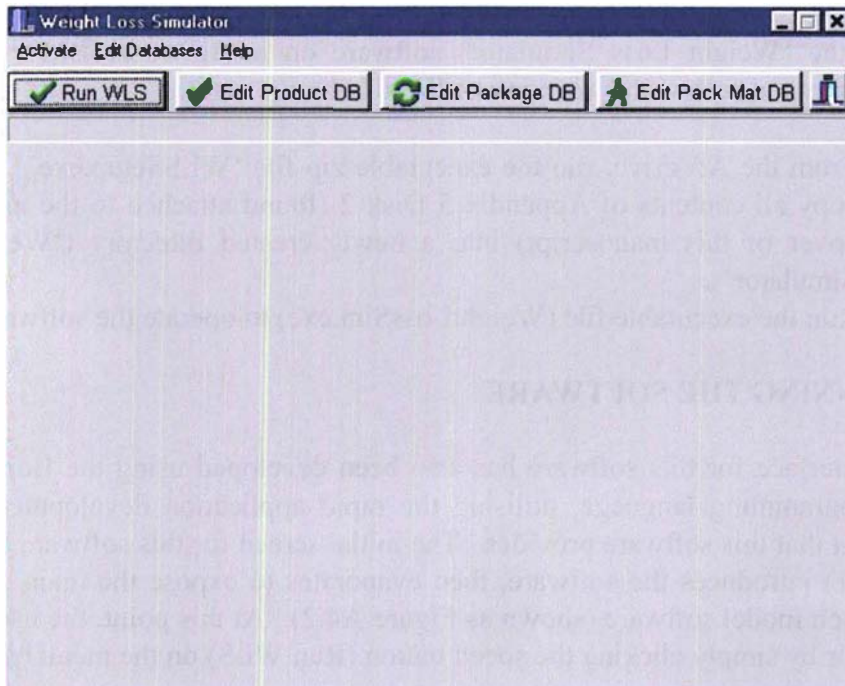


Figure A4.2. The main screen for the 'Weight Loss Simulator' software - where the simulation model is activated using the Run Simulation Speed Button.

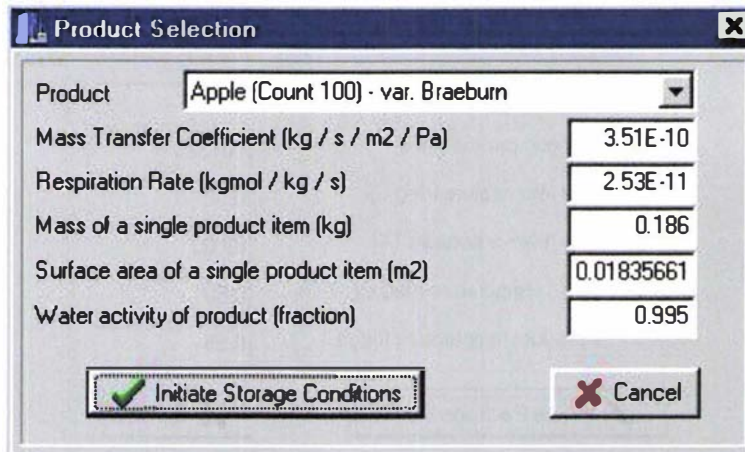


Figure A4.3. The first dialogue screen for implementation of product data for the 'Weight Loss Simulator' software.

In this dialogue box (Figure A4.4), relative humidity, storage temperature conditions etc. are required for the packaging system. By clicking on the 'Initiate Package Details' button, the storage conditions are included in the simulation data, and package configuration details can be implemented.

The package details incorporate dimensions and materials required for construction of the packaging system. These data cannot be edited, as they are implemented from a database of packaging systems (using the 'Edit Package DB' speed button on the main form's menu bar). The data in this dialogue box (Figure A4.5) are implemented upon clicking of the 'Calculate' button. This reveals a further dialogue box of data pertaining to the individual packaging materials used in construction of the packaging system (Figure A4.6). These data are for the users information only, and cannot be edited at this time (can be edited, or new materials introduced using the 'Edit Pack Mat DB' speed button on the main form's menu bar).

Clicking the 'Continue' button implements the solution period to begin for the packaging system. During this process, the screen is updated to show the progress of the software in calculation of the solution (Figure A4.7). Upon completion of the simulation, a full summary of system results and conditions are updated to the screen (Figure A4.8).

Storage Conditions

Fluid in Storage Environment: Air

Fluid atmospheric pressure (Pa): 101325

Storage facility temperature (deg C): 0.50

Storage facility relative humidity (%): 89.00

In-package fluid temperature (deg C): 0.50

In-package product temperature (deg C): 0.55

Figure A4.4. The second dialogue screen for implementation of storage data for the 'Weight Loss Simulator' software.

Package Configuration Details

Package Configuration: 10kg Corrugated Tomato Pack

Package Width: 0.3

Package Height: 0.185

Package Length: 0.38

Package Porosity: 0.506629

Number of Product items in Package: 92

Number of Boundary Packaging Materials in Configuration: 2

Number of Internal Packaging Materials in Configuration: 0

Boundary Packaging Materials	Total Vent Area	Flow Vent Area	Fluid Flow Rate	Material Mass	Total Material Area	Transmission Area
623 C Corrugated Board	0.021	0	0	0.2727	0.3496	0.3496
62623 CB Corrugated Board	0	0	0	0.1443	0.111	0.111

Internal Packaging Materials

Figure A4.5. The third dialogue screen for implementation of packaging system data for the 'Weight Loss Simulator' software.

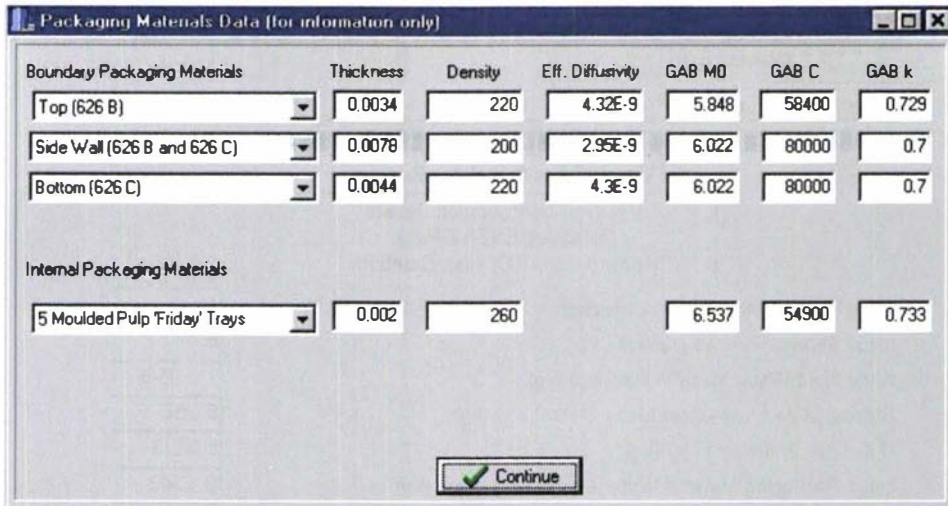


Figure A4.6. The packaging materials dialog box. The data this dialog contains is shown only for information, and cannot be edited at this time. If this is necessary, use of the 'Edit Pack Mat DB' menu button is required.

These visual components outline the increase in water content of the fluid and packaging materials. These components also outline the steady-state relative humidity achieved in the package, and the rate of product weight loss. Upon checking of the WeightSim directory, a file should exist with the data from the simulation (SimResults.txt). A summary of the SimResults.txt datafile is shown in Figure A4.9.

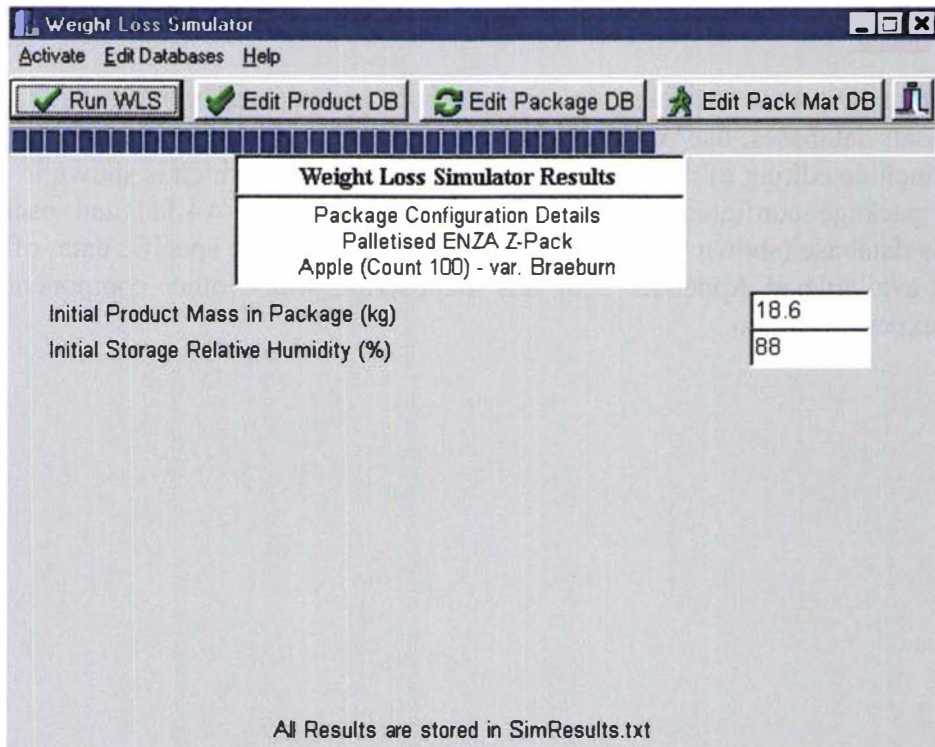


Figure A4.7. The status of the screen during simulation by the 'Weight Loss Simulator' software. The progress bar (in blue) indicates simulation progress.

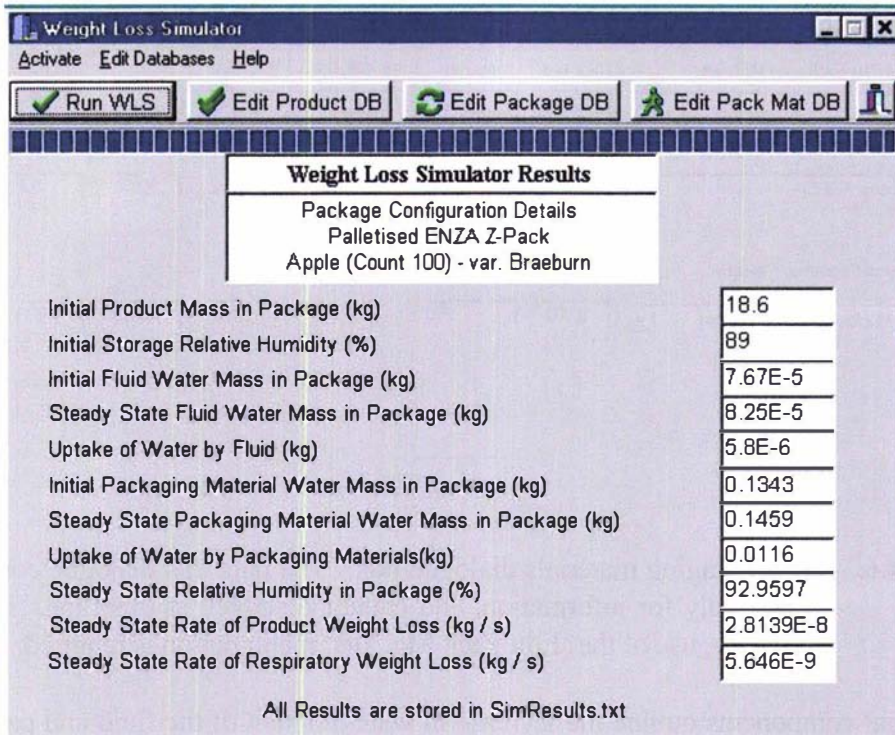


Figure A4.8. The summary of results as produced upon completion by the Simulation software.

A4.4. EDITING THE PRODUCT, PACKAGE AND PACKAGING MATERIALS DATABASES

To include new products, packaging configurations and packaging materials in each of the relevant databases, use of the 'Edit' buttons on the menu bar is advised. These options include editing of the product database (the editor of which is shown in Figure A4.10), package configurations database (shown in Figure A4.11) and packaging materials database (shown in Figure A4.12). These all require specific data, of which some is available in Appendix 2 of this manuscript, whilst other components may require experimentation.

Weight Loss Simulator Results	
Package Configuration :	Palletised ENZA Z-Pack
Product Type :	Apple (Count 100) - var. Braeburn
Product Information :	
Product Mass Transfer Coefficient	3.51E-09 kg/m ² /s/Pa
Product Respiration Coefficient	2.53E-11 kgmol/kg/s
Mass of Product in Package	18.6 kg
Surface Area of Product	1.83566 m ²
Product Temperature	0.69 deg C
Product Water Activity	0.995 dimensionless
Fluid Information :	
Fluid Pressure	101325 Pa
External Fluid Temperature	0.1 deg C
External Fluid Relative Humidity	86 %
Internal Fluid Temperature	0.68 deg C
Package Information :	
Height of Package	0.257 m
Width of Package	0.313 m
Length of Package	0.482 m
Porosity of Package	0.457348 fraction
Number of Boundary Packaging Materials	3
Number of Internal Packaging Materials	1
Packaging Material Information :	
Boundary Material 1	Top (626 B)
Boundary Material 2	Side Wall (626 B and 626 C)
Boundary Material 3	Bottom (626 C)
Internal Material 1	5 Moulded Pulp 'Friday' Trays
Results :	
Initial Product Mass	18.6 kg
Initial Fluid Relative Humidity	86 %
Initial Fluid Mass	7.40E-05 kg
Final Fluid Mass	8.80E-05 kg
Initial Packaging Material Mass	0.1278 kg
Final Packaging Material Mass	0.1651 kg
Steady-state Fluid RH	97.9313 %
Steady-state Product Water Loss	6.78E-08 kg / s
Steady-state Product Respiration Loss	5.65E-09 kg / s

Figure A4.9. A summary of the results file as produced by the Simulation software. This can be readily imported into a spread-sheeting package for data analysis.

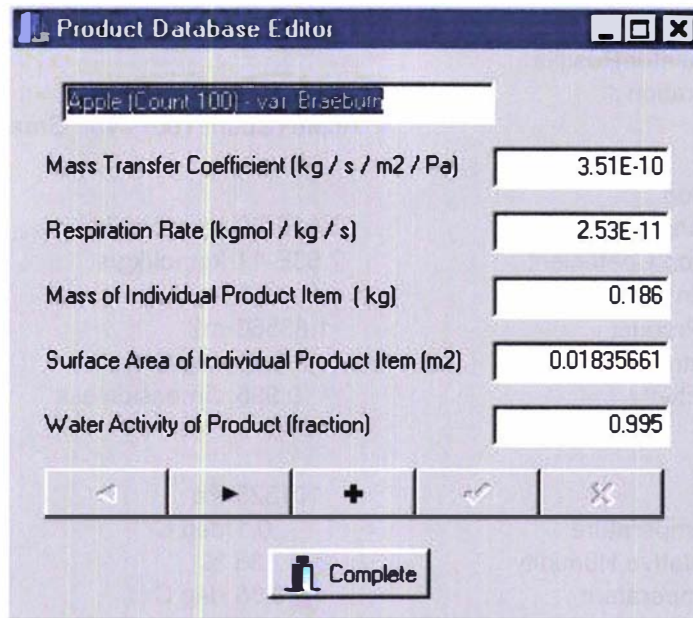


Figure A4.10. The product database editor, which allows input of specialised data regarding products in package configurations.

Product data for many products can be gathered from Chapter 6. Data can then be saved to the database by posting an edit using the ✓ key on the Navigator button at the base of the dialogue page (this is the case with all database edit processes). This prototype software does not include a large range of products, but additions will be forthcoming in subsequent versions. The package configuration database editor (Figure A4.11) requires general data regarding dimensions and construction of the packaging system. Much of the data required for this database is measurable from the packaging system.

By clicking the 'Edit Pack Mat DB' menu button, a screen requiring specialised data about the packaging materials is revealed (Figure A4.12). Data requirements (such as isotherm coefficients, thickness and water vapour transmission rates) are relatively specific as well as sparse, so may require some specialised experimental work for characterisation.

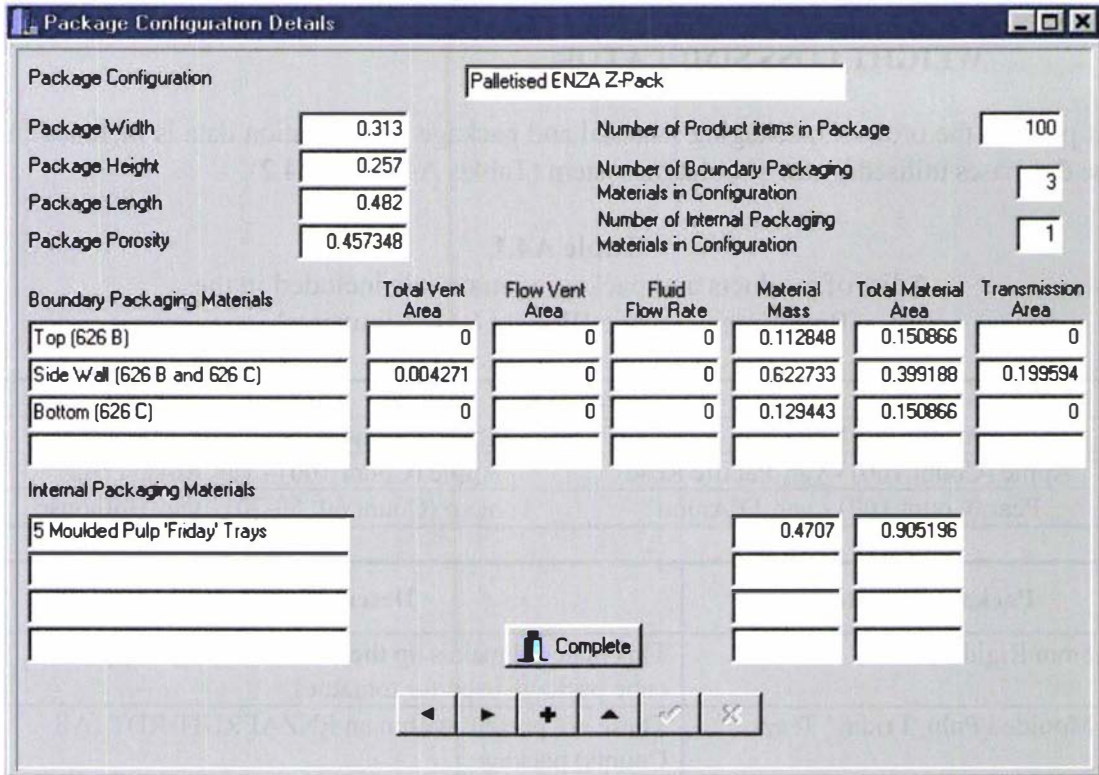


Figure A4.11. The package configuration database editor, which allows input of data for packaging configurations and constructions.

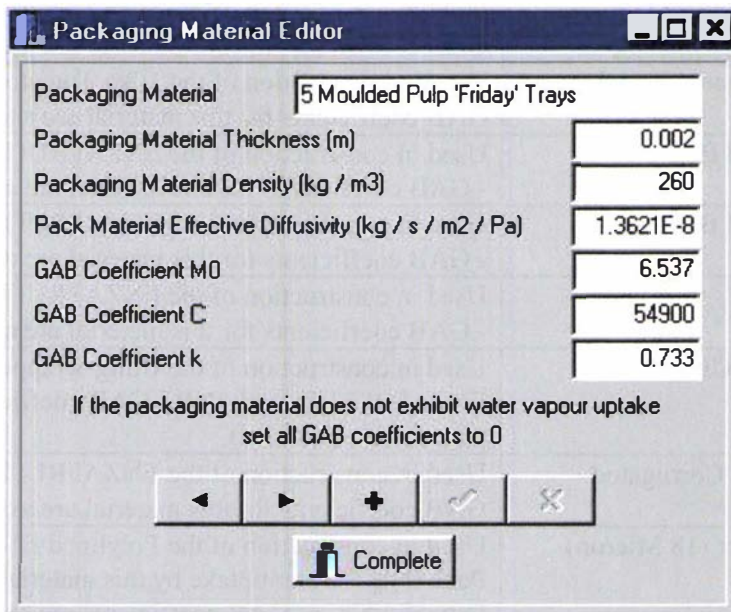


Figure A4.12. The packaging materials database editor, which allows input of data for packaging materials.

A4.5. CURRENT PACKAGE AND PRODUCT INCLUSIONS IN THE WEIGHT LOSS SIMULATOR

At present, the product, packaging material and package configuration data is included in the databases utilised by the simulation system (Tables A4.1 and A4.2).

Table A4.1.

A list of products and packaging materials included in the Beta Version of the 'Weight Loss Simulator'

Products	
Apple (Cnts 80,100,120) - var. Braeburn	Apple (Count 100) - var. Cox Orange
Apple (Count 100) - var. Pacific Rose	Apple (Count 100) - var. Royal Gala
Pear (Count 100) - var. D'Anjou	Tomato (Count 60, 60-70) - var. Hothouse

Packaging Materials	Description
1.8mm Rigid Plastic	This material makes up the construction of the plastic cube package used for tomatoes.
2 Moulded Pulp 'Friday' Trays	These are present within an ENZAFRUIT RDT (All Counts) package.
5 Moulded Pulp 'Friday' Trays	These are present within an ENZAFRUIT Z-Pack (Counts 60 - 110) package.
6 Moulded Pulp 'Friday' Trays	These are present within an ENZAFRUIT Z-Pack (Counts 120 - 150) package.
623 C Corrugated Board	Used in construction of the 10kg Tomato Pack (NB - GAB coefficients for this material are assumed)
62623 CB Corrugated Board	Used in construction of the 10kg Tomato Pack (NB - GAB coefficients for this material are assumed)
626 C Corrugated Board	Used in construction of the ENZAFRUIT Z-Pack (NB - GAB coefficients for this material are assumed)
626 B Corrugated Board	Used in construction of the ENZAFRUIT Z-Pack (NB - GAB coefficients for this material are assumed)
626 B + 626 C	Used in construction of the ENZAFRUIT Z-Pack (NB - GAB coefficients for this material are assumed)
626 B + 626 C + Cling	Used in construction of the Cling-wrapped ENZAFRUIT Z-Pack (NB - GAB coefficients for this material are assumed)
Duo-arch 6226 C Corrugated Board	Used in construction of the ENZAFRUIT RDT (NB - GAB coefficients for this material are assumed)
Standard Polyliner (18 Micron)	Used in construction of the Polylined ENZAFRUIT Z-Pack (NB - Water uptake by this material is assumed to negligible, so GAB coefficients are set to 0)

Table A4.2.

A list of packages included in the Beta Version of the 'Weight Loss Simulator'

Package Configurations	Description
10kg Corrugated Cardboard Tomato Package	A corrugated cardboard package commonly used for transport packaging by 'Harvest NZ'.
15kg Plastic Tomato Package	A plastic cube box was used for packing tomatoes into to reduce the rate of weight loss.
Cling-wrapped ENZAFRUIT Z-Pack (exposed on 2 faces only)	This is the standard ENZAFRUIT Z-Pack with a cling wrap over the 2 faces exposed to the coolstore air.
ENZAFRUIT Z-Pack (exposed on 2 faces only)	This is the standard ENZAFRUIT Z-Pack exposed to the coolstore air on only 2 faces.
Non-ventilated ENZAFRUIT Z-Pack (exposed on 2 faces only)	This is the standard ENZAFRUIT Z-Pack without ventilation or handholes and exposed to the coolstore air on only 2 faces.
Sealed, Polylined ENZAFRUIT Z-Pack	This is the standard ENZAFRUIT Z-Pack with a sealed polyliner within the corrugated cardboard package.
Standard Polylined ENZAFRUIT Z-Pack	This is the standard ENZAFRUIT Z-Pack with a 24 hole, 'standard' polyliner within the corrugated cardboard package.
ENZAFRUIT RDT (exposed on 2 faces only)	This is the standard ENZAFRUIT RDT exposed to the coolstore air on only 2 faces.

A4.6. FUTURE MODIFICATIONS OF SOFTWARE

This software was developed as a prototype simulation tool, for research only (with the aim of its imminent use by industry representatives). This is therefore a disclaimer - the developer does not accept any responsibility for software development downfalls. In addition, this developer does not accept responsibility for the software's wrongful or improper use.

Future modifications that are planned for this software include;

- Inclusion of a graphical description of each product, packaging system and packaging material implemented in the software.
- Presentation of results in a graphical manner from the final results screen, allowing comparison of previously simulated systems.

A4.6. FILES INCLUDED FOR SOFTWARE OPERATION

A number of files have been included (as Appendix 5) for operation of the 'Weight Loss Simulator' software. These files are outlined in Table A4.3 and their purpose briefly discussed where necessary.

Table A4.3.

Table of files included in Appendix 5
(Disk 2 - attached to back cover of this manuscript)

Filename	Description
In the <i>WeightSim</i> Directory;	
<i>WeightLossSim.exe</i>	The Executable file for running the 'Weight Loss Simulator' software.
<i>SimResults.txt</i>	The results file created after running of each simulation (NB This is overwritten after each simulation)
In the <i>Databases</i> Directory;	
<i>Product.DB</i>	Database containing product information for products listed in Table A4.1.
<i>Packaging Material.DB</i>	Database containing packaging material information for materials listed in Table A4.1.
<i>Package Details.DB</i>	Database containing package information for packaging configurations listed in Table A4.2.